Regulation von Thioredoxin-1 und Mitochondrien-abhängigen zellulären Funktionen im kardiovaskulären System

Inaugural-Dissertation

zur Erlangung des Doktorgrades
der Mathematisch-Naturwissenschaftlichen Fakultät
der Heinrich-Heine-Universität Düsseldorf

vorgelegt von

Philipp Jakobs
aus Geilenkirchen

Düsseldorf, Mai 2018

aus dem Institut für
der Heinrich-Heine-Universität Düsseldorf

Gedruckt mit der Genehmigung der
Mathematisch-Naturwissenschaftlichen Fakultät der
Heinrich-Heine-Universität Düsseldorf

Berichterstatter:

1. Prof. Dr. Judith Haendeler

2. Prof. Dr. Axel Gödecke

Tag der mündlichen Prüfung:

04.07.2018

Erklärung

Ich versichere an Eides statt, dass die Dissertation von mir selbstständig und ohne unzulässige fremde Hilfe unter Beachtung der „Grundsätze zur Sicherung guter wissenschaftlicher Praxis an der Heinrich-Heine-Universität Düsseldorf“ erstellt worden ist.

_____

(Philipp Jakobs)

Düsseldorf, Mai 2018

Inhaltsverzeichnis

Gefäßalterung

Allgemein kann das Altern definiert werden als fortschreitender Funktionsverlust aller Gewebe, welcher zu einer gestörten Funktion des Organismus führt. Das Altern ist ein unabhängiger Risikofaktor für das Auftreten einer Vielzahl von Erkrankungen. Externe Risikofaktoren, wie z.B. Ernährung oder Luftverschmutzung, können den Alterungsprozess modulieren und damit die Entstehung von Krankheiten beschleunigen oder verzögern. Auf Einflüsse dieser Umweltfaktoren gehe ich im nächsten Kapitel ein.

Kardiovaskuläre Erkrankungen stellen die häufigste Todesursache dar. 2016 starben über 17 Millionen Menschen an kardiovaskulären Erkrankungen, was 32 % der Gesamttodesfälle weltweit ausmachte (https://ourworldindata.org/causes-of-death). Eine der Hauptursachen für kardiovaskuläre Erkrankungen sind Veränderungen der Gefäße bis hin zum Gefäßverschluss. Blutgefäße kann man untergliedern in Arterien und Venen, die zu den großen Gefäßen gehören, sowie Arteriolen, Kapillaren und Venolen, die zu den kleinen Gefäßen zählen. Im Folgenden gehe ich nur noch auf Arterien ein. Die innerste Schicht der Arterien ist das Endothel. Diese sogenannte Tunica intima bildet eine einschichtige Barriere zwischen dem Blutstrom und den äußeren Schichten der Gefäßwand (Tunica interna). Komplettiert wird diese durch Schichten glatter Muskelzellen (Tunica media), die von einer Bindegewebsschicht umgeben sind (Tunica externa) (Abbildung 1). Das Endothel erfüllt wichtige Funktionen in den Gefäßen.

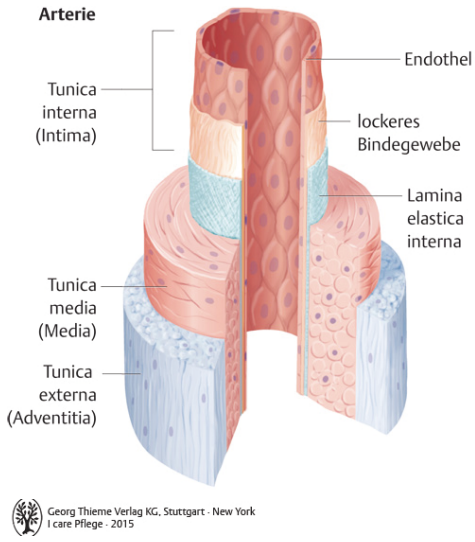

Abbildung 1: Schematischer Aufbau von Arterien: Tunica interna: Besteht aus einer Schicht von Endothelzellen und Bindegewebe. Tunica media: Besteht aus Schichten von glatten Muskelzellen und elastischen Fasern. Tunica externa: Bindegewebsschicht (Bley et al. 2015)

Zum einen bildet das Endothel eine nicht adhärente Oberfläche für Leukozyten, sodass diese nicht anheften können. Des Weiteren verhindert es die Aktivierung von Thrombozyten durch die Bildung von Heparin oder Prostazyklinen. Außerdem sorgt das Endothel für den Austausch von Nährstoffen und Sauerstoff zwischen dem umliegenden Gewebe und dem Blut. Endothelzellen spielen zudem eine wichtige Rolle bei der Dilatation und Konstriktion von arteriellen Gefäßen, die hauptsächlich über Stickstoffmonoxid (NO) reguliert werden. NO ist ein lösliches Gas, das aus der Aminosäu-

re L-Arginin mit Hilfe des Co-Faktors Tetrahydribiopterin (BH4) durch das Enzym Stickstoffmonoxid-Synthase (NOS) gebildet wird (Palmer et al. 1988). Es gibt drei Isoformen von NOS, die neuronale (nNOS), die induzierbare (iNOS) und die endotheliale (eNOS) NOS. Alle drei Isoformen sind im kardiovaskulären System vorhanden (Tsutsui et al. 2009), wobei die eNOS und nNOS konstitutiv exprimiert sind. Über zyklisches Guanosinmonophosphat (cGMP), das durch die Freisetzung von NO aus dem Endothel von Guanylatzyklase in den glatten Muskelzellen gebildet wird, reguliert NO die Relaxation dieser (Moncada et al. 1991). Zudem ist das endotheliale NO wichtig zur Verhinderung der Thrombozytenaktivierung und Inhibition der Expression von Adhäsionsmolekülen auf der Endothelzelloberfläche (Radomski et al. 1987). Neben der Vermeidung der Entstehung von Thrombosen verhindert NO die Ausschüttung von in Thrombozyten gebildeten Wachstumsfaktoren, welche die Proliferation von glatten Muskelzellen stimulieren. Zudem schützt NO Endothelzellen vor Apoptose (Dimmeler et al. 1997; Dimmeler et al. 1997; Dimmeler and Zeiher 1999; Haendeler et al. 1999). Mit fortschreitendem Alter wird weniger NO synthetisiert, was zu einer endothelialen Dysfunktion führt (Zeiher et al. 1993; Luscher and Noll 1995; Tschudi et al. 1996). Die endotheliale Dysfunktion geht einher mit erhöhter Endothelzell-Apoptose und damit dem Verlust der Integrität des Endothels.

Einfluss von ultrafeinen Kohlenstoffpartikeln als Luftverschmutzungsbestandteil auf die Lunge und von Koffein als Ernährungskomponente auf das kardiovaskuläre System

Luftverschmutzung ist ein externer Risikofaktor, welcher kardiovaskuläre Erkrankungen hervorrufen kann. Jährlich sterben zwischen 3 und 4 Millionen Menschen an den Folgen der Luftverschmutzung (Lim et al. 2012; Lelieveld et al. 2015). Einen wesentlichen Anteil an der Luftverschmutzung haben Feststoffteilchen (particulate matter, PM). Sie werden klassifiziert in grobe (Durchmesser < 10 µm, ≥ 2,5 µm), feine (Durchmesser < 2,5 µm, ≥ 0,1 µm) und ultrafeine Partikel (Durchmesser < 0,1 µm). PMs haben unterschiedliche Zusammensetzungen, die abhängig von der Quelle sind. Kohlenstoffhaltige Partikel entstehen durch Verbrennungsprozesse, sei es durch Verkehr, Industrie oder Haushalt. Sie sind zwar kohlenstoffbasiert, können auf ihrer Oberfläche aber noch verschiedene Substanzen, wie z.B. polyzyklische aromatische Kohlenwasserstoffe und reaktive Metalle, binden (Miller et al. 2012). Die Inhalation von PMs sorgt für eine starke oxidative Stressreaktion in der Lunge. Diese Reaktion wird durch verschiedene enzymatische Signalwege verstärkt und führt letztendlich zu einer systemischen vaskulären Stressreaktion. Es zeigte sich, dass auch reine ultrafeine Kohlenstoffpartikel oxidativen Stress in Lungenepithelzellen induzieren und in diesen zur zellulären Seneszenz führen (Büchner et al. 2013). Zudem konnte unsere Arbeitsgruppe in dieser Studie nachweisen, dass ultrafeine Kohlenstoffpartikel die NO Bioverfügbarkeit und die Proteinmenge an eNOS in Endothelzellen reduzieren sowie Seneszenz erhöhen (Büchner et al. 2013). Dies ist im Einklang mit Befunden, dass PM-induzierter oxidativer Stress die Verfügbarkeit von NO in Endothelzellen verringert und Inhalation von Dieselabgasen, im Gegen-

satz zu gefilterter Luft, zu einer verschlechterten Endothel-abhängigen Vasodilatation und verringerter endothelialer Bioverfügbarkeit von NO führt (Mills et al. 2005).

Um nun zu verstehen, welche Signalwege durch ultrafeine Kohlenstoffpartikel in der Lunge verändert werden, wurde in Kollaboration mit der Partikel-Toxikologie des IUF der Einfluss von ultrafeinen Kohlenstoffpartikeln sowohl *ex vivo* auf Lungenepithelzellen wie *in vivo* auf die Lunge der Maus untersucht. Es zeigte sich, dass ultrafeine Kohlenstoffpartikel den „epidermal growth factor receptor" (EGFR) auf der Zelloberfläche aktivieren. Diese Aktivierung war abhängig von der durch ultrafeine Kohlenstoffpartikel induzierten Ko-Lokalisation von EGFR und Caveolin-1 in sogenannten „lipid rafts". „Lipid rafts" sind spezielle Bereiche u.a. in der Plasmamembran. Sie weisen einen hohen Gehalt an Sphingomyelinen, Glycosphingolipiden und Cholesterin auf. „Lipid rafts" sind an verschiedenen intrazellulären Prozessen beteiligt wie u.a. der Sortierung von Proteinen und der Signaltransduktion (Sezgin et al. 2017). Durch die durch ultrafeine Kohlenstoffpartikel induzierte Ko-Lokalisation von EGFR und Caveolin-1 in den „lipid rafts" kommt es zur nachfolgenden Aktivierung von „extracellular signal-regulated kinases 1/2" (ERK1/2) und „RAC-alpha serine/threonine-protein kinase 1" (Proteinase Bα/Akt1). Um die Aktivierung dieser Kinasen durch ultrafeine Kohlenstoffpartikel auch *in vivo* nachzuweisen, wurde in Lungenlysaten von Wildtyp Mäusen und Caveolin-1-defizienten Tieren nach Partikel-Instillation die Aktivierung von ERK1/2 und Akt1 untersucht. Es zeigte sich, dass es in Caveolin-1-defizienten Mäusen nicht zu einer Aktivierung durch Partikel kam. Zudem konnte in der Lunge von Caveolin-1-defizienten Mäusen keine durch ultrafeine Kohlenstoffpartikel induzierte pro-inflammatorische Reaktion nachgewiesen werden (Stöckmann,…, **Jakobs**, et al. 2018). Daher scheint Caveolin-1 zusammen mit dem EGFR wichtig für die durch ultrafeine Kohlenstoffpartikel induzierten Veränderungen zu sein.

Verschiedene Studien assoziieren den Verlust der Zell-Zell-Kommunikation mit dem Auftreten von zellulärer Seneszenz und Alterung (Lopez-Otin et al. 2013). Da unsere Arbeitsgruppe bereits nachgewiesen hatte, dass ultrafeine Kohlenstoffpartikel in nicht-inflammatorischen Konzentrationen Seneszenz in Lungenepithelzellen induzieren (Büchner et al. 2013), wurde nun untersucht, ob es in diesen Zellen auch zum Verlust der Zell-Zell-Kommunikation kommt.

Die Behandlung von Lungenepithelzellen mit ultrafeinen Kohlenstoffpartikeln über eine Dauer von 14 Tagen führte nicht nur zu einer Akkumulation des Zellzyklusinhibitors p21 und dem Verlust der redox-sensitiven Histon-Deacetylase Sirtuin-1, sondern auch zur Reduktion der Connexin-43 Proteinmenge. Connexin-43 ist maßgeblich für die Zell-Zell-Kommunikation in Lungenepithelzellen verantwortlich. Sich daran anschließende Untersuchungen zeigten, dass ultrafeine Kohlenstoffpartikel nicht nur die Menge an Connexin-43 reduzierten, sondern auch die Translokation von Connexin-43 von der Plasmamembran in das Zytosol induzierten. Daher scheint auch in Lungenepithelzellen die Seneszenzinduktion mit dem Verlust der Zell-Zell-Kommunikation einherzugehen (Spannbrucker,…, **Jakobs,** et al. 2018).

Neben Luftverschmutzung, in der ultrafeine Kohlenstoffpartikel zu der Entstehung von Krankheiten in der Lunge beitragen, hat Ernährung einen wesentlichen Einfluss auf das kardiovaskuläre System. Verschiedene Kohortenstudien zeigten eine Assoziation zwischen Kaffeekonsum und einem verringerten Mortalitätsrisiko bei einer Vielzahl von Erkrankungen. Dabei korrelierte die Anzahl der Todesfälle nach Herz- und Atemwegserkrankungen, nach Schlaganfällen und durch Diabetes Typ II negativ mit dem Kaffeekonsum (van Dam and Feskens 2002; van Dam and Hu 2005; Freedman et al. 2012; Gunter et al. 2017). Zudem scheint der protektive Effekt von Koffein dosisabhängig zu sein, da ein Konsum von vier oder mehr Tassen Kaffee pro Tag im Vergleich mit einem niedrigeren Konsum das Risiko von Erkrankungen verringert (O'Keefe et al. 2013). In einer vorangegangenen Studie unserer Arbeitsgruppe konnte nachgewiesen werden, dass nach dem Trinken von vier Tassen Kaffee eine Serumkonzentration von ca. 30-50 µM Koffein im Menschen erreicht wird (Spyridopoulos et al. 2008). Bisher waren als Wirkmechanismen für Koffein eine Inhibition von Adenosinrezeptoren und Phosphodiesterasen sowie eine Erhöhung von intrazellulärem Calcium beschrieben worden. Jedoch ergaben Dosis-Wirkungsstudien, dass alle diese Effekte von Koffein nur mit Konzentrationen über 200 µM erzielt werden können (Smellie et al. 1979; Benowitz 1990; Lasley et al. 2001; Fisone et al. 2004; Daly 2007; Ribe et al. 2008; Banerjee et al. 2014). Da jedoch durch das Trinken von 4 Tassen Kaffee im menschlichen Blut nur eine Konzentration von ca. 30-50 µM erreicht werden kann, ist unklar, welche molekularen Prozesse durch maximal 50 µM Koffein in Zellen verändert werden. Erste Untersuchungen unserer Arbeitsgruppe zeigten, dass diese physiologischen Konzentrationen von Koffein die migratorische Kapazität von Endothelzellen in einer Mitochondrien-abhängigen Weise *ex vivo* und *in vivo* verbessern (Spyridopoulos et al. 2008). Daher sollten die zugrunde liegenden Mechanismen, wie Koffein die mitochondrielle Funktion und die Migration von Endothelzellen verbessert, aufgeklärt werden.

Eine frühere Studie von McAllister et al. gab einen Hinweis auf den Zellzyklusinhibitor CDKN1B/p27 („cyclin dependent kinase inhibitor 1B“) als einen möglichen Mediator von Migrationsprozessen. In dieser Arbeit war gezeigt worden, dass p27-defiziente Fibroblasten nicht in der Lage sind zu migrieren, was sich durch Gabe von rekombinantem p27 kompensieren ließ. Zudem wurde nachgewiesen, dass der pro-migratorische Effekt von p27 abhängig von seiner nichtnukleären Lokalisation ist (McAllister et al. 2003).

Daher lag die Vermutung nahe, dass p27 auch eine Rolle in der Endothelzellmigration spielt. Da die migratorische Kapazität von Endothelzellen von funktionellen Mitochondrien abhängig ist (Spyridopoulos et al. 2008), wurde zunächst untersucht, wo p27 in Endothelzellen lokalisiert ist. Interessanterweise konnten wir zeigen, dass p27 auch in den Mitochondrien von Endothelzellen vorhanden ist. Ein Zusammenhang mit Koffein konnte anhand der Tatsache, dass die Menge an mitochondriellem p27 durch Behandlung von Endothelzellen mit 50 µM Koffein signifikant gesteigert wurde, gezeigt werden (Ale-Agha*, Goy*, **Jakobs*** et al. 2018).

Um einen Nachweis zu führen, dass p27 für die Endothelzellmigration benötigt wird, wurde seine Expression mit „small interfering RNAs“ (siRNAs) herunterreguliert (Abbildung 2A). Dabei zeigte sich, dass sowohl die basale als auch die Koffein-induzierte Migration durch den „Knockdown“ von p27 in Endothelzellen komplett aufgehoben wird (Abbildung 2B). Dies zeigt, dass Endothelzellen p27 für die Migration benötigen. Allerdings konnte damit nicht geklärt werden, ob diese Funktion von nukleärem oder mitochondriellem p27 ausgeübt wird. Daher wurden nach der siRNA-vermittelten Herunterregulation von endogenem p27 Varianten überexprimiert, die entweder exklusiv im Zellkern (nuc p27) oder in den Mitochondrien (mito p27) lokalisiert sind. In diesem „rescue“-Versuch konnten wir zeigen, dass nur das mitochondrielle p27 dem „Knockdown“ von endogenem p27 entgegenwirken und damit die migratorische Kapazität wiederherstellen kann (Abbildung 2C) (Ale-Agha*, Goy*, **Jakobs*** et al. 2018).

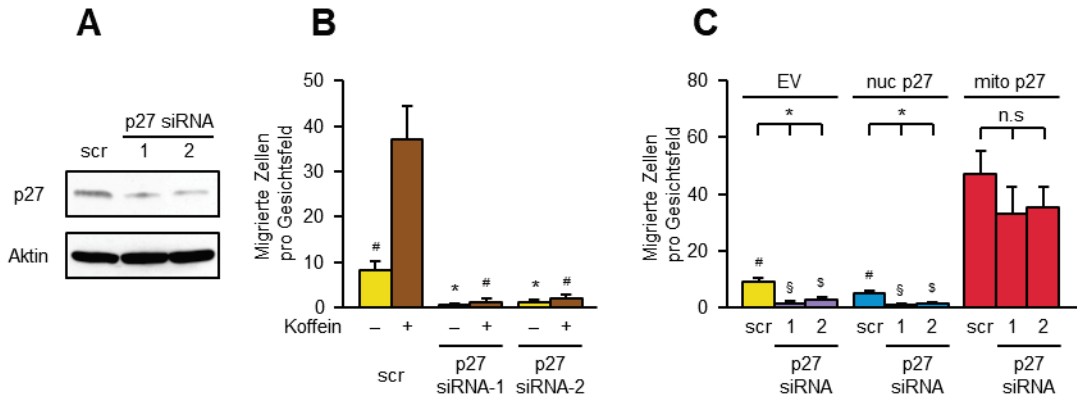

Abbildung 2: Mitochondrielles p27 ist essentiell für die Migration von Endothelzellen. Endothelzellen wurden mit zwei p27-spezifischen siRNAs (p27 siRNA-1 und -2) sowie einer „scrambled“ siRNA (scr) als Kontrolle transfiziert. (**A**) Nachweis der Herunterregulation: Repräsentativer Immunoblot von p27 und Aktin als Ladekontrolle. (**B**) Die migratorische Kapazität der transfizierten Zellen ohne und mit Koffeinbehandlung wurde in einem „scratch-wound assay“ untersucht. Die Anzahl der migrierten Zellen wurde nach deren Anfärbung mit Image J ermittelt. Gezeigt sind Mittelwerte +/- Standardfehler (n=5,*p<0,05 vs. scr –Koffein, #p<0,05 vs. scr +Koffein). (**C**) Nach der Transfektion mit den siRNAs wurden die Zellen zusätzlich mit einem Leervektor („empty vector“-EV) oder Expressionsvektoren für mitochondrielles (mito p27) oder nukleäres p27 (nuc p27) transfiziert und die Zellmigration wie in (**B**) gemessen. Gezeigt sind Mittelwerte +/- Standardfehler (n=5-6, *p<0,05 vs. zugehörigem scr, $^{\#}$<p0,05 vs. scr/mito p27, §p<0,05 vs. p27 siRNA-1/mito p27, $^{\$}$p<0,05 vs. p27 siRNA-2/mito p27) (Ale-Agha*, Goy*, **Jakobs*** et al. 2018).

Der pro-migratorische Effekt von mitochondriellem p27 konnte durch die Zugabe von Koffein allerdings nicht weiter gesteigert werden. Dies deutet darauf hin, dass Koffein und mitochondrielles p27 entweder den gleichen pro-migratorischen Signalweg regulieren oder jeder der beiden Stimuli für sich alleine die migratorische Kapazität maximal induziert, sodass kein additiver Effekt beobachtet werden kann. Da die Endothelzellmigration abhängig von funktionellen Mitochondrien ist, wurde untersucht, wie mitochondrielles p27 und nukleäres p27 mitochondrielle Parameter beeinflussen. Dazu wurde das mitochondrielle Membranpotential nach Überexpression von mitochondriellen bzw. nukleärem p27 in Endothelzellen gemessen. Im Einklang mit den Befunden zur Migration konnte nur das mitochondrielle p27 das Membranpotential verbessern (Ale-Agha*, Goy*, **Jakobs*** et al. 2018).

Im nächsten Schritt sollte aufgeklärt werden, welche Bereiche in p27 für seine Translokation in die Mitochondrien, den pro-migratorischen Effekt und die Verbesserung der mitochondriellen Funktio-

nen verantwortlich sind. Es war bereits beschrieben worden, dass die subzelluläre Verteilung von p27 über die Phosphorylierung von mindestens vier verschiedenen Aminosäureresten reguliert wird, Serin 10, Threonin 157, Threonin 187 und Threonin 198. Die Phosphorylierung dieser vier Reste ist offenbar entscheidend für die nicht-nukleäre Lokalisierung von p27, allerdings ist der Beitrag der einzelnen Aminosäuren nicht vollständig geklärt (Boehm et al. 2002; Viglietto et al. 2002).

Zunächst sollte untersucht werden, wie sich der Verlust der Bereiche, die diese Aminosäuren enthalten, auf die Endothelzellmigration auswirkt. Dazu wurden in dem p27 Expressionsvektor mit der mitochondrialen Zielsequenz Deletionen eingeführt, in denen der N-Terminus mit Serin 10 oder der C-terminale Bereich, der alle anderen Phosphorylierungsstellen beinhaltet, fehlt. Zusätzlich wurde eine Mutante kloniert, in der beide Termini deletiert sind. In allen Mutanten war die „cyclin dependent kinase inhibitor"-Domäne (CDÌ) intakt.

Alle drei Mutanten zeigten nach Überexpression einen verringerten pro-migratorischen Effekt im Vergleich zum kompletten Protein, wobei die Doppelmutante die pro-migratorische Aktivität komplett verloren hatte. Zudem erhöhte die Expression von mitochondriellem p27 den ATP Gehalt in den Mitochondrien, wozu keine der Deletionsmutanten in der Lage war. Zusammenfassend kann man feststellen, dass sowohl der C- wie auch der N- Terminus von mitochondriellem p27 für die funktionelle Kapazität von Endothelzellen benötigt wird (Ale-Agha*, Goy*, **Jakobs*** et al. 2018).

Um die Phosphorylierungsstellen, die wichtig für die Funktion von mitochondriellem p27 sind, weiter einzugrenzen, fokussierten wir uns im Folgenden auf Serin 10 und Threonin 187, da Threonin 157 und 198 wichtig für die Zellzyklusregulation sind (Larrea et al. 2008). Dieser Prozess ist an den Zellkern gebunden, was vermuten lässt, dass die Phosphorylierung dieser beiden Aminosäuren wahrscheinlich hauptsächlich an der Regulation der nukleären Lokalisierung beteiligt ist. Zudem konnten wir feststellen, dass sowohl Serin 10 als auch Threonin 187 durch die Behandlung mit 50 µM Koffein verstärkt phosphoryliert werden. Um den Einfluss dieser Phosphorylierungen auf Endothelzellmigration zu untersuchen, wurde im nächsten Schritt eine p27 Mutante kloniert, die zielgerichtet in Mitochondrien gehen kann und bei der Serin 10 und Threonin 187 durch die nicht phosphorylierbare Aminosäure Alanin ersetzt wurden.

Die Überexpression dieser Mutante konnte die Migration von Endothelzellen nicht induzieren, was eindeutig beweist, dass Serin 10 und Threonin 187, zumindest in der mitochondrialen Fraktion von p27 und höchstwahrscheinlich auch ihre Phosphorylierung in den Mitochondrien, für die pro-migratorische Aktivität erforderlich sind. Um herauszufinden, ob Serin 10 und Threonin 187 und deren Phosphorylierung auch wichtig für den Import in die Mitochondrien sind, wurde ein Expressionsvektor für eine analoge Mutante kloniert, die allerdings keine Mitochondrienimportsequenz besaß. Es stellte sich heraus, dass die Fähigkeit, in die Mitochondrien importiert zu werden, durch die Veränderung von Serin 10 und Threonin 187 in nicht phosphorylierbare Aminosäurereste stark eingeschränkt war. Dies legt nahe, dass die Phosphorylierung dieser beiden Aminosäuren nicht

nur wichtig für die pro-migratorische Aktivität von p27 ist, sondern auch in seine Translokation in die Mitochondrien involviert ist (Ale-Agha*, Goy*, **Jakobs*** et al. 2018).

Da funktionelle Mitochondrien im Herzen nicht nur Energie für die Pumpfunktion bereitstellen müssen, sondern auch mit extern oder intern induzierten Veränderungen, wie z.B. während und nach dem Myokardinfarkt, umgehen müssen, stellten wir die Hypothese auf, dass eine nicht-Zellzyklus-bezogene Funktion von p27, nach unseren Daten höchstwahrscheinlich in den Mitochondrien, auch für das Herz wichtig sein könnte (Ale-Agha*, Goy*, **Jakobs*** et al. 2018). Um eine potentielle p27-Abhängigkeit der Funktionalität von Mitochondrien zu untersuchen, wurde die Atmungskettenaktivität von isolierten Herzmitochondrien aus adulten p27-defizienten Mäusen und Wildtyp Geschwistertieren anhand des Sauerstoffverbrauchs bestimmt. Die Mitochondrien aus p27-defizienten Mäusen zeigten eine signifikant verringerte Komplex I-abhängige Atmung, was zeigt, dass diese Tiere eine beeinträchtigte mitochondriale Funktionalität aufweisen. Des Weiteren konnte eine Gabe von 0,05 % Koffein im Trinkwasser der Tiere für 10 Tage, die zu einer Serumkonzentration von ca. 30-50 µM Koffein führt, die mitochondrielle Atmung in den Herzen von p27-defizienten Mäusen im Gegensatz zu Wildtyp Tieren nicht verbessern (Ale-Agha*, Goy*, **Jakobs*** et al. 2018).

Neben den Kardiomyozyten spielen Fibroblasten eine wichtige Rolle im Herzen. Nach einer Verletzung, wie z.B. einem Herzinfarkt, müssen Fibroblasten in Myofibroblasten differenzieren, um den durch Zellverlust entstandenen Bereich mit mechanisch stabilen, kontraktilen Zellen auszufüllen. Ein Hauptstimulus für diese Differenzierung von Fibroblasten ist der „transforming growth factor β1“ (TGFβ1) (Hinz 2010). Interessanterweise ist diese Differenzierung mit einer Erhöhung des Mitochondriengehalts und der mitochondriellen Atmung assoziiert (Negmadjanov et al. 2015). Daher wollten wir als Nächstes herausfinden, welchen Einfluss Koffein und mitochondrielles p27 auf die Myofibroblasten-Differenzierung haben, da beide Mitochondrienfunktionen positiv beeinflussen. Die induzierte Myofibroblasten-Differenzierung wurde anhand der Hochregulation von „α smooth muscle actin“ (αSMA), einem Marker für diesen Prozess, gemessen. Eine Erhöhung der αSMA Menge durch TGFβ1 konnte nur in kardialen Fibroblasten aus Wildtypmäusen, nicht aber in p27-defizienten Fibroblasten nachgewiesen werden (Abbildung 3A und B). Dieser Effekt konnte, zumindest partiell und wiederum nur in den p27-profizienten Fibroblasten, auch durch Koffeinbehandlung erreicht werden (Abbildung 3A und B), was darauf hindeutet, dass die mitochondrielle Translokation von p27 daran beteiligt sein könnte. Um zu zeigen, dass mitochondrielles p27 ausreicht, um für den „Knockout“ von p27 zu kompensieren, wurden p27-defiziente Zellen mit einem lentiviralen Expressionsvektor für mitochondriell-adressiertes p27 transduziert. Die Re-Expression von mitochondriellem p27 auf dem p27-defizienten genetischen Hintergrund war ausreichend, um die TGFβ1-induzierte Myofibroblasten-Differenzierung wiederherzustellen (Abbildung 3C). Dies zeigt einen kausalen Zusammenhang zwischen mitochondriellen p27 und der Fähigkeit zur Myofibroblasten-Differenzierung (Ale-Agha*, Goy*, **Jakobs*** et al. 2018).

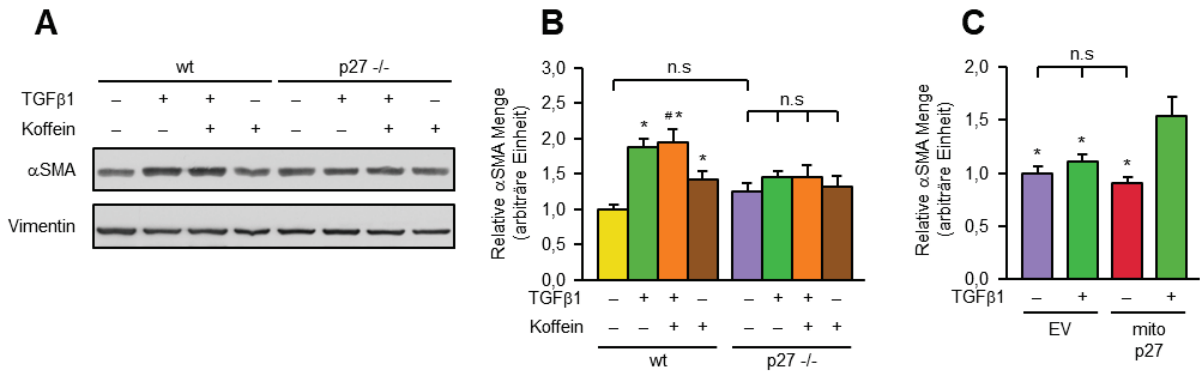

Abbildung 3: Mitochondrielles p27 wird für die Myofibroblastendifferenzierung von kardialen Fibroblasten benötigt. (**A** und **B**) Kardiale Fibroblasten wurden aus dem Herzen von Wildtypmäusen (wt) und p27-defizienten Geschwistertieren (p27 -/-) isoliert und die Myofibroblastendifferenzierung TGFβ1 induziert; zusätzlich wurden die Zellen mit 50 µM Koffein behandelt. Als Marker für die Myofibroblasten-Differenzierung wurde αSMA mittels Immunoblot detektiert: Vimentin wurde als Ladekontrolle verwendet. (**A**) Repräsentativer Immunoblot (**B**) Semiquantitative Analyse von αSMA normiert auf Vimentin. Gezeigt sind Mittelwerte +/- Standardfehler (n=5-8, *p<0,05 vs. wt unbehandelt, #p<0,05 vs. wt +Koffein, n.s. =nicht signifikant). (**C**) p27-defiziente kardiale Fibroblasten wurden lentiviral mit einem Leervektor („empty vector"-EV) oder einem Expressionsvektor für mitochondriell-adressiertes p27 (mito p27) transduziert und Myofibroblasten-Differenzierung TGFβ1 induziert. Semiquantitative Analyse von αSMA normiert auf Vimentin, gezeigt sind die Mittelwerte +/- Standardfehler (n=5, *p<0,05 vs. mito p27 +TGFβ1) (Ale-Agha*, Goy*, **Jakobs*** et al. 2018).

Abschließend wurde der Einfluss von Koffein im Zusammenhang mit mitochondriellem p27 in Assoziation mit Alterung in einem *in vivo* Modell getestet.

Altern ist mit einer verringerten mitochondriellen Atmungskapazität verbunden (Pence and Yarbro 2018). In diesem Zusammenhang wollten wir herausfinden, ob eine 10-tägige Koffeingabe in 22 Monate alten Mäusen die mitochondrielle Atmung verbessert. Wir konnten eine Verbesserung der Atmung in Herzmitochondrien nachweisen, welche nach Koffeingabe einen ähnlich hohen Komplex I-abhängigen Sauerstoffverbrauch aufwiesen wie die Mitochondrien aus adulten Mäusen (Abbildung 4) (Ale-Agha*, Goy*, **Jakobs*** et al. 2018).

Interessanterweise konnten wir zudem zeigen, dass die mitochondrielle Atmung in den Herzen adulter p27-defizienter Mäuse ähnlich war wie in den alten Wildtypmäusen, die kein Koffein erhalten hatten und sich durch Koffeingabe nicht steigern ließ (Abbildung 4) (Ale-Agha*, Goy*, **Jakobs*** et al. 2018).

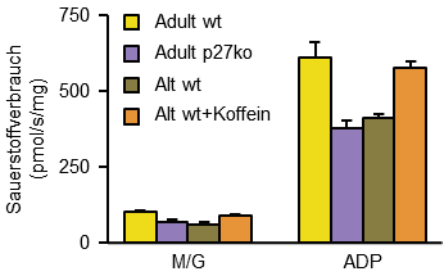

Abbildung 4: Koffein verbessert die Atmungskettenaktivität in Mausherzmitochondrien in Abhängigkeit von p27. Untersucht wurden Herzmitochondrien aus adulten Wildtyp Mäusen (Adult wt) und p27-defizienten Geschwistertieren (Adult p27ko) sowie aus alten Wildtyp Tieren, die entweder 10 Tage Trinkwasser mit 0,05 % Koffein (Alt wt+Koffein) oder nur Trinkwasser (Alt wt) erhalten hatten. Der Sauerstoffverbrauch wurde nach Zugabe von Malat/Glutamat (M/G) bzw. Adenosindiphosphat (ADP) gemessen. Gezeigt sind die Mittelwerte +/- Standardfehler (n=6 pro Gruppe) (Ale-Agha*, Goy*, **Jakobs*** et al. 2018).

Dies suggeriert, dass das Fehlen von p27 die Funktionalität des Herzens in einer ähnlichen Weise verschlechtert wie das Altern. In diesem Kontext konnten wir auch nachweisen, dass Koffein im Trinkwasser der Tiere den mitochondriellen p27 Gehalt im Herzen erhöht (Ale-Agha*, Goy*, **Jakobs*** et al. 2018). Dies zeigt, dass die Koffein-induzierte Verbesserung der mitochondriellen Atmung mit gesteigertem mitochondriellen p27 einhergeht.

Zusammenfassend konnten wir nachweisen, dass die Zunahme von mitochondriellem p27 einen neuen Wirkmechanismus von Koffein bezüglich der funktionellen Verbesserung verschiedener Zellen des kardiovaskulären Systems darstellt.

Pro- und anti-oxidative Systeme

Während des Alterungsprozesses und bei einer Vielzahl von Erkrankungen kommt es zudem zu einer Zunahme von reaktiven Sauerstoffspezies (reactive oxygen species, ROS). Zu den ROS gehören unter anderem die Sauerstoff-basierten freien Radikale, wie das Superoxid-Anion ($O_2^{-}\bullet$), sowie das nicht radikale Wasserstoffperoxid (H_2O_2) (Halliwell and Cross 1994). In physiologischen Konzentrationen sind ROS wichtig für intrazelluläre Signaltransduktionsprozesse (Finkel 2011), weswegen es ein Gleichgewicht zwischen der Bildung und dem Abbau von ROS gibt. Wenn es jedoch zu einem Anstieg an ROS oder einer Verminderung der anti-oxidativen Kapazität kommt, entsteht oxidativer Stress. Oxidativer Stress wird bei der Gefäßalterung beobachtet (Haendeler et al. 2004) und sorgt für eine ROS-vermittelte Schädigung von Nukleinsäuren, Proteinen und Lipiden. Diese Schädigungen tragen zum Alterungsprozess per se (Haigis and Yankner 2010) und dadurch zu Alters-assoziierten Erkrankungen bei (Paravicini and Touyz 2006).

In jeder Zelle gibt es ein Gleichgewicht zwischen intrazellulären pro-oxidativen und anti-oxidativen Systemen. Dies wird als sogenannte „Redox Balance“ bezeichnet. Zu den pro-oxidativen Systemen gehören unter anderem die Nicotinamid Adenin Dinukleotid Phosphat (NADPH) Oxidasen (NOXn), die Mitochondrien sowie die entkoppelte eNOS. Zu der NOX Familie gehören 7 Mitglieder, NOX1-NOX5 sowie die beiden dualen NOX Duox1 und Duox2 (Bedard and Krause 2007). Die in Endothelzellen am höchsten exprimierte NADPH Oxidase ist die konstitutiv aktive NOX4. Die Herunterregulation von NOX4 verzögert die Einleitung replikativer Seneszenz in Endothelzellen (Lener et al. 2009). Des Weiteren konnte unsere Arbeitsgruppe zeigen, dass durch oxidativen Stress induzierte, vorzeitige Seneszenz in primären humanen Endothelzellen sowohl zu einer Erhöhung der NOX4 Menge als auch einer verstärkten Bildung totaler und mitochondrieller ROS führt (Goy et al. 2014). Ein weiterer Produzent von ROS sind die Mitochondrien. Eine ihrer wesentlichen Funktionen ist die oxidative Phosphorylierung. An der oxidativen Phosphorylierung sind fünf Multienzymkomplexe beteiligt, wobei die Komplexe I-IV die mitochondriale Atmungskette darstellen und Komplex V die ATP Synthase. Es wird angenommen, dass die Atmungskette die Hauptquelle von ROS unter physiologischen Bedingungen ist (Boveris and Chance 1973; Sohal and Sohal 1991). In dieser gibt es zwei Hauptsysteme, die für die Superoxid-Anion Synthese verantwortlich sind: Die

NADH Dehydrogenase im Komplex I (Galkin and Brandt 2005) sowie Komplex III (Drose and Brandt 2008). Im Zuge der oxidativen Phosphorylierung werden zwischen 0,4 und 4 % des Sauerstoffs zu Superoxid konvertiert (Shigenaga et al. 1994; Evans et al. 2002; Carreras et al. 2004). Kommt es in den Mitochondrien nicht zum Abbau der Superoxidanionen, kann dies zu den bereits beschriebenen Schädigungen von Makromolekülen, darunter der mitochondrialen DNA führen (Shigenaga et al. 1994; Tanaka et al. 1996). Interessanterweise wurde gezeigt, dass der Alterungsprozess die Schädigungen der Mitochondrien verstärkt, da dieser mit einer Erhöhung der ROS Konzentration einhergeht (Seo et al. 2010). Ein weiterer ROS Donor ist die entkoppelte e NOS. Wie oben bereits erwähnt, ist Tetrahydrobiopterin (BH4) ein essentieller Co-Faktor für alle NOS. BH4 ist entscheidend für die Stabilisierung von NOS-Dimeren, welche die funktionelle Einheit bei der Produktion von NO darstellen (Moens and Kass 2006; Ketonen and Mervaala 2008; Moens et al. 2008). Wird die Menge an BH4 reduziert, verändert sich die Dimerstruktur und es kommt zur Entkopplung des Enzyms. Dabei ist die enzymatische Reduktion von molekularem Sauerstoff nicht länger an die Umsetzung von L-Arginin gekoppelt, sodass kein NO mehr gebildet wird, sondern an seiner Stelle das Superoxid-Anion. Die Entkopplung der eNOS führt somit zu einer erhöhten ROS Produktion und verringerten NO Bildung und führt langfristig zur endothelialen Dysfunktion (Moens and Kass 2006).

Um den vielen ROS Quellen entgegenzuwirken besitzt das kardiovaskuläre System eine Vielzahl von anti-oxidativen Systemen. Dazu gehören die Superoxid Dismutasen (SODn), die Katalase, das Glutathion (GSH) System, Glutathion Peroxidasen (GPxn), Peroxiredoxine und die Thioredoxin Systeme.

Superoxidanionen werden von SODn zu molekularem Sauerstoff und H_2O_2 umgewandelt. Es gibt drei verschiedene Isoformen der SOD in Eukaryoten, die Mangan SOD (MnSOD), die Kupfer/Zink SOD (Cu/Zn SOD) und die extrazelluläre SOD (ecSOD). Die SOD mit Mangan im aktiven Zentrum ist ausschließlich in den Mitochondrien lokalisiert (Wallace 2005), die Kupfer/Zink SOD hingegen befindet sich im Zytoplasma (Fridovich 1983). Die ecSOD, die auch Kupfer/Zink im aktiven Zentrum hat, liegt hauptsächlich in der extrazellulären Matrix vor (Marklund 1984).

Das aus der Dismutation entstandene Wasserstoffperoxid kann durch verschiedene Enzyme zu Wasser reduziert werden. Die Katalase ist ein intrazelluläres Enzym, das hauptsächlich in den Peroxisomen (Masters et al. 1986), aber auch zu einem gewissen Teil im Zytosol vorkommt. Sie wandelt Wasserstoffperoxid in einer zweistufigen Reaktion zu Wasser und molekularem Sauerstoff um (Chance et al. 1979). Die Proteine der GPx Familie können ebenfalls Wasserstoffperoxid, aber auch Lipidperoxide reduzieren. Dabei wird GSH zum Glutathiondisulfid (GSSG) oxidiert. Das entstandene GSSG wird mit Hilfe der GSH Reduktase mit NADPH als Kosubstrat wieder zu GSH reduziert, wodurch ein Kreislauf entsteht und GSH für die Glutathion Peroxidasen im Zytosol wieder zur Verfügung steht (Lu 2009). Zudem gibt es auch eine GPx in den Mitochondrien, die dort anfallendes Wasserstoffperoxid abbaut. Neben den GPx können auch Peroxiredoxine H_2O_2 sowohl im

Zytosol als auch in den Mitochondrien abbauen. Die Peroxiredoxine benötigen dafür entweder das mitochondrielle oder das zytosolische Thioredoxin-System, da bei der Umwandlung von Wasserstoffperoxid in Wasser Peroxiredoxine oxidiert werden und dann durch die Thioredoxin Systeme regeneriert werden müssen, um weitere H_2O_2 Moleküle abbauen zu können (Rhee et al. 2001). Die Thioredoxin Systeme bestehen aus den Proteinen Thioredoxin-2 (Trx-2) und Thiroedoxin-2 Reduktase (TrxR2) bzw. Thioredoxin-1 (Trx-1) und Thioredoxin-1 Reduktase (TrxR1). Trx-2 und die zugehörige Reduktase sind in den Mitochondrien lokalisiert. Trx-2 reduziert oxidiertes Peroxiredoxin 3 und wird selber wiederum durch TrxR2 in Abhängigkeit von NADPH reduziert. Durch die Detoxifizierung der Mitochondrien schützt Trx-2 vor dem durch oxidative Stimuli induzierten Zelltod (Chen et al. 2002). Trx-2 bindet außerdem an ASK1 (apoptosis signal-regulating kinase 1) (Zhang et al. 2004; Huang et al. 2015) und inhibiert so deren Aktivität und die damit verbundene Caspase-abhängige Apoptose (Saxena et al. 2010). Da der Fokus meiner Arbeit auf Thioredoxin-1 liegt, werde ich im folgenden Kapitel gesondert auf das Thioredoxin-1 System eingehen.

Das Thioredoxin-1 System

Trx-1 ist eine 12 kDa große Oxidoreduktase, die erstmal 1964 in *Escherichia coli* beschrieben wurde (Laurent et al. 1964). Im Bereich der Aminosäuren 32-35 besitzt Trx-1 in Säugern eine konservierte Sequenz aus Cystein-Glycin-Prolin-Cystein, die den Redox Gleichgewichtszustand reguliert. Durch die Nähe der beiden Cysteine ist die Oxidation durch die Bildung einer internen Disulfidbrückenbindung möglich. Das reversibel oxidierte Trx-1 wird unter NADPH Verbrauch durch die Trx-1 Reduktase wieder zur aktiven Form reduziert (Schallreuter and Wood 1986) (Abbildung 5).

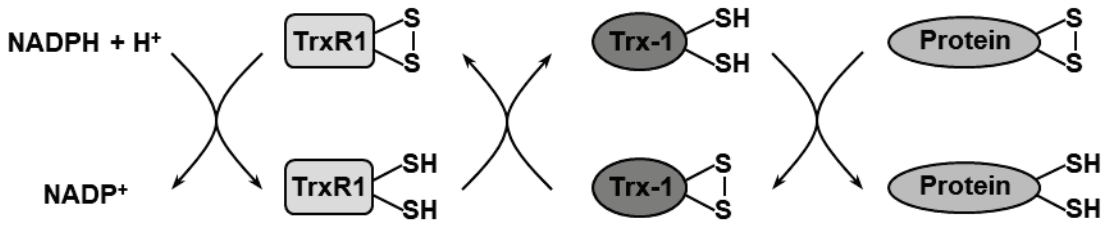

Abbildung 5: Das Thioredoxin-1 System. Thioredoxin-1 (Trx-1) reduziert oxidierte Proteine und wird dadurch oxidiert. Regeneriert wird Trx-1 durch Thioredoxin-1 Reduktase (TrxR1) in Abhängigkeit von NADPH. Adaptiert aus (Zschauer et al. 2013).

Neben den beiden Cysteinen an den Positionen 32 und 35 besitzt Trx-1 drei weitere Cysteine an den Positionen 62, 69 und 73. Es konnte gezeigt werden, dass neben der Disulfidbrückenbindung an den Cysteinen C32 und C35 unter oxidativen Bedingungen eine zweite Disulfidbindung zwischen C62 und C69 entstehen kann, die einen Einfluss auf die dreidimensionale Struktur des Proteins hat (Watson et al. 2003; Hashemy and Holmgren 2008). Die Sensitivität des Trx-1 Systems wurde in einem kinetischen Model demonstriert in dem gezeigt wurde, dass Veränderungen in der Konzentration oder Aktivität einzelner Mitglieder die Kinetik anderer Mitglieder beeinflussen (Pillay et al. 2011). Neben der Oxidation der Cysteine von Trx-1 gibt es weitere post-translationale Modifikationen (PTM). Eine dieser PTMs im Endothel ist die S-Nitrosierung. Dabei bindet NO an das

Cystein an Position 69, was zu einer Steigerung der Redoxaktivität von Trx-1 führt (Haendeler et al. 2004) (Abbildung 6). Unter stark oxidativen Bedingungen bilden sich zwei Disulfidbrücken in dem Enzym aus, sodass dann Trx-1 an Cystein 73 S-nitrosiert werden kann (Barglow et al. 2011). Dies verringert dann die enzymatische Aktivität von Trx-1 (Hashemy and Holmgren 2008).

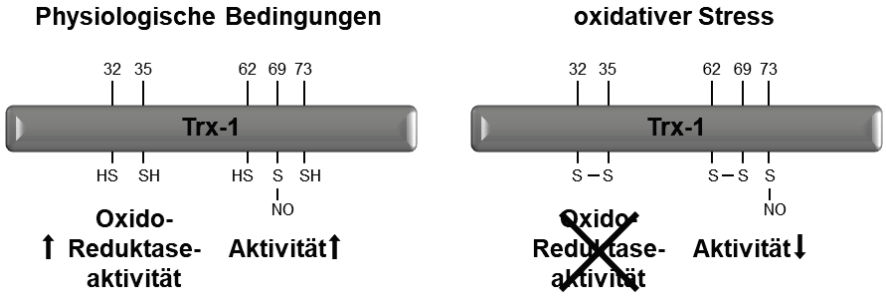

Abbildung 6: Regulation der Thioredoxin-1 Aktivität. Thioredoxin-1 (Trx-1) besitzt 5 essentielle Cysteine, die wichtig für seine Aktivität sind. Unter physiologischen Bedingungen reduziert Trx-1 oxidierte Proteine über die Cysteine 32 und 35. Ist C69 S-nitrosiert, ist die Oxidoreduktase Aktivität von Trx-1 gesteigert. Unter oxidativem Stress kann es zur Ausbildung von zwei intramolekularen Disulfidbrücken kommen. Die Disulfidbrücke zwischen C32 und C35 verhindert die Reduktion oxidierter Proteine durch Trx-1. Bildet sich zusätzlich eine Disulfidbrücke zwischen C62 und C69 kann Cystein 73 S-nitrosiert werden (**Jakobs** et al. 2017).

Neben diesen Modifikationen an Cysteinresten kann Trx-1 außerdem an Tyrosin 49 durch Peroxynitrit nitriert werden. Es konnte gezeigt werden, dass es nach Ischämie/Reperfusion (I/R) zu einer verstärkten Nitrierung kommt und die Trx-1 Aktivität reduziert ist. Dies ging einher mit einer reduzierten Interaktion mit ASK1 (Tao et al. 2006). Ähnliches konnte in Bezug auf das Altern festgestellt werden. In älteren Mäusen trat im Vergleich mit jungen Tieren eine verstärkte Trx-1 Nitrierung im Herzen auf. Das legt den Schluss nahe, dass die älteren Herzen wegen der verringerten Trx-1 Aktivität nicht mehr in der Lage sind, Verletzungen des Herzens zu kompensieren (Zhang et al. 2007).

Trx-1 reguliert die Funktion vieler Proteine durch Interaktion, wobei diese Interaktionen teilweise abhängig vom Redoxstatus von Trx-1 sind. So ist die Interaktion mit der Adenosinmonophosphat-aktivierten Proteinkinase (AMPK), die essentiell für die zelluläre Energiehomöostase ist, notwendig, um die Cysteine in der AMPK in reduzierter Form zu erhalten, damit AMPK aktiviert werden kann (Shao et al. 2014). Durch die Interaktion mit Aktin und ASK1 wirkt Trx-1 anti-apoptotisch. In unserer Arbeitsgruppe konnte gezeigt werden, dass die Interaktion von Aktin mit Trx-1 in Endothelzellen letzteres vor Degradation schützt. Zudem wird durch diese Interaktion eine durch oxidativen Stress induzierte Stressfaserbildung inhibiert (Zschauer et al. 2011). Neben Aktin kann Trx-1 an den N-Terminus von ASK1 binden. Die Interaktion verringert die Aktivität von ASK1, wird aber durch oxidativen Stress oder eine Mutation der Cysteine 32 und 35 aufgehoben (Saitoh et al. 1998). Die Interaktion zwischen ASK1 und Trx-1 kann durch den negativen Regulator von Trx-1, das „Trx binding protein-2“ (TBP-2), auch bekannt als „vitamin D3 upregulated protein 1“ (VDUP1) oder „thioredoxin interacting protein“ (TXNIP), verhindert werden (Junn et al. 2000). Dadurch kommt es zur Aktivierung der ASK1, da TXNIP – und nicht mehr ASK1 – an Trx-1 bindet.

Die Interaktion von Trx-1 mit anderen Proteinen ist nicht auf das Zytoplasma begrenzt. Trx-1 wird durch Bindung an α-Karyopherin in den Kern importiert (Schroeder et al. 2007). Nukleäre Interaktionspartner von Trx-1 sind unter anderem „hypoxia-inducible factor-1α" (HIF-1α) (Ema et al. 1999), Glukokortikoid Rezeptor (Makino et al. 1999), „nuclear factor kappa-light-chain-enhancer of activated B cells" (NF-κB) (Lillig and Holmgren 2007) und „nuclear factor (erythroid-derived 2)-like 2" (Nrf2). Nrf2 wird im folgenden Kapitel im Zusammenhang mit Atherosklerose und Ischämie/Reperfusions-Schäden im Herzen genauer erläutert.

Einfluss von Nrf2 und Trx-1 alleine sowie im Zusammenspiel auf Atherosklerose und nach Ischämie/Reperfusions-Schäden im Herzen

Die Entstehung von Atherosklerose wird mit schlechter Ernährung oder fehlender physischer Bewegung assoziiert. Diese Risikofaktoren können zu einer Schädigung der Endothelzellschicht (Danaei et al. 2009; Folsom et al. 2011) und damit verbunden zur Einwanderung von pro-inflammatorischen Zellen, Proliferation von glatten Muskelzellen und einer Intergrin-abhängigen Rekrutierung von Thrombozyten führen. Die Gesamtheit dieser Prozesse geht mit der Entstehung von atherosklerotischen Plaque einher. Dadurch wird das Gefäßlumen verengt, bis es letztendlich zum Verschluss kommt. Trx-1 und Nrf2 alleine sowie im Zusammenspiel wirken der Entstehung und Progression von Atherosklerose und Ischämie/Reperfusions (I/R)-Schäden im Herzen entgegen (Abbildung 7). Nrf2 aktiviert Promotoren durch Bindung an sogenannte „antioxidant response elements" (AREs). Es reguliert das Trx-1 System, da Trx-1 und TrxR1 AREs in ihren Promoterregionen besitzen. Dies führt zur Expressionserhöhung von Trx-1 und TrxR1, wenn Nrf2 aktiviert wird (Sakurai et al. 2005; Im et al. 2012; Kim et al. 2012). Im Gegenzug konnte gezeigt werden, dass Überexpression von Trx-1 die Nrf2 Aktivität und die Bindung an AREs steigert (Hansen et al. 2004; Schroeder et al. 2007). Dies zeigt einen positiven Feedback Loop von Trx-1 und Nrf2 (Abbildung 7) (**Jakobs** et al. 2017).

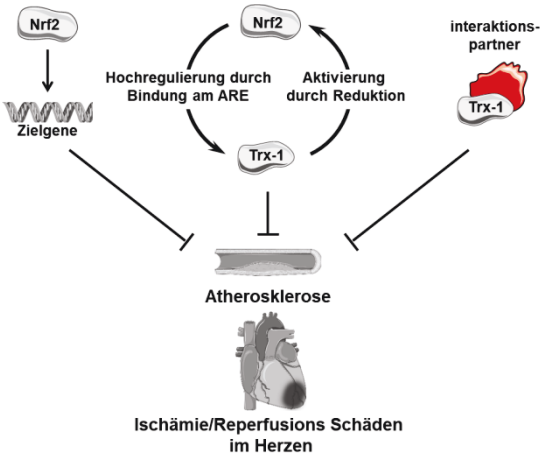

Abbildung 7: Einfluss von Nrf2 und Trx-1 alleine und im Zusammenspiel in Atherosklerose und nach Ischämie/Reperfusions Schäden im Herzen (**Jakobs** et al. 2017)**.**

Nrf2 ist entscheidend für die Funktionalität von Endothelzellen, was sich daran zeigt, dass der „Knockdown" von Nrf2 zu einer reduzierten Endothelzellmigration führt, welche wesentlich für die

Integrität des Endothels ist. (Valcarcel-Ares et al. 2012). Bei Behandlung von Endothelzellen mit starken Oxidantien, wie z.B. mit hypochloriger Säure (HOCl), wird Nrf2 aktiviert und dadurch die Hämoxygenase-1 (HO-1) verstärkt exprimiert. HO-1 katalysiert die Degradation von Häm zu Biliverdin, welches als Antioxidant wirkt (Stocker et al. 1987; Stocker et al. 1987; Baranano et al. 2002). Im Gegensatz dazu erlaubt Inhibition der HO-1 eine HOCl-induzierte Apoptose in Endothelzellen (Wei et al. 2009). Nrf2 kann außerdem durch Sulforaphan aktiviert werden. Sulforaphan ist ein Isothiocyanat, das in Kohl und Brokkoli vorkommt. Es reduziert die Expression von VCAM-1 (vascular cell adhesion molecule-1) im Endothel von Wildtyp Mäusen, nicht aber in Nrf2 defizienten Tieren (Zakkar et al. 2009). VCAM-1 bewirkt die Adhäsion verschiedener pro-atherogener Zellen an das Endothel. Zusammenfassend zeigen diese Studien daher, dass Nrf2 im Endothel anti-inflammatorisch und damit atheroprotektiv wirkt. Neben der schützenden Funktion von Nrf2 bei der Entstehung und/oder Progression von Atherosklerose, konnte auch eine protektive Wirkung von Nrf2 bei I/R-Schäden nachgewiesen werden. So führt der Verschluss der linken Koronararterie zu einer Verdopplung der Infarktgröße in Nrf2 defizienten Mäusen. Präkonditionierung durch 2-4 Episoden von 5-minütiger Ischämie und Reperfusion erhöht die Nrf2 Proteinmenge und reduziert signifikant die Infarktgröße in Wildtyp Tieren. Hingegen hat eine Präkonditionierung in Nrf2 knockout Mäusen keinen protektiven Effekt (Xu et al. 2014). Interessanterweise induzieren Glukokortikoide Zielgene von Nrf2, wie z.B. HO-1, in einer Prostaglandin D Synthase abhängigen Weise. Katusamata et al. konnten zeigen, dass Glukokortikoide keinen protektiven Effekt mehr nach I/R-Schaden in Nrf2 defizienten Tieren haben, da eine nukleäre Translokation von Nrf2 zum Schutz beim I/R-Schaden notwendig und Glukokortikoid abhängig ist (Katsumata et al. 2014). Auch Behandlung mit Nahrungsmittelinhaltsstoffen, wie z.B. Resveratrol oder α-Liponsäure, bewirkt eine Nrf2 abhängige Verbesserung der Herzfunktion nach Ischämie und Reperfusion. Dabei wird eine verstärkte Translokation von Nrf2 in den Nukleus beobachtet, was dann ebenfalls eine Expressionssteigerung der HO-1 bedingt (Deng et al. 2013).

Auch für Trx-1 wurde eine protektive Rolle sowohl bei I/R-Schäden als auch bei Entstehung und Progression der Atherosklerose beschrieben. Eine herzspezifische Überexpression von Trx-1 verbessert die systolische und diastolische ventrikuläre Funktion nach Ischämie und Reperfusion (Turoczi et al. 2003). Zudem zeigte sich eine gesteigerte Komplex I Aktivität in den Herzmitochondrien dieser Mäuse (Ago et al. 2006). Die verbesserten kardialen und mitochondrialen Funktionen lassen darauf schließen, dass eine zusätzliche Erhöhung der Trx-1 Proteinmenge die oxidativen Schäden nach Ischämie und Reperfusion reduzieren kann. Dies zeigte sich auch darin, dass die Trx-1 Proteinmenge nach Myokardinfarkt verringert ist. Postkonditionierung kann den Trx-1 Spiegel in sechs Monate alten Tieren wiederherstellen und hat daher eine protektive Wirkung. In 12 Monate und 20 Monate alten Mäusen dagegen ist der protektive Effekt der Postkonditionierung nicht vorhanden und zudem wird auch kein kompensatorischer Effekt bezüglich der Trx-1 Menge beobachtet (Perez et al. 2016). Diese Daten deuten daraufhin, dass der positive Effekt der Postkonditionierung sowohl vom Trx-1 Spiegel, aber auch vom Alter abhängig ist.

Im Zusammenhang mit der Entstehung und Progression der Atherosklerose konnte gezeigt werden, dass es nach Überexpression von Trx-1 zu einer erhöhten Smad3 Phosphorylierung und einer Inhibition der durch oxidiertes „low density lipoprotein“ (oxLDL) induzierten Expression der Adhäsionsmoleküle VCAM-1 und ICAM-1 (intercellular adhesion molecule-1) kommt (Chen et al. 2010). Ein wichtiger negativer Regulator von Trx-1 ist, wie zuvor beschrieben, TXNIP. In einem etablierten Tiermodell der Atherosklerose entstehung führte TXNIP Defizienz zu einer Verringerung der Anzahl atherosklerotischer Plaques (Byon et al. 2015). Zudem weisen diese Tiere eine erhöhte Trx-1 Aktivität, geringere ROS Mengen und reduzierte Expression von VCAM-1, ICAM-1 und MCP-1 (monocyte chemoattractant protein 1) im Gefäß auf. Eine mechanistische Erklärung für die verringerte Expression von MCP-1 liegt in der Abhängigkeit seiner Transkription von dem Transkriptionsfaktor c-Jun. Eine Überexpression von Trx-1 in Endothelzellen unterdrückt dessen nukleäre Translokation, wodurch es zur verringerten Expression von MCP-1 kommt. Dadurch wird weniger MCP-1, das für die Rekrutierung von Monozyten und Makrophagen verantwortlich ist, aus dem Endothel freigesetzt. Zudem hält Trx-1 „apurinic/apyrimidinic endodeoxyribonuklease 1“ (APEX1) vermehrt im Zytosol, sodass das für die erhöhte DNA-Bindungsaktivität von c-Jun benötigte APEX1 nicht in den Kern transportiert werden kann (Chen et al. 2010). In meiner Arbeit konnte ich zeigen, dass Trx-1 durch APEX1 in Endothelzellen reguliert wird. Dies wird im folgenden Kapitel beschrieben.

Regulation von Trx-1 durch APEX1

APEX1 ist ein 37 kDa großes Protein, das zwei funktionelle Domänen, eine Redox-Domäne und eine DNA Reparatur-Domäne, enthält (Abbildung 8). Der C-Terminus enthält die DNA Reparatur-Domäne mit der Endonuklease Aktivität des Proteins, die wichtig für seine Funktion im sogenannten „base excision repair“ ist (Xanthoudakis et al. 1994). Im N-terminalen Teil von APEX1 ist die Redox-Domäne lokalisiert (Abbildung 8). Dadurch hat APEX1 eine Redoxaktivität, weshalb das Protein oftmals auch „redox factor-1“ (Ref-1) genannt wird. Die Redox aktiven Cysteine in der Redox-Domäne sind die Cysteine 65 und 93 (Walker et al. 1993). Durch diese Cysteine kann APEX1 eine Reihe von oxidierten Transkriptionsfaktoren reduzieren und so deren DNA Bindung verstärken.

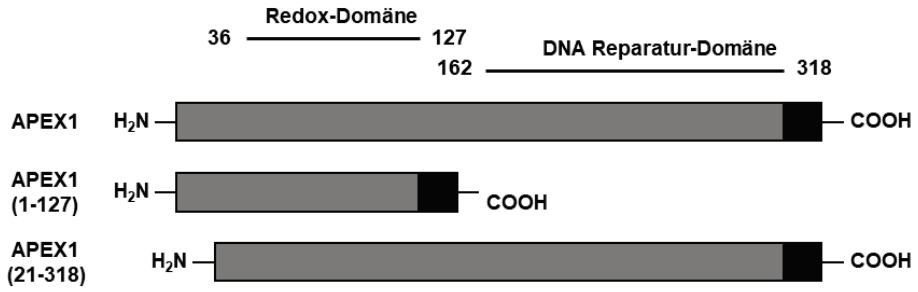

Abbildung 8: Funktionelle Domänen und Deletionsmutanten von APEX1.

Dazu zählen beispielsweise „activator protein-1“ (AP-1) (Xanthoudakis and Curran 1992), NF-κB (Nishi et al. 2002) und HIF-1α (Huang et al. 1996). Es konnte gezeigt werden, dass APEX1 neben der Schutzfunktion bei DNA Schädigungen und der Redoxaktivität anti-apoptotische Eigenschaften in verschiedenen Tumorzelllinien aufweist (Kelley and Fishel 2008). Diese wurden anfangs mit der DNA Reparaturdomäne assoziiert (Fung and Demple 2005). Es konnte aber nachgewiesen werden, dass die Redox-Domäne eine wichtige Rolle für die anti-apoptotische Funktion von APEX1 einnimmt (Zou et al. 2007). Ob APEX1 auch in humanen Endothelzellen anti-apoptotisch wirkt, ist bisher nicht bekannt. Ein Ziel dieser Doktorarbeit war es, eine potentielle anti-apoptotische Funktion von APEX1 in diesem Zelltyp zu untersuchen und, falls APEX1 eine derartige Funktion haben sollte, die zugrunde liegenden Mechanismen aufzuklären.

Zunächst wurde dafür ein Expressionsvektor für APEX1 kloniert und dieser in humane Endothelzellen transfiziert. Die Überexpression von APEX1 in Endothelzellen inhibiert sowohl die Caspase 3 Aktivität, welche als Apoptoseindikator angesehen werden kann, wie auch die mit Hilfe einer Annexin V Färbung gemessene Apoptose (Abbildung 9A) (Dyballa-Rukes*, **Jakobs*** et al. 2017). Induktion von Apoptose führt dazu, dass Annexin V von der inneren Plasmamembran nach außen gestülpt wird. Da bei der Anfärbung nur Annexin V auf der Zelloberfläche detektiert wird, stellen Annexin V-positive Zellen apoptotische Zellen dar.

Die anti-apoptotische Wirkung von APEX1 konnte sowohl unter basalen Bedingungen als auch unter oxidativem Stress nachgewiesen werden (Abbildung 9A) (Dyballa-Rukes*, **Jakobs*** et al. 2017). Um die anti-apoptotische Wirkung von APEX1 kausal nachzuweisen, wurde dann die Menge an APEX1 durch verschiedene siRNAs herunterreguliert und die Apoptoserate gemessen. Es zeigte sich eine gesteigerte Apoptose in Endothelzellen (Abbildung 9B) (Dyballa-Rukes*, **Jakobs*** et al. 2017).

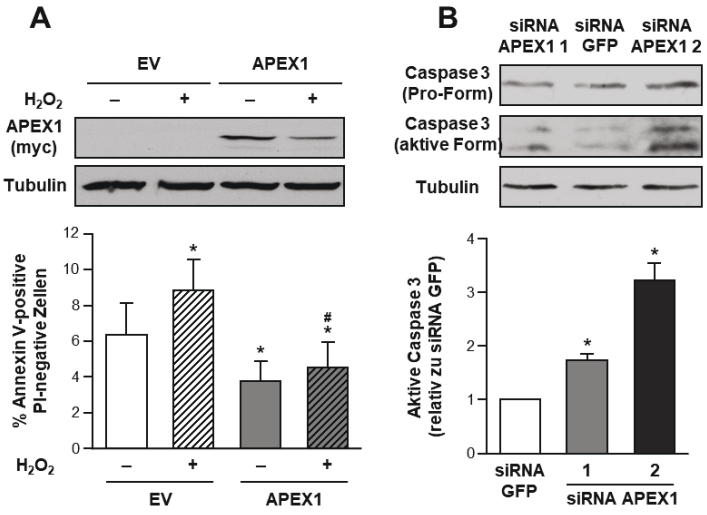

Abbildung 9: APEX1 schützt primäre humane Endothelzellen vor Apoptose. (**A**) Endothelzellen wurden mit einem Leervektor („empty vector“–EV) oder einem Expressionsvektor für APEX1 transfiziert und mit H_2O_2 behandelt. Oben: Nachweis der Expression von APEX1 mittels Immunoblot, das überexprimierte Protein wurde anhand des C-terminalen myc Epitop-tags detektiert, Tubulin diente als Ladekontrolle. Unten: Der Anteil apoptotischer Zellen wurde nach Annexin V/Propidium-Iodid Färbung durchflusszytometrisch bestimmt. Gezeigt sind Mittelwerte +/- Standardfehler (n=6,*p<0,05 vs. EV -H_2O_2,#p<0,05 vs. EV +H_2O_2). (**B**) Endothelzellen wurden mit zwei APEX1-spezifischen siRNAs (siRNA APEX1-1

und -2) sowie einer gegen grün fluoreszierendes Protein gerichteten siRNA (siRNA GFP) als Kontrolle transfiziert. Als Surrogatmarker für Apoptoseinduktion wurde die Spaltung der Pro-Form von Caspase 3 in die aktive Form mittels Immunoblot ermittelt, Tubulin diente als Ladekontrolle. Oben: Repräsentativer Immunoblot. Unten: Semiquantitative Analyse der Caspase 3 Spaltung normiert auf Tubulin. Gezeigt sind Mittelwerte +/- Standardfehler relativ zu den mit der siRNA GFP transfizierten Zellen (n=3,*p<0,05 vs. siRNA GFP) (Dyballa-Rukes*, **Jakobs*** et al. 2017).

Diese Daten zeigen erstmalig, dass APEX1 in humanen Endothelzellen anti-apoptotisch wirkt.

Im nächsten Schritt sollte aufgeklärt werden, welche Rolle die beiden unterschiedlichen funktionellen Domänen von APEX1 (Abbildung 8) bei der Apoptose-Inhibition spielen. Daher wurden zunächst Expressionsvektoren für APEX1 Deletionsmutanten kloniert. Der einen Mutante fehlen die Aminosäuren 128-318 (APEX1 (1-127)) und damit die DNA Reparatur-Domäne (Abbildung 8). Der zweiten Mutante fehlen lediglich die ersten 20 Aminosäuren am N-Terminus (APEX1 (21-318)). Eine Überexpression von APEX1 (1-127) hatte einen ähnlich protektiven Effekt auf Endothelzellen wie APEX1. Dies führt zu dem Schluss, dass die anti-apoptotische Wirkung von APEX1 unabhängig von der DNA Reparatur-Domäne ist. Interessanterweise zeigte sich, dass bei Expression der Mutante APEX1 (21-318) nicht nur der protektive Effekt von APEX1 aufgehoben wird, sondern dass das Fehlen der ersten 20 Aminosäuren zu einer signifikanten Erhöhung der Apoptose führt. Aufgrund dieser Ergebnisse sollte der Mechanismus, wie APEX1 anti-apoptotisch wirkt und warum APEX1 (21-318) Apoptose induziert, aufgeklärt werden. Unsere Arbeitsgruppe konnte in mehreren Arbeiten die essentielle Funktion von Trx-1 beim Schutz von Endothelzellen vor Apoptose nachweisen (Haendeler et al. 2002; Haendeler et al. 2004; Schroeder et al. 2007; Zschauer et al. 2011). Daher wurde als Nächstes der Einfluss einer Überexpression von APEX1 und APEX1 (21-318) auf die Trx-1 Proteinmenge untersucht (Abbildung 10A).

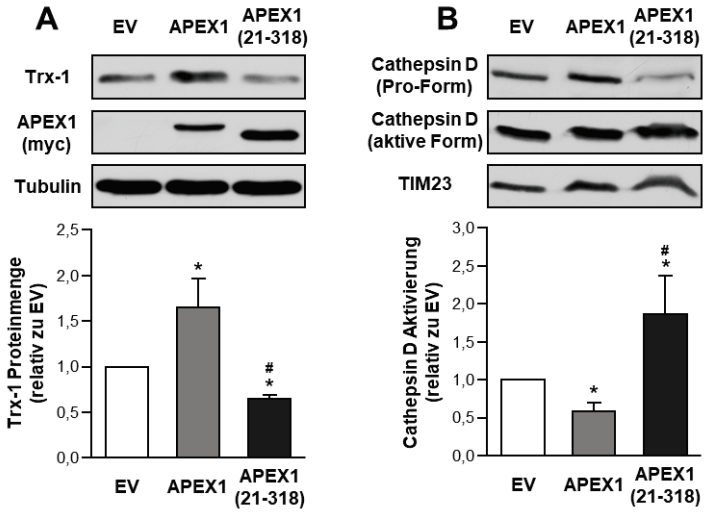

Abbildung 10: APEX1 im Gegensatz zum N-terminal verkürzten APEX1 steigert die Thioredoxin-1 Proteinmenge und inhibiert die Cathepsin D Aktivierung. (**A** und **B**) Endothelzellen wurden mit einem Leervektor („empty vector"– EV) oder Expressionsvektoren für APEX1 bzw. die N-terminal verkürzte Variante APEX1 (21-318) transfiziert. (**A**) Thioredoxin-1 (Trx-1) und die überexprimierten APEX1 Varianten wurden mittels Immunoblot nachgewiesen, letztere anhand des C-terminalen myc Epitop-tags (APEX1(myc)); Tubulin diente als Ladekontrolle. Oben: Repräsentative Immunoblots. Unten: Semiquantitative Analyse der Trx-1 Menge normiert auf Tubulin. Gezeigt sind Mittelwerte +/- Standardfehler relativ zu den mit dem Leervektor transfizierten Zellen (n=4,*p<0,05 vs. EV, #p<0,05 vs. APEX1). (**B**) Die Aktivierung von Cathepsin D wurde anhand der proteolytischen Spaltung der Pro-Form in die aktive Form mittels Immunoblot bestimmt, TIM23 diente als Ladekontrolle. Oben: Repräsentative Immunoblots. Unten: Semiquantitative Analyse der Cathepsin D Aktivierung. Gezeigt sind Mittelwerte +/- Standardfehler relativ zu den mit dem Leervektor transfizierten Zellen (n=5,*p<0,05 vs. EV, #p<0,05 vs.APEX1) (Dyballa-Rukes*, **Jakobs*** et al. 2017).

Es stellte sich heraus, dass die Überexpression von APEX1 die Trx-1 Proteinmenge signifikant gegenüber dem Leervektor steigern konnte (Abbildung 10A). Dagegen wurde durch die Transfektion mit dem APEX1 (21-318) Expressionsvektor die Trx-1 Proteinmenge signifikant reduziert. Da Trx-1 durch die lysosomale Protease Cathepsin D (Cat D) degradiert werden kann und dies zur Apoptose von Endothelzellen führt (Haendeler et al. 2005; Goy et al. 2014), wurde untersucht, ob die Cat D Aktivität von APEX1 reguliert werden kann. Die Überexpression von APEX1 reduziert die Aktivität von Cat D, wohingegen APEX1 (21-318) die Aktivität in Endothelzellen steigert (Abbildung 10B) (Dyballa-Rukes*, **Jakobs*** et al. 2017). Da Trx-1 und APEX1 die Aktivität von verschiedenen Transkriptionsfaktoren (TF) regulieren (Hirota et al. 1997; Wei et al. 2000), ist es vorstellbar, dass nicht nur die Cat D Aktivität erhöht ist, sondern bereits die RNA Menge. Daher wurde die Cat D RNA Menge nach Transfektion mit den APEX1 Expressionsvektoren bestimmt. Weder die Überexpression von APEX1, noch die von APEX1 (21-318) führten zu quantitativen Veränderungen in Cat D RNA, sodass der Cat D Aktivitätszunahme ein anderer Mechanismus zugrunde zu liegen scheint. Aktives Cat D entsteht in einer mehrstufigen, bis heute nicht bis ins letzte Detail verstandenen proteolytischen Prozessierung aus dem inaktiven Pro-Enzym (Minarowska et al. 2008). Da die Überexpression von APEX1 die Spaltung der Pro-Form von Cat D in die aktive Form hemmt, lag die Vermutung nahe, dass APEX1 möglicherweise mit diesem Pro-Enzym einen Komplex bildet. Mittels Immunpräzipitation wurde gezeigt, dass APEX1 mit der Pro-Form von Cat D assoziiert ist, wohingegen APEX1 (21-318) keinen Komplex damit bildet. Das führt zu dem Schluss, dass APEX1 die Prozessierung von Cat D in die aktive Form aufgrund der Bindung inhibieren kann. Um herauszufinden, ob APEX1 den pro-apoptotischen Effekt der Mutante APEX1 (21-318) kompensieren kann, wurden beide koexprimiert. Erstaunlicherweise konnte APEX1 in den Kotransfektionen den pro-apoptotischen Effekt der Mutante nicht kompensieren (Abbildung 11A-C) (Dyballa-Rukes*, **Jakobs*** et al. 2017).

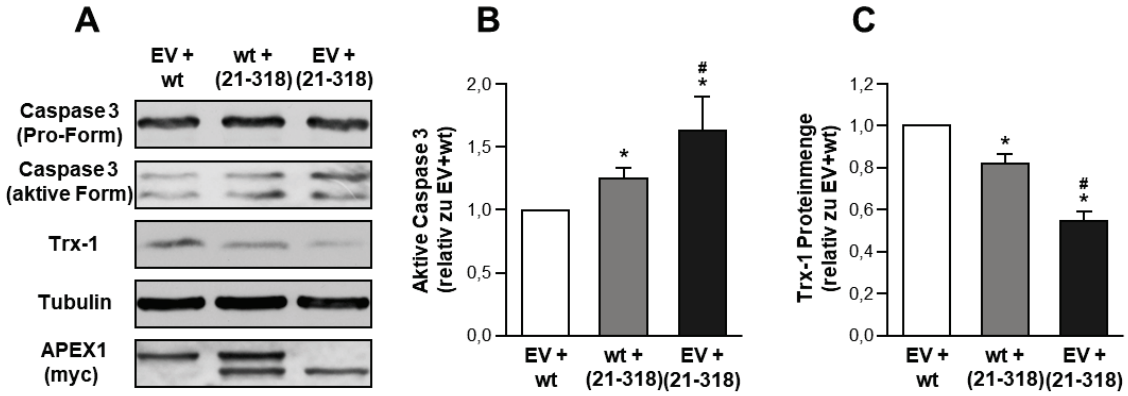

Abbildung 11: APEX1 kann den pro-apoptotischen Effekt von APEX1 (21-318) nicht kompensieren. (**A**-**C**) Endothelzellen wurden mit 1:1 Gemischen eines Leervektor („empty vector"–EV) und Expressionsvektoren für APEX1 (EV+wt) bzw. die N-terminal verkürzte Variante APEX1 (21-318) (EV+(21-318)) bzw. einem Gemisch der beiden Expressionsvektoren (wt+(21-318)) transfiziert. Als Surrogatmarker für Apoptoseinduktion wurde die Spaltung der Pro-Form von Caspase 3 in die aktive Form mittels Immunoblot ermittelt. Thioredoxin-1 (Trx-1) und die Expression der beiden überexprimierten APEX1 Varianten wurden mit der gleichen Technik nachgewiesen, letztere anhand des C-terminalen myc Epitop-tags (APEX1(myc)); Tubulin diente als Ladekontrolle. (**A**) Repräsentative Immunoblots. (**B**) Semiquantitative Analyse der Caspase 3 Spaltung normiert auf Tubulin. Gezeigt sind Mittelwerte +/- Standardfehler relativ zu den mit EV+wt transfizierten Zellen (n=5, *p<0,05 vs. EV +wt, #p<0,05 vs. wt +(21-318)). (**C**) Semiquantitative Analyse der Trx-1

Menge normiert auf Tubulin. Gezeigt sind Mittelwerte +/- Standardfehler relativ zu den mit EV+wt transfizierten Zellen (n=4, *p<0,05 vs. EV +wt, #p<0,05 vs. wt +(21-318)) (Dyballa-Rukes*, **Jakobs*** et al. 2017).

Außerdem war in diesen Experimenten weiterhin wie bei alleiniger Überexpression von APEX1 (21-318) die Spaltung von Caspase 3 in die aktive Form verstärkt und die Trx-1 Proteinmenge reduziert (Abbildung 11A-C) (Dyballa-Rukes*, **Jakobs*** et al. 2017). Diese Daten zeigen, dass APEX1 (21-318) dominant gegenüber dem vollständigen Protein ist. Zudem scheinen die ersten 20 Aminosäuren essentiell für den anti-apoptotischen Effekt von APEX1 in Endothelzellen zu sein. Um dies noch detaillierter nachzuweisen, wurde ein Expressionsvektor kloniert, mit dem nur die ersten 20 Aminosäuren von APEX1 (APEX1 (1-20)) exprimiert werden. Die Überexpression von APEX1 (1-20) konnte sowohl die basale wie auch H_2O_2-induzierte Apoptose sowie die Spaltung der Pro-Caspase 3 in die aktive Form inhibieren (Abbildung 12A und B) (Dyballa-Rukes*, **Jakobs*** et al. 2017).

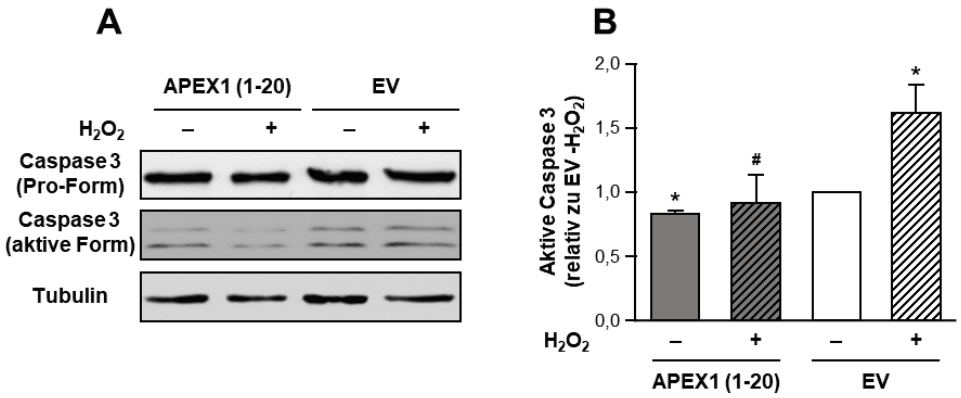

Abbildung 12: Die ersten 20 Aminosäuren von APEX1 schützen Endothelzellen vor Apoptose. (**A** und **B**) Endothelzellen wurden mit einem Leervektor („empty vector"–EV) oder einem Expressionsvektor für ein Protein, das nur die ersten 20 Aminosäuren von APEX1 mit einem C-terminalen myc Epitop-tag (APEX1 (1-20)) transfiziert und mit H_2O_2 behandelt. Als Surrogatmarker für Apoptoseinduktion wurde die Spaltung der Pro-Form von Caspase 3 in die aktive Form mittels Immunoblot ermittelt, Tubulin diente als Ladekontrolle. (**A**) Repräsentative Immunoblots. (**B**) Semiquantitative Analyse der Caspase 3 Spaltung normiert auf Tubulin. Gezeigt sind Mittelwerte +/- Standardfehler relativ zu den mit EV transfizierten, unbehandelten Zellen (n=4,*p<0,05 vs. EV $-H_2O_2$, #p<0,05 vs. EV $+H_2O_2$) (Dyballa-Rukes*, **Jakobs*** et al. 2017).

Um herauszufinden, ob eine Erhöhung der Trx-1 Menge dem pro-apoptotischen Effekt von APEX1 (21-318) entgegenwirken kann, wurde Trx-1 mittels lentiviraler Transduktion permanent in Endothelzellen exprimiert. Anschließend wurden die Zellen mit dem APEX1 (21-318) Expressionsvektor transfiziert und die aktive Caspase 3 mittels Immunoblot nachgewiesen. Zellen, die nur APEX1 (21-318) exprimieren, zeigten eine Erhöhung der aktiven Caspase 3. Allerdings konnte der pro-apoptotischen Effekt von APEX1 (21-318) durch permanente Re-Expression von Trx-1 aufgehoben werden, was sich in einer verminderten aktiven Caspase 3 widerspiegelte (Abbildung 13A und B) (Dyballa-Rukes*, **Jakobs*** et al. 2017).

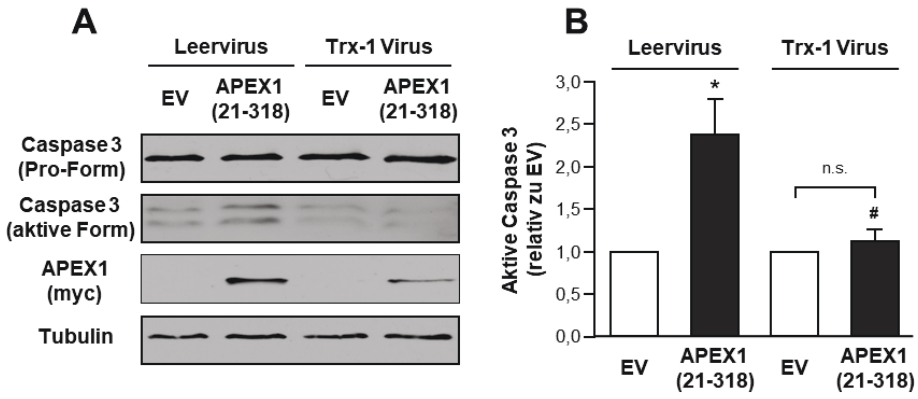

Abbildung 13: Permanente Expression von Thioredoxinx-1 kompensiert die pro-apoptotische Wirkung von APEX1 (21-318). (A und **B)** Endothelzellen wurden mit einem lentiviralen Expressionsvektor für Thioredoxin-1 (Trx-1 Virus) oder, als Kontrolle, einem Leervirus transduziert. Nach der Transduktion wurden die Zellen zusätzlich mit einem Leervektor („empty vector"-EV) oder einem Expressionsvektor für APEX1 (21-318) transfiziert. Als Surrogatmarker für Apoptoseinduktion wurde die Spaltung der Pro-Form von Caspase 3 in die aktive Form mittels Immunoblot ermittelt, die Expression der N-terminal deletierten APEX1 Variante wurde anhand des C-terminalen myc Epitop-tags mit der gleichen Technik nachgewiesen APEX1 (21-318)); Tubulin diente als Ladekontrolle. (**A**) Repräsentative Immunoblots. (**B**) Semi-quantitative Analyse der Caspase 3 Spaltung normiert auf Tubulin. Gezeigt sind Mittelwerte +/- Standardfehler relativ zu den jeweils mit EV transfizierten Zellen (n=4,*p<0,05 vs. Leervirus/EV, #p<0,05 vs. Leervirus/APEX1 (21-318) (Dyballa-Rukes*, **Jakobs*** et al. 2017).

Zudem wollten wir in einem *in vivo* Modell den Einfluss von erhöhtem oxidativen Stress auf das Trx-1 Level im Endothel untersuchen. Diese Untersuchungen wurden in Kooperation mit unserem amerikanischen Partnerlabor an der University of Virginia in Charlottesville im Rahmen des internationalen Graduiertenkollegs (IRTG1902) durchgeführt. Dazu wurde das Modell der permanenten Ligatur der Carotis communis verwendet, in dem es nachgewiesenermaßen zu erhöhtem oxidativem Stress im Gefäß kommt (Chiu and Chien 2011). Es stellte sich heraus, dass der dreiwöchige Verschluss der Halsschlagader zum dramatischen Verlust von Trx-1 im Endothel führt (Dyballa-Rukes*, **Jakobs*** et al. 2017).

Zusammenfassend ist zu sagen, dass APEX1 anti-apoptotisch in Endothelzellen wirkt, indem es mit der Pro-Form von Cat D einen Komplex bildet und dadurch die Prozessierung von Cat D hemmt. Damit ist die Cat D Aktivität reduziert und es kommt nicht zum Abbau von Trx-1. Durch die Erhaltung der Trx-1 Proteinmenge sind dann die Endothelzellen vor Apoptose geschützt (Abbildung 14) (Dyballa-Rukes*, **Jakobs*** et al. 2017).

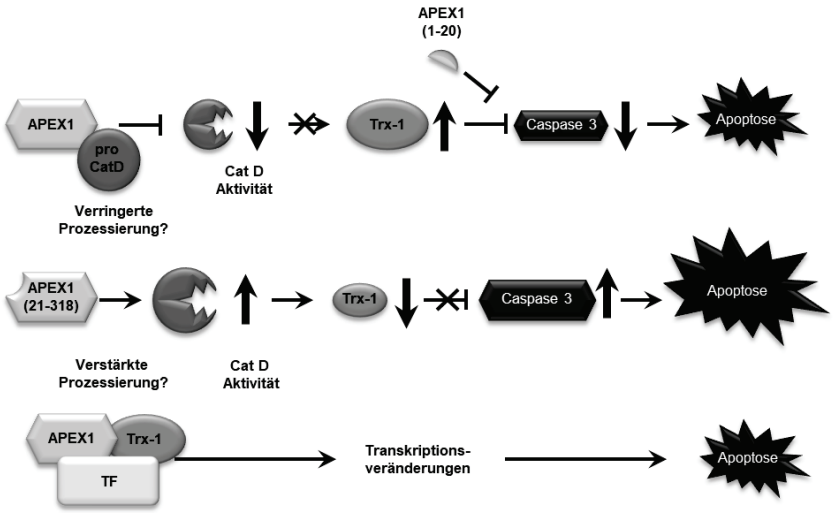

Abbildung 14: Schematische Zusammenfassung der Regulation von Trx-1 durch APEX1 und APEX1 (21-318) (Dyballa-Rukes*, **Jakobs*** et al. 2017)**.**

Ausblick

Ein Ziel dieser Doktorarbeit war es, eine potentielle anti-apoptotische Funktion von APEX1 in Endothelzellen zu untersuchen und, falls APEX1 eine derartige Funktion haben sollte, die zugrunde liegenden Mechanismen aufzuklären. Es konnte erstmals nachgewiesen werden, dass APEX1 anti-apoptotisch in humanen Endothelzellen wirkt, indem es mit der Pro-Form von Cat D einen Komplex bildet und dadurch wahrscheinlich die Prozessierung von Cat D hemmt (Dyballa-Rukes*, **Jakobs*** et al. 2017). Durch die daraus resultierende reduzierte Cat D Aktivität kommt es nicht zum Abbau von Trx-1, wodurch die Endothelzellen vor Apoptose geschützt werden (Abbildung 14). Außerdem konnte gezeigt werden, dass die anti-apoptotische Funktion von APEX1 abhängig von den ersten 20 Aminosäuren des Proteins ist und Überexpression dieses Anteils des Proteins ausreichend für den Apoptoseschutz ist (Dyballa-Rukes*, **Jakobs*** et al. 2017). Um die schützende Funktion von APEX1 (1-20) genauer zu untersuchen, werden wir im nächsten Schritt dieses Peptid, das am N-Terminus entweder mit Fluoresceinisothiocyanat (FITC) oder Biotin gekoppelt ist, in Kooperation mit der Firma JPT aus Berlin generieren. Mit dem FITC gekoppelten APEX1 Peptid soll zunächst eine Methode etabliert werden, mit der es in Endothelzellen eingebracht werden kann. Mit Hilfe des Protein-Transduktions-Reagens PROTEOfectene, welches einen Protein-Lipid-Komplex bildet, können Peptide über Endozytose in Zellen eingeschleust werden. Daher werden unterschiedliche PROTEOfectene/Peptid Mischungsverhältnisse eingesetzt und bezüglich der Effizienz, mit der das Peptid von Endothelzellen aufgenommen wird, untersucht. Ziel ist es, eine Effizienz von mindestens 80 % zu erreichen. Anschließend werden wir untersuchen, ob das APEX1 (1-20) Peptid Apoptoseinduktion inhibieren kann und wenn ja, ob es therapeutisch oder präventiv eingesetzt werden kann. Unser Ziel wird es sein, das Peptid als Kurzzeittherapeutikum einzusetzen, da die langfristige Behandlung mit einem möglichen anti-apoptotischen Peptid auch viele negative Effekte, wie z.B. Tumorwachstum, hervorrufen könnte. Daher wollen wir zunächst Apoptose

mit Lipopolysaccharid (LPS) als einem Auslöser von Sepsis in Endothelzellen induzieren und dann untersuchen, ob eine Vorinkubation mit dem APEX1 (1-20) Peptid diese Apoptose hemmen kann. Sollte dies der Fall sein, wollen wir ebenfalls untersuchen, ob eine Gabe des Peptids auch nach LPS Behandlung noch protektiv sein kann. Wenn wir einen anti-apoptotischen Effekt *in vitro* zeigen können, soll im nächsten Schritt getestet werden, ob das APEX1 (1-20) Peptid *in vivo* nach intravenöser Gabe von Endothelzellen aufgenommen wird. Für diesen *in* vivo Ansatz wird jedoch das Biotin gekoppelte Peptid genutzt, da wir dieses über Streptavidin, welches an das im Vergleich mit FITC wesentlich stärkere Fluorochrom Phycoerythrin gekoppelt ist, in Gewebeschnitten nachweisen können. Durch Kofärbung für einen Endothelzellmarker, wie z.B. CD31, kann festgestellt werden, ob das Peptid sich in diesen Zellen wiederfindet.

Weiterhin soll das Biotin gekoppelte APEX1 (1-20) Peptid verwendet werden, um zu untersuchen, an welche Proteine das Peptid bindet. Daher wollen wir die Far Western Blot Methode etablieren, bei der, analog zum Immunoblot, zelluläre Proteine nach elektrophoretischer Trennung auf eine Membran übertragen werden. Allerdings wird hierbei anstelle eines Antikörpers das Peptid verwendet, das an seine auf der Membran immobilisierten Interaktionspartner bindet. Die Detektion dieser Komplexe erfolgt über Meerrettichperoxidase-gekoppeltes Streptavidin und eine Chemilumineszenzreaktion wie auch bei einem Immunoblot. Sollten wir dabei positive Signale erhalten, sollen die Interaktionspartner des APEX1 (1-20) Peptids mittels Bindung an Streptavidin-Agarose und anschließende Massenspektrometrie (MS) identifiziert werden.

Des Weiteren konnte im Rahmen dieser Arbeit nachgewiesen werden, dass Koffein Endothelzellmigration in Abhängigkeit von mitochondriellem p27 induziert. Zudem war die Komplex I-abhängige Atmungskettenaktivität von Herzmitochondrien sowie die Differenzierung von kardialen Fibroblasten in Myofibroblasten von p27 abhängig (Ale-Agha*, Goy*, **Jakobs*** et al. 2018). Während dieses zuletzt genannten Differenzierungsprozesses kommt es zur Ausbildung von sogenannten Stressfasern aus αSMA, die den Zellen mechanische Stabilität und Kontraktilität verleihen. Von unserer Arbeitsgruppe war bereits für Endothelzellen gezeigt worden, dass die Ausbildung von derartigen Aktin-Faserbündeln mit einer Herunterregulation von Trx-1 verbunden ist, da es einen gegenseitigen Schutz von Aktin und Trx-1 gibt, wobei deren physikalische Assoziation zum einen Trx-1 vor Degradation und zum anderen Aktin vor der Ausbildung von Stressfasern schützt (Zschauer et al. 2011). Man kann annehmen, dass diese Phänomene auch bei der Myofibroblastendifferenzierung eine Rolle spielen, wobei hierbei allerdings dieser gegenseitige Schutz aufgehoben werden sollte, um die in diesem Fall notwendige Ausbildung von Stressfasern zu erlauben. Daher soll in Zukunft untersucht werden, wie Trx-1 in kardialen Fibroblasten nach Behandlung mit TGFβ1 reguliert wird und ob eine mögliche Regulation auch abhängig von mitochondriellem p27 ist.

Zudem ist es unerlässlich, die Funktionen von p27 im Mitochondrium genauer zu verstehen. Dazu sollen Interaktionspartner von p27 identifiziert werden, welche möglicherweise Rückschlüsse auf

die Funktion von p27 im Mitochondrium zulassen. Hierfür wollen wir zunächst aus Endothelzellen, die nach Transfektion mit dem entsprechenden Expressionsvektor mitochondrielles p27 mit einem myc-Epitop überexprimieren, dieses mittels eines myc Antikörpers immunpräzipitieren und seine Bindungspartner identifizieren. Zudem soll untersucht werden, ob die Interaktionspartner von mitochondriellem p27 durch Koffein verändert werden.

Zusammenfassung

Das Altern ist ein unabhängiger Risikofaktor für eine Vielzahl von Erkrankungen. Externe Risikofaktoren, wie z.B. Luftverschmutzung oder Ernährung, können den Alterungsprozess beeinflussen und damit die Entstehung von Krankheiten beschleunigen oder verzögern. Während des Alterungsprozesses kommt es zu einer Störung der Redoxhomöostase, verbunden mit einer Erhöhung von reaktiven Sauerstoffspezies und zu einer Einschränkung der mitochondriellen Atmung.

Ziel dieser Arbeit war die Aufklärung von molekularen Mechanismen, die in der Lunge und im Herzkreislaufsystem zu den genannten Veränderungen beitragen, um langfristig präventive oder therapeutische Strategien entwickeln zu können. In der Lunge als Eintrittsorgan für Partikel kommt es zu Veränderungen der Lungenepithelzellen. In dieser Arbeit konnte gezeigt werden, dass ultrafeine Kohlenstoffpartikel als ein Hauptbestandteil der Luftverschmutzung, abhängig von Caveolin-1 und von reaktiven Sauerstoffspezies, den epidermalen Wachstumsfaktor Rezeptor und daraus resultierend die Protein Kinase B sowie die Mitogen-aktivierte Protein Kinase aktivieren. Zudem bedingen Kohlenstoffpartikel den Verlust der Zell-Zell Kommunikation, ein weiteres bekanntes Zeichen des Alterungsprozesses und von chronisch obstruktiver Lungenerkrankung. Im Zusammenhang mit Ernährung konnte am Beispiel von Koffein eine Funktionsverbesserung in verschiedenen Zellen des kardiovaskulären Systems gezeigt werden. Koffein steigert die Komplex I-abhängige Atmung der Mitochondrien im Herzen, verstärkt die migratorische Kapazität der Endothelzellen und fördert die Differenzierung von kardialen Fibroblasten in Myofibroblasten. Auch die zuletzt genannten Effekte sind abhängig von der Atmungskettenfunktion. Der zugrunde liegende Mechanismus ist eine durch Koffein-induzierte Translokation des Zellzyklusinhibitors CDKN1B/p27 in die Mitochondrien. Die Funktionalität von Mitochondrien wird eingeschränkt durch Erhöhung von reaktiven Sauerstoffspezies. Deren Produktion wirken verschiedene anti-oxidative Systeme entgegen. Ein wesentliches dieser Systeme im Endothel ist das Thioredoxin-1 System. Neben seiner Funktion als Oxidoreduktase wirkt Thioredoxin-1 anti-apoptotisch. In dieser Arbeit wurde „apurinic/apyrimidinic endodeoxyribonuklease 1“ (APEX1) erstmalig als Regulator von Thioredoxin-1 identifiziert. APEX1 verhindert durch Inhibition der proteolytischen Aktivierung der Protease Cathepsin D die Degradation von Thioredoxin-1 und so die Induktion von Apoptose in Endothelzellen. Für diesen protektiven Effekt sind die ersten 20 Aminosäuren von APEX1 ausreichend.

Die Ergebnisse dieser Arbeit untermauern, dass die Mitochondrien und die Redoxhomöostase eine wesentliche Rolle im Alterungsprozess und damit bei Alters-assoziierten Erkrankungen spielen. Verbesserung der Mitochondrienfunktion durch Erhöhung von CDKN1B/p27 in den Mitochondrien und/oder Gabe eines Peptides, das die ersten 20 Aminosäuren von APEX1 enthält, könnten neue Ansätze zur Prävention oder Therapie Alters-assoziierter Erkrankungen darstellen.

Summary

Aging is an independent risk factor for multiple diseases. External risk factors like air pollution or diet can influence the aging process and thereby enhance or delay the development of diseases. Aging is associated with a disturbance of the redox homeostasis accompanied by an increase of reactive oxygen species and impairment in mitochondrial respiration.

The aim of this work was to elucidate molecular mechanisms that contribute to the aforementioned changes in the lung and in the cardiovascular system in order to develop preventive or therapeutic strategies. Inhalation of particles leads to alterations of lung epithelial cells. In this work it could be shown that ultrafine carbon particles as a major component of air pollution activate the epidermal growth factor as well as the protein kinase B and the mitogen-activated protein kinase in a caveolin-1 and reactive oxygen species dependent manner. Moreover, treatment with ultrafine carbon particles leads to loss of cell-cell-communication, which is a further hallmark of aging and chronic obstructive pulmonary disease. In the context of diet, caffeine improves functions of different cells within the cardiovascular system. Caffeine increases complex I dependent respiration in heart mitochondria, enhances migratory capacity of endothelial cells, and improves differentiation of cardiac fibroblast into myofibroblasts. The latter two effects also depend on mitochondrial respiration. The underlying mechanism is a caffeine-induced translocation of the cell cycle inhibitor CDKN1B/p27 into mitochondria. The functionality of mitochondria is reduced by increased reactive oxygen species formation. Their production is counteracted by various anti-oxidative systems. One of the most important of these systems in the endothelium is the Thioredoxin-1 system. Besides the function as an oxidoreductase, Thioredoxin-1 acts anti-apoptotic. In this study apurinic/apyrimidinic endodeoxyribonuklease 1 (APEX1) was for the first time identified as a regulator of Thioredoxin-1. APEX1 inhibits the degradation of Thioredoxin-1 by inhibiting the proteolytic activation of the protease Cathepsin D and, thus, apoptosis induction in endothelial cells. The first 20 amino acids of APEX1 are sufficient for this protective effect.

The results of this work confirm that mitochondria and redox homeostasis play an essential role in the aging process and thereby in age-associated diseases. Improvement of mitochondrial function by increasing CDKN1B/p27 in the mitochondria and/or administration of a peptide containing the first 20 amino acids of APEX1 may represent new approaches to prevent or treat age-associated diseases.

Literaturverzeichnis

Ago, T., I. Yeh, M. Yamamoto, M. Schinke-Braun, J. A. Brown, B. Tian and J. Sadoshima (2006). "Thioredoxin1 upregulates mitochondrial proteins related to oxidative phosphorylation and TCA cycle in the heart." Antioxid Redox Signal **8**(9-10): 1635-1650.

Ale-Agha, N., C. Goy, P. Jakobs, I. Spyridopoulos, S. Gonnissen, N. Dyballa-Rukes, K. Aufenvenne, F. Von Ameln, et al. (2018). "CDKN1B/p27 is localized in mitochondria and improves respiration-dependent processes in the cardiovascular system - new mode of action for caffeine." PLoS Biol **Im Druck**.

Banerjee, P., Z. Ali, B. Levine and D. R. Fowler (2014). "Fatal caffeine intoxication: a series of eight cases from 1999 to 2009." J Forensic Sci **59**(3): 865-868.

Baranano, D. E., M. Rao, C. D. Ferris and S. H. Snyder (2002). "Biliverdin reductase: a major physiologic cytoprotectant." Proc Natl Acad Sci U S A **99**(25): 16093-16098.

Barglow, K. T., C. G. Knutson, J. S. Wishnok, S. R. Tannenbaum and M. A. Marletta (2011). "Site-specific and redox-controlled S-nitrosation of thioredoxin." Proc Natl Acad Sci U S A **108**(35): E600-606.

Bedard, K. and K. H. Krause (2007). "The NOX family of ROS-generating NADPH oxidases: physiology and pathophysiology." Physiol Rev **87**(1): 245-313.

Benowitz, N. L. (1990). "Clinical pharmacology of caffeine." Annu Rev Med **41**: 277-288.

Bley, C.-H., M. Centgraf, A. Cieslik, J. Hack and L. Hohloch (2015). I care Anatomie, Physiologie. Stuttgart, Georg Thieme.

Boehm, M., T. Yoshimoto, M. F. Crook, S. Nallamshetty, A. True, G. J. Nabel and E. G. Nabel (2002). "A growth factor-dependent nuclear kinase phosphorylates p27(Kip1) and regulates cell cycle progression." EMBO J **21**(13): 3390-3401.

Boveris, A. and B. Chance (1973). "The mitochondrial generation of hydrogen peroxide. General properties and effect of hyperbaric oxygen." Biochem J **134**(3): 707-716.

Büchner, N., N. Ale-Agha, S. Jakob, U. Sydlik, K. Kunze, K. Unfried, J. Altschmied and J. Haendeler (2013). "Unhealthy diet and ultrafine carbon black particles induce senescence and disease associated phenotypic changes." Exp Gerontol **48**(1): 8-16.

Byon, C. H., T. Han, J. Wu and S. T. Hui (2015). "Txnip ablation reduces vascular smooth muscle cell inflammation and ameliorates atherosclerosis in apolipoprotein E knockout mice." Atherosclerosis **241**(2): 313-321.

Carreras, M. C., M. C. Franco, J. G. Peralta and J. J. Poderoso (2004). "Nitric oxide, complex I, and the modulation of mitochondrial reactive species in biology and disease." Mol Aspects Med **25**(1-2): 125-139.

Chance, B., H. Sies and A. Boveris (1979). "Hydroperoxide metabolism in mammalian organs." Physiol Rev **59**(3): 527-605.

Chen, B., D. Guan, Z. J. Cui, X. Wang and X. Shen (2010). "Thioredoxin 1 downregulates MCP-1 secretion and expression in human endothelial cells by suppressing nuclear translocation of activator protein 1 and redox factor-1." Am J Physiol Cell Physiol **298**(5): C1170-1179.

Chen, Y., J. Cai, T. J. Murphy and D. P. Jones (2002). "Overexpressed human mitochondrial thioredoxin confers resistance to oxidant-induced apoptosis in human osteosarcoma cells." J Biol Chem **277**(36): 33242-33248.

Chiu, J. J. and S. Chien (2011). "Effects of disturbed flow on vascular endothelium: pathophysiological basis and clinical perspectives." Physiol Rev **91**(1): 327-387.

Daly, J. W. (2007). "Caffeine analogs: biomedical impact." Cell Mol Life Sci **64**(16): 2153-2169.

Danaei, G., E. L. Ding, D. Mozaffarian, B. Taylor, J. Rehm, C. J. Murray and M. Ezzati (2009). "The preventable causes of death in the United States: comparative risk assessment of dietary, lifestyle, and metabolic risk factors." PLoS Med **6**(4): e1000058.

Deng, C., Z. Sun, G. Tong, W. Yi, L. Ma, B. Zhao, L. Cheng, J. Zhang, et al. (2013). "alpha-Lipoic acid reduces infarct size and preserves cardiac function in rat myocardial ischemia/reperfusion injury through activation of PI3K/Akt/Nrf2 pathway." PLoS One **8**(3): e58371.

Dimmeler, S., J. Haendeler, M. Nehls and A. M. Zeiher (1997). "Suppression of apoptosis by nitric oxide via inhibition of interleukin-1beta-converting enzyme (ICE)-like and cysteine protease protein (CPP)-32-like proteases." J Exp Med **185**(4): 601-607.

Dimmeler, S., V. Rippmann, U. Weiland, J. Haendeler and A. M. Zeiher (1997). "Angiotensin II induces apoptosis of human endothelial cells. Protective effect of nitric oxide." Circ Res **81**(6): 970-976.

Dimmeler, S. and A. M. Zeiher (1999). "Nitric oxide-an endothelial cell survival factor." Cell Death Differ **6**(10): 964-968.

Drose, S. and U. Brandt (2008). "The mechanism of mitochondrial superoxide production by the cytochrome bc1 complex." J Biol Chem **283**(31): 21649-21654.

Dyballa-Rukes, N., P. Jakobs, A. Eckers, N. Ale-Agha, V. Serbulea, K. Aufenvenne, T. C. Zschauer, L. L. Rabanter, et al. (2017). "The Anti-Apoptotic Properties of APEX1 in the

Endothelium Require the First 20 Amino Acids and Converge on Thioredoxin-1." Antioxid Redox Signal **26**(12): 616-629.

Ema, M., K. Hirota, J. Mimura, H. Abe, J. Yodoi, K. Sogawa, L. Poellinger and Y. Fujii-Kuriyama (1999). "Molecular mechanisms of transcription activation by HLF and HIF1alpha in response to hypoxia: their stabilization and redox signal-induced interaction with CBP/p300." EMBO J **18**(7): 1905-1914.

Evans, J. L., I. D. Goldfine, B. A. Maddux and G. M. Grodsky (2002). "Oxidative stress and stress-activated signaling pathways: a unifying hypothesis of type 2 diabetes." Endocr Rev **23**(5): 599-622.

Finkel, T. (2011). "Signal transduction by reactive oxygen species." J Cell Biol **194**(1): 7-15.

Fisone, G., A. Borgkvist and A. Usiello (2004). "Caffeine as a psychomotor stimulant: mechanism of action." Cell Mol Life Sci **61**(7-8): 857-872.

Folsom, A. R., H. Yatsuya, J. A. Nettleton, P. L. Lutsey, M. Cushman and W. D. Rosamond (2011). "Community prevalence of ideal cardiovascular health, by the American Heart Association definition, and relationship with cardiovascular disease incidence." J Am Coll Cardiol **57**(16): 1690-1696.

Freedman, N. D., Y. Park, C. C. Abnet, A. R. Hollenbeck and R. Sinha (2012). "Association of coffee drinking with total and cause-specific mortality." N Engl J Med **366**(20): 1891-1904.

Fridovich, I. (1983). "Superoxide dismutases: regularities and irregularities." Harvey Lect **79**: 51-75.

Fung, H. and B. Demple (2005). "A vital role for Ape1/Ref1 protein in repairing spontaneous DNA damage in human cells." Mol Cell **17**(3): 463-470.

Galkin, A. and U. Brandt (2005). "Superoxide radical formation by pure complex I (NADH:ubiquinone oxidoreductase) from Yarrowia lipolytica." J Biol Chem **280**(34): 30129-30135.

Goy, C., P. Czypiorski, J. Altschmied, S. Jakob, L. L. Rabanter, A. C. Brewer, N. Ale-Agha, N. Dyballa-Rukes, et al. (2014). "The imbalanced redox status in senescent endothelial cells is due to dysregulated Thioredoxin-1 and NADPH oxidase 4." Exp Gerontol **56**: 45-52.

Gunter, M. J., N. Murphy, A. J. Cross, L. Dossus, L. Dartois, G. Fagherazzi, R. Kaaks, T. Kuhn, et al. (2017). "Coffee Drinking and Mortality in 10 European Countries: A Multinational Cohort Study." Ann Intern Med **167**(4): 236-247.

Haendeler, J., J. Hoffmann, J. F. Diehl, M. Vasa, I. Spyridopoulos, A. M. Zeiher and S. Dimmeler (2004). "Antioxidants inhibit nuclear export of telomerase reverse transcriptase and delay replicative senescence of endothelial cells." Circ Res **94**(6): 768-775.

Haendeler, J., J. Hoffmann, V. Tischler, B. C. Berk, A. M. Zeiher and S. Dimmeler (2002). "Redox regulatory and anti-apoptotic functions of thioredoxin depend on S-nitrosylation at cysteine 69." Nat Cell Biol **4**(10): 743-749.

Haendeler, J., J. Hoffmann, A. M. Zeiher and S. Dimmeler (2004). "Antioxidant effects of statins via S-nitrosylation and activation of thioredoxin in endothelial cells: a novel vasculoprotective function of statins." Circulation **110**(7): 856-861.

Haendeler, J., R. Popp, C. Goy, V. Tischler, A. M. Zeiher and S. Dimmeler (2005). "Cathepsin D and H2O2 stimulate degradation of thioredoxin-1: implication for endothelial cell apoptosis." J Biol Chem **280**(52): 42945-42951.

Haendeler, J., V. Tischler, J. Hoffmann, A. M. Zeiher and S. Dimmeler (2004). "Low doses of reactive oxygen species protect endothelial cells from apoptosis by increasing thioredoxin-1 expression." FEBS Lett **577**(3): 427-433.

Haendeler, J., A. M. Zeiher and S. Dimmeler (1999). "Nitric oxide and apoptosis." Vitam Horm **57**: 49-77.

Haigis, M. C. and B. A. Yankner (2010). "The aging stress response." Mol Cell **40**(2): 333-344.

Halliwell, B. and C. E. Cross (1994). "Oxygen-derived species: their relation to human disease and environmental stress." Environ Health Perspect **102 Suppl 10**: 5-12.

Hansen, J. M., W. H. Watson and D. P. Jones (2004). "Compartmentation of Nrf-2 redox control: regulation of cytoplasmic activation by glutathione and DNA binding by thioredoxin-1." Toxicol Sci **82**(1): 308-317.

Hashemy, S. I. and A. Holmgren (2008). "Regulation of the catalytic activity and structure of human thioredoxin 1 via oxidation and S-nitrosylation of cysteine residues." J Biol Chem **283**(32): 21890-21898.

Hinz, B. (2010). "The myofibroblast: paradigm for a mechanically active cell." J Biomech **43**(1): 146-155.

Hirota, K., M. Matsui, S. Iwata, A. Nishiyama, K. Mori and J. Yodoi (1997). "AP-1 transcriptional activity is regulated by a direct association between thioredoxin and Ref-1." Proc Natl Acad Sci U S A **94**(8): 3633-3638.

Huang, L. E., Z. Arany, D. M. Livingston and H. F. Bunn (1996). "Activation of hypoxia-inducible transcription factor depends primarily upon redox-sensitive stabilization of its alpha subunit." J Biol Chem **271**(50): 32253-32259.

Huang, Q., H. J. Zhou, H. Zhang, Y. Huang, F. Hinojosa-Kirschenbaum, P. Fan, L. Yao, L. Belardinelli, et al. (2015). "Thioredoxin-2 inhibits mitochondrial reactive oxygen species generation and apoptosis stress kinase-1 activity to maintain cardiac function." Circulation **131**(12): 1082-1097.

Im, J. Y., K. W. Lee, J. M. Woo, E. Junn and M. M. Mouradian (2012). "DJ-1 induces thioredoxin 1 expression through the Nrf2 pathway." Hum Mol Genet **21**(13): 3013-3024.

Jakobs, P., V. Serbulea, N. Leitinger, A. Eckers and J. Haendeler (2017). "Nuclear Factor (Erythroid-Derived 2)-Like 2 and Thioredoxin-1 in Atherosclerosis and Ischemia/Reperfusion Injury in the Heart." Antioxid Redox Signal **26**(12): 630-644.

Junn, E., S. H. Han, J. Y. Im, Y. Yang, E. W. Cho, H. D. Um, D. K. Kim, K. W. Lee, et al. (2000). "Vitamin D3 up-regulated protein 1 mediates oxidative stress via suppressing the thioredoxin function." J Immunol **164**(12): 6287-6295.

Katsumata, Y., K. Shinmura, Y. Sugiura, S. Tohyama, T. Matsuhashi, H. Ito, X. Yan, K. Ito, et al. (2014). "Endogenous prostaglandin D2 and its metabolites protect the heart against ischemia-reperfusion injury by activating Nrf2." Hypertension **63**(1): 80-87.

Kelley, M. R. and M. L. Fishel (2008). "DNA repair proteins as molecular targets for cancer therapeutics." Anticancer Agents Med Chem **8**(4): 417-425.

Ketonen, J. and E. Mervaala (2008). "Effects of dietary sodium on reactive oxygen species formation and endothelial dysfunction in low-density lipoprotein receptor-deficient mice on high-fat diet." Heart Vessels **23**(6): 420-429.

Kim, J. H., Y. K. Choi, K. S. Lee, D. H. Cho, Y. Y. Baek, D. K. Lee, K. S. Ha, J. Choe, et al. (2012). "Functional dissection of Nrf2-dependent phase II genes in vascular inflammation and endotoxic injury using Keap1 siRNA." Free Radic Biol Med **53**(3): 629-640.

Larrea, M. D., J. Liang, T. Da Silva, F. Hong, S. H. Shao, K. Han, D. Dumont and J. M. Slingerland (2008). "Phosphorylation of p27Kip1 regulates assembly and activation of cyclin D1-Cdk4." Mol Cell Biol **28**(20): 6462-6472.

Lasley, R. D., M. S. Jahania and R. M. Mentzer, Jr. (2001). "Beneficial effects of adenosine A(2a) agonist CGS-21680 in infarcted and stunned porcine myocardium." Am J Physiol Heart Circ Physiol **280**(4): H1660-1666.

Laurent, T. C., E. C. Moore and P. Reichard (1964). "Enzymatic Synthesis of Deoxyribonucleotides. Iv. Isolation and Characterization of Thioredoxin, the Hydrogen Donor from Escherichia Coli B." J Biol Chem **239**: 3436-3444.

Lelieveld, J., J. S. Evans, M. Fnais, D. Giannadaki and A. Pozzer (2015). "The contribution of outdoor air pollution sources to premature mortality on a global scale." Nature **525**(7569): 367-371.

Lener, B., R. Koziel, H. Pircher, E. Hutter, R. Greussing, D. Herndler-Brandstetter, M. Hermann, H. Unterluggauer, et al. (2009). "The NADPH oxidase Nox4 restricts the replicative lifespan of human endothelial cells." Biochem J **423**(3): 363-374.

Lillig, C. H. and A. Holmgren (2007). "Thioredoxin and related molecules--from biology to health and disease." Antioxid Redox Signal **9**(1): 25-47.

Lim, S. S., T. Vos, A. D. Flaxman, G. Danaei, K. Shibuya, H. Adair-Rohani, M. Amann, H. R. Anderson, et al. (2012). "A comparative risk assessment of burden of disease and injury attributable to 67 risk factors and risk factor clusters in 21 regions, 1990-2010: a systematic analysis for the Global Burden of Disease Study 2010." Lancet **380**(9859): 2224-2260.

Lopez-Otin, C., M. A. Blasco, L. Partridge, M. Serrano and G. Kroemer (2013). "The hallmarks of aging." Cell **153**(6): 1194-1217.

Lu, S. C. (2009). "Regulation of glutathione synthesis." Mol Aspects Med **30**(1-2): 42-59.

Luscher, T. F. and G. Noll (1995). "The pathogenesis of cardiovascular disease: role of the endothelium as a target and mediator." Atherosclerosis **118 Suppl**: S81-90.

Makino, Y., N. Yoshikawa, K. Okamoto, K. Hirota, J. Yodoi, I. Makino and H. Tanaka (1999). "Direct association with thioredoxin allows redox regulation of glucocorticoid receptor function." J Biol Chem **274**(5): 3182-3188.

Marklund, S. L. (1984). "Extracellular superoxide dismutase in human tissues and human cell lines." J Clin Invest **74**(4): 1398-1403.

Masters, C., M. Pegg and D. Crane (1986). "On the multiplicity of the enzyme catalase in mammalian liver." Mol Cell Biochem **70**(2): 113-120.

McAllister, S. S., M. Becker-Hapak, G. Pintucci, M. Pagano and S. F. Dowdy (2003). "Novel p27(kip1) C-terminal scatter domain mediates Rac-dependent cell migration independent of cell cycle arrest functions." Mol Cell Biol **23**(1): 216-228.

Miller, M. R., C. A. Shaw and J. P. Langrish (2012). "From particles to patients: oxidative stress and the cardiovascular effects of air pollution." Future Cardiol **8**(4): 577-602.

Mills, N. L., H. Tornqvist, S. D. Robinson, M. Gonzalez, K. Darnley, W. MacNee, N. A. Boon, K. Donaldson, et al. (2005). "Diesel exhaust inhalation causes vascular dysfunction and impaired endogenous fibrinolysis." Circulation **112**(25): 3930-3936.

Minarowska, A., M. Gacko, A. Karwowska and L. Minarowski (2008). "Human cathepsin D." Folia Histochem Cytobiol **46**(1): 23-38.

Moens, A. L. and D. A. Kass (2006). "Tetrahydrobiopterin and cardiovascular disease." Arterioscler Thromb Vasc Biol **26**(11): 2439-2444.

Moens, A. L., E. Takimoto, C. G. Tocchetti, K. Chakir, D. Bedja, G. Cormaci, E. A. Ketner, M. Majmudar, et al. (2008). "Reversal of cardiac hypertrophy and fibrosis from pressure overload by tetrahydrobiopterin: efficacy of recoupling nitric oxide synthase as a therapeutic strategy." Circulation **117**(20): 2626-2636.

Moncada, S., R. M. Palmer and E. A. Higgs (1991). "Nitric oxide: physiology, pathophysiology, and pharmacology." Pharmacol Rev **43**(2): 109-142.

Negmadjanov, U., Z. Godic, F. Rizvi, L. Emelyanova, G. Ross, J. Richards, E. L. Holmuhamedov and A. Jahangir (2015). "TGF-beta1-mediated differentiation of fibroblasts is associated with increased mitochondrial content and cellular respiration." PLoS One **10**(4): e0123046.

Nishi, T., N. Shimizu, M. Hiramoto, I. Sato, Y. Yamaguchi, M. Hasegawa, S. Aizawa, H. Tanaka, et al. (2002). "Spatial redox regulation of a critical cysteine residue of NF-kappa B in vivo." J Biol Chem **277**(46): 44548-44556.

O'Keefe, J. H., S. K. Bhatti, H. R. Patil, J. J. DiNicolantonio, S. C. Lucan and C. J. Lavie (2013). "Effects of habitual coffee consumption on cardiometabolic disease, cardiovascular health, and all-cause mortality." J Am Coll Cardiol **62**(12): 1043-1051.

Palmer, R. M., D. S. Ashton and S. Moncada (1988). "Vascular endothelial cells synthesize nitric oxide from L-arginine." Nature **333**(6174): 664-666.

Paravicini, T. M. and R. M. Touyz (2006). "Redox signaling in hypertension." Cardiovasc Res **71**(2): 247-258.

Pence, B. D. and J. R. Yarbro (2018). "Aging impairs mitochondrial respiratory capacity in classical monocytes." Exp Gerontol **108**: 112-117.

Perez, V., D. A. V, T. Mazo, T. Marchini, L. Caceres, P. Evelson and R. J. Gelpi (2016). "Ischemic postconditioning confers cardioprotection and prevents reduction of Trx-1 in young mice, but not in middle-aged and old mice." Mol Cell Biochem **415**(1-2): 67-76.

Pillay, C. S., J. H. Hofmeyr and J. M. Rohwer (2011). "The logic of kinetic regulation in the thioredoxin system." BMC Syst Biol **5**: 15.

Radomski, M. W., R. M. Palmer and S. Moncada (1987). "Endogenous nitric oxide inhibits human platelet adhesion to vascular endothelium." Lancet **2**(8567): 1057-1058.

Rhee, S. G., S. W. Kang, T. S. Chang, W. Jeong and K. Kim (2001). "Peroxiredoxin, a novel family of peroxidases." IUBMB Life **52**(1-2): 35-41.

Ribe, D., D. Sawbridge, S. Thakur, M. Hussey, C. Ledent, I. Kitchen, S. Hourani and J. M. Li (2008). "Adenosine A2A receptor signaling regulation of cardiac NADPH oxidase activity." Free Radic Biol Med **44**(7): 1433-1442.

Saitoh, M., H. Nishitoh, M. Fujii, K. Takeda, K. Tobiume, Y. Sawada, M. Kawabata, K. Miyazono, et al. (1998). "Mammalian thioredoxin is a direct inhibitor of apoptosis signal-regulating kinase (ASK) 1." EMBO J **17**(9): 2596-2606.

Sakurai, A., M. Nishimoto, S. Himeno, N. Imura, M. Tsujimoto, M. Kunimoto and S. Hara (2005). "Transcriptional regulation of thioredoxin reductase 1 expression by cadmium in vascular endothelial cells: role of NF-E2-related factor-2." J Cell Physiol **203**(3): 529-537.

Saxena, G., J. Chen and A. Shalev (2010). "Intracellular shuttling and mitochondrial function of thioredoxin-interacting protein." J Biol Chem **285**(6): 3997-4005.

Schallreuter, K. U. and J. M. Wood (1986). "The role of thioredoxin reductase in the reduction of free radicals at the surface of the epidermis." Biochem Biophys Res Commun **136**(2): 630-637.

Schroeder, P., R. Popp, B. Wiegand, J. Altschmied and J. Haendeler (2007). "Nuclear redox-signaling is essential for apoptosis inhibition in endothelial cells--important role for nuclear thioredoxin-1." Arterioscler Thromb Vasc Biol **27**(11): 2325-2331.

Seo, A. Y., A. M. Joseph, D. Dutta, J. C. Hwang, J. P. Aris and C. Leeuwenburgh (2010). "New insights into the role of mitochondria in aging: mitochondrial dynamics and more." J Cell Sci **123**(Pt 15): 2533-2542.

Sezgin, E., I. Levental, S. Mayor and C. Eggeling (2017). "The mystery of membrane organization: composition, regulation and roles of lipid rafts." Nat Rev Mol Cell Biol **18**(6): 361-374.

Shao, D., S. Oka, T. Liu, P. Zhai, T. Ago, S. Sciarretta, H. Li and J. Sadoshima (2014). "A redox-dependent mechanism for regulation of AMPK activation by Thioredoxin1 during energy starvation." Cell Metab **19**(2): 232-245.

Shigenaga, M. K., T. M. Hagen and B. N. Ames (1994). "Oxidative damage and mitochondrial decay in aging." Proc Natl Acad Sci U S A **91**(23): 10771-10778.

Smellie, F. W., C. W. Davis, J. W. Daly and J. N. Wells (1979). "Alkylxanthines: inhibition of adenosine-elicited accumulation of cyclic AMP in brain slices and of brain phosphodiesterase activity." Life Sci **24**(26): 2475-2482.

Sohal, R. S. and B. H. Sohal (1991). "Hydrogen peroxide release by mitochondria increases during aging." Mech Ageing Dev **57**(2): 187-202.

Spannbrucker, T., N. Ale-Agha, C. Goy, N. Dyballa-Rukes, P. Jakobs, J. Altschmied, K. Unfried and J. Haendeler (2018). "Induction of cellular senescence and loss of gap junctional intercellular communication by carbon nanoparticle exposure of lung epithelial cells." Exp Gerontol **in Revision**.

Spyridopoulos, I., S. Fichtlscherer, R. Popp, S. W. Toennes, B. Fisslthaler, T. Trepels, A. Zernecke, E. A. Liehn, et al. (2008). "Caffeine enhances endothelial repair by an AMPK-dependent mechanism." Arterioscler Thromb Vasc Biol **28**(11): 1967-1974.

Stocker, R., A. N. Glazer and B. N. Ames (1987). "Antioxidant activity of albumin-bound bilirubin." Proc Natl Acad Sci U S A **84**(16): 5918-5922.

Stocker, R., Y. Yamamoto, A. F. McDonagh, A. N. Glazer and B. N. Ames (1987). "Bilirubin is an antioxidant of possible physiological importance." Science **235**(4792): 1043-1046.

Stockmann, D., T. Spannbrucker, N. Ale-Agha, P. Jakobs, C. Goy, N. Dyballa-Rukes, T. Hornstein, A. Kumper, et al. (2018). "Non-Canonical Activation of the Epidermal Growth Factor Receptor by Carbon Nanoparticles." Nanomaterials (Basel) **8**(4).

Tanaka, M., S. A. Kovalenko, J. S. Gong, H. J. Borgeld, K. Katsumata, M. Hayakawa, M. Yoneda and T. Ozawa (1996). "Accumulation of deletions and point mutations in mitochondrial genome in degenerative diseases." Ann N Y Acad Sci **786**: 102-111.

Tao, L., X. Jiao, E. Gao, W. B. Lau, Y. Yuan, B. Lopez, T. Christopher, S. P. RamachandraRao, et al. (2006). "Nitrative inactivation of thioredoxin-1 and its role in postischemic myocardial apoptosis." Circulation **114**(13): 1395-1402.

Tschudi, M. R., M. Barton, N. A. Bersinger, P. Moreau, F. Cosentino, G. Noll, T. Malinski and T. F. Luscher (1996). "Effect of age on kinetics of nitric oxide release in rat aorta and pulmonary artery." J Clin Invest **98**(4): 899-905.

Tsutsui, M., H. Shimokawa, Y. Otsuji, Y. Ueta, Y. Sasaguri and N. Yanagihara (2009). "Nitric oxide synthases and cardiovascular diseases: insights from genetically modified mice." Circ J **73**(6): 986-993.

Turoczi, T., V. W. Chang, R. M. Engelman, N. Maulik, Y. S. Ho and D. K. Das (2003). "Thioredoxin redox signaling in the ischemic heart: an insight with transgenic mice overexpressing Trx1." J Mol Cell Cardiol **35**(6): 695-704.

Valcarcel-Ares, M. N., T. Gautam, J. P. Warrington, L. Bailey-Downs, D. Sosnowska, R. de Cabo, G. Losonczy, W. E. Sonntag, et al. (2012). "Disruption of Nrf2 signaling impairs angiogenic capacity of endothelial cells: implications for microvascular aging." J Gerontol A Biol Sci Med Sci **67**(8): 821-829.

van Dam, R. M. and E. J. Feskens (2002). "Coffee consumption and risk of type 2 diabetes mellitus." Lancet **360**(9344): 1477-1478.

van Dam, R. M. and F. B. Hu (2005). "Coffee consumption and risk of type 2 diabetes: a systematic review." JAMA **294**(1): 97-104.

Viglietto, G., M. L. Motti and A. Fusco (2002). "Understanding p27(kip1) deregulation in cancer: down-regulation or mislocalization." Cell Cycle **1**(6): 394-400.

Walker, L. J., C. N. Robson, E. Black, D. Gillespie and I. D. Hickson (1993). "Identification of residues in the human DNA repair enzyme HAP1 (Ref-1) that are essential for redox regulation of Jun DNA binding." Mol Cell Biol **13**(9): 5370-5376.

Wallace, D. C. (2005). "A mitochondrial paradigm of metabolic and degenerative diseases, aging, and cancer: a dawn for evolutionary medicine." Annu Rev Genet **39**: 359-407.

Watson, W. H., J. Pohl, W. R. Montfort, O. Stuchlik, M. S. Reed, G. Powis and D. P. Jones (2003). "Redox potential of human thioredoxin 1 and identification of a second dithiol/disulfide motif." J Biol Chem **278**(35): 33408-33415.

Wei, S. J., A. Botero, K. Hirota, C. M. Bradbury, S. Markovina, A. Laszlo, D. R. Spitz, P. C. Goswami, et al. (2000). "Thioredoxin nuclear translocation and interaction with redox factor-1 activates the activator protein-1 transcription factor in response to ionizing radiation." Cancer Res **60**(23): 6688-6695.

Wei, Y., X. M. Liu, K. J. Peyton, H. Wang, F. K. Johnson, R. A. Johnson and W. Durante (2009). "Hypochlorous acid-induced heme oxygenase-1 gene expression promotes human endothelial cell survival." Am J Physiol Cell Physiol **297**(4): C907-915.

Xanthoudakis, S. and T. Curran (1992). "Identification and characterization of Ref-1, a nuclear protein that facilitates AP-1 DNA-binding activity." EMBO J **11**(2): 653-665.

Xanthoudakis, S., G. G. Miao and T. Curran (1994). "The redox and DNA-repair activities of Ref-1 are encoded by nonoverlapping domains." Proc Natl Acad Sci U S A **91**(1): 23-27.

Xu, B., J. Zhang, J. Strom, S. Lee and Q. M. Chen (2014). "Myocardial ischemic reperfusion induces de novo Nrf2 protein translation." Biochim Biophys Acta **1842**(9): 1638-1647.

Zakkar, M., K. Van der Heiden, A. Luong le, H. Chaudhury, S. Cuhlmann, S. S. Hamdulay, R. Krams, I. Edirisinghe, et al. (2009). "Activation of Nrf2 in endothelial cells protects arteries from exhibiting a proinflammatory state." Arterioscler Thromb Vasc Biol **29**(11): 1851-1857.

Zeiher, A. M., H. Drexler, B. Saurbier and H. Just (1993). "Endothelium-mediated coronary blood flow modulation in humans. Effects of age, atherosclerosis, hypercholesterolemia, and hypertension." J Clin Invest **92**(2): 652-662.

Zhang, H., L. Tao, X. Jiao, E. Gao, B. L. Lopez, T. A. Christopher, W. Koch and X. L. Ma (2007). "Nitrative thioredoxin inactivation as a cause of enhanced myocardial ischemia/reperfusion injury in the aging heart." Free Radic Biol Med **43**(1): 39-47.

Zhang, R., R. Al-Lamki, L. Bai, J. W. Streb, J. M. Miano, J. Bradley and W. Min (2004). "Thioredoxin-2 inhibits mitochondria-located ASK1-mediated apoptosis in a JNK-independent manner." Circ Res **94**(11): 1483-1491.

Zou, G. M., M. H. Luo, A. Reed, M. R. Kelley and M. C. Yoder (2007). "Ape1 regulates hematopoietic differentiation of embryonic stem cells through its redox functional domain." Blood **109**(5): 1917-1922.

Zschauer, T. C., K. Kunze, S. Jakob, J. Haendeler and J. Altschmied (2011). "Oxidative stress-induced degradation of thioredoxin-1 and apoptosis is inhibited by thioredoxin-1-actin interaction in endothelial cells." Arterioscler Thromb Vasc Biol **31**(3): 650-656.

Zschauer, T. C., S. Matsushima, J. Altschmied, D. Shao, J. Sadoshima and J. Haendeler (2013). "Interacting with thioredoxin-1--disease or no disease?" Antioxid Redox Signal **18**(9): 1053-1062.

Eigene Veröffentlichungen

1. **The anti-apoptotic properties of APEX1 in the endothelium require the first twenty amino acids and converge on Thioredoxin-1**
   Dyballa-Rukes N*, **Jakobs P***, Eckers A*, Ale-Agha N, Serbulea V, Aufenvenne K, Zschauer T-C, Rabanter LL, Jakob S, Von Ameln F, Eckermann O, Leitinger N, Goy C, Altschmied J[#], Haendeler J[#]
   Antioxid Redox Signal. 2017; 26: 616-629 *Gleichberechtigte Erstautoren; [#]Gleichberechtigte Letztautoren
2. **Nuclear factor (erythroid-derived 2)-like 2 and Thioredoxin-1 in atherosclerosis and ischemia/reperfusion injury in the heart**
   Jakobs P*, Serbulea V*, Leitinger N, Eckers A[#], Haendeler J[#]
   Antioxid Redox Signal. 2017; 26: 630-644 *Gleichberechtigte Erstautoren; [#]Gleichberechtigte Letztautoren
3. **CDKN1B/p27 is localized in mitochondria and improves respiration-dependent processes in the cardiovascular system – new mode of action for caffeine**
   Ale-Agha N*, Goy C*, **Jakobs P***, Spyridopoulos I, Gonnissen S, Dyballa-Rukes N, Aufenvenne K, Von Ameln F, Zurek M, Spannbrucker T, Eckermann O, Jakob S, Gorressen S, Abrams M, Grandoch M, Fischer JW, Köhrer K, Deenen R, Unfried K, Altschmied J[#], Haendeler J[#]
   Plos Biology. 2018: im Druck *Gleichberechtigte Erstautoren; [#]Gleichberechtigte Letztautoren
4. **Non-canonical activation of the epidermal growth factor receptor by carbon nanoparticles**
   Stöckmann D*, Spannbrucker T*, Ale-Agha N, **Jakobs P**, Goy C, Dyballa-Rukes N, Hornstein T, Kümper A, Kraegeloh A, Haendeler J, Unfried K
   Nanomaterials. 2018; 8 *Gleichberechtigte Erstautoren
5. **Induction of cellular senescence and loss of gap junctional intercellular communication by carbon nanoparticle exposure of lung epithelial cells**
   Spannbrucker T*, Ale-Agha N*, Goy C, Dyballa-Rukes N, **Jakobs P**, Altschmied J, Unfried K, Haendeler J
   Exp Gerontol. 2018; in Revision *Gleichberechtigte Erstautoren

The anti-apoptotic properties of APEX1 in the endothelium require the first twenty amino acids and converge on Thioredoxin-1

Dyballa-Rukes N*, **Jakobs P***, Eckers A*, Ale-Agha N, Serbulea V, Aufenvenne K, Zschauer T-C, Rabanter LL, Jakob S, Von Ameln F, Eckermann O, Leitinger N, Goy C, Altschmied J#, Haendeler J#

Antioxid Redox Signal. 2017; 26: 616-629 *Gleichberechtigte Erstautoren; #Gleichberechtigte Letztautoren

Autoren:

Dybala-Rukes N: Erstautorin, war an der Planung und Durchführung aller Versuche beteiligt, führte die Datenanalyse durch und war zudem am Entwurf des Manuskripts beteiligt.

Jakobs P: Erstautor, war an der Planung und Durchführung aller Versuche beteiligt, führte die Datenanalyse durch und war zudem am Entwurf des Manuskripts beteiligt. Plante mit Frau Haendeler alle Versuche für die Revision.

Eckers A: Erstautorin, war an der Planung und Durchführung aller Versuche beteiligt, führte die Datenanalyse durch und war zudem am Entwurf des Manuskripts beteiligt.

Ale-Agha N: Führte zusammen mit Frau Aufenvenne Immunfluoreszenzfärbungen durch.

Serbulea V: Führte Tierversuche und deren Analyse durch immunhistochemische Färbungen durch.

Aufenvenne K: Führte Immunoblots und zusammen mit Frau Ale-Agha Immunfluoreszenzfärbungen durch.

Zschauer T-C: Führte Immunoblots und Immunfluoreszenzfärbungen durch. Klonierte die APEX1 Konstrukte.

Rabanter LL: Führte Immunoblots und Immunfluoreszenzfärbungen durch.

Jakob S: Führte FACS Messungen und zusammen mit Frau Ale-Agha Immunfluoreszenzfärbungen durch.

Von Ameln F: Führte RNA Isolierungen und PCR-Analysen durch, klonierte mit Philipp Jakobs den für die Revision wichtigen Expressionsvektor für APEX1 (1-20).

Eckermann O: Führte RNA Isolierungen und PCR-Analysen sowie FACS Messungen durch.

Leitinger N: Führte zusammen mit Vlad Serbulea Tierversuche und deren Analyse durch immunhistochemische Färbungen durch.

Goy C: Führte Caspase 3 und Cathepsin D Aktivitätsmessungen sowie deren Analyse durch, beteiligte sich an den Immunoblots mit Philipp Jakobs.

Altschmied J: Senior Autor, war an der Konzeption der Studie federführend beteiligt. Erstellte das Konzept für alle Klonierungen von Expressionsvektoren, erstellte die Abbildungen, schrieb das Manuskript.

Haendeler J: Senior Autorin, hatte die Idee zur Studie, war an der Versuchsplanung beteiligt, schrieb und finalisierte das Manuskript.

Mary Ann Liebert, Inc. publishers

Prof. Dr. Jojo Haendeler
University of Duesseldorf
IUF - Leibniz Research Institute for Environmental Medicine
Auf`m Hennekamp 50
40225 Duesseldorf
Germany

May 16, 2018

Dear Dr. Haendeler:

Copyright permission is granted to Philipp Jakobs to use the figures from the articles below for his thesis.

"Nuclear Factor (Erythroid-Derived 2)-Like 2 and Thioredoxin-1 in Atherosclerosis and Ischemia/Reperfusion Injury in the Heart"
By Philipp Jakobs, Vlad Serbulea, Norbert Leitinger, Anna Eckers, and Judith Haendeler
Antioxidants & Redox Signaling Volume: 26 Issue 12: April 20, 2017
http://doi.org/10.1089/ars.2016.6795

"The Anti-Apoptotic Properties of APEX1 in the Endothelium Require the First 20 Amino Acids and Converge on Thioredoxin-1"
By Nadine Dyballa-Rukes, Philipp Jakobs, Anna Eckers, Niloofar Ale-Agha, Vlad Serbulea, Karin Aufenvenne, Tim-Christian Zschauer, Lothar L. Rabanter, Sascha Jakob, Florian von Ameln, Olaf Eckermann, Norbert Leitinger, Christine Goy, Joachim Altschmied, and Judith Haendeler
Antioxidants & Redox Signaling Volume: 26 Issue 12: April 20, 2017
http://doi.org/10.1089/ars.2016.6799

Kind Regards,

Karen Ballen
Manager, Copyright Permission
Mary Ann Liebert, Inc., publishers
KBallen@liebertpub.com

ANTIOXIDANTS & REDOX SIGNALING
Volume 26, Number 12, 2017

DOI: 10.1089/ars.2016.6799

FORUM ORIGINAL RESEARCH COMMUNICATION

The Anti-Apoptotic Properties of APEX1 in the Endothelium Require the First 20 Amino Acids and Converge on Thioredoxin-1

Nadine Dyballa-Rukes,[1,*] Philipp Jakobs,[1,*] Anna Eckers,[1,*] Niloofar Ale-Agha,[1] Vlad Serbulea,[2] Karin Aufenvenne,[1] Tim-Christian Zschauer,[1] Lothar L. Rabanter,[1] Sascha Jakob,[1] Florian von Ameln,[1] Olaf Eckermann,[1] Norbert Leitinger,[2,3] Christine Goy,[1] Joachim Altschmied,[1,*] and Judith Haendeler[1,4,*]

Abstract

The APEX nuclease (multifunctional DNA repair enzyme) 1 (APEX1) has a disordered N-terminus, a redox, and a DNA repair domain. APEX1 has anti-apoptotic properties, which have been linked to both domains depending on cell type and experimental conditions.

Aims: As protection against apoptosis is a hallmark of vessel integrity, we wanted to elucidate whether APEX1 acts anti-apoptotic in primary human endothelial cells and, if so, what the underlying mechanisms are.

Results: APEX1 inhibits apoptosis in endothelial cells by reducing Cathepsin D (CatD) cleavage, potentially by binding to the unprocessed form. Diminished CatD activation results in increased Thioredoxin-1 protein levels leading to reduced Caspase 3 activation. Consequently, apoptosis rates are decreased. This depends on the first twenty amino acids in APEX1, because APEX1 (21-318) induces CatD activity, decreases Thioredoxin-1 protein levels, and, thus, increases Caspase 3 activity and apoptosis. Along the same lines, APEX1 (1-20) inhibits Caspase 3 cleavage and apoptosis. Furthermore, re-expression of Thioredoxin-1 *via* lentiviral transduction rescues endothelial cells from APEX1 (21-318)-induced apoptosis. In an *in vivo* model of restenosis, which is characterized by oxidative stress, endothelial activation, and smooth muscle cell proliferation, Thioredoxin-1 protein levels are reduced in the endothelium of the carotids.

Innovation: APEX1 acts anti-apoptotic in endothelial cells. This anti-apoptotic effect depends on the first 20 amino acids of APEX1.

Conclusion: As proper function of the endothelium during life span is a hallmark for individual health span, a detailed characterization of the functions of the APEX1N-terminus is required to understand all its cellular properties. *Antioxid. Redox Signal.* 26, 616–629.

Keywords: APEX1, Trx-1, N-terminus, anti-apoptotic

Introduction

THE APEX NUCLEASE (multifunctional DNA repair enzyme) 1 (APEX1) is an ubiquitously expressed protein with dual functions; it can act as (i) an apurinic/apyrimidinic endonuclease in base excision repair pathways and (ii) as a redox factor, why it has also been called redox factor 1 (Ref-1). APEX1 has been described as anti-apoptotic and growth promoting in several tumor cell lines and tumors (25). First, these activities were only associated with the DNA repair

[1]IUF-Leibniz Research Institute for Environmental Medicine, Duesseldorf, Germany.
[2]Department of Pharmacology, University of Virginia, Charlottesville, Virginia.
[3]Cardiovascular Research Center, University of Virginia, Charlottesville, Virginia.
[4]Medical Faculty, Central Institute of Clinical Chemistry and Laboratory Medicine, University of Duesseldorf, Duesseldorf, Germany.
*N.D.-R., P.J., A.E. are equally contributing first authors and J.A. and J.H. are equally contributing last authors to this work.

Innovation

Anti-apoptotic properties of the multifunctional protein APEX1 have previously been described in tumor cells. However, it was not clear, which domain of APEX1 is required for this function. In this study, we describe for the first time that APEX1 suppresses apoptosis in primary human endothelial cells. The N-terminal 20 amino acids of APEX1 are fully sufficient for apoptosis protection and the downstream target is Thioredoxin-1. Thus, small peptide approaches using the N-terminus of APEX-1 could in the future be relevant for disease protection.

domain. However, over the last decade, it has become clear that the redox domain in APEX1 also plays an important role in the anti-apoptotic function in normal somatic cells.

Therefore, several studies were performed to identify small-molecule inhibitors specifically targeting the different domains in APEX1 to understand specific functions of this protein in normal and tumor cells [for review see Ref. (31)].

The endothelium plays a central role as a barrier between the blood stream and the surrounding tissue. However, numerous environmental factors have a negative impact on the endothelium by changing the circulating levels of cytokines, chemokines, and/or growth factors. Those mediators influence the endothelium and seem to importantly contribute to endothelial dysfunction (8, 37, 44).

One hallmark of endothelial dysfunction is the damage of endothelial cells leading to apoptotic cell death (3). Several studies have been undertaken to improve endothelial function by inhibiting endothelial cell apoptosis (12, 28, 40, 43, 47). Already decades ago, it was evident that oxygen deprivation for a certain time led to endothelial cell death, which, on the contrary, was also induced by the process of reoxygenation. This was associated with a burst in reactive oxygen species (ROS) damaging the endothelium and resulting in apoptosis induction. One central transcription factor protecting the endothelium under hypoxia and reoxygenation is the Hypoxia Inducible Factor 1 alpha (HIF1α) (5, 23, 42). The regulation of HIF1α under those conditions has been attributed to APEX1 (16, 21), and thus, APEX1 has an anti-apoptotic and prosurvival function when the oxygen concentration is unphysiological. However, till now, the role of APEX1 in apoptosis protection under basal conditions and a potential function of its different domains have not been investigated.

Moreover, several studies suggested that APEX1 acts in concert with Thioredoxin-1 (Trx-1) to regulate the activity of numerous transcription factors and thereby influences cellular functions (2, 4, 9, 16, 22, 41). Indeed, a colocalization between endogenous Trx-1 and APEX1 in primary human endothelial cells has been shown (30).

Therefore, we investigated for the first time the effects of APEX1 on basal apoptosis in primary human endothelial cells and showed that its anti-apoptotic activity depends on the N-terminus of the protein, but is independent of the DNA repair domain. Since the N-terminus of APEX1 has recently been described as important for nuclear targeting and interaction specificity (29), we also investigated the functions of the N-terminus of APEX1. Moreover, we also demonstrated a role for Trx-1 in the anti-apoptotic function of APEX1.

Results

The integrity of the endothelium is essential for proper vessel function. APEX1 is a bifunctional protein, which contains two nonoverlapping domains – a redox domain and a DNA repair domain. The redox function – needed for reductive activation of transcription factors – requires the region between amino acids 36 and 127, with the cysteines in position 65 and 93 being critical for redox activity. On the contrary, the DNA repair domain resides in the C-terminus starting at amino acid 162 and extending to the end of APEX1 (39, 45). In contrast to these domains, the functions of the N-terminus of APEX1 are less well defined.

APEX1 acts anti-apoptotic under hypoxic conditions in endothelial cells (21). The underlying mechanisms are supposed to include the activation of HIF1α and NF-κB. However, the role of APEX1 under basal conditions has not been investigated. Therefore, we first cloned an expression vector for APEX1 and transiently overexpressed it in primary human endothelial cells. APEX1 significantly inhibited Caspase 3/7 activity and apoptosis measured by Annexin V-positive/propidium iodide (PI)-negative cells (Fig. 1A, B and Supplementary Fig. S1; Supplementary Data are available online at www.liebertpub.com/ars). Besides basal apoptosis, induction of oxidative stress-induced apoptosis was also completely blocked by APEX1 (Fig. 1B and Supplementary Fig. S1).

APEX1 deficiency leads to early embryonic lethality with the embryos dying shortly after implantation, indicating a critical role for APEX1 in normal cellular functions. Notably, many cells in the very early APEX1 knockout embryos are characterized by pyknotic nuclei, that is, chromatin condensation, which is a feature of apoptosis (46). Thus, we also examined apoptosis induction after partial knockdown of endogenous APEX1 with siRNA avoiding complete depletion of the protein (Fig. 1C). Reduction of APEX1 levels resulted in increased apoptosis and cleaved Caspase 3 (Fig. 1D, E and Supplementary Fig. S1).

Next, we generated two mutants of APEX1 to understand (i) the role of the DNA repair domain [APEX1 (1-127)] and (ii) of the N-terminus [APEX1 (21-318)] in apoptosis protection (Fig. 2A). Both mutants can be expressed to a similar extent as full-length APEX1 in endothelial cells (Fig. 2B, C and Supplementary Fig. S2). The localization pattern shown in Figure 2B demonstrates that all three proteins can be found in the nucleus and in the cytosol. However, APEX1 (21-318) seems to have increased cytosolic localization. Nevertheless, it can be excluded that the first 20 amino acids in APEX1 are alone responsible for nuclear localization in endothelial cells. With respect to apoptosis protection, APEX1 (1-127) inhibited apoptosis, whereas APEX1 (21-318) significantly increased apoptosis when compared to empty vector control as well as to APEX1 (Fig. 2C). These results lead to the conclusion that the DNA repair domain of APEX1 is dispensable for apoptosis protection in endothelial cells.

Unexpected and more surprising were the data obtained with the N-terminally truncated mutant APEX1 (21-318). Therefore, we next sought to determine mechanisms underlying the anti-apoptotic properties of the full-length protein and the pro-apoptotic properties of APEX1 (21-318). To reinforce the findings obtained with Annexin V binding, we also measured Caspase 3/7 activity. Indeed, APEX1 inhibited

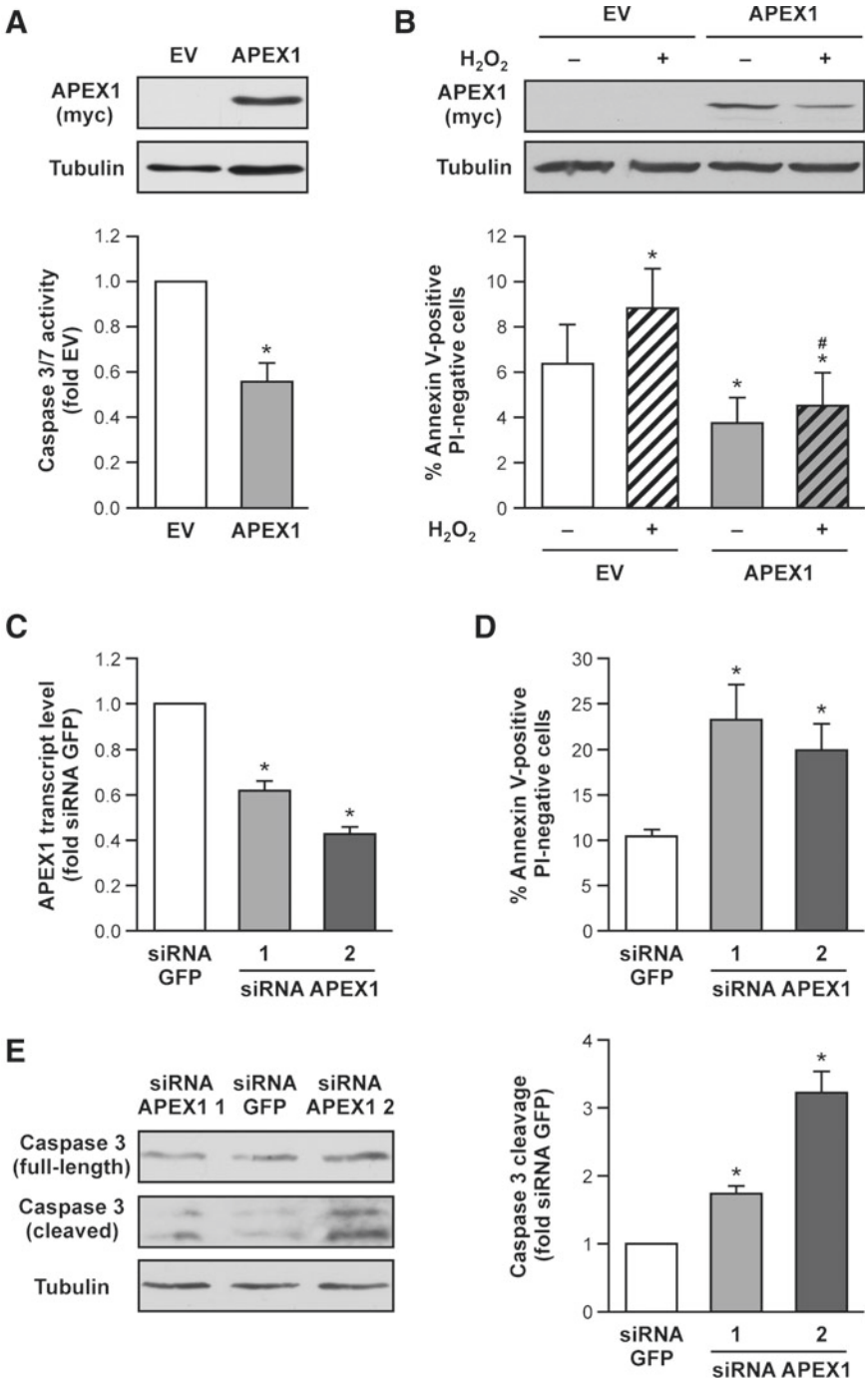

FIG. 1. APEX1 protects primary human endothelial cells against apoptosis. **(A)** Endothelial cells were transfected with an empty vector (EV) or an APEX1 expression vector (APEX1) and assayed for Caspase 3/7 activity 1 day after transfection. *Top panel*: Overexpressed APEX1 was detected by immunoblot with an antibody against the C-terminal myc-tag [APEX1 (myc)], Tubulin served as a loading control. *Bottom panel*: Caspase 3/7 activity. Data are mean ± SEM and were normalized to EV transfected cells ($n = 3$, $^{*}p < 0.05$ *vs.* EV). **(B)** Cells were transfected as in **(A)** and treated with 200 μM H_2O_2 for 18 h. *Top panel*: Overexpressed APEX1 was detected by immunoblot with an antibody against the C-terminal myc-tag [APEX1 (myc)], Tubulin served as a loading control. *Bottom panel*: The percentage of Annexin V-positive/PI-negative cells was determined by flow cytometry. Data are mean ± SEM ($n = 6$, $^{*}p < 0.05$ *vs.* EV − H_2O_2, $^{\#}p < 0.05$ *vs.* EV + H_2O_2). **(C–E)** Endothelial cells were transfected with two different siRNAs targeting the APEX1 transcript and a siRNA directed against GFP as a control and assayed for APEX1 mRNA, early apoptosis, and cleaved Caspase 3 1 day after transfection. **(C)** APEX1 transcript levels were determined by semiquantitative real-time PCR using RPL32 for normalization. Data are mean ± SEM and were normalized to siRNA GFP transfected cells ($n = 4$, $^{*}p < 0.05$ *vs.* siRNA GFP). **(D)** The percentage of Annexin V-positive/PI-negative cells was determined by flow cytometry. Data are mean ± SEM ($n = 4$–5, $^{*}p < 0.05$ *vs.* siRNA GFP). **(E)** Immunoblots were used to determine the amounts of full-length [Caspase 3 (full length)] and cleaved Caspase 3 [Caspase 3 (cleaved)], Tubulin served as a loading control. *Left panel*: Representative immunoblots. *Right panel*: Semiquantitative analysis of cleaved Caspase 3; data are mean ± SEM and were normalized to siRNA GFP transfected cells ($n = 3$, $^{*}p < 0.05$ *vs.* siRNA GFP). PCR, polymerase chain reaction; SEM, standard error of the mean.

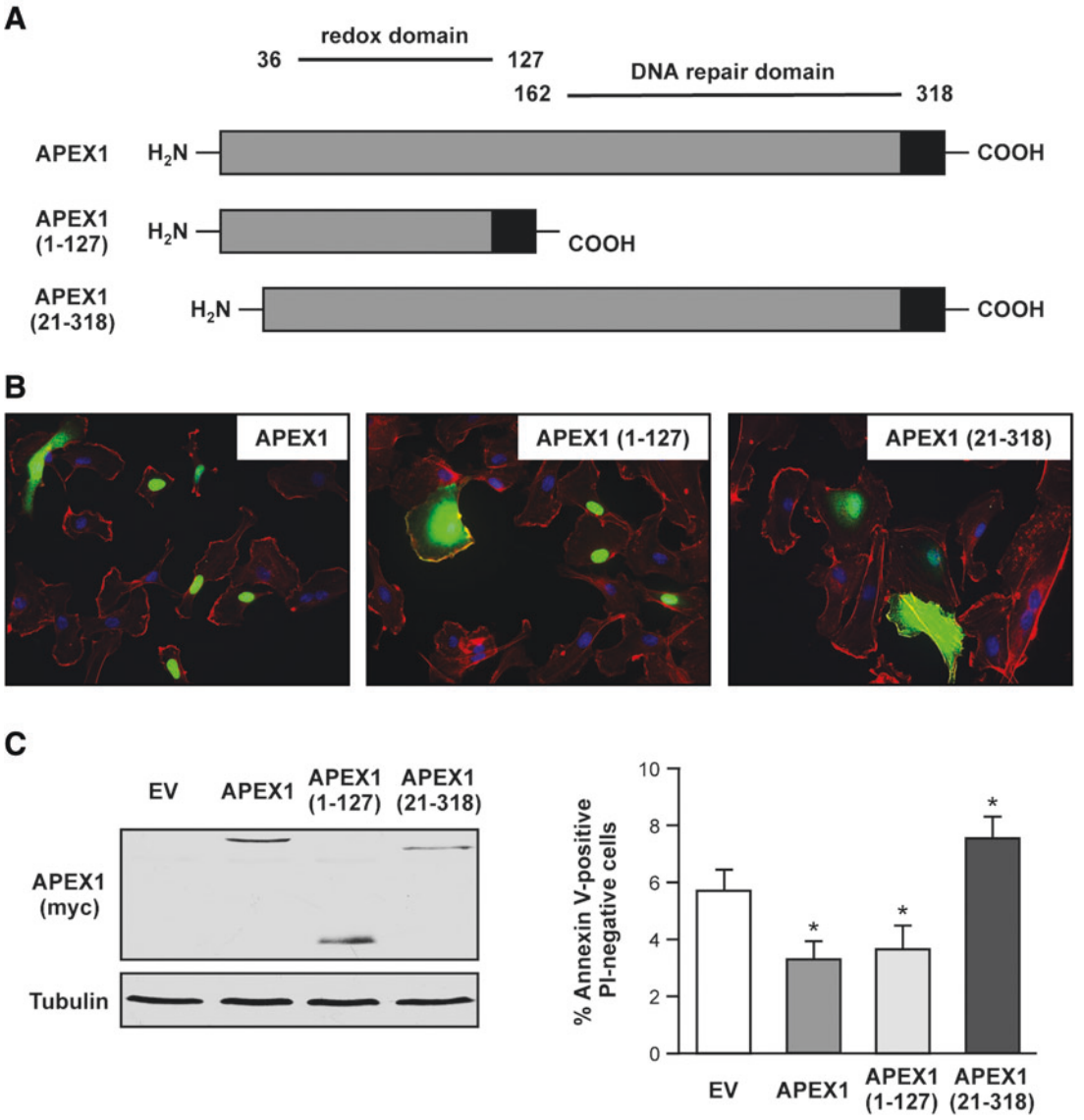

FIG. 2. The N-terminal 20 amino acids of APEX1 are required for apoptosis protection. (A) Functional domains and deletion mutants of APEX1. Shown are the redox domain of APEX1, which begins C-terminal to amino acid 36 and ends at amino acid 127, and the DNA repair domain encompassing the complete C-terminus beginning at amino acid 162. The mutant APEX1 (1-127) lacks the complete DNA repair domain, in APEX1 (21-318) the first 20 amino acids are missing. The C-terminal myc-tag is symbolized by a *black rectangle*. **(B)** Subcellular localization of truncated APEX1 proteins. Endothelial cells were transfected with expression vectors for full-length APEX1 or the two mutants and analyzed by immunostaining 1 day after transfection. APEX1 variants were detected with a fluorescently labeled anti-myc-tag antibody (*green*); actin filaments were stained with Alexa Fluor 568-coupled phalloidin (*red*), and nuclei were counterstained with DAPI (*blue*). **(C)** Endothelial cells were transfected with an EV or expression vectors for full-length APEX1 (APEX1) or the two deletion mutants. *Left panel*: Overexpressed APEX1 proteins were detected by immunoblot with an antibody against the C-terminal myc-tag [APEX1 (myc)], Tubulin served as a loading control. *Right panel*: The percentage of Annexin V-positive/PI-negative cells was determined by flow cytometry. Data are mean ± SEM ($n = 6$, $^*p < 0.05$ *vs.* EV). To see this illustration in color, the reader is referred to the web version of this article at www.liebertpub.com/ars

Caspase 3/7 activation (Fig. 3A). In contrast, but in accordance with the data obtained before (Fig. 2C), APEX1 (21-318) significantly increased Caspase 3/7 activity when compared to empty vector control as well as to cells overexpressing full-length APEX1.

We have previously shown that Trx-1 is essential for the protection of endothelial cells against apoptosis (17, 20, 36, 48). Therefore, we next investigated the effects of APEX1 and APEX1 (21-318) on Trx-1 protein levels. Interestingly, we found that expression of full-length APEX1 increased the amount of Trx-1, whereas APEX1 (21-318) significantly reduced Trx-1 protein levels (Fig. 3B and Supplementary Fig. S3). Since Trx-1 is degraded by the lysosomal protease Cathepsin D (CatD) (15, 19), and microinjection of CatD in fibroblasts leads to Caspase 3 activation and apoptosis induction (34), we next determined the activity of CatD by the

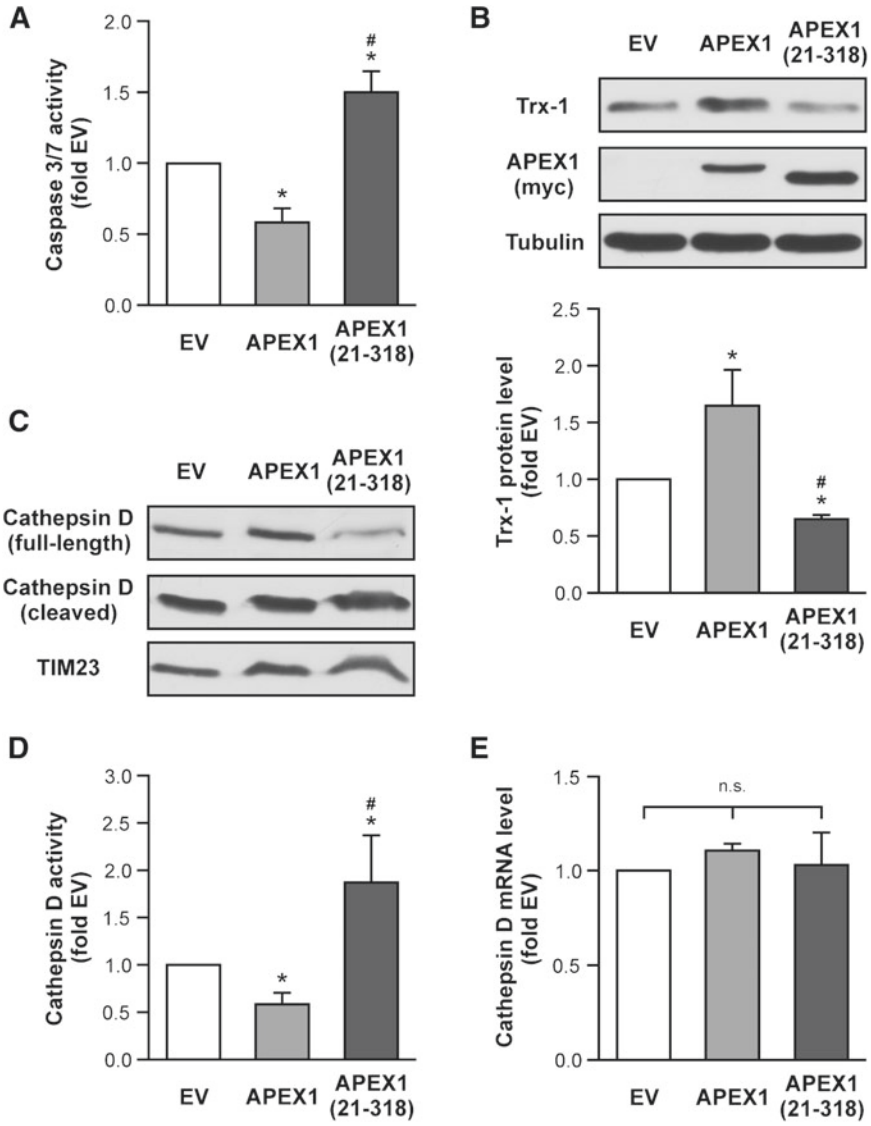

FIG. 3. Full-length APEX1 in contrast to the N-terminal deletion mutant increases Thioredoxin-1 levels by inhibiting CatD. Endothelial cells were transfected with an EV or expression vectors for full-length APEX1 (APEX1) or the N-terminally truncated mutant APEX1 (21-318). **(A)** Caspase 3/7 activity was measured 1 day after transfection. Data are mean ± SEM and were normalized to EV transfected cells ($n = 4$, $^{*}p < 0.05$ *vs.* EV, $^{\#}p < 0.05$ *vs.* APEX1). **(B)** Immunoblots were used to determine Thioredoxin-1 (Trx-1) levels and to verify expression of APEX1 and APEX1 (21-318) [APEX1 (myc)], Tubulin served as a loading control. *Top panel*: Representative immunoblots. *Bottom panel*: Semiquantitative analysis of Trx-1 protein amounts; data are mean ± SEM and were normalized to EV transfected cells ($n = 4$, $^{*}p < 0.05$ *vs.* EV, $^{\#}p < 0.05$ *vs.* APEX1). **(C)** Levels of full-length CatD and its cleavage product, which is indicative of activation, were analyzed by immunoblot, TIM23 served as loading control. **(D)** CatD activity was measured by a fluorometric assay. Data are mean ± SEM and were normalized to EV transfected cells ($n = 5$, $^{*}p < 0.05$ *vs.* EV, $^{\#}p < 0.05$ *vs.* APEX1). **(E)** Transcript levels were analyzed by semiquantitative real-time PCR using ERK2 for normalization. Data are mean ± SEM and were normalized to EV transfected cells ($n = 3$, n.s., not significant).

amount of cleaved CatD in an immunoblot (Fig. 3C and Supplementary Fig. S3) as well as with a quantitative activity assay (Fig. 3D). Again, APEX1 reduced CatD activity, whereas APEX1 (21-318) drastically increased active CatD.

Because APEX1 and Trx-1 have been implicated in the regulation of transcription factors (22, 41), we also determined CatD RNA levels after APEX1 overexpression. As demonstrated in Figure 3E, neither the full-length protein nor APEX1 (21-318) affected CatD RNA levels. Thus, the reduction in full-length CatD and concomitant increase in cleaved CatD in cells overexpressing APEX1 (21-318) indeed mirror the enhanced CatD activity. Our data indicate that APEX1 (21-318) overexpression reduces Trx-1 protein levels and induces apoptosis. Next, we examined whether we can counteract the pro-apoptotic effect of APEX1 (21-318) by blocking CatD using the cell-permeable CatD inhibitor, Pepstatin A-penetratin. Indeed, inhibition of CatD abrogated APEX1 (21-318)-induced apoptosis and restored Trx-1 protein levels (Supplementary Figs. 1 and S sup1).

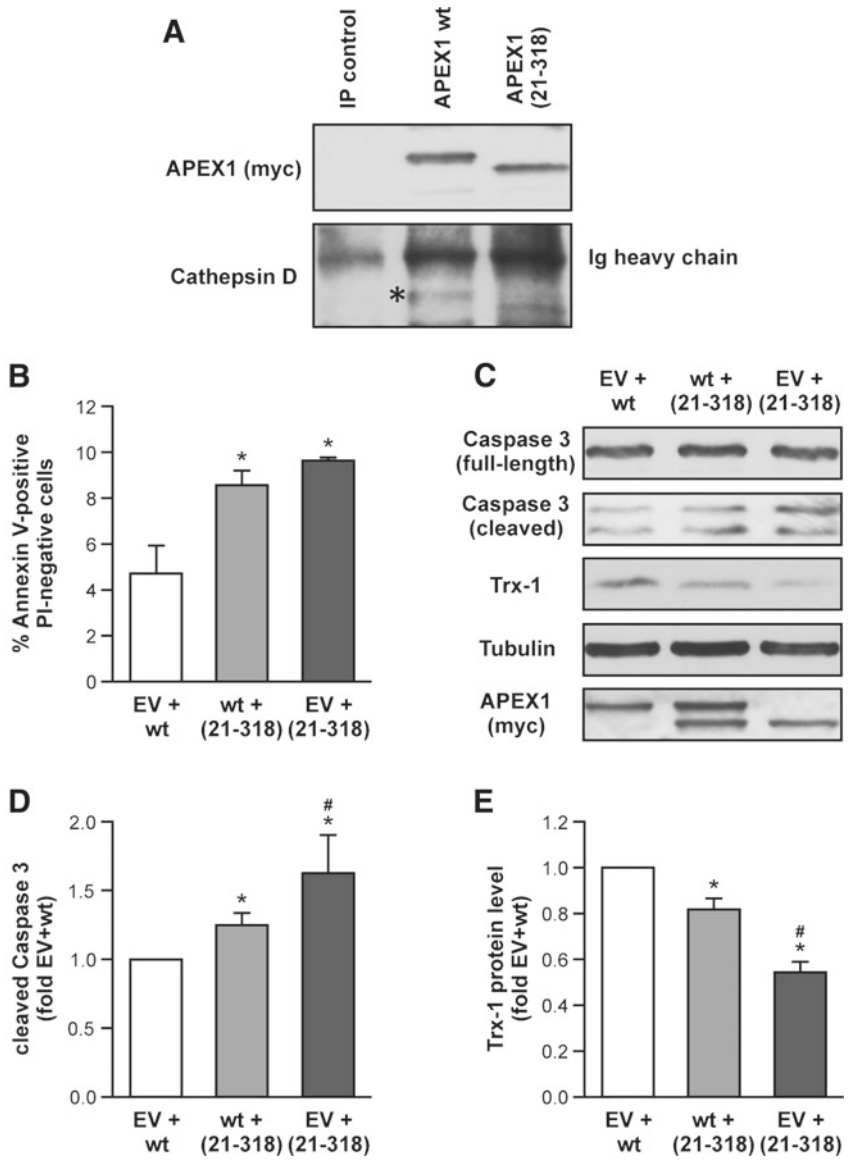

FIG. 4. Functional competition between APEX1 wt and the N-terminally deleted mutant APEX1 (21-318). (A) Endothelial cells were transfected with expression vectors for APEX1 wt and APEX1 (21-318) as indicated. One day after transfection, the cells were lysed and the lysates used for an immunoprecipitation with an anti-myc-tag antibody. A 1:1 mixture of both lysates was used for a control immunoprecipitation (IP control) using an anti-FLAG antibody. The precipitates were resolved by SDS-PAGE. Immunoblots were used to detect the APEX1 proteins [APEX1 (myc)] and CatD. The *asterisk* indicates full-length CatD. **(B–E)** Endothelial cells were transfected with 1:1 mixtures of expression vectors for APEX1 wt, APEX1 (21-318), and an EV as indicated. One day after transfection, the cells were either analyzed for early apoptosis or lysed, and the lysates were subjected to SDS-PAGE. **(B)** Percentage of Annexin V-positive/PI-negative cells; data are mean ± SEM ($n = 3$–5, $^{*}p < 0.05$ *vs.* EV+wt). **(C)** Representative immunoblots of full-length [Caspase 3 (full-length)], cleaved Caspase 3 [Caspase 3 (cleaved)], and Thioredoxin-1 (Trx-1), Tubulin served as a loading control. Expression of APEX1 wt and APEX1 (21-318) was verified with an antibody against the C-terminal myc-tag [APEX1 (myc)]. **(D)** Semiquantitative analysis of cleaved Caspase 3; data are mean ± SEM and were normalized to cells transfected with EV+wt [$n = 5$, $^{*}p < 0.05$ *vs.* EV+wt, $^{\#}p < 0.05$ *vs.* wt+(21-318)]. **(E)** Semiquantitative analysis of Trx-1 protein levels; data are mean ± SEM and were normalized to cells transfected with EV+wt [$n = 4$, $^{*}p < 0.05$ *vs.* EV+wt, $^{\#}p < 0.05$ *vs.* wt+(21-318)].

Since full-length APEX1 and APEX1 (21-318) have an influence on CatD, we next investigated whether CatD is in a complex with APEX1. Indeed, we found that the unprocessed CatD is associated with APEX1, but not with APEX1 (21-318) (Fig. 4A and Supplementary Fig. S4). Thus, one could speculate that association of APEX1 and CatD inhibits processing and thus activation of CatD. On the contrary, APEX1 (21-318) enhanced CatD cleavage, suggesting that APEX1 (21-318) might affect one or more of the proteases involved in CatD processing, which is required for its activation (33).

To further understand whether APEX1 wild type (wt) and APEX1 (21-318) compete against each other, we performed cotransfection experiments using equal amounts of empty vector and APEX1 wt, APEX1 wt and APEX1 (21-318), or

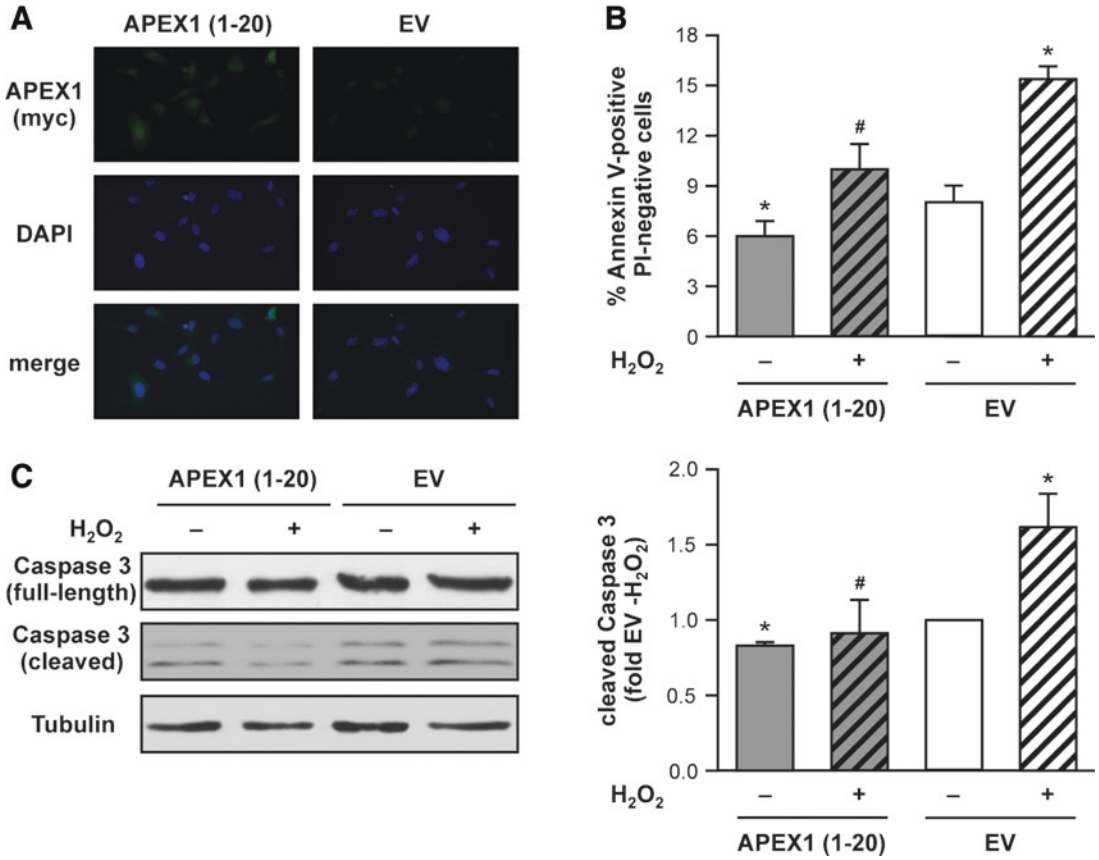

FIG. 5. APEX1 (1-20) inhibits apoptosis and Caspase 3 cleavage. Endothelial cells were transfected with an expression vector for APEX1 (1-20) or an EV and analyzed 1 day after transfection. **(A)** APEX1 (1-20) was detected with a fluorescently labeled anti-myc-tag antibody (*green*), and nuclei were counterstained with DAPI (*blue*). **(B)** The transfected cells were treated with 200 μM H_2O_2 for 18 h or left untreated. The percentage of Annexin V-positive/PI-negative cells was determined by flow cytometry. Data are mean ± SEM ($n = 5$, $^{*}p < 0.05$ *vs.* EV $-H_2O_2$, $^{\#}p < 0.05$ *vs.* EV + H_2O_2). **(C)** Cells were treated as in **(B)**, and the amounts of full-length [Caspase 3 (full-length)] and cleaved Caspase 3 [Caspase 3 (cleaved)] were determined by immunoblot, Tubulin served as a loading control. *Left panel*: Representative immunoblots. *Right panel*: Semiquantitative analysis of cleaved Caspase 3; data are mean ± SEM and were normalized to EV transfected untreated cells ($n = 4$, $^{*}p < 0.05$ *vs.* EV $-H_2O_2$, $^{\#}p < 0.05$ *vs.* EV + H_2O_2). To see this illustration in color, the reader is referred to the web version of this article at www.liebertpub.com/ars

empty vector and APEX1 (21-318). As expected, co-transfection of empty vector and APEX1 (21-318) displayed the highest apoptosis induction (Fig. 4B). Interestingly, co-transfection of APEX1 wt and APEX1 (21-318) resulted in increased apoptosis induction compared to empty vector and APEX1 wt. Thus, the presence of APEX1 (21-318) seems to overcome the protective effect of APEX1 wt. Along the same line, APEX1 (21-318) increased cleaved Caspase 3 (Fig. 4C, D and Supplementary Fig. S4) and reduced Trx-1 protein levels (Fig. 4C, E and Supplementary Fig. S4).

These data further support an important role for the first 20 amino acids of APEX1 in apoptosis protection in endothelial cells. Therefore, we next cloned an expression vector for only the N-terminal region [APEX1 (1-20)] and investigated the impact of APEX1 (1-20) on basal- and H_2O_2-induced apoptosis and Caspase 3 activation. After expression of APEX1 (1-20), we first analyzed its localization pattern. The small protein can be found in the nucleus and in the cytosol (Fig. 5A). Overexpression of APEX1 (1-20) in endothelial cells resulted in inhibition of basal- and H_2O_2-induced apoptosis as well as Caspase 3 cleavage (Fig. 5B, C and Supplementary Fig. S5). Of note, the effects of APEX1 (1-20) are less pronounced than those of APEX1 wt (Fig. 1A, B). However, these data clearly demonstrate that the first 20 amino acids of APEX1 have anti-apoptotic properties in endothelial cells.

Next, we wanted to determine whether permanent re-expression of Trx-1 can overcome the pro-apoptotic effects of APEX1 (21-318). The stable re-expression of Trx-1 as well as expression of APEX1 (21-318) and cleavage of Caspase 3 were analyzed by immunostaining and immunoblots (Fig. 6 and Supplementary Fig. S6). As demonstrated in Figure 6B, only cells, which overexpress APEX1 (21-318), show an increase in cleaved Caspase 3 under conditions, where the protein levels of Trx-1 are not increased. This effect was completely blunted in cells with increased Trx-1 protein levels. Thus, the amount of Trx-1 protein determines the fate of endothelial cells.

Finally, we used an *in vivo* model of restenosis induction by carotid ligation. This model is characterized by increased oxidative stress, smooth muscle cell proliferation, and activation of the endothelium (10). The protein levels of Trx-1 and APEX1 in this model have not been determined before. However, activation of the endothelium and smooth muscle

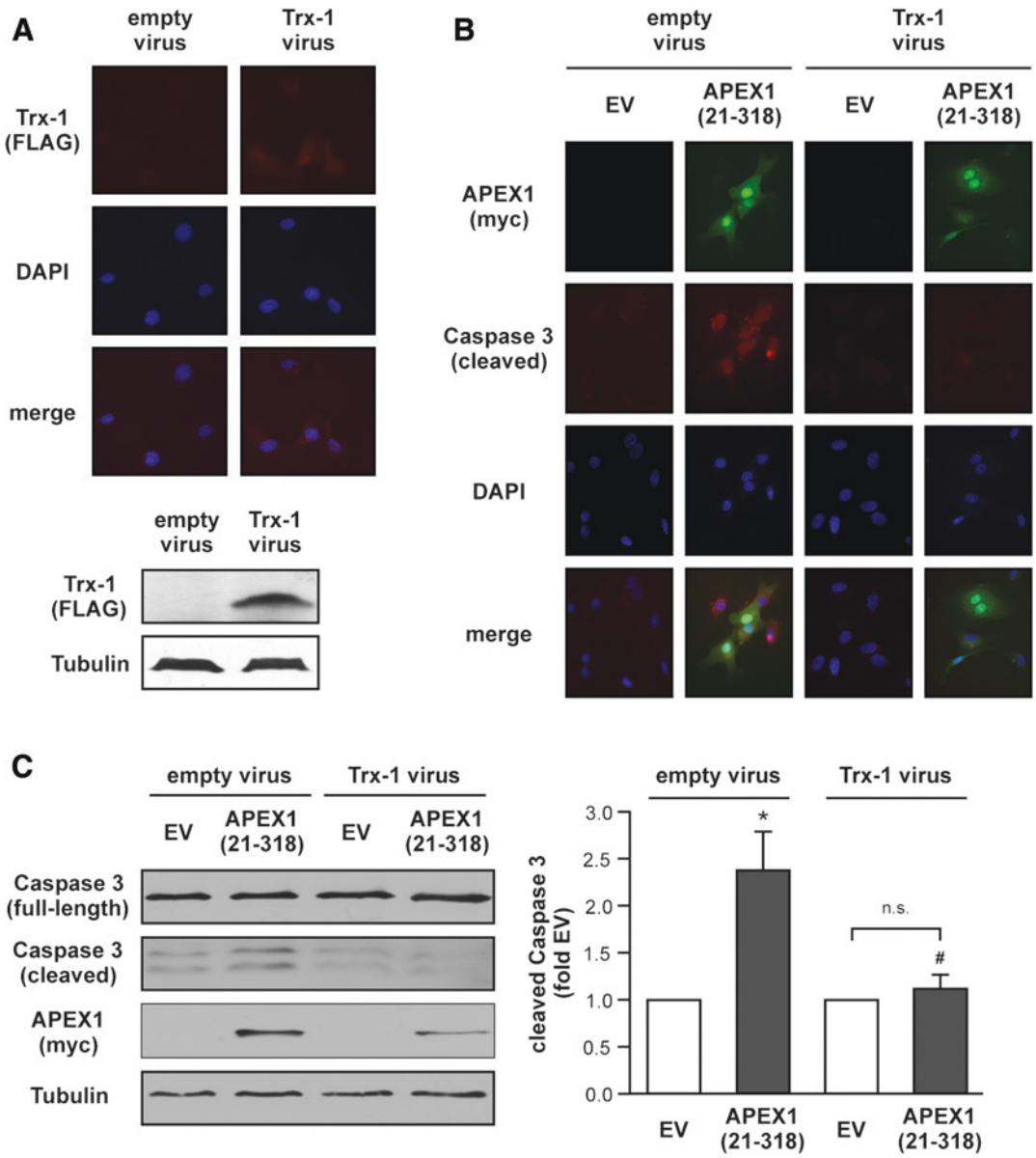

FIG. 6. Permanent Thioredoxin-1 re-expression prevents apoptosis induction and CatD activation by APEX1 (21-318). Endothelial cells were transduced with a lentiviral expression vector for FLAG-tagged Thioredoxin-1 (Trx-1 virus) or a lentivirus not containing the Trx-1 coding sequence (empty virus). Five days after transduction, the cells were transfected with an EV or an expression vector for APEX1 (21-318) and analyzed 1 day after transfection. **(A)** *Top panel*: Cells transduced with the different viruses and transfected with EV were stained for Thioredoxin-1 expressed from the lentivirus using a fluorescently labeled anti-FLAG antibody [Trx-1 (FLAG)] (*red*), and nuclei were counterstained with DAPI (*blue*). *Bottom panel*: Lysates from these cells were analyzed by immunoblot, Tubulin served as a loading control. **(B)** Cells transduced with the different viruses and transfected with EV or the expression vector for APEX1 (21-318) were stained for the APEX1 mutant with a fluorescently labeled anti-myc-tag antibody [APEX1 (myc)] (*green*) and with a fluorescently labeled antibody detecting cleaved Caspase 3 [Caspase 3 (cleaved)] (*red*), nuclei were counterstained with DAPI (*blue*). **(C)** Immunoblots were used to determine the amounts of full-length [Caspase 3 (full-length)] and cleaved Caspase 3 [Caspase 3 (cleaved)] and to verify expression of APEX1 (21-318) [APEX1 (myc)], Tubulin served as a loading control. *Left panel*: Representative immunoblots. *Right panel*: Semiquantitative analysis of cleaved Caspase 3; data are mean ± SEM and were normalized to the corresponding EV transfected cells [$n = 4$, $^{*}p < 0.05$ *vs.* empty virus/EV, $^{\#}p < 0.05$ *vs.* empty virus/APEX1 (21-318), n.s., not significant]. To see this illustration in color, the reader is referred to the web version of this article at www.liebertpub.com/ars

cell proliferation have been associated with altered APEX1 pathways like disturbed localization of APEX1, reduced activation of the transcription factor c-Jun, and increased ROS formation (11, 27). Furthermore, oxidative stress has been demonstrated to reduce Trx-1 levels in the endothelium (15, 19). Therefore, we investigated the protein levels of Trx-1 and APEX1 in CD31-positive cells in this model. As demonstrated in Figure 7, ligation leads to a loss of Trx-1 in the endothelium, whereas APEX1 levels seem to be unaltered in the endothelium but increased in smooth muscle cells.

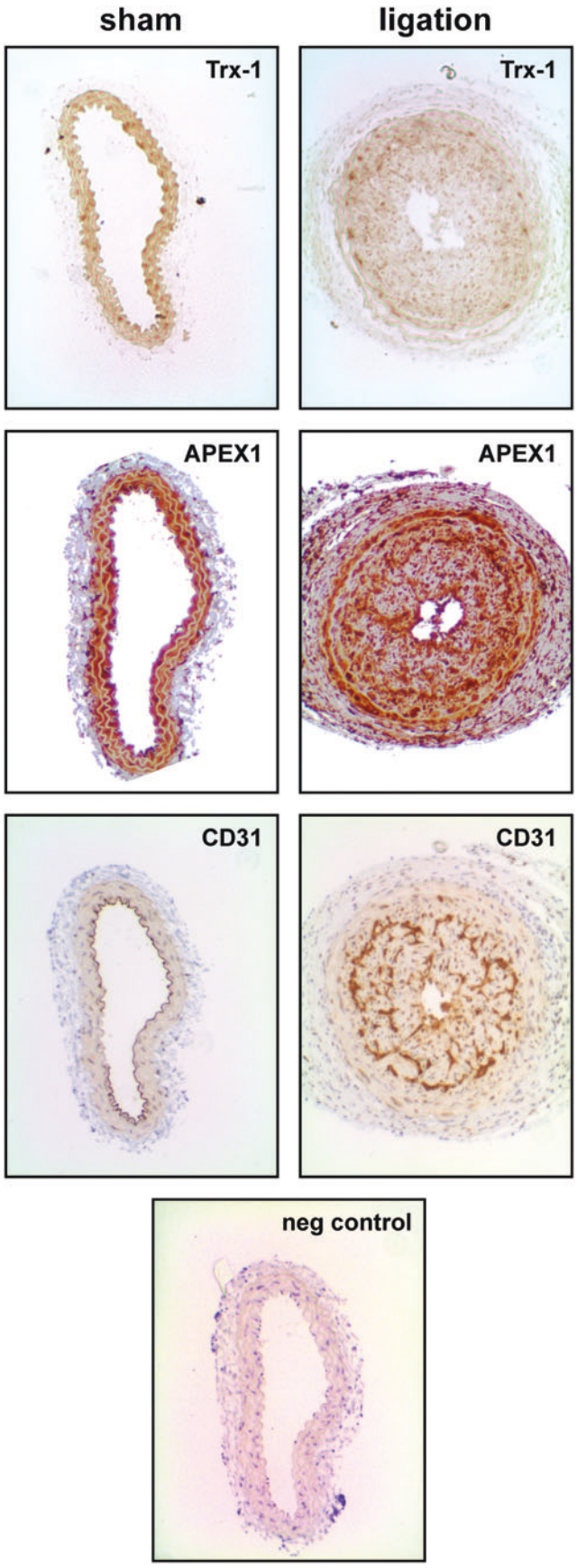

Discussion

The data of the present study show for the first time that APEX1 acts anti-apoptotic under physiological conditions by inhibiting CatD activity, and thus, Trx-1 degradation and Caspase 3 activation. This anti-apoptotic property depends on the first 20 amino acids of APEX1, since the APEX1 (21-318) mutant increases CatD cleavage and activity and induces Trx-1 degradation and Casapse-3 activation. Moreover, expression of a protein encompassing only these 20 amino acids can protect endothelial cells against apoptosis (Fig. 8). Under conditions of oxidative stress *ex vivo* and *in vivo*, Trx-1 is degraded and endothelial function is reduced.

Anti-apoptotic properties of APEX1 have been demonstrated in the hypoxic endothelium by Hall *et al.* (21). The authors showed that hypoxic conditions reduced APEX1 protein levels and transient overexpression inhibited apoptosis induction. It was speculated that the anti-apoptotic effect of APEX1 under hypoxia is dependent on NF-κB. However, under the hypoxic conditions chosen by Hall *et al.* (2% O_2), NF-κB was not activated, but APEX1 was still anti-apoptotic. In contrast, the anti-apoptotic effect of APEX1 in TNFα-treated endothelial cells was dependent on NF-κB activation. Therefore, it was suggested that APEX1 could act anti-apoptotic by stabilizing HIF1α under hypoxic conditions (21). This is supported by findings, which demonstrated that inhibition of APEX1 redox function reduced the transcription factor activity not only of NF-κB but also of HIF1α (13). Thus, APEX1 can influence transcription factors, but dependent on the conditions, different transcription factors are regulated by APEX1. Under our experimental conditions, APEX1 was neither able to induce the DNA binding activity of the p65 subunit of NF-κB (TransAM activity assay: $98\% \pm 12\%$ compared to EV transfected cells, $n=4$) nor could we find increased HIF1α protein levels (Supplementary Figs. 2 and S sup2).

However, we found here an additional mechanism, by which APEX1 stabilizes Trx-1 protein levels through inhibition of CatD processing, and thus, activation of this protease. Trx-1 is known to be essential for endothelial function as well as for survival of cells and organisms. Trx-1-deficient mice die shortly after implantation (32), demonstrating that Trx-1 is essential for early development of the mouse embryo. Along the same line, partial knockdown of Trx-1 in endothelial cells leads to cell death (20). Furthermore, senescence induction in endothelial cells is accompanied by loss of Trx-1 and can be rescued by lentiviral re-expression of Trx-1 (15). Therefore, our newly discovered mechanism,

FIG. 7. Carotid ligation reduces Thioredoxin-1 levels in the endothelium, while APEX1 is unaltered. Twelve-week-old mice were subjected to unilateral carotid artery ligation for 21 days (ligation), and the uninjured side served as control (sham). Paraffin sections of the carotids were stained for Thioredoxin-1 (Trx-1), APEX1, and CD31, in the negative control, primary antibodies were omitted. All sections were counterstained with Hematoxylin. Representative sections of a total of seven animals per group are shown. To see this illustration in color, the reader is referred to the web version of this article at www.liebertpub.com/ars

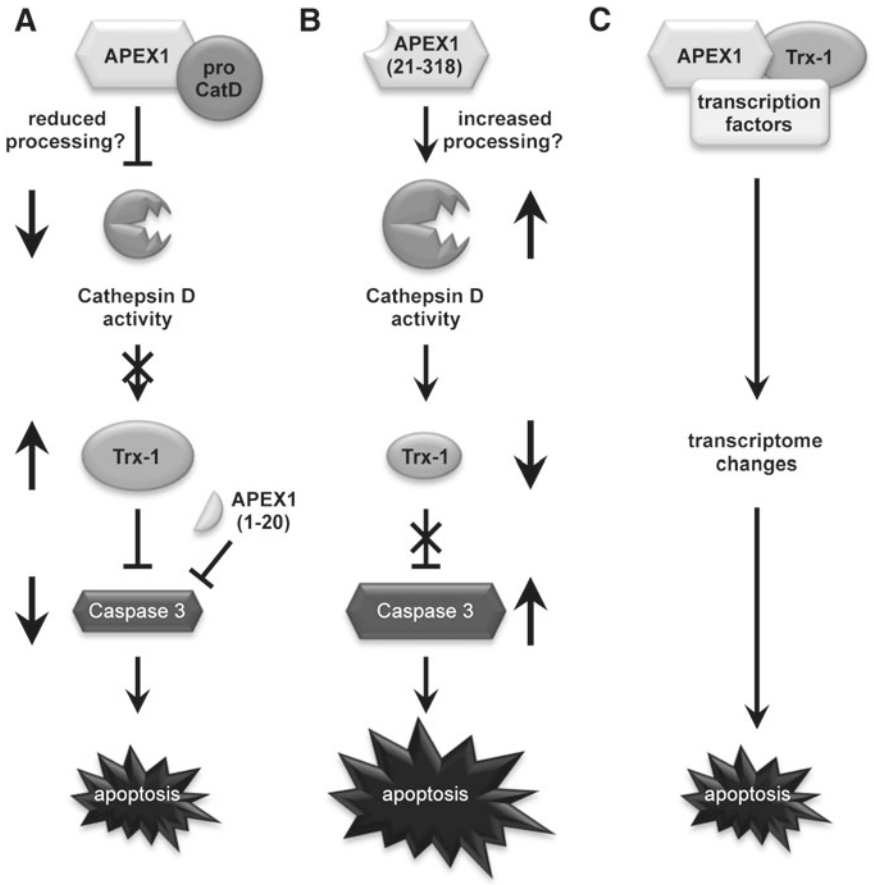

FIG. 8. Schematic representation of pathways for apoptosis protection by APEX1 and Trx-1. (A) APEX1 is associated with full-length cathepsin D (pro CatD) and inhibits its activation by diminishing its processing. This leads to reduced degradation of Thioredoxin-1 (Trx-1), and thus, an increase in the level of Trx-1. Trx-1, in turn, inhibits Caspase 3 and thereby suppresses apoptosis induction. The first 20 amino acids of APEX1 are able to protect against apoptosis by reducing Caspase 3 cleavage. **(B)** The N-terminally truncated mutant APEX1 (21-318) does not bind to unprocessed CatD. By an as yet unknown mechanism the mutant promotes CatD activation resulting in a loss of Trx-1 protein, diminished Caspase 3 inhibition, and increased apoptosis rates. **(C)** APEX1- in concert with Trx-1-regulates transcription factor activities leading to transcriptome changes and apoptosis inhibition.

which increases Trx-1 protein levels in endothelial cells, could be of therapeutic interest.

Unfortunately, it has to be noted that APEX1 as well as Trx-1 have been well described to be essential for tumor growth and both proteins are expressed in a variety of different tumors. One of the most important functions of APEX1 and Trx-1 in tumor development is the anti-apoptotic property of both enzymes. Interestingly, in cancer biology, the DNA repair domain of APEX1 seems to play an important role in protecting the tumors [for reviews see Refs. (6, 25)], whereas in endothelial cells, the DNA repair domain is dispensable for its anti-apoptotic properties – as we demonstrate here. Moreover, a huge effort has been undertaken to also characterize the redox domain within APEX1. This resulted in the design of small molecules to specifically inhibit the redox activity of APEX1. Those small molecules inhibited cancer cell growth as well as network formation of tumor endothelial cells (26). Thus, inhibition of the redox function of APEX1 could also be important for cancer therapy.

However, our experiments clearly show that the N-terminal 20 amino acids, and thus, most likely not the redox domain of APEX1, are required for apoptosis protection in endothelial cells. Structural analyses of APEX1 show that the first 62 amino acids of APEX1 seemingly do not adopt an ordered structure, while the remainder of the protein is characterized by extensive α-helices and β-sheets (PDBsum entry 3u8u at www.ebi.ac.uk/thornton-srv/databases/cgi-bin/pdbsum/GetPage.pl). The first 20 amino acids of APEX1 have been described as the nuclear localization signal (24). However, APEX1 (21-318) is still present in the nucleus (Fig. 2B and Supplementary Figs. 3 and S sup3), which excludes cytosolic retention as a potential mechanism for apoptosis induction by the truncated APEX1 (21-318) protein.

Moreover, the 33 N-terminal residues of APEX1 are required for complex formation with nucleophosmin, and it has been proposed that this interaction regulates the ability of the endonuclease to remove damaged RNA molecules (38). Damaged RNA molecules can be taken up by lysosomes (14), and thus, it is conceivable that a dysregulation of RNA metabolism can interfere with lysosomal activity. Therefore, impairment of RNA quality control might play a role in the regulation of cell death. Interestingly, in a model of *Helicobacter pylori* infection of gastrointestinal epithelial cells, it has been demonstrated that APEX1 can be acetylated at the lysine residues in position 6 or 7. This modification is important for its recruitment to a multiprotein complex on so-called negative calcium response elements. However, the acetylation status of APEX1 did not affect the transcriptional activity of p53 (7).

Notably, we did not observe changes in the CatD mRNA levels after overexpression of APEX1 (21-318), suggesting that the extreme N-terminus of APEX1 might not be involved in the activation of transcription factors regulating CatD expression, but may rather be involved in the processing of the enzyme precursor(s). Our data indicate that APEX1 interacts with unprocessed CatD (Fig. 4A), which might inhibit its processing. Interestingly, this interaction is not observed with the mutant APEX1 (21-318), which increases CatD cleavage and activity (Fig. 3C, D). Therefore, one could speculate that the N-terminally deleted APEX1 protein enhances the processing of CatD. However, the activation of

CatD requires multiple proteases, not all of which have been identified so far (33), and therefore, uncovering the mode of action of APEX1 (21-318) requires further studies, including complete characterization of the CatD processing cascade. However, other mechanisms could also be imagined, and future studies will hopefully uncover the mechanism by which APEX1 regulates CatD activation.

Innovation and Conclusion

In conclusion, we present here that characterization of the redox domain and the DNA repair domains of APEX1 is probably not sufficient to understand the full spectrum of its functions, because the N-terminus of APEX1 is required for the anti-apoptotic properties in the normal endothelium. Moreover, the N-terminus of APEX1 is crucial for the maintenance of Trx-1 protein levels. Re-expression of Trx-1 can block the pro-apoptotic properties of APEX1 (21-318), demonstrating that a certain Trx-1 level is essential to protect the endothelium. This can be also seen *in vivo* in the ligation model, in which loss of Trx-1 is present in the restenosis areas.

Besides the post-translational mechanisms demonstrated here, the regulation of transcription factors by APEX1 in concert with Trx-1 should not be overlooked (Fig. 8). Thus, depending on the cellular conditions, multiple APEX1- and Trx-1-dependent pathways might contribute to protection of the endothelium.

Materials and Methods

Cell culture

Primary human endothelial cells were cultured as previously described (17). After detachment with trypsin, cells were grown for at least 18 h as described (17).

Transient transfection of endothelial cells

Cells were transiently transfected with plasmid DNA using SuperFect (17) and with siRNAs using HiPerFect as described previously (18). Transfection reagents and siRNAs were purchased from Qiagen (Hilden, Germany).

Apoptosis assay

Detection of cell death was performed by flow cytometry using Annexin V-APC binding and PI staining as described previously (36); early apoptotic cells are Annexin V positive and PI negative.

Caspase 3/7 activity assay

Caspase 3/7 activity was measured using the Caspase 3 activity assay (Cell Signaling Technology, Frankfurt, Germany) with the following modifications: samples were lysed in CHAPS buffer (50 mM HEPES pH 7.5, 10% Sucrose, 0.5% Triton X-100, 0.1% CHAPS), including protease inhibitor cocktail (BioTool, Munich, Germany). Treatment of identically transfected endothelial cells with ZVAD (20 μM; Enzo Life Sciences GmbH, Lörrach, Germany) served as a negative control for the Caspase 3/7 activity measurements and was always subtracted from the corresponding sample. The remaining activity thus reflects solely Caspase 3/7 activity. DMSO was used as solvent control. Caspase 3/7 activity was normalized to protein content.

CatD activity assay

CatD activity was measured using CatD activity fluorimetric assay (BioVision, Milpitas, CA) according to the manufacturer's instructions. Human recombinant CatD (Sigma, Deisenhofen, Germany) was used as a positive control. Negative control samples were incubated with 1 μg/ml pepstatin A. The CatD activity was normalized to protein content.

Determination of NF-κB p65 DNA binding activity

The DNA binding activity of the p65 subunit of the transcription factor NF-κB was determined with the TransAM® NFκB p65 Transcription Factor ELISA Kit (Active Motif, La Hulpe, Belgium) according to the manufacturer's instructions.

Immunofluorescence staining

Endothelial cells were fixed in 4% paraformaldehyde, permeabilized for 15 min using 0.3% Triton X-100 and 3% bovine serum albumin in phosphate-buffered saline (PBS). For a direct immunostaining, cells were incubated with an anti-FLAG antibody directly conjugated with Alexa Fluor 594 (1:25; New England Biolabs, Frankfurt, Germany), an anti-myc-tag antibody directly conjugated with Alexa Fluor 488 (1:25; New England Biolabs, Frankfurt, Germany), or an anti-cleaved Caspase 3 antibody directly conjugated with Alexa Fluor 594 (1:25; New England Biolabs, Frankfurt, Germany) in PBS overnight at 4°C. Actin filaments were stained with Alexa Fluor 568-coupled phalloidin for 30 min at room temperature (1:100; Invitrogen, Karlsruhe, Germany). Nuclei were stained with 4′,6-diamidino-2-phenylindole (DAPI; Invitrogen, Karlsruhe, Germany) for 5 min at room temperature. Cells were washed and mounted with ProLong Gold antifade mounting medium (Invitrogen, Karlsruhe, Germany). Fluorescence images were taken with an AXIOVERT 200 M microscope (Zeiss, Jena, Germany, 40 × magnification, oil).

Preparation of protein lysates

Endothelial cells were washed with PBS and scraped off the dishes on ice. After centrifugation, the resulting pellet was lysed in RIPA-buffer for 30 min on ice. After removing cellular debris by centrifugation (16,000 × g, 15 min, 4°C), protein concentrations were measured using the Bradford protein assay (BioRad, Munich, Germany).

Immunoblotting

Immunoblotting was performed as previously described (18). Blotting membranes were incubated with primary antibodies directed against myc-tag, Caspase 3, HIF1α (1:500 and 1:300, respectively, all Cell Signaling Technology, Frankfurt, Germany), Trx-1, CatD (both 1:500; Abcam, Berlin, Germany), TIM23 (1:500; BD Biosciences, Heidelberg, Germany), Topoisomerase I (1:250; Santa Cruz Biotechnology, Heidelberg, Germany), PTP1B (1:1000; ECM Biosciences, Cologne, Germany), or Tubulin, FLAG (1:50,000 and 1:300, respectively, both Sigma, Deisenhofen, Germany) overnight at 4°C, before they were washed and incubated with secondary antibodies according to standard

procedures. Detection was performed by enhanced chemiluminescence using the ECL reagent (GE Healthcare, Freiburg, Germany) and standard X-ray films. Semi-quantitative analyses were performed on scanned X-ray films using ImageJ 1.42q (1).

Immunoprecipitation

Lysates (500 μg) were immunoprecipitated with 5 μg anti-myc-tag antibody or 5 μg anti-FLAG antibody overnight at 4°C. After incubation with protein A and G Sepharose (GE Healthcare, Solingen, Germany) for 2 h at 4°C, the beads were washed, resuspended in SDS-PAGE sample buffer, and subjected to gel electrophoresis on a 10% SDS-PAGE gel.

Cloning of APEX1 expression vectors

The APEX1 coding sequence without the translation termination codon was amplified from human endothelial cell cDNA using the primers hAPEX1 NT for1 (5′-CTCGAG AATTCCACCATGCCGAAGCGTGGGAAAAAG-3′) and hAPEX1 CT rev1 (5′-GCGCAAGCTTCAGTGCTAGGTA TAGGGTGAT-3′). The resulting amplification product was cut with *Eco*RI and *Hin*dIII and inserted into pcDNA.3.1™/myc-His(-) (Invitrogen, Karlsruhe, Germany) opened with the same enzymes, thereby creating a contiguous reading frame from the APEX1 coding sequence into the the C-terminal myc/His_6-epitope-tag. An identical approach was chosen for the two APEX1 deletion mutants APEX1 (1-127) and APEX1 (21-318). For the mutant APEX1 (21-318), an ATG initiation codon was introduced directly 5′ to the codon for proline in position 21. To create the expression vector for the mutant APEX1 (1-20) the downstream primer contained the coding sequence for a myc-epitope tag, and the resulting amplification product was used to replace the myc-His_6-epitope tag in pcDNA.3.1/myc-His(-). The identity of all plasmids was confirmed by restriction enzyme digestion and DNA sequencing of the APEX1 coding region.

Semiquantitative reverse transcriptase polymerase chain reaction

RNA isolation and cDNA synthesis were performed as previously described (18). Gene-specific mRNA levels were determined by semiquantitative real-time polymerase chain reaction using a Rotor-Gene Q (Qiagen, Hilden, Germany). For the detection of the CatD cDNA, the primers hCTSD Ex07/08 for1 (5′-TCAGGGCGAGTACATGATCC-3′) and hCTSD Ex09 rev1 (5′-ATGTCCATGCCCATGAAGCC-3′) were used, for the APEX1 cDNA hAPEX1 Ex04 for1 (5′-ACAAGGAAGGGTACAGTGGC-3′) and hAPEX1 Ex05 rev1 (5′-GCCTTCCTGATCATGCTCCT-3′). The ERK2 and RPL32 cDNAs were amplified as controls for normalization using the primers hERK2 Ex08 for1 (5′-TGCTAG ATTCCAGCCAGGAT-3′) and hERK2 Ex09 rev1 (5′-ACGGCTCAAAGGAGTCAAAG-3′) or hmRPL32 Ex02 for1 (5′-GTGAAGCCCAAGATCGTCAA-3′) and hmRPL32 Ex03 rev1 (5′-TTGTTGCACATCAGCAGCAC-3′), respectively. All primer pairs were designed such that the two different primers are separated by an intron. Relative expression of APEX1 and CatD was calculated by the $\Delta\Delta C_t$ method (35).

Production of lentiviral particles and transduction of endothelial cells

Virus production, concentration, and titration, as well as transduction of endothelial cells were performed as previously described (15). Endothelial cells were transduced with a multiplicity of infection of 15.

Animals

Wild-type mice were purchased from Jackson Laboratories (Bar Harbor, ME). Fourteen age-matched male mice aged 12 weeks on a regular chow diet were used for the carotid ligation procedure. The University of Virginia Animal Care and Use Committee approved all procedures and protocols used in this study.

Carotid ligation

Twelve-week-old mice received a daily heparin dose of 600 U/kg/day beginning 30 min before surgery and continuing for 4 days postsurgery. Mice were anesthetized with an intraperitoneal injection of 80 mg/kg Ketamine. The ventral surface of the neck was shaved, wiped with betadine and 70% ethanol, and a midline incision was made through the skin. The right common carotid artery was exposed and completely ligated just proximal to the carotid bifurcation. The left carotid artery served as an uninjured control. Both carotid arteries were harvested 21 days after injury and embedded transversely in paraffin. Six micrometer cross-sections of vessels were prepared and stained for Trx-1, APEX1, and CD31; for the negative control, the primary antibody was omitted. Paraffin sections were removed from xylene, deparaffinized, and rehydrated with dH_2O. Briefly, the staining involved endogenous peroxidase staining for 30 min, antigen retrieval for 20 min, blocking with avidin/biotin blocking kit (Vector Laboratories, Burlingame, CA), secondary antibody staining for 1 h, followed by immunoperoxidase staining with Vectastain Elite ABC Kit (PK-6100; Vector Laboratories), and finally visualizing the stain using DAB (3,3-diaminobenzidine) HRP substrate. Hematoxylin was used as the counterstain for all sections imaged.

Acknowledgments

P.J. is a scholarship holder of the IRTG1902. This work was, in part, supported by the following grants: Deutsche Forschungsgemeinschaft (HA2868/9-1, HA2868/10-1, IRTG1902 P2) and Forschungskommission of the Medical Faculty, University of Duesseldorf (28/2014) to J.H.; NIH grant R01 DK096076 to N.L.; Deutsche Forschungsgemeinschaft (AL288/2-1, IRTG1902 P1) to J.A. V.S. was supported by a training grant NIH T32 GM007055-42 and an American Heart Association predoctoral fellowship 15PRE25560036.

Author Disclosure Statement

No competing financial interests exist.

References

1. Abramoff MD, Magelhaes PJ, and Ram SJ. Image processing with ImageJ. *Biophotonics Int* 11: 36–42, 2004.

2. Akamatsu Y, Ohno T, Hirota K, Kagoshima H, Yodoi J, and Shigesada K. Redox regulation of the DNA binding activity in transcription factor PEBP2. The roles of two conserved cysteine residues. *J Biol Chem* 272: 14497–14500, 1997.
3. Altschmied J and Haendeler J. Thioredoxin-1 and endothelial cell aging: role in cardiovascular diseases. *Antioxid Redox Signal* 11: 1733–1740, 2009.
4. Ando K, Hirao S, Kabe Y, Ogura Y, Sato I, Yamaguchi Y, Wada T, and Handa H. A new APE1/Ref-1-dependent pathway leading to reduction of NF-kappaB and AP-1, and activation of their DNA-binding activity. *Nucleic Acids Res* 36: 4327–4336, 2008.
5. Arany Z, Huang LE, Eckner R, Bhattacharya S, Jiang C, Goldberg MA, Bunn HF, and Livingston DM. An essential role for p300/CBP in the cellular response to hypoxia. *Proc Natl Acad Sci U S A* 93: 12969–12973, 1996.
6. Bapat A, Fishel ML, and Kelley MR. Going ape as an approach to cancer therapeutics. *Antioxid Redox Signal* 11: 651–668, 2009.
7. Bhattacharya V, McSweeney PA, Shi Q, Bruno B, Ishida A, Nash R, Storb RF, Sauvage LR, Hammond WP, and Wu MH. Enhanced endothelialization and microvessel formation in polyester grafts seeded with CD34(+) bone marrow cells. *Blood* 95: 581–585, 2000.
8. Brook RD. Cardiovascular effects of air pollution. *Clin Sci (Lond)* 115: 175–187, 2008.
9. Chen B, Guan D, Cui ZJ, Wang X, and Shen X. Thioredoxin 1 downregulates MCP-1 secretion and expression in human endothelial cells by suppressing nuclear translocation of activator protein 1 and redox factor-1. *Am J Physiol Cell Physiol* 298: C1170–C1179, 2010.
10. Chiu JJ and Chien S. Effects of disturbed flow on vascular endothelium: pathophysiological basis and clinical perspectives. *Physiol Rev* 91: 327–387, 2011.
11. Chyu KY, Dimayuga PC, Zhao X, Nilsson J, Shah PK, and Cercek B. Altered AP-1/Ref-1 redox pathway and reduced proliferative response in iNOS-deficient vascular smooth muscle cells. *Vasc Med* 9: 177–183, 2004.
12. Feuerstein G, Yue TL, Ma X, and Ruffolo RR. Novel mechanisms in the treatment of heart failure: inhibition of oxygen radicals and apoptosis by carvedilol. *Prog Cardiovasc Dis* 48: 17–24, 1998.
13. Fishel ML, Jiang Y, Rajeshkumar NV, Scandura G, Sinn AL, He Y, Shen C, Jones DR, Pollok KE, Ivan M, Maitra A, and Kelley MR. Impact of APE1/Ref-1 redox inhibition on pancreatic tumor growth. *Mol Cancer Ther* 10: 1698–1708, 2011.
14. Fujiwara Y, Furuta A, Kikuchi H, Aizawa S, Hatanaka Y, Konya C, Uchida K, Yoshimura A, Tamai Y, Wada K, and Kabuta T. Discovery of a novel type of autophagy targeting RNA. *Autophagy* 9: 403–409, 2013.
15. Goy C, Czypiorski P, Altschmied J, Jakob S, Rabanter LL, Brewer AC, Ale-Agha N, Dyballa-Rukes N, Shah AM, and Haendeler J. The imbalanced redox status in senescent endothelial cells is due to dysregulated Thioredoxin-1 and NADPH oxidase 4. *Exp Gerontol* 56: 45–52, 2014.
16. Gurusamy N, Malik G, Gorbunov NV, and Das DK. Redox activation of Ref-1 potentiates cell survival following myocardial ischemia reperfusion injury. *Free Radic Biol Med* 43: 397–407, 2007.
17. Haendeler J, Hoffmann J, Tischler V, Berk BC, Zeiher AM, and Dimmeler S. Redox regulatory and anti-apoptotic functions of thioredoxin depend on S-nitrosylation at cysteine 69. *Nat Cell Biol* 4: 743–749, 2002.
18. Haendeler J, Mlynek A, Buchner N, Lukosz M, Graf M, Guettler C, Jakob S, Farrokh S, Kunze K, Goy C, Guardiola-Serrano F, Schaal H, Cortese-Krott M, Deenen R, Kohrer K, Winkler C, and Altschmied J. Two isoforms of sister-of-mammalian grainyhead have opposing functions in endothelial cells and in vivo. *Arterioscler Thromb Vasc Biol* 33: 1639–1646, 2013.
19. Haendeler J, Popp R, Goy C, Tischler V, Zeiher AM, and Dimmeler S. Cathepsin D and H_2O_2 stimulate degradation of thioredoxin-1: implication for endothelial cell apoptosis. *J Biol Chem* 280: 42945–42951, 2005.
20. Haendeler J, Tischler V, Hoffmann J, Zeiher AM, and Dimmeler S. Low doses of reactive oxygen species protect endothelial cells from apoptosis by increasing thioredoxin-1 expression. *FEBS Lett* 577: 427–433, 2004.
21. Hall JL, Wang X, Van A, Zhao Y, and Gibbons GH. Overexpression of Ref-1 inhibits hypoxia and tumor necrosis factor-induced endothelial cell apoptosis through nuclear factor-kappab-independent and -dependent pathways. *Circ Res* 88: 1247–1253, 2001.
22. Hirota K, Matsui M, Iwata S, Nishiyama A, Mori K, and Yodoi J. AP-1 transcriptional activity is regulated by a direct association between thioredoxin and Ref-1. *Proc Natl Acad Sci U S A* 94: 3633–3638, 1997.
23. Huang LE, Arany Z, Livingston DM, and Bunn HF. Activation of hypoxia-inducible transcription factor depends primarily upon redox-sensitive stabilization of its alpha subunit. *J Biol Chem* 271: 32253–32259, 1996.
24. Jackson EB, Theriot CA, Chattopadhyay R, Mitra S, and Izumi T. Analysis of nuclear transport signals in the human apurinic/apyrimidinic endonuclease (APE1/Ref1). *Nucleic Acids Res* 33: 3303–3312, 2005.
25. Kelley MR and Fishel ML. DNA repair proteins as molecular targets for cancer therapeutics. *Anticancer Agents Med Chem* 8: 417–425, 2008.
26. Kelley MR, Luo M, Reed A, Su D, Delaplane S, Borch RF, Nyland RL, II, Gross ML, and Georgiadis MM. Functional analysis of novel analogues of E3330 that block the redox signaling activity of the multifunctional AP endonuclease/redox signaling enzyme APE1/Ref-1. *Antioxid Redox Signal* 14: 1387–1401, 2011.
27. Kim CS, Son SJ, Kim EK, Kim SN, Yoo DG, Kim HS, Ryoo SW, Lee SD, Irani K, and Jeon BH. Apurinic/apyrimidinic endonuclease1/redox factor-1 inhibits monocyte adhesion in endothelial cells. *Cardiovasc Res* 69: 520–526, 2006.
28. Kureishi Y, Luo Z, Shiojima I, Bialik A, Fulton D, Lefer DJ, Sessa WC, and Walsh K. The HMG-CoA reductase inhibitor simvastatin activates the protein kinase Akt and promotes angiogenesis in normocholesterolemic animals. *Nat Med* 6: 1004–1010, 2000.
29. Li M and Wilson DM, III. Human apurinic/apyrimidinic endonuclease 1. *Antioxid Redox Signal* 20: 678–707, 2014.
30. Lukosz M, Jakob S, Büchner N, Zschauer TC, Altschmied J, and Haendeler J. Nuclear redox signaling. *Antioxid Redox Signal* 12: 713–742, 2010.
31. Luo M, Delaplane S, Jiang A, Reed A, He Y, Fishel M, Nyland RL, II, Borch RF, Qiao X, Georgiadis MM, and Kelley MR. Role of the multifunctional DNA repair and redox signaling protein Ape1/Ref-1 in cancer and endothelial cells: small-molecule inhibition of the redox function of Ape1. *Antioxid Redox Signal* 10: 1853–1867, 2008.
32. Matsui M, Oshima M, Oshima H, Takaku K, Maruyama T, Yodoi J, and Taketo MM. Early embryonic lethality caused

by targeted disruption of the mouse thioredoxin gene. *Dev Biol* 178: 179–185., 1996.
33. Minarowska A, Gacko M, Karwowska A, and Minarowski L. Human cathepsin D. *Folia Histochem Cytobiol* 46: 23–38, 2008.
34. Roberg K, Kagedal K, and Ollinger K. Microinjection of cathepsin d induces caspase-dependent apoptosis in fibroblasts. *Am J Pathol* 161: 89–96, 2002.
35. Schmittgen TD and Livak KJ. Analyzing real-time PCR data by the comparative C(T) method. *Nat Protoc* 3: 1101–1108, 2008.
36. Schroeder P, Popp R, Wiegand B, Altschmied J, and Haendeler J. Nuclear redox-signaling is essential for apoptosis inhibition in endothelial cells—important role for nuclear thioredoxin-1. *Arterioscler Thromb Vasc Biol* 27: 2325–2331, 2007.
37. Toda N. Age-related changes in endothelial function and blood flow regulation. *Pharmacol Ther* 133: 159–176, 2012.
38. Vascotto C, Fantini D, Romanello M, Cesaratto L, Deganuto M, Leonardi A, Radicella JP, Kelley MR, D'Ambrosio C, Scaloni A, Quadrifoglio F, and Tell G. APE1/Ref-1 interacts with NPM1 within nucleoli and plays a role in the rRNA quality control process. *Mol Cell Biol* 29: 1834–1854, 2009.
39. Walker LJ, Robson CN, Black E, Gillespie D, and Hickson ID. Identification of residues in the human DNA repair enzyme HAP1 (Ref-1) that are essential for redox regulation of Jun DNA binding. *Mol Cell Biol* 13: 5370–5376, 1993.
40. Walter DH, Haendeler J, Galle J, Zeiher AM, and Dimmeler S. Cyclosporin A inhibits apoptosis of human endothelial cells by preventing release of cytochrome C from mitochondria. *Circulation* 98: 1153–1157, 1998.
41. Wei SJ, Botero A, Hirota K, Bradbury CM, Markovina S, Laszlo A, Spitz DR, Goswami PC, Yodoi J, and Gius D. Thioredoxin nuclear translocation and interaction with redox factor-1 activates the activator protein-1 transcription factor in response to ionizing radiation. *Cancer Res* 60: 6688–6695, 2000.
42. Wei Z, Costa K, Al-Mehdi AB, Dodia C, Muzykantov V, and Fisher AB. Simulated ischemia in flow-adapted endothelial cells leads to generation of reactive oxygen species and cell signaling. *Circ Res* 85: 682–689., 1999.
43. Werner C, Gensch C, Poss J, Haendeler J, Bohm M, and Laufs U. Pioglitazone activates aortic telomerase and prevents stress-induced endothelial apoptosis. *Atherosclerosis* 216: 23–34, 2011.
44. Widlansky ME, Gokce N, Keaney JF, Jr, and Vita JA. The clinical implications of endothelial dysfunction. *J Am Coll Cardiol* 42: 1149–1160, 2003.
45. Xanthoudakis S, Miao GG, and Curran T. The redox and DNA-repair activities of Ref-1 are encoded by nonoverlapping domains. *Proc Natl Acad Sci U S A* 91: 23–27, 1994.
46. Xanthoudakis S, Smeyne RJ, Wallace JD, and Curran T. The redox/DNA repair protein, Ref-1, is essential for early embryonic development in mice. *Proc Natl Acad Sci U S A* 93: 8919–8923, 1996.
47. Zhang X, Hu K, and Li CY. Protection against oxidized low-density lipoprotein-induced vascular endothelial cell death by integrin-linked kinase. *Circulation* 104: 2762–2766, 2001.
48. Zschauer TC, Kunze K, Jakob S, Haendeler J, and Altschmied J. Oxidative stress-induced degradation of thioredoxin-1 and apoptosis is inhibited by thioredoxin-1-actin interaction in endothelial cells. *Arterioscler Thromb Vasc Biol* 31: 650–656, 2011.

Address correspondence to:
Prof. Judith Haendeler
IUF-Leibniz Research Institute
for Environmental Medicine
Auf'm Hennekamp 50
40225 Duesseldorf
Germany

E-mail: juhae001@uni-duesseldorf.de

Dr. Joachim Altschmied
IUF-Leibniz Research Institute
for Environmental Medicine
Auf'm Hennekamp 50
40225 Duesseldorf
Germany

E-mail: joalt001@uni-duesseldorf.de

Date of first submission to ARS Central, June 26, 2016; date of final revised submission, November 9, 2016; date of acceptance, November 11, 2016.

Abbreviations Used

APEX1 = APEX nuclease (multifunctional DNA repair enzyme) 1
CatD = cathepsin D
CD31 = platelet/endothelial cell adhesion molecule 1 (PECAM-1)
HIF1α = hypoxia inducible factor 1 alpha
NF-κB = nuclear factor kappa B
PI = propidium iodide
ROS = reactive oxygen species
TIM23 = translocase of inner mitochondrial membrane 23
Trx-1 = thioredoxin-1

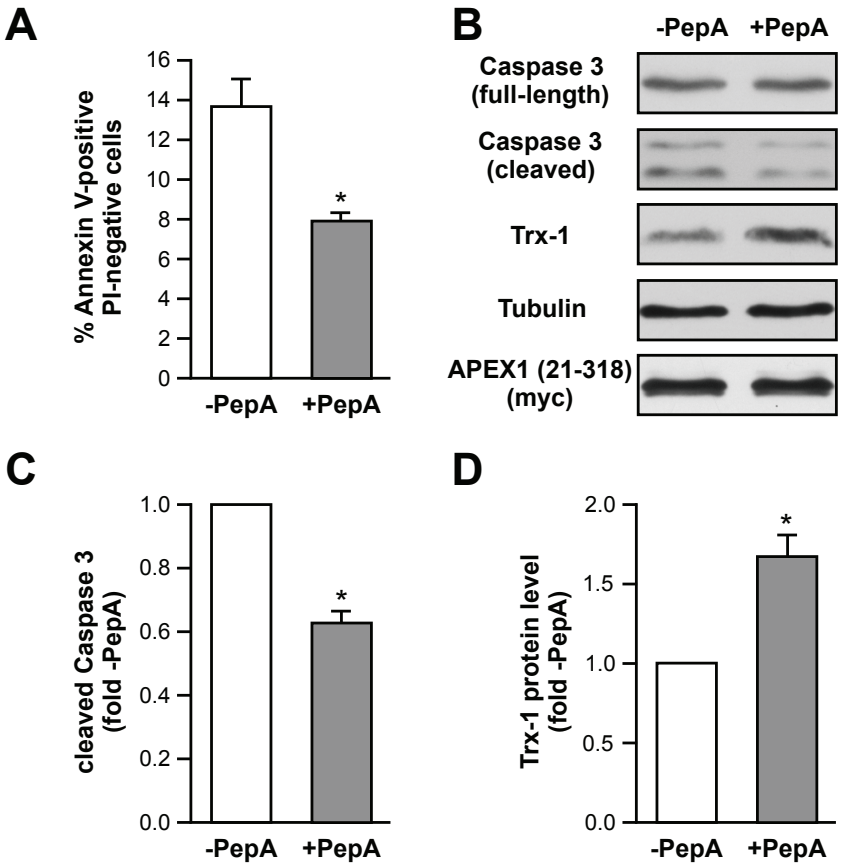

Supplementary Figure 1: Inhibition of Cathepsin D reduces apoptosis and Caspase-3 activation by APEX1 (21-318) and prevents Thioredoxin-1 degradation. EC were transfected with an expression vector for the N-terminally truncated APEX1 (21-318) and treated with 1 µM PepstatinA-penetratin (+PepA) or left untreated (-PepA). 1 day after transfection the cells were either analyzed for early apoptosis or lysed and the lysates were subjected to SDS-PAGE. **(A)** Percentage of Annexin V-positive/PI-negative cells; data are mean ± SEM (n=3, *p<0.05 vs. -PepA). **(B)** Representative immunoblots of full-length (Caspase 3 (full-length)), cleaved Caspase 3 (Caspase 3 (cleaved)) and Thioredoxin-1 (Trx-1); Tubulin served as a loading control. APEX1 (21-318) overexpression was verified with an antibody against the C-terminal myc-tag (APEX1 (21-318) (myc)). **(C)** Semi-quantitative analysis of cleaved Caspase 3; data are mean ± SEM and were normalized to untreated cells (n=3, *p<0.05 vs. -PepA). **(D)** Semi-quantitative analysis of Trx-1 protein levels; data are mean ± SEM and were normalized to untreated cells (n=3, *p<0.05 vs. -PepA).

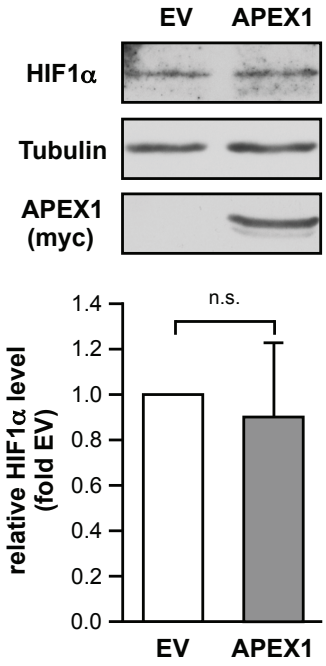

Supplementary Figure 2: Overexpression of APEX1 does not change HIF1α levels. EC were transfected with an empty vector (EV) or an expression vector for full-length APEX1 (APEX1). 1 day after transfection the cells were lysed and the lysates subjected to SDS-PAGE. HIF1α was detected by immunoblot, Tubulin served as a loading control. APEX1 overexpression was verified with an antibody against the C-terminal myc-tag (APEX1 (myc)). Top panel: Representative immunoblots. Bottom panel: semi-quantitative analysis of HIF1α protein amounts; data are mean ± SEM and were normalized to EV transfected cells (n=4, n.s. = not significant).

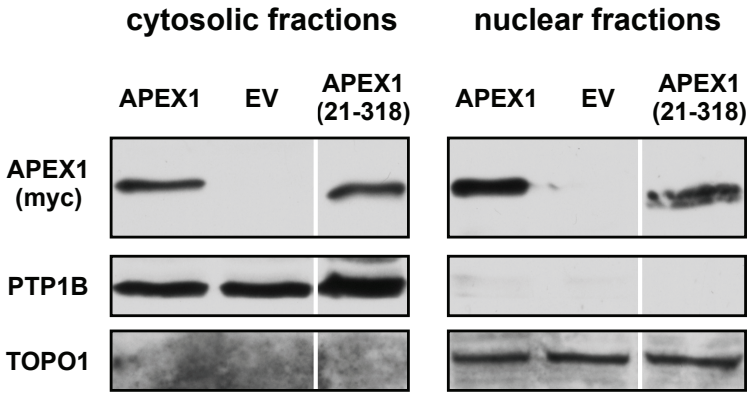

Supplementary Figure 3: Deletion of the N-terminal 20 amino acids of APEX1 does not change subcellular localization. EC were transfected with an empty vector (EV) or expression vectors for full-length APEX1 (APEX1) or the N-terminally truncated mutant APEX1 (21-318). 1 day after transfection cells were fractionated into cytosolic and nuclear fractions using the NE-PER™ Nuclear and Cytoplasmic Extraction Reagent (ThemoFischer Scientific, Schwerte, Germany). The fractions were subjected to SDS-PAGE and the APEX1 variants were detected by immunoblot (APEX1 (myc)). The purity of the fractions was assessed by detection of Protein-Tyrosine Phosphatase 1B (PTP1B) as cytosolic marker and Topoisomerase I (TOPO1) as nuclear marker. As can be seen, APEX1 and APEX1 (21-318) are both found in the cytosol and in the nucleus.

Nuclear factor (erythroid-derived 2)-like 2 and Thioredoxin-1 in atherosclerosis and ischemia/reperfusion injury in the heart

Jakobs P*, Serbulea V*, Leitinger N, Eckers A#, Haendeler J#

Antioxid Redox Signal. 2017; 26: 630-644 *Gleichberechtigte Erstautoren; #Gleichberechtigte Letztautoren

Autoren:

Jakobs P: Erstautor, schrieb den Teil zu Thioredoxin-1 in Atherosklerose und nach Ischämie/Reperfusions Schäden im Herzen. Erstellte alle Abbildungen.

Serbulea V: Erstautor, schrieb den Teil zu Nrf2 Teil in Atherosklerose und nach Ischämie/Reperfusions Schäden im Herzen.

Leitinger N: Ko-Autor, Schrieb zusammen mit Frau Haendeler und Frau Eckers die Einleitung und das Fazit. Zudem korrigierte er den von Vlad Serbulea geschriebenen Nrf2 Teil.

Eckers A: Senior-Autorin, Schrieb zusammen Frau Haendeler und Herrn Leitinger die Einleitung und das Fazit. Korrigierte alle Abbildungen.

Haendeler J: Senior-Autorin, Schrieb zusammen mit Herrn Leitinger und Frau Eckers die Einleitung und das Fazit. Zudem korrigierte sie den von Philipp Jakobs geschriebenen Thioredoxin-1 Teil, revidierte das gesamte Manuskript

Mary Ann Liebert, Inc. publishers

Prof. Dr. Jojo Haendeler
University of Duesseldorf
IUF - Leibniz Research Institute for Environmental Medicine
Auf`m Hennekamp 50
40225 Duesseldorf
Germany

May 16, 2018

Dear Dr. Haendeler:

Copyright permission is granted to Philipp Jakobs to use the figures from the articles below for his thesis.

"Nuclear Factor (Erythroid-Derived 2)-Like 2 and Thioredoxin-1 in Atherosclerosis and Ischemia/Reperfusion Injury in the Heart"
By Philipp Jakobs, Vlad Serbulea, Norbert Leitinger, Anna Eckers, and Judith Haendeler
Antioxidants & Redox Signaling Volume: 26 Issue 12: April 20, 2017
http://doi.org/10.1089/ars.2016.6795

"The Anti-Apoptotic Properties of APEX1 in the Endothelium Require the First 20 Amino Acids and Converge on Thioredoxin-1"
By Nadine Dyballa-Rukes, Philipp Jakobs, Anna Eckers, Niloofar Ale-Agha, Vlad Serbulea, Karin Aufenvenne, Tim-Christian Zschauer, Lothar L. Rabanter, Sascha Jakob, Florian von Ameln, Olaf Eckermann, Norbert Leitinger, Christine Goy, Joachim Altschmied, and Judith Haendeler
Antioxidants & Redox Signaling Volume: 26 Issue 12: April 20, 2017
http://doi.org/10.1089/ars.2016.6799

Kind Regards,

Karen Ballen
Manager, Copyright Permission
Mary Ann Liebert, Inc., publishers
KBallen@liebertpub.com

ANTIOXIDANTS & REDOX SIGNALING
Volume 26, Number 12, 2017

DOI: 10.1089/ars.2016.6795

Discoveries

FORUM REVIEW ARTICLE

Nuclear Factor (Erythroid-Derived 2)-Like 2 and Thioredoxin-1 in Atherosclerosis and Ischemia/Reperfusion Injury in the Heart

Philipp Jakobs,[1,*] Vlad Serbulea,[2,*] Norbert Leitinger,[2,3] Anna Eckers,[1,#] and Judith Haendeler[1,4,#]

Abstract

Significance: Redox signaling is one of the key elements involved in cardiovascular diseases. Two important molecules are the transcription factor nuclear factor erythroid 2-related factor 2 (Nrf2) and the oxidoreductase thioredoxin-1 (Trx-1).
Recent Advances: During the previous years, a lot of studies investigated Nrf2 and Trx-1 as protective proteins in cardiovascular disorders. Moreover, post-translational modifications of those molecules were identified that play an important role in the cardiovascular system. This review will summarize changes in the vasculature in atherosclerosis and ischemia reperfusion injury of the heart and the newest findings achieved with Nrf2 and Trx-1 therein. Interestingly, Nrf2 and Trx-1 can act together as well as independently of each other in protection against atherosclerosis and ischemia and reperfusion injury.
Critical Issues: In principle, pharmacological activation of a transcription factor-like Nrf2 can be dangerous, since a transcription regulator has multiple targets and the pleiotropic effects of such activation should not be ignored. Moreover, overactivation of Nrf2 as well as long-term treatment with Trx-1 could be deleterious for the cardiovascular system.
Future Directions: Therefore, the length of treatment with Nrf2 activators and/or Trx-1 has first to be studied in more detail in cardiovascular disorders. Moreover, a combination of Nrf2 activators and Trx-1 should be investigated and taken into consideration. *Antioxid. Redox Signal.* 26, 630–644.

Keywords: atherosclerosis, ischemia and reperfusion injury, Nrf2, Trx-1

Introduction

Several cardiovascular diseases are tightly linked to disturbances in the redox status of the heart and vasculature, for example, atherosclerosis and acute and chronic myocardial infarction (MI). Several redox molecules, which play an important role in cardiovascular disorders, have been described and intensively reviewed. Decades ago, it had become evident that the antioxidative defense is impaired in cardiovascular disorders and thus, therapies using vitamin C and vitamin E have been conducted. In our days, it is evident that neither vitamin C nor vitamin E nor a combination is a successful therapy in cardiovascular disorders [for review, see Moser and Chun (72) and Saremi and Arora (90)]. Since application of vitamin C and E as antioxidants was rather unspecific, several studies were performed to understand why the antioxidative defense is impaired in cardiovascular disorders.

In the cardiovascular system, important antioxidative molecules are catalase, superoxide dismutases (SOD), glutathione, glutathione S-transferases, glutathione peroxidases, heme oxygenases, thioredoxin reductases, and thioredoxins. The expression of those antioxidative molecules can be

[1]IUF-Leibniz Research Institute for Environmental Medicine, Duesseldorf, Germany.
[2]Department of Pharmacology, University of Virginia, Charlottesville, Virginia.
[3]Cardiovascular Research Center, University of Virginia, Charlottesville, Virginia.
[4]Central Institute of Clinical Chemistry and Laboratory Medicine, Medical Faculty, University of Duesseldorf, Duesseldorf, Germany.
*Equal contributing first authors.
#Equal contributing senior authors.

regulated by the transcription factor Nuclear factor erythroid 2-related factor 2 (Nrf2). Genetic variants in Nrf2 and Nrf2 regulated genes have been associated with cardiovascular diseases (86). Therefore, activation of Nrf2 can be one potential therapeutic option in cardiovascular diseases. Over the previous years, it had become clear that thioredoxin-1 (Trx-1) was not only regulated by Nrf2 *via* the two antioxidant response elements (AREs) in its promoter but also that Trx-1 regulated Nrf2 by keeping Nrf2 in its reduced state and thus allowing Nrf2 to increase expression of antioxidative enzymes (63). Moreover, Trx-1 has been shown to regulate proteins by direct interaction in the cardiovascular system (114) and is, therefore, not solely an antioxidative molecule and could be of therapeutic interest in cardiovascular disorders. A combination of activation of Nrf2 and an increase in Trx-1 could be considered.

Thus, this review will first introduce Nrf2 and Trx-1 and then the effects of Nrf2 and Trx-1 in atherosclerosis and in ischemia reperfusion injury will be described.

Nuclear Factor Erythroid 2-Related Factor 2

Nrf2 is a transcription factor that binds to AREs in promoter regions of target genes to coordinate transcription of genes in response to oxidative stress. Nrf2 belongs to the transcription factor family of cap 'n' collar basic region leucine zipper (CNC-bZIP) proteins. Under basal conditions, Nrf2 remains sequestered in the cytoplasm by the Kelch-like ECH-associated protein 1 (Keap1) (Fig. 1). Keap1 is a cysteine rich protein that binds Nrf2 through cysteine residues, thereby inhibiting nuclear translocation of Nrf2 (56, 103). Protein levels of Nrf2 are moderate, because association with Keap1 leads not only to cytoplasmic retention but also to ubiquitination and proteasomal degradation of Nrf2 in a Cullin3-dependent manner, preventing basal expression of Nrf2 target genes (68). Oxidants and electrophiles serve as Nrf2 activators; however, the exact mechanism of activation remains unclear. Experimental evidence suggests that electrophilic molecules or oxidants induce the release of Nrf2 from the cytosolic complex by oxidation of cysteines within Keap1.

Regarding expression of Nrf2 itself, analyses with luciferase reporter systems demonstrated that activity of the Nrf2 promoter was enhanced by treatment with 3H-1,2-dithiole-3-thione (59). Moreover, 3H-1,2-dithiole-3-thione also increased Nrf2 messenger RNA (mRNA) and protein levels in the rat cardiac H9c2 cell line, which was accompanied with reduced intracellular reactive oxygen species (ROS) levels (11).

During vascular development, enhanced expression of Nrf2 has been reported in the tip cells of retinal vessels. Two models, one involving Nrf2 deficiency and another involving an endothelial-specific Nrf2 knockout, showed reduced angiogenic sprouting in the retina without changes in vascular endothelial growth factor (VEGF), implying that Nrf2 is a cell-autonomous regulator of angiogenesis (106).

Target genes of Nrf2 regulate drug metabolism, redox homeostasis, DNA repair, and inflammatory processes. The most prominent examples are SOD, Glutathione-S-transferase (GST), heme oxygenase-1 (HO-1), and thioredoxin reductase 1 (TrxR1). Besides increased sensitivity against oxidative stress, Nrf2-deficient mice show disturbances in lipid metabolism, which will be addressed in more detail in the sections: ''Role of Nrf2 in Atherosclerosis, Especially in the Endothelium'' and

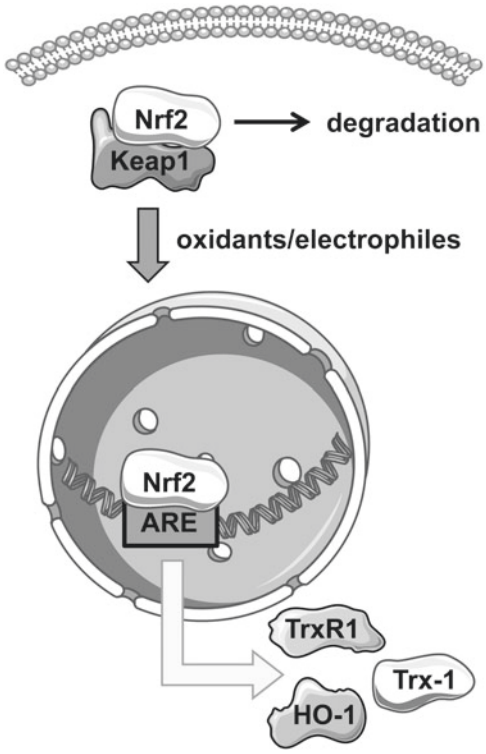

FIG. 1. Nrf2 signaling. Under basal conditions, the transcription factor Nrf2 remains sequestered in the cytoplasm *via* interaction with Keap1. To maintain low concentrations of Nrf2, it is constantly degraded by the proteasome. On electrophilic or oxidative stress, Nrf2 is released from the complex and shuttles to the nucleus, able to bind to AREs. This leads to enhanced expression of target genes such as HO-1, TrxR1, and Trx-1. AREs, antioxidant response elements; HO-1, heme oxygenase-1; Keap1, Kelch-like ECH-associated protein 1; Nrf2, nuclear factor erythroid 2-related factor 2; Trx-1, thioredoxin-1; TrxR1, thioredoxin reductase 1.

''Role of Nrf2 and Trx-1 in Atherosclerosis, Especially in Macrophages.'' The importance for Keap1 in regulation of Nrf2 has also been demonstrated by the deletion of Keap1 in hepatocytes of mice. This leads to a constitutive activation of Nrf2. In models of steatohepatitis, improved hepatic steatosis and reduced apoptosis have been observed in those Keap1-deficient mice. However, chronic liver inflammation and fibrosis progression were not inhibited by loss of Keap1 (85), suggesting that sustained activation of Nrf2 could be detrimental.

Another important target of Nrf2 is the ubiquitin-proteasome complex, which has also been discussed as a therapeutic target in cardiovascular diseases (77). In mouse embryonic fibroblasts, the 20S proteasome is regulated by Nrf2 in response to oxidative stress. One hour of hydrogen peroxide (H_2O_2) treatment resulted in elevated proteasomal activity after 24 h and small interfering RNA (siRNA) knockdown of Nrf2 prevented this activation. Thus, Nrf2 serves to limit the levels of damaged or oxidized proteins by promoting their degradation (81).

Since Nrf2 activation induces the expression of protective enzymes against oxidative stress, modulation of Nrf2 activity arose as a potential therapeutic approach. Interestingly, many

Nrf2 inducers are plant-derived natural compounds (6, 42). Nrf2 signaling is important in various diseases such as cancers, respiratory disorders, neuronal diseases, diabetes, and cardiovascular diseases [reviewed in Magesh *et al.* (64)]. A critical consideration in targeting Nrf2 therapeutically is that this transcription factor is believed to regulate the expression of up to 10% of all mammalian genes (98); therefore, one has to bear in mind that modulation of Nrf2 may lead to unexpected outcomes. A phase 3 randomized trial revealed an increased risk for heart failure in patients with type 2 diabetes treated once daily with bardoxolone, a potent Nrf2 activator (15), highlighting the aforementioned problem. On the other hand, brusatol has been reported to enhance the efficiency of chemotherapy by inhibiting Nrf2 (87). However, it was also shown that brusatol can have adverse effects in non-tumorous cells and enhances the sensitivity to chemical stress induced by bardoxolone, further supporting how critical it is to tamper with Nrf2 using inhibitors and activators (76).

Post-Translational Modifications of Nrf2

Besides the regulation of Nrf2 expression and its interaction with Keap1 as described earlier, there is recent evidence that Nrf2 is also modified post-translationally, which results in changes in Nrf2 activity and/or localization.

Protein kinase C (PKC)-dependent phosphorylation of Nrf2 at serine 40 has been described in oxidative stress in a tumor cell line, leading to increased nuclear localization of Nrf2 (41). Similar observations were made in rat pheochromocytoma (PC12) cells. Treatment with the nitric oxide (NO) donor S-Nitroso-N-acetyl-DL-penicillamine (SNAP) induced serine phosphorylation of Nrf2, analyzed by immunoprecipitation and use of a phospho-serine antibody. Interestingly, this study not only reported enhanced phosphorylation of Nrf2 but also enhanced nitrosation of Keap1. The abrogation of nuclear localization of Nrf2 by concomitant use of a pharmacological PKC inhibitor did not affect nitrosation of Keap1. Thus, nitrosation of Keap1 seems not to be responsible for the localization of Nrf2 (100). Enhanced nuclear Nrf2 activity was also observed after acetylation of lysines 588 and 591, which was dependent on cAMP responsive element binding protein (CREB). In this study, the authors showed that enhanced activity of the deacetylase NAD-dependent deacetylase sirtuin-1 (SIRT1) or mutation of both lysines (588 and 591) in Nrf2 promoted cytosolic accumulation of Nrf2 (50).

Interplay Between Nrf2 and Trx-1

It has been demonstrated that parts of the Trx-1 system are regulated by the transcription factor Nrf2, because Trx-1 and its reductase, TrxR1, each harbor AREs in their promoter region (43, 53, 89), leading to increased Trx-1 expression on nuclear Nrf2 activation under several conditions (Fig. 1). Reciprocally, it has been shown that overexpression of Trx-1 enhanced Nrf2 activity and that binding to AREs was increased, as analyzed by a protein-DNA binding assay after immunoprecipitation of nuclear Trx-1 (34, 91). This suggests a potential direct interaction of both proteins as well as a crosstalk between Nrf2 and Trx-1. A recent study describes the influence of Trx-1 on nuclear localization of SKN-1, the ortholog of Nrf2 in *Caenorhabditis elegans.* It was observed that loss of Trx-1 in the whole organism led to enhanced nuclear localization of SKN-1, demonstrating that interaction and crosstalk of Nrf2 signaling and the Trx-1 system contribute to inter- and intra-organ communication (67).

The cross-regulation between Nrf2 and Trx-1 either leads to protection from organ failure and maintenance of cellular homeostasis or, in the case of loss of functionality of these proteins, promotes pathophysiological complications. It is necessary to understand the underlying molecular mechanisms of the crosstalk between Nrf2 and Trx-1 to be able to develop new kinds of treatment of cardiovascular diseases or to improve the already established therapies. Moreover, the Nrf2-independent functions of Trx-1 seem to play a role in cardioprotection and will be introduced later.

Thioredoxin-1

The Trx-1 system consists of the two major proteins, Trx-1 and TrxR1. The conserved redox motif, with amino acids—CGPC—at positions 32–35 in human Trx-1, serves as a regulator of the cellular redox-steady-state equilibrium. Because of the proximity of both cysteines, a rapid oxidation accompanied by formation of an internal disulfide bridge is possible. This reversible oxidation of Trx-1 is recovered under nicotinamide adenine dinucleotide phosphate (NADPH) consumption through TrxR1, resulting in restoration of Trx-1 in its reduced form. Trx-1 contains three more cysteine residues at positions 62, 69, and 73; it has been shown that, in addition to intramolecular disulfide bridge formation between C32 and C35, a second S-S bridge can form between C62 and C69 under oxidative conditions with distinct impact on the three-dimensional structure of Trx-1 (Fig. 2) (35, 105).

As a thiol-disulfide-oxidoreductase, Trx-1 acts as a reducing agent for oxidized proteins. The two-step mechanism, by which the target molecule is reduced with concomitant oxidation of Trx-1 at C32 and/or C35, has been extensively reviewed elsewhere (61). The sensitivity of the Trx-1 system has been demonstrated by kinetic modeling, which showed that changes of concentrations or activities of single members of this crucial redox cycle affect kinetics of other members (82).

Post-Translational Modifications of Trx-1

Oxidation of cysteines is not the only post-translational modification (PTM) that occurs within Trx-1. For example, another fundamental PTM of Trx-1 in the endothelium is S-nitrosation (Fig. 2). Binding of NO to cysteine 69 elevated the redox activity of Trx-1 and enhanced the resistance to apoptosis (31). Nitrosation of Trx-1 under physiological conditions seems to occur in a selective manner. When Trx-1 was oxidized, nitrosation induced by incubation with nitrosated glutathione (GSNO) was observed mainly at C73 (3) (Fig. 2). However, it is unclear whether these findings are due to the oxidation at the historically considered active site at C32 and C35, or whether they are due to disulfide bridge formation between C62 and C69, which also occurs under oxidative stress. The most likely explanation is that oxidation of C62 and C69 prevents S-nitrosation of C69.

Besides nitrosation, Trx-1 is also nitrated, which is a modification of mostly tyrosines by peroxynitrite ($ONOO^-$). In various studies, nitration of Trx-1 in the cardiovascular

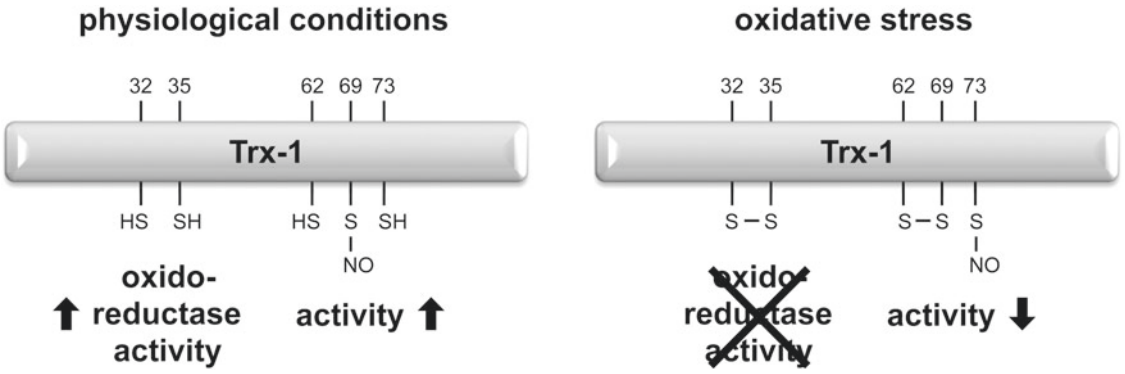

FIG. 2. Regulation of Trx-1 activity. Trx-1 has five essential cysteines that are important for its activity. Under physiological conditions, Trx-1 reduced oxidized proteins *via* C32 and C35. C69 is S-nitrosated, which increases the oxidoreductase activity of C32 and C35. Under conditions of oxidative stress, Trx-1 activity is reduced. C32 and C35 as well as C62 and C69 form disulfide bridges, and C73 is S-nitrosated.

system was investigated. Tao *et al.* demonstrated a decade ago inactivation of Trx-1 by 3-N-morpholinosydnonimine (SIN-1), which is often used to generate superoxide radical anions and NO at the same time to yield $ONOO^-$, *in vitro*.

Moreover, it has been shown that ischemia/reperfusion (I/R) reduced the activity of Trx-1 and enhanced its nitration. This was paralleled with reduced interaction of apoptosis signal-regulating kinase 1 (ASK-1) (96). Similar findings were observed in old mice compared with young mice, indicating that nitration of Trx-1 in the heart is even more pronounced in old mice (112), suggesting that the inability of the old heart to cope with an insult is due to reduced Trx-1 activity. In high-glucose-treated cardiomyocytes, inactivation of Trx-1 due to a drastic increase of nitration was observed without changes in expression levels. This was even more pronounced after sham-simulated ischemia reperfusion, suggesting that high-glucose sensitization of cardiomyocytes is dependent on nitration and, thus, inactivation of Trx-1 (62).

Regulation of Proteins by Trx-1

Interaction of Trx-1 with other proteins often depends on its redox status. This is reasonable, because Trx-1 reduces oxidized proteins to restore their function. For example, interaction of Trx-1 with the energy-sensing protein and cardioprotective 5′ AMP-activated protein kinase (AMPK) is required to maintain cysteines within AMPK in a reduced state, which is crucial for its activation (92). However, interaction that is dependent on cysteines in the active site may also inhibit the function of the target molecule. In the endothelium, apoptosis is a crucial event, since endothelial cells (EC) serve as a barrier organ and maintenance of the functional monolayer integrity is essential for blood vessel homeostasis. It has been demonstrated that Trx-1 is able to inhibit apoptosis by interacting with the N-terminus of ASK-1. This interaction results in decreased ASK-1 activity and was abrogated under oxidative stress conditions or mutation of cysteines 32 and 35 (88). Another study demonstrated that overexpressed Trx-1 led to degradation of ASK-1 in EC.

Furthermore, usage of Trx-1C32S and Trx-1C35S mutants revealed that a single cysteine is sufficient to inhibit ASK-1 activity, which was even seen in the presence of H_2O_2. However, the responsible cysteine—if it is only one—in ASK-1 remains to be investigated. The interaction between ASK-1 and Trx-1 can be inhibited by Trx binding protein-2 (TBP-2), also referred to as vitamin D3 upregulated protein 1 (VDUP1), or thioredoxin interacting protein (TXNIP) (46). Therefore, TXNIP is a negative regulator of Trx-1 and counteracts its protective properties.

In addition, Trx-1 possesses anti-inflammatory capacities. Overexpression of Trx-1 in EC downregulates the release of monocyte chemoattractant protein 1 (MCP-1), an inducible cytokine that recruits monocytes and macrophages. This was shown to be accompanied by suppressing nuclear translocation of apurinic/apyrimidinic endonuclease redox effector factor-1 (APEX-1) and reduced DNA-binding activity of activator protein 1 (AP-1) (12). This study lacks experiments regarding involvement of interaction between Trx-1 and APEX-1, but it has been shown that direct interaction of Trx-1 with APEX-1 leads to transcriptome changes due to modulation of AP-1 activity in HeLa cells (38).

Modulation of activity or functionality of other proteins in a covalent or indirect manner (75) by Trx-1 is not restricted to the cytoplasm (114). Trx-1 is able to shuttle to the nucleus in a karyopherin-α-dependent manner (91). Nuclear interaction partners of Trx-1 include hypoxia-inducible factor-1 α (HIF-1α), glucocorticoid receptor, nuclear factor kappa-light-chain-enhancer of activated B cells (NF-κB), and, as already mentioned, Nrf2 (23, 61, 65).

Atherosclerosis

The onset of atherosclerosis has been associated with the common lifestyle of industrial nations, which includes lack of exercise, overconsumption of sugars, fats, and cholesterol. Each of these habits can result in a damaged vasculature (19, 26). Multiple layers of the vasculature can be damaged and lead to the formation of atherosclerotic lesions and plaques. Distinct cell types, which become dysfunctional during atherogenesis, include EC, smooth muscle cells (SMCs), and macrophages. The endothelium, formed by a monolayer of EC, is located closest to the blood flow and forms a semipermeable barrier between blood contents and the media and adventitia. As a consequence, EC need to be sensitive to

chemical and physical changes in the body to induce relaxation or contraction of blood vessels [for review, see Mehta and Malik (69)].

Loss of EC or injury to the endothelial monolayer can result in remodeling of the vessel wall, which is marked by invasion of inflammatory cells, proliferation of SMCs, and integrin-dependent recruitment of platelets as early events in the development of atherosclerotic plaques [for review, see Bui *et al.* (8)]. Endothelial dysfunction contributes to the development of atherosclerosis. As an initial event, EC become activated and start to express leukocyte adhesion molecules. After recruitment of monocytes, oxidized low-density lipoprotein (OxLDL) through scavenger receptors such as CD36 leads to the formation of foam cells (25), a hallmark of atherosclerotic lesions. A recent study has shown that SMCs in atherosclerotic lesions may be derived from proliferating progenitor cells in the adventitia (94).

Role of Nrf2 in Atherosclerosis, Especially in the Endothelium

In EC, knockdown of Nrf2, or overexpression of its repressor Keap1, led to a reduction of EC migration and tube formation. Moreover, it was demonstrated that Caspase-3/7 activity was increased under basal conditions and was even more pronounced after treatment with 3 μM H_2O_2 for 18 h (101). Knockdown of Keap1 also protected EC from tumor necrosis factor α (TNF-α)-induced ROS formation and monocyte adhesion. In addition, an injection of Keap1 siRNA before lipopolysaccharide (LPS) injection reduced the NO_x content and TNF-α plasma levels in mice (52). Further evidence supporting the benefit of an intact Nrf2-ARE system is provided in a study by Zakkar *et al.*, which shows that absence of Nrf2 leads to vascular cell adhesion molecule-1 (VCAM-1) expression in EC whereas activation of Nrf2 leads to the opposite (111).

To address the hypothesis that activation of Nrf2 at atheroprone sites (commonly at branch points with low shear stress) will prevent EC activation and atherogenesis, the investigators pharmacologically activated Nrf2 using sulforaphane. Sulforaphane treatment was shown to reduce VCAM-1 expression in sites of low shear stress in wild-type (WT) but not Nrf2-null mice (111). This study provides evidence that Nrf2 regulation in EC is intimately linked with initiation and progression of atherosclerosis.

In addition to oxidants, it has been demonstrated that shear stress induces Nrf2 target gene expression, which was abrogated after Nrf2 knockdown. These expression patterns were antagonized by preincubation of human EC with oxypurinol or diphenyleneiodonium (DPI; NADPH oxidase and Xanthine oxidase inhibitors) (104). This study found that both oscillatory and laminar flow enhanced Nrf2 nuclear localization, whereas only laminar flow induced the expression of Nrf2 target genes. This suggests that Nrf2 has anti-atherogenic properties, since the pro-atherogenic oscillatory flow did not enhance binding to the ARE (40).

Surprisingly, various studies observed that Nrf2 acts in a pro-atherogenic manner. Sussan *et al.* reported that aortic plaques are reduced in young and old $Nrf2^{-/-}$ $ApoE^{-/-}$ mice, and that this was gender independent (93). Yet another study found that Nrf2-related gene expression was lower in aged of $LDLR^{-/-}$ mice placed on a high-fat diet (18). As a possible reason for these discrepancies, the authors discuss methodological differences to the earlier study, as well as differences in mouse models used (apolipoprotein E [ApoE] *vs.* LDL receptor [LDLR] deficiency). Reduction in lesion size was reported in Nrf2-deficient mice, and as a molecular mechanism, this is believed to be due to induction of interleukin (IL)-1 in cholesterol crystals *via* the NACHT, LRR, and PYD domains-containing protein 3 (NLRP3) inflammasome, activated by Nrf2 (27). These various contradictory findings underline the complexity of both modulating the signaling of a transcription factor-like Nrf2 and cardiovascular diseases such as atherosclerosis.

Studies show that disruption of Nrf2 activity allows EC to succumb to oxidative stress and leads to the development of coronary artery disease (21). The presence of SOD in the endothelium is reduced in patients with coronary artery disease, implying a deficiency in the Nrf2-mediated antioxidant response (60). Conversely, it has also been shown that reducing superoxide production by decreasing NADPH oxidase expression results in smaller lesions in a mouse model of atherosclerosis (4). Successful attenuation of atherosclerosis was also achieved in aged high-fat-diet-fed mice when subjected to antioxidant treatment (18). However, the use of exogenous antioxidants in humans to combat atherosclerosis and cardiovascular disease, in general, has not been very successful (73), stressing the importance to understand the intracellular redox homeostasis and defense mechanisms in more detail.

In addition to the oxidized lipids and pro-inflammatory cytokines, EC proximal to atherosclerotic lesions are also exposed to highly oxidative molecules, such as hypochlorous acid (HOCl). HOCl is formed by myeloperoxidase, which is present both intercellularly in EC and extracellularly at lesion sites (107). Treating EC with HOCl will induce expression of HO-1, an Nrf2-dependent antioxidant enzyme promoting cell viability. Inhibition of HO-1 by protoporphyrin-IX results in apoptosis of HOCl-stimulated EC. In the case of atherosclerosis, hypoxia is another factor that comes into play. It was found that intermittent hypoxia, an inducer of atherosclerosis and vascular inflammation, leads to a decrease of reduced glutathione (GSH) and an increase of modified glutathione (GSSG) (33). Sustained hypoxia was also found to induce pro-inflammatory gene expression in EC, while concurrently inducing Nrf2 and Nrf2-dependent transcription of HO-1 (83).

Another key function of EC is the production of NO by endothelial nitric oxide synthase (eNOS) to combat coagulation and regulate vascular tone (16). Dysfunction of the EC in atherosclerosis develops on a few different levels, ranging from cell viability to promotion of inflammation. These problems arise from the high level of oxidative stress associated with atherosclerosis. An essential factor that distinguishes the atheroprotective and atherogenic sites along the endothelium is expression of Nrf2. A study that investigated atherosclerotic susceptibility of sites within the mouse vasculature found that lesion development inversely correlated with shear stress experienced by the EC (111). EC located at branch points in the vasculature were noted to have a higher likelihood of forming atherosclerotic lesions compared with cells found in areas of high shear stress and laminar flow.

The production of VCAM-1 in EC has been associated with atherosclerosis (111). During the development of

atherosclerosis, OxLDL particles gather within the arterial intima. The bioactive components of these particles (oxidized phospholipids [OxPL]) induce VCAM-1 production in neighboring EC. VCAM-1 promotes monocyte binding to lesions in the endothelium. The accumulation of immune cells, which adopt a pro-inflammatory state, provides an environment filled with inflammatory stimuli (MCP-1, IL-1β, TNF-α) and subsequent oxidative stress. It was also found that VCAM-1 is induced in a p38-dependent manner, and Nrf2 activation suppresses this signaling (111). Sites of high shear stress dampen the effect of pro-inflammatory stimuli on EC. The converse was found in sites of low shear stress where they were observed to be highly vulnerable to plaque formation and greatly increased levels of VCAM-1 expression (111).

Thus, Nrf2 plays an important role in protecting the endothelium from damage and inhibiting the onset of endothelial dysfunction and, subsequently, atherosclerosis.

Role of Trx-1 in Atherosclerosis, Especially in the Endothelium

The function of Trx-1 in atherosclerosis and especially in the endothelium has not been studied in depth, since regulation of Nrf2 results in an increase in Thioredoxin-1 Reductase and, thus, in increased Trx-1 activity. In a few studies, it has been demonstrated that overexpression of Trx-1 enhanced Smad3 phosphorylation and inhibited the OxLDL-induced expression of adhesion molecules VCAM and intercellular adhesion molecule (ICAM) in human EC. Moreover, Smad3 was identified as an interaction partner of Trx-1, as was shown by immunoprecipitation of Trx-1 in EC lysates after adenoviral transduction with either Trx-1 WT or Trx-1 C32/35S (13).

One important player in the inflammasome is the TXNIP. TXNIP interacts with Trx-1 and is, therefore, inhibited. Trx-1 activity was investigated in vascular smooth muscle cells (VSMCs) isolated from WT and TXNIP ApoE-deficient mice. TXNIP-deficient mice show increased Trx-1 activity and reduced ROS levels. TXNIP ablation also leads to reduced expression of VCAM, ICAM, and MCP-1 (9). Changes of the TXNIP/Trx-1 interaction have been found in another *in vivo* study. Atherosclerosis, as an age-associated disease, was analyzed in old mice (25 months), which were fed with resveratrol for 3 months. These authors demonstrated a reduction of TXNIP expression and an improvement of aortic distensibility, a parameter reflecting elasticity. Although they found no changes in Trx-1 mRNA levels, it is likely that the release of Trx-1 from the complex with TXNIP is responsible for the improved outcome (5).

Given the fact that Trx-1 is one of the most important antiapoptotic proteins in the endothelium and loss of EC importantly contributes to the onset of atherosclerosis and associated events, for example, MI, it is reasonable to conclude that Trx-1 is a protective molecule in the vascular wall.

Role of Nrf2 and Trx-1 in Atherosclerosis, Especially in Macrophages

A consequence of atherogenic VCAM-1 and proinflammatory gene expression in EC is the infiltration of macrophages and monocytes into the lesions, as VCAM-1 induction promotes binding of monocytes to the endothelium. The migration of monocytes through the endothelium is an important event in the development of atherosclerosis, as blocking monocyte recruitment significantly slows disease development (70). These monocytes are exposed to many inflammatory mediators, including, but not limited to, MCP-1, TNF-α, and IL-1β. Details of monocyte interaction with the endothelium in atherosclerosis have been reviewed by Moore and Tabas (71). Nrf2 and Trx-1 play critical roles in controlling inflammation and immune system function. Disruption of Nrf2 results in increased mortality of endotoxin- and cecal ligation-challenged mice (97). The intracellular role of Nrf2 and Trx-1 in macrophages remains the same as in other cells, a defense mechanism against oxidative stress (45). At the intracellular level, Nrf2 and Trx-1 are believed to protect immune cells, namely macrophages, from ROS generated during inflammation (57).

High-cholesterol diets dramatically increase the presence of LDL in the circulation, and atherosclerotic lesions are burdened with high levels of oxidative stress, resulting in an environment filled with oxidized peptides and lipids. OxLDL, namely the phospholipid surface of the lipoprotein, produces OxPL. OxPL comprise one of the primary bioactive components of OxLDL, and OxPL constitute the active component of minimally modified low-density lipoprotein (mmLDL). OxPL promote monocyte adhesion to the endothelium (28) and an inflammatory response in macrophages. The hallmark of OxPL-dependent macrophage polarization is the induction of Nrf2-dependent gene expression, as represented by the markers HO-1 and TrxR1, to name a few (47).

OxPL inhibit phagocytosis, one of the principle functions of macrophages, promoting further inflammation and plaque accumulation. OxPL induce a novel macrophage phenotype, known as Mox, which has a unique gene expression profile as compared with the pro-inflammatory (M1) and anti-inflammatory (M2) macrophages. Mox is characterized as having mild (in comparison to M1) pro-inflammatory gene expression as well as significant Nrf2-dependent gene expression (Fig. 3). The Mox macrophages make up one third of the macrophages present in atherosclerotic lesions (Fig. 3) (47).

Trx-1 can be secreted by cells to promote M2 macrophage polarization, leading to atheroprotection (22) (Fig. 4). Full-length extracellular Trx-1 has also been shown to inhibit complement deposition on human EC, effectively competing with a complement for its binding site (54). A truncated form of Trx-1 shown to exist *in vivo*, known as Trx80, has the opposite effect, leading to complement activation *via* the classical and alternative pathways (54). Activation of Nrf2 has also been shown to attenuate inflammation and prevent tissue damage in a mouse model of sickle cell disease, a mechanism believed to be driven primarily by the heme-metabolizing action of HO-1 (51).

Polarized macrophages are associated with the development of atherosclerosis. M1 macrophages have pro-inflammatory and pro-atherogenic properties, whereas M2 macrophages show the opposite (66). Therefore, one could speculate that changing the balance between M1/M2 macrophages could lead to either progression or improvement of atherogenic events with the potential to treat atherosclerosis. As mentioned already in the Introduction section, Trx-1 has an anti-inflammatory potential. It was demonstrated that treatment

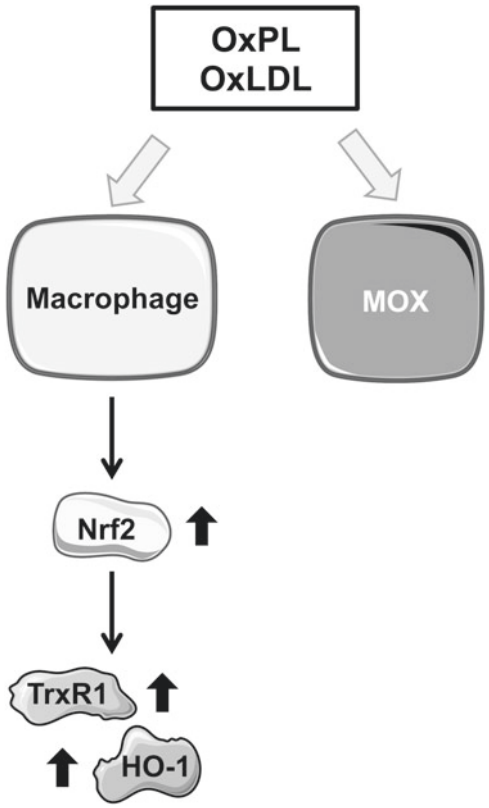

FIG. 3. Role of Nrf2 in macrophages in atherosclerosis. Oxidized phospholipids induce inflammatory responses in macrophages, accompanied by Nrf2 induction and increased expression of Nrf2 target genes. A novel macrophage phenotype is induced, MOX, which has a unique gene expression profile as compared with the pro-inflammatory (M1) and anti-inflammatory (M2) macrophages.

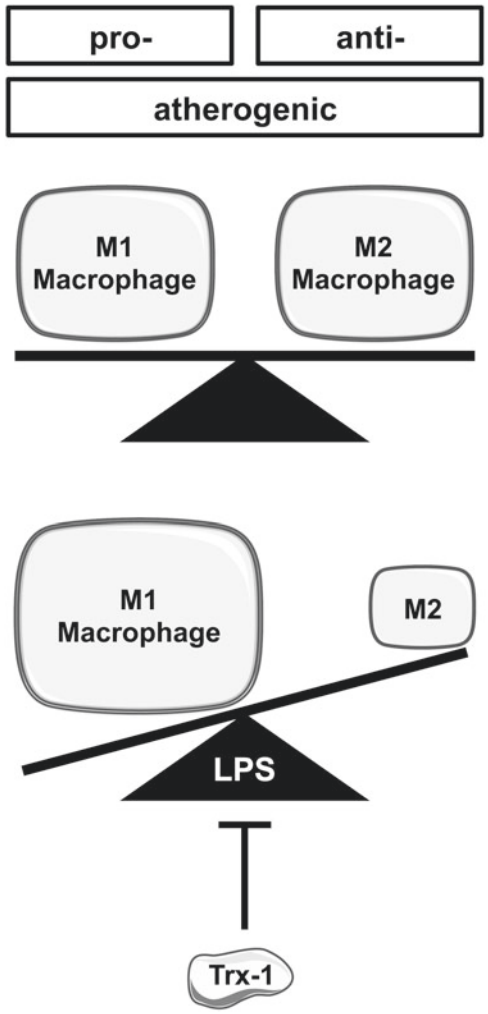

FIG. 4. Role Trx-1 in the balance of M1 and M2 macrophages in atherosclerosis. The balance between the pro-atherogenic M1 macrophages and the anti-atherogenic M2 macrophages is disturbed during atherosclerosis. The LPS-induced shift to M1 macrophages can be antagonized by Trx-1. LPS, lipopolysaccharide.

with recombinant human Trx-1 in murine peritoneal isolated macrophages led to enhancement of the expression of CD206 and IL-10, which are markers of M2 macrophages. Moreover, LPS stimulation led to an increase in TNF-α expression, a marker for M1 macrophages, which was abrogated after treatment with Trx-1 (Fig. 4). As an *in vivo* atherosclerosis model, mice have been chosen in which the mouse *ApoE* gene is replaced by the human ApoE2. These mice virtually exhibit all characteristics of type III hyperlipoproteinemia in humans. Those mice are markedly defective in clearing β-migrating VLDL particles, and they spontaneously develop atherosclerotic plaques, even on a regular diet. Treatment with Trx-1 showed increased macrophage polarization in the animals (22).

Taken together, Nrf2 and Trx-1 signaling is crucial at the level of macrophage invasion as well, and it exerts protective functions in antagonizing progression of atherosclerosis.

Role of Nrf2 and Trx-1 in Atherosclerosis, Especially in VSMCs

Besides EC, a large part of the disease progression relies on the activity of VSMCs and macrophages. The intimal hyperplasia is mediated by growth factors such as platelet-derived growth factor (PDGF) (48). PDGF activation of SMCs induces ROS production in an NADPH-oxidase-dependent manner and disrupts cellular homeostasis (58). PDGF stimulates SMCs to migrate and proliferate, and a recent study using a lineage tracing approach identified a role for progenitor cells in the adventitia (94) in promoting arterial occlusion. It has been shown in SMCs that Nrf2 is a key regulator of cell migration and neointimal hyperplasia (2). PDGF activation of SMCs also leads to the activation of Nrf2 (2), possibly as a feedback mechanism, to counteract increased ROS production and reinstate a cellular redox balance.

The complex interplay between the endothelium and VSMCs has been demonstrated by analyzing changes of the redox balance in a co-culture model. In this approach, a reduction of superoxide and H_2O_2 levels was observed in VSMCs co-cultured with microvascular EC. These changes were independent of NADPH oxidase expression patterns,

but rather due to upregulation of antioxidant systems such as Trx-1 and copper/zinc superoxide dismutase (Cu/Zn SOD). These findings highlight, at least under non-pathological conditions, that Trx-1 not only protects the endothelium itself but also that EC serve as a protector against ROS generation by upregulation of Trx-1 in VSMCs (110).

I/R Injury in the Heart

Ischemia is the result of the blockage of a vessel, for example, due to a blood clot, which can last from minutes to hours. After removal of the causal blockage physically or by drugs, blood flow is restored during the reperfusion phase. Tissue damage and the severity of cell dysfunction, injury, and/or death are, on one hand, dependent on the extent as well as on the duration of ischemia. Moreover, during reperfusion, the harmful event for cells is an oxidative burst (102, 115).

It has long been known that the dimensions of MI can be decreased by repetitive episodes of ischemia, even at the remote sites. Ischemic preconditioning (IPC) as well as remote preconditioning can improve heart function after MI. This remote preconditioning has been applied successfully before percutaneous coronary intervention (36, 39). In addition, ischemic postconditioning (POC) has been applied in humans as well. Excellent insights into the signaling events evoked by pre- or postconditioning events have been summarized elsewhere (37).

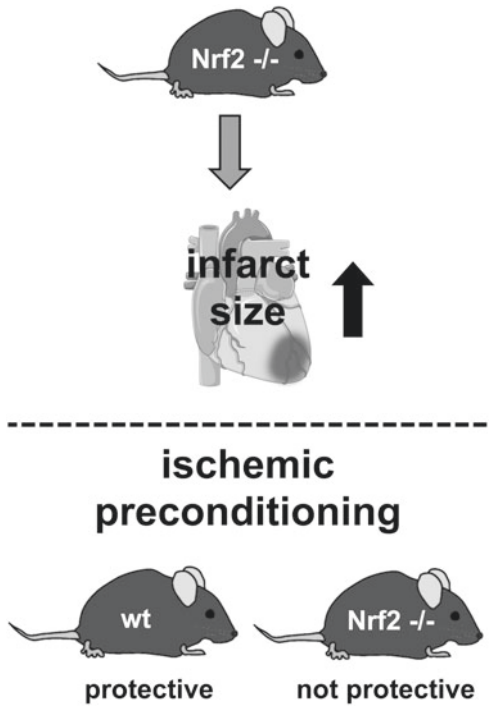

FIG. 5. Nrf2 protects from ischemia reperfusion injury and is required for ischemic preconditioning. Nrf2-deficient mice show enhanced infarct size compared with wild-type mice after occlusion of the left anterior descending artery. Ischemic preconditioning was dependent on Nrf2, because Nrf2 knockout mice did not benefit from ischemic preconditioning.

Role of Nrf2 in I/R Injury in the Heart

Involvement of Nrf2 in I/R-related processes has been shown by a comparison of WT mice with Nrf2-deficient mice. Of note, Nrf2 knockout mice have been reported to show an impaired cardiovascular phenotype, for example, due to left ventricular diastolic dysfunction and higher expression of eNOS (24). These findings underscore the important function of Nrf2 in the cardiovascular system. Occlusion of the left anterior descending (LAD) artery for 30 min revealed a twofold increase in infarct size in $Nrf2^{-/-}$ mice (Fig. 5) (109). In the same study, it was observed that Nrf2 is required for successful preconditioning, since two cycles of IPC did not result in cardiac protection in the absence of Nrf2 (Fig. 5). Since ROS levels are elevated after I/R, the oxidant-sensing Nrf2 transcription factor might be a promising target to ameliorate injuries after I/R. This is supported by several studies using potential Nrf2 activators.

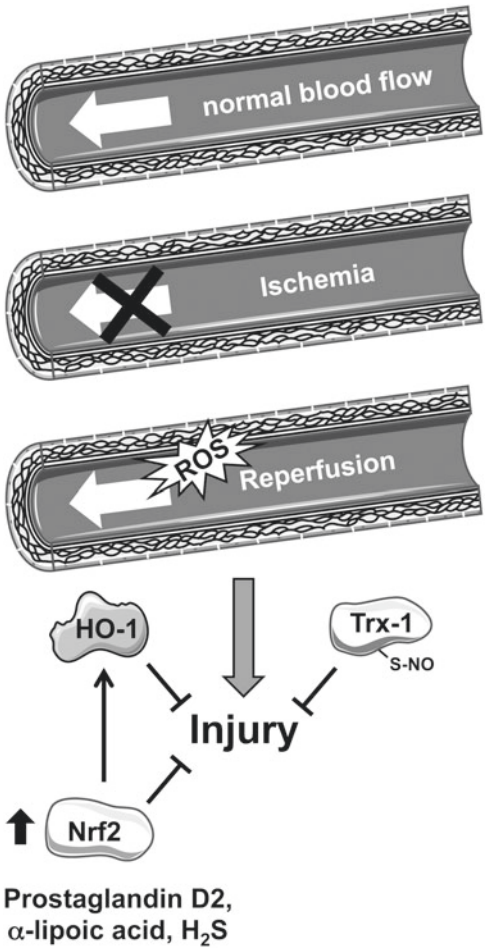

FIG. 6. Activation of Nrf2 and application of Trx-1 protect from ischemia reperfusion injury. Prostaglandin D2, alpha-lipoic acid, and H_2S, given before reperfusion, reduced oxidative stress and improved cardiac function due to increased nuclear Nrf2 activation and expression of target genes, for example, HO-1. Application of human Trx-1 before reperfusion decreased apoptosis in cardiac tissue of mice, and this was even more pronounced when using S-nitrosated human Trx-1. H_2S, hydrogen sulfide.

Glucocorticoids induce Nrf2 target genes, for example, HO-1, in a lipocalin-type prostaglandin D synthase-dependent manner. Glucocorticoids are unable to act cardioprotective in the Nrf2-deficient heart after I/R injury. Moreover, endogenous prostaglandin D2 increased nuclear translocation of Nrf2, reduced infarct size, and partially preserved heart function (Fig. 6) (49). Alpha-lipoic acid, which can be found in food such as broccoli, spinach, and tomatoes, is clinically approved (17).

Preconditioning with alpha-lipoic acid partially preserved heart function by reducing myocardial infarct size, cardiomyocyte apoptosis, and inflammation in I/R injury in rats. This seems to be dependent on increased nuclear localization and activation of Nrf2 target genes such as HO-1 (Fig. 6) (20). Recently, hydrogen sulfide (H_2S) has been suggested to be a cardioprotective molecule. Preconditioning with H_2S for 24 h reduced infarct size after I/R injury in an Nrf2-dependent manner, since this protection was not seen in Nrf2-deficient mice (Fig. 6) (10). The Nrf2-dependent, protective effect of H_2S preconditioning was also seen in diabetic mice (78). Resveratrol is a polyphenol that can be found in red grapes and wine. Resveratrol has been observed to exert antioxidative properties, for instance, by inducing the expression of enzymes such as manganese superoxide dismutase (MnSOD) and Catalase (44). Recently, Cheng *et al.* (14) demonstrated that resveratrol treatment before reperfusion after 30 min of ischemia improved cardiac function and reduced infarct size in the rat heart. This study is of potential interest, because the administration of resveratrol was 5 min before reperfusion and, thus, it could be of clinical significance.

The underlying mechanisms induced by resveratrol cannot be attributed to nuclear localization of Nrf2 alone, although an involvement of Nrf2 in the beneficial effects of resveratrol in mice and rats has been shown (14). However, the poor bioavailability and the concentrations of resveratrol, which would have to be used in humans, are critical. Moreover, the timing and the duration of treatment are unclear (84). Therefore, larger controlled human trials are needed to investigate those points and to then determine the contribution of Nrf2 (7).

Taken together, several natural molecules are cardioprotective in an Nrf2-dependent manner.

Role of Trx-1 in I/R in the Heart

With respect to Trx-1, it has been demonstrated that cardiac-specific overexpression of Trx-1 in mice improved systolic and diastolic post-ischemic ventricular function (99). Reduction of endogenous Trx-1 activity by using dominant negative-Trx-1 transgenic mice abolished this protective effect. Interestingly, this was accompanied by improved mitochondrial function measured in isolated mitochondria from those Trx-1 transgenic mice (79). Trx-1 protein levels are reduced after MI induced by I/R in young mice and could be partly restored after post-conditioning (Fig. 7). Middle-aged (12 months) and old (20 months) mice also showed lower Trx-1 levels after I/R; however, this could not be rescued by post-conditioning (Fig. 7). The protective effect of post-conditioning seems to decline with age, as was described already for preconditioning (1, 108). However, findings regarding age-dependent decline of ischemic conditioning are controversial. In a recent study, no association between age, gender or cardiovascular medication, and remote IPC could be observed in patients undergoing coronary artery bypass grafting (55).

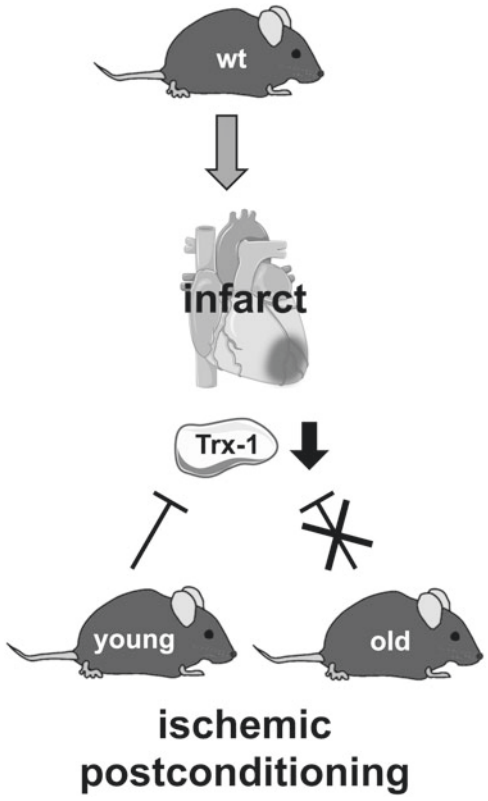

FIG. 7. The protective role of Trx-1 in ischemic post-conditioning is dependent on age. Young and old mice show reduced Trx-1 protein levels after myocardial infarction. The decrease in Trx-1 protein levels can only be restored in young mice by ischemic postconditioning.

As mentioned earlier, reperfusion leads to an overload of ROS due to an oxidative burst. High levels of ROS resulted in loss of Trx-1, which was demonstrated by Perez *et al.*, 120 min after reperfusion. Loss of Trx-1 then leads to an ''over''-adaptive response, which explains the opposite finding of an increase of Trx-1 24 h after the reperfusion phase (80). Analyzing Trx-1 levels in cardiac tissue biopsies collected from cardiopulmonary bypass surgeries revealed an increase of Trx-1 in patients who were preconditioned by four cycles of 5 min upper arm ischemia followed by a 5 min reperfusion phase (113). This reveals one possible molecular mechanism for the improved outcome, for example, in MI after applying IPC. However, injury induced by myocardial I/R is accompanied by apoptosis.

Since Trx-1 exerts anti-apoptotic functions, for example, due to nitrosation at cysteine 69 in EC (30), it is most likely that enhancement of nitrosated Trx-1 during MI results in decreased apoptosis. Indeed, a reduction of apoptosis was observed in I/R cardiac tissue of mice, which received human Trx-1 10 min before reperfusion. This effect was even more pronounced after using S-nitrosated Trx-1 (Fig. 6) (95). Interestingly, under conditions of oxidative stress, Trx-1 is degraded (32). This reduction of Trx-1 is also seen in mice subjected to a high-fat diet. As a consequence, increased apoptosis of cardiac myocytes is detected after ischemia in mice on a high-fat diet (92).

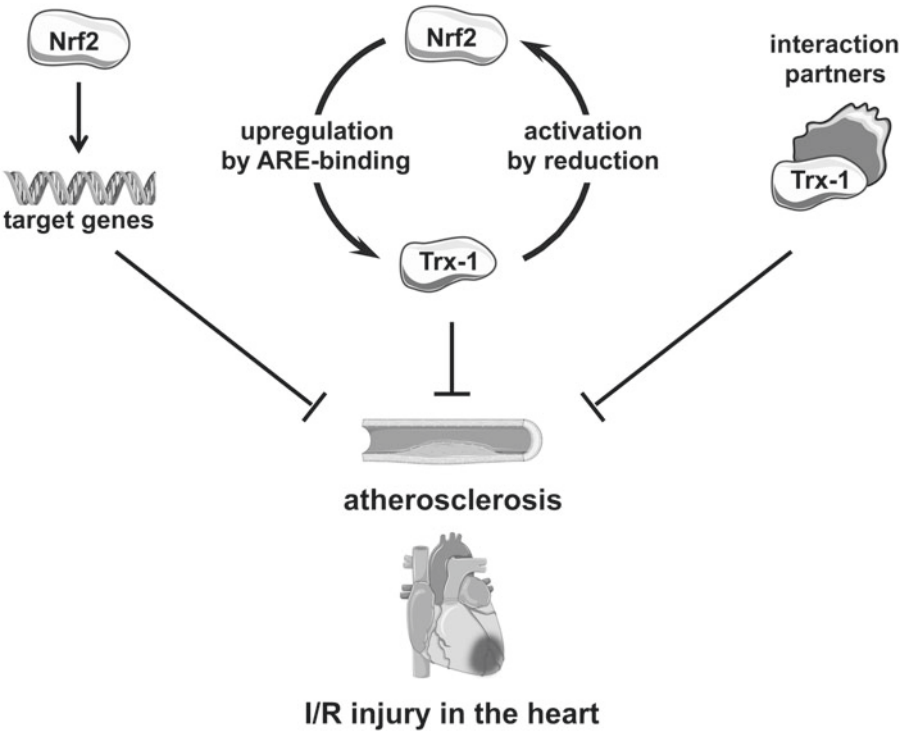

FIG. 8. Nrf2 and Trx-1 alone or in concert are protective in atherosclerosis and ischemia and reperfusion injury in the heart. Nrf2 is protective by induction of different target genes. Trx-1 can bind different interaction partners, thereby inhibiting deleterious actions or increasing protective functions of the respective proteins. Nrf2 can induce Trx-1 expression by binding to AREs in the Trx-1 promoter—concomitantly, Trx-1 reduces Nrf2 to keep it in the active form in the nucleus. This Nrf2 Trx-1 crosstalk can protect from atherosclerosis and ischemia and reperfusion injury in the heart.

Taken together, these studies support the notion that Trx-1 is cardioprotective in I/R.

Role of Nrf2 and Trx-1 in I/R in the Heart

Nrf2 and Trx-1 have also been shown to act in concert in I/R injury. An APEX-1/Trx-1/Nrf2/NF-κB axis was proposed. Although no or low interaction of APEX-1 with NF-κB and Nrf2 in nuclear extracts of left ventricular tissues could be observed after I/R, increased association of NF-κB and Nrf2 with APEX-1 was found in preconditioned hearts using four cycles of ischemia. Immunoprecipitated NFκB pulled down Trx-1 in the preconditioned heart, which was dependent on the presence of APEX-1 as shown by application of antisense oligonucleotides for APEX-1. In general, the amount of nuclear Trx-1 and Nrf2 was reduced after I/R, which could be restored after preconditioning (29). Moreover, the beneficial effect of H_2S was dependent not only on Nrf2 but also on Trx-1, as it was lost in mice with cardiac-specific overexpression of a dominant negative mutant of Trx-1 (74). These findings indicate a crucial role in IPC by crosstalk and association of these two proteins.

Therefore, the extent of injury after I/R, occurring in some of the most frequent causes of deaths such as MI, is dependent on both Nrf2 signaling and functional Trx-1. Interestingly, both proteins also play a role in pre- or post-conditioning. However, further studies regarding the impact of the Nrf2/Trx-1 crosstalk, elucidating detailed action on the molecular level, are necessary.

Conclusions/Future Directions

In summary, both Nrf2 and Trx-1 play an important role in atherosclerosis and ischemia and reperfusion injury of the heart alone as well as in concert (Fig. 8).

Interventions regarding nutritional and/or pharmacological activation of Nrf2 to improve heart and vessel function in atherosclerosis or ischemia/reperfusion should be well reflected. Since Nrf2 is a transcription factor, it regulates the expression of multiple genes, which even vary from organ to organ. Thus, pleiotropic effects cannot be overseen when modulating Nrf2 activity therapeutically. Moreover, overactivation of Nrf2 may be deleterious; length and starting point of treatment should be deliberate.

Treatment with Trx-1 could be beneficial even after MI. However, the most relevant patients who one has to deal with over the next decades are people over 75. From the studies in mice, Trx-1 alone will probably not be protective.

Since Nrf2 can increase Trx-1 mRNA and protein levels may be a combination therapy leading to increased and enhanced nuclear Nrf2, active Trx-1 protein could be of potential interest. Nevertheless, more studies in mice and humans are needed to address those potential therapeutic options.

Acknowledgments

P.J. is a scholarship holder of the IRTG1902. This work was, in part, supported by the Deutsche Forschungsgemeinschaft (HA2868/9-1 and 10-1, IRTG1902 P2); by the Forschungskommission of the Medical Faculty, University of Duesseldorf (28/2014) to J.H.; and by an NIH grant R01 DK096076 to N.L.V.S. was supported by a training grant NIH T32 GM007055-42 and an American Heart Association pre-doctoral fellowship 15PRE25560036. Single elements for figures were taken from the Powerpoint image bank of Servier Medical Art (www.servier.com/Powerpoint-image-bank), which is licensed under a Creative Commons Attribution 3.0 Unported License (http://creativecommons.org/licenses/by/3.0).

References

1. Abete P, Testa G, Cacciatore F, Della-Morte D, Galizia G, Langellotto A, and Rengo F. Ischemic preconditioning in the younger and aged heart. *Aging Dis* 2: 138–148, 2011.
2. Ashino T, Yamamoto M, Yoshida T, and Numazawa S. Redox-sensitive transcription factor Nrf2 regulates vascular smooth muscle cell migration and neointimal hyperplasia. *Arterioscler Thromb Vasc Biol* 33: 760–768, 2013.
3. Barglow KT, Knutson CG, Wishnok JS, Tannenbaum SR, and Marletta MA. Site-specific and redox-controlled S-nitrosation of thioredoxin. *Proc Natl Acad Sci U S A* 108: E600–E606, 2011.
4. Barry-Lane PA, Patterson C, van der Merwe M, Hu Z, Holland SM, Yeh ET, and Runge MS. p47phox is required for atherosclerotic lesion progression in ApoE(-/-) mice. *J Clin Invest* 108: 1513–1522, 2001.
5. Bedarida T, Baron S, Vibert F, Ayer A, Henrion D, Thioulouse E, Marchiol C, Beaudeux JL, Cottart CH, and Nivet-Antoine V. Resveratrol decreases TXNIP mRNA and protein nuclear expressions with an arterial function improvement in old mice. *J Gerontol A Biol Sci Med Sci* 71: 720–729, 2016.
6. Bocci V and Valacchi G. Nrf2 activation as target to implement therapeutic treatments. *Front Chem* 3: 4, 2015.
7. Bonnefont-Rousselot D. Resveratrol and cardiovascular diseases. *Nutrients* 8: 250, 2016.
8. Bui QT, Prempeh M, and Wilensky RL. Atherosclerotic plaque development. *Int J Biochem Cell Biol* 41: 2109–2113, 2009.
9. Byon CH, Han T, Wu J, and Hui ST. Txnip ablation reduces vascular smooth muscle cell inflammation and ameliorates atherosclerosis in apolipoprotein E knockout mice. *Atherosclerosis* 241: 313–321, 2015.
10. Calvert JW, Jha S, Gundewar S, Elrod JW, Ramachandran A, Pattillo CB, Kevil CG, and Lefer DJ. Hydrogen sulfide mediates cardioprotection through Nrf2 signaling. *Circ Res* 105: 365–374, 2009.
11. Cao Z, Zhu H, Zhang L, Zhao X, Zweier JL, and Li Y. Antioxidants and phase 2 enzymes in cardiomyocytes: chemical inducibility and chemoprotection against oxidant and simulated ischemia-reperfusion injury. *Exp Biol Med (Maywood)* 231: 1353–1364, 2006.
12. Chen B, Guan D, Cui ZJ, Wang X, and Shen X. Thioredoxin 1 downregulates MCP-1 secretion and expression in human endothelial cells by suppressing nuclear translocation of activator protein 1 and redox factor-1. *Am J Physiol Cell Physiol* 298: C1170–C1179, 2010.
13. Chen B, Wang W, Shen T, and Qi R. Thioredoxin1 downregulates oxidized low-density lipoprotein-induced adhesion molecule expression via Smad3 protein. *PLoS One* 8: e76226, 2013.
14. Cheng L, Jin Z, Zhao R, Ren K, Deng C, and Yu S. Resveratrol attenuates inflammation and oxidative stress induced by myocardial ischemia-reperfusion injury: Role of Nrf2/ARE pathway. *Int J Clin Exp Med* 8: 10420–10428, 2015.
15. Chin MP, Wrolstad D, Bakris GL, Chertow GM, de Zeeuw D, Goldsberry A, Linde PG, McCullough PA, McMurray JJ, Wittes J, and Meyer CJ. Risk factors for heart failure in patients with type 2 diabetes mellitus and stage 4 chronic kidney disease treated with bardoxolone methyl. *J Card Fail* 20: 953–958, 2014.
16. Cines DB, Pollak ES, Buck CA, Loscalzo J, Zimmerman GA, McEver RP, Pober JS, Wick TM, Konkle BA, Schwartz BS, Barnathan ES, McCrae KR, Hug BA, Schmidt AM, and Stern DM. Endothelial cells in physiology and in the pathophysiology of vascular disorders. *Blood* 91: 3527–3561, 1998.
17. Coleman MD, Eason RC, and Bailey CJ. The therapeutic use of lipoic acid in diabetes: a current perspective. *Environ Toxicol Pharmacol* 10: 167–172, 2001.
18. Collins AR, Lyon CJ, Xia X, Liu JZ, Tangirala RK, Yin F, Boyadjian R, Bikineyeva A, Pratico D, Harrison DG, and Hsueh WA. Age-accelerated atherosclerosis correlates with failure to upregulate antioxidant genes. *Circ Res* 104: e42–e54, 2009.
19. Danaei G, Ding EL, Mozaffarian D, Taylor B, Rehm J, Murray CJ, and Ezzati M. The preventable causes of death in the United States: comparative risk assessment of dietary, lifestyle, and metabolic risk factors. *PLoS Med* 6: e1000058, 2009.
20. Deng C, Sun Z, Tong G, Yi W, Ma L, Zhao B, Cheng L, Zhang J, Cao F, and Yi D. alpha-Lipoic acid reduces infarct size and preserves cardiac function in rat myocardial ischemia/reperfusion injury through activation of PI3K/Akt/Nrf2 pathway. *PLoS One* 8: e58371, 2013.
21. Donovan EL, McCord JM, Reuland DJ, Miller BF, and Hamilton KL. Phytochemical activation of Nrf2 protects human coronary artery endothelial cells against an oxidative challenge. *Oxid Med Cell Longev* 2012: 132931, 2012.
22. El Hadri K, Mahmood DF, Couchie D, Jguirim-Souissi I, Genze F, Diderot V, Syrovets T, Lunov O, Simmet T, and Rouis M. Thioredoxin-1 promotes anti-inflammatory macrophages of the M2 phenotype and antagonizes atherosclerosis. *Arterioscler Thromb Vasc Biol* 32: 1445–1452, 2012.
23. Ema M, Hirota K, Mimura J, Abe H, Yodoi J, Sogawa K, Poellinger L, and Fujii-Kuriyama Y. Molecular mechanisms of transcription activation by HLF and HIF1alpha in response to hypoxia: their stabilization and redox signal-induced interaction with CBP/p300. *EMBO J* 18: 1905–1914, 1999.
24. Erkens R, Kramer CM, Luckstadt W, Panknin C, Krause L, Weidenbach M, Dirzka J, Krenz T, Mergia E, Suvorava T, Kelm M, and Cortese-Krott MM. Left ventricular diastolic dysfunction in Nrf2 knock out mice is associated with cardiac hypertrophy, decreased expression of SERCA2a, and preserved endothelial function. *Free Radic Biol Med* 89: 906–917, 2015.
25. Febbraio M, Hajjar DP, and Silverstein RL. CD36: A class B scavenger receptor involved in angiogenesis, atherosclerosis, inflammation, and lipid metabolism. *J Clin Invest* 108: 785–791, 2001.
26. Folsom AR, Yatsuya H, Nettleton JA, Lutsey PL, Cushman M, Rosamond WD, and Investigators AS. Community prevalence of ideal cardiovascular health, by the American Heart Association definition, and relationship with cardiovascular disease incidence. *J Am Coll Cardiol* 57: 1690–1696, 2011.
27. Freigang S, Ampenberger F, Spohn G, Heer S, Shamshiev AT, Kisielow J, Hersberger M, Yamamoto M, Bachmann MF, and Kopf M. Nrf2 is essential for cholesterol crystal-induced inflammasome activation and exacerbation of atherosclerosis. *Eur J Immunol* 41: 2040–2051, 2011.

28. Furnkranz A, Schober A, Bochkov VN, Bashtrykov P, Kronke G, Kadl A, Binder BR, Weber C, and Leitinger N. Oxidized phospholipids trigger atherogenic inflammation in murine arteries. *Arterioscler Thromb Vasc Biol* 25: 633–638, 2005.
29. Gurusamy N, Malik G, Gorbunov NV, and Das DK. Redox activation of Ref-1 potentiates cell survival following myocardial ischemia reperfusion injury. *Free Radic Biol Med* 43: 397–407, 2007.
30. Haendeler J, Hoffmann J, Tischler V, Berk BC, Zeiher AM, and Dimmeler S. Redox regulatory and anti-apoptotic functions of thioredoxin depend on S-nitrosylation at cysteine 69. *Nat Cell Biol* 4: 743–749, 2002.
31. Haendeler J, Hoffmann J, Zeiher AM, and Dimmeler S. Antioxidant effects of statins via S-nitrosylation and activation of thioredoxin in endothelial cells: A novel vasculoprotective function of statins. *Circulation* 110: 856–861, 2004.
32. Haendeler J, Popp R, Goy C, Tischler V, Zeiher AM, and Dimmeler S. Cathepsin D and H_2O_2 stimulate degradation of thioredoxin-1: implication for endothelial cell apoptosis. *J Biol Chem* 280: 42945–42951, 2005.
33. Han Q, Yeung SC, Ip MS, and Mak JC. Intermittent hypoxia-induced NF-kappaB and HO-1 regulation in human endothelial EA.hy926 cells. *Cell Biochem Biophys* 66: 431–441, 2013.
34. Hansen JM, Watson WH, and Jones DP. Compartmentation of Nrf-2 redox control: regulation of cytoplasmic activation by glutathione and DNA binding by thioredoxin-1. *Toxicol Sci* 82: 308–317, 2004.
35. Hashemy SI and Holmgren A. Regulation of the catalytic activity and structure of human thioredoxin 1 via oxidation and S-nitrosylation of cysteine residues. *J Biol Chem* 283: 21890–21898, 2008.
36. Hausenloy DJ, Mwamure PK, Venugopal V, Harris J, Barnard M, Grundy E, Ashley E, Vichare S, Di Salvo C, Kolvekar S, Hayward M, Keogh B, MacAllister RJ, and Yellon DM. Effect of remote ischaemic preconditioning on myocardial injury in patients undergoing coronary artery bypass graft surgery: A randomised controlled trial. *Lancet* 370: 575–579, 2007.
37. Heusch G. Molecular basis of cardioprotection: Signal transduction in ischemic pre-, post-, and remote conditioning. *Circ Res* 116: 674–699, 2015.
38. Hirota K, Matsui M, Iwata S, Nishiyama A, Mori K, and Yodoi J. AP-1 transcriptional activity is regulated by a direct association between thioredoxin and Ref-1. *Proc Natl Acad Sci U S A* 94: 3633–3638, 1997.
39. Hoole SP, Heck PM, Sharples L, Khan SN, Duehmke R, Densem CG, Clarke SC, Shapiro LM, Schofield PM, O'Sullivan M, and Dutka DP. Cardiac Remote Ischemic Preconditioning in Coronary Stenting (CRISP Stent) Study: A prospective, randomized control trial. *Circulation* 119: 820–827, 2009.
40. Hosoya T, Maruyama A, Kang MI, Kawatani Y, Shibata T, Uchida K, Warabi E, Noguchi N, Itoh K, and Yamamoto M. Differential responses of the Nrf2-Keap1 system to laminar and oscillatory shear stresses in endothelial cells. *J Biol Chem* 280: 27244–27250, 2005.
41. Huang HC, Nguyen T, and Pickett CB. Phosphorylation of Nrf2 at Ser-40 by protein kinase C regulates antioxidant response element-mediated transcription. *J Biol Chem* 277: 42769–42774, 2002.
42. Hybertson BM, Gao B, Bose SK, and McCord JM. Oxidative stress in health and disease: the therapeutic potential of Nrf2 activation. *Mol Aspects Med* 32: 234–246, 2011.
43. Im JY, Lee KW, Woo JM, Junn E, and Mouradian MM. DJ-1 induces thioredoxin 1 expression through the Nrf2 pathway. *Hum Mol Genet* 21: 3013–3024, 2012.
44. Ingles M, Gambini J, Miguel MG, Bonet-Costa V, Abdelaziz KM, El Alami M, Vina J, and Borras C. PTEN mediates the antioxidant effect of resveratrol at nutritionally relevant concentrations. *Biomed Res Int* 2014: 580852, 2014.
45. Ishii T, Itoh K, Takahashi S, Sato H, Yanagawa T, Katoh Y, Bannai S, and Yamamoto M. Transcription factor Nrf2 coordinately regulates a group of oxidative stress-inducible genes in macrophages. *J Biol Chem* 275: 16023–16029, 2000.
46. Junn E, Han SH, Im JY, Yang Y, Cho EW, Um HD, Kim DK, Lee KW, Han PL, Rhee SG, and Choi I. Vitamin D3 up-regulated protein 1 mediates oxidative stress via suppressing the thioredoxin function. *J Immunol* 164: 6287–6295, 2000.
47. Kadl A, Meher AK, Sharma PR, Lee MY, Doran AC, Johnstone SR, Elliott MR, Gruber F, Han J, Chen W, Kensler T, Ravichandran KS, Isakson BE, Wamhoff BR, and Leitinger N. Identification of a novel macrophage phenotype that develops in response to atherogenic phospholipids via Nrf2. *Circ Res* 107: 737–746, 2010.
48. Kaiser M, Weyand CM, Bjornsson J, and Goronzy JJ. Platelet-derived growth factor, intimal hyperplasia, and ischemic complications in giant cell arteritis. *Arthritis Rheum* 41: 623–633, 1998.
49. Katsumata Y, Shinmura K, Sugiura Y, Tohyama S, Matsuhashi T, Ito H, Yan X, Ito K, Yuasa S, Ieda M, Urade Y, Suematsu M, Fukuda K, and Sano M. Endogenous prostaglandin D2 and its metabolites protect the heart against ischemia-reperfusion injury by activating Nrf2. *Hypertension* 63: 80–87, 2014.
50. Kawai Y, Garduno L, Theodore M, Yang J, and Arinze IJ. Acetylation-deacetylation of the transcription factor Nrf2 (nuclear factor erythroid 2-related factor 2) regulates its transcriptional activity and nucleocytoplasmic localization. *J Biol Chem* 286: 7629–7640, 2011.
51. Keleku-Lukwete N, Suzuki M, Otsuki A, Tsuchida K, Katayama S, Hayashi M, Naganuma E, Moriguchi T, Tanabe O, Engel JD, Imaizumi M, and Yamamoto M. Amelioration of inflammation and tissue damage in sickle cell model mice by Nrf2 activation. *Proc Natl Acad Sci U S A* 112: 12169–12174, 2015.
52. Kim JH, Choi YK, Lee KS, Cho DH, Baek YY, Lee DK, Ha KS, Choe J, Won MH, Jeoung D, Lee H, Kwon YG, and Kim YM. Functional dissection of Nrf2-dependent phase II genes in vascular inflammation and endotoxic injury using Keap1 siRNA. *Free Radic Biol Med* 53: 629–640, 2012.
53. Kim YC, Yamaguchi Y, Kondo N, Masutani H, and Yodoi J. Thioredoxin-dependent redox regulation of the antioxidant responsive element (ARE) in electrophile response. *Oncogene* 22: 1860–1865, 2003.
54. King BC, Nowakowska J, Karsten CM, Kohl J, Renstrom E, and Blom AM. Truncated and full-length thioredoxin-1 have opposing activating and inhibitory properties for

human complement with relevance to endothelial surfaces. *J Immunol* 188: 4103–4112, 2012.
55. Kleinbongard P, Neuhauser M, Thielmann M, Kottenberg E, Peters J, Jakob H, and Heusch G. Confounders of cardioprotection by remote ischemic preconditioning in patients undergoing coronary artery bypass grafting. *Cardiology* 133: 128–133, 2016.
56. Kobayashi A, Kang MI, Okawa H, Ohtsuji M, Zenke Y, Chiba T, Igarashi K, and Yamamoto M. Oxidative stress sensor Keap1 functions as an adaptor for Cul3-based E3 ligase to regulate proteasomal degradation of Nrf2. *Mol Cell Biol* 24: 7130–7139, 2004.
57. Kobayashi E, Suzuki T, and Yamamoto M. Roles nrf2 plays in myeloid cells and related disorders. *Oxid Med Cell Longev* 2013: 529219, 2013.
58. Kong G, Lee S, and Kim KS. Inhibition of rac1 reduces PDGF-induced reactive oxygen species and proliferation in vascular smooth muscle cells. *J Korean Med Sci* 16: 712–718, 2001.
59. Kwak MK, Itoh K, Yamamoto M, and Kensler TW. Enhanced expression of the transcription factor Nrf2 by cancer chemopreventive agents: role of antioxidant response element-like sequences in the nrf2 promoter. *Mol Cell Biol* 22: 2883–2892, 2002.
60. Landmesser U, Merten R, Spiekermann S, Buttner K, Drexler H, and Hornig B. Vascular extracellular superoxide dismutase activity in patients with coronary artery disease: relation to endothelium-dependent vasodilation. *Circulation* 101: 2264–2270, 2000.
61. Lillig CH and Holmgren A. Thioredoxin and related molecules—From biology to health and disease. *Antioxid Redox Signal* 9: 25–47, 2007.
62. Luan R, Liu S, Yin T, Lau WB, Wang Q, Guo W, Wang H, and Tao L. High glucose sensitizes adult cardiomyocytes to ischaemia/reperfusion injury through nitrative thioredoxin inactivation. *Cardiovasc Res* 83: 294–302, 2009.
63. Lukosz M, Jakob S, Büchner N, Zschauer TC, Altschmied J, and Haendeler J. Nuclear redox signaling. *Antioxid Redox Signal* 12: 713–742, 2010.
64. Magesh S, Chen Y, and Hu L. Small molecule modulators of Keap1-Nrf2-ARE pathway as potential preventive and therapeutic agents. *Med Res Rev* 32: 687–726, 2012.
65. Makino Y, Yoshikawa N, Okamoto K, Hirota K, Yodoi J, Makino I, and Tanaka H. Direct association with thioredoxin allows redox regulation of glucocorticoid receptor function. *J Biol Chem* 274: 3182–3188, 1999.
66. Mantovani A, Garlanda C, and Locati M. Macrophage diversity and polarization in atherosclerosis: A question of balance. *Arterioscler Thromb Vasc Biol* 29: 1419–1423, 2009.
67. McCallum KC, Liu B, Fierro-Gonzalez JC, Swoboda P, Arur S, Miranda-Vizuete A, and Garsin DA. TRX-1 regulates SKN-1 nuclear localization cell non-autonomously in *Caenorhabditis elegans*. *Genetics* 203: 387–402, 2016.
68. McMahon M, Itoh K, Yamamoto M, and Hayes JD. Keap1-dependent proteasomal degradation of transcription factor Nrf2 contributes to the negative regulation of antioxidant response element-driven gene expression. *J Biol Chem* 278: 21592–21600, 2003.
69. Mehta D and Malik AB. Signaling mechanisms regulating endothelial permeability. *Physiol Rev* 86: 279–367, 2006.
70. Mestas J and Ley K. Monocyte-endothelial cell interactions in the development of atherosclerosis. *Trends Cardiovasc Med* 18: 228–232, 2008.
71. Moore KJ and Tabas I. Macrophages in the pathogenesis of atherosclerosis. *Cell* 145: 341–355, 2011.
72. Moser MA and Chun OK. Vitamin C and heart health: A review based on findings from epidemiologic studies. *Int J Mol Sci* 17: 1328, 2016.
73. Myung SK, Ju W, Cho B, Oh SW, Park SM, Koo BK, and Park BJ. Efficacy of vitamin and antioxidant supplements in prevention of cardiovascular disease: systematic review and meta-analysis of randomised controlled trials. *BMJ* 346: f10, 2013.
74. Nicholson CK, Lambert JP, Molkentin JD, Sadoshima J, and Calvert JW. Thioredoxin 1 is essential for sodium sulfide-mediated cardioprotection in the setting of heart failure. *Arterioscler Thromb Vasc Biol* 33: 744–751, 2013.
75. Nishiyama A, Masutani H, Nakamura H, Nishinaka Y, and Yodoi J. Redox regulation by thioredoxin and thioredoxin-binding proteins. *IUBMB Life* 52: 29–33, 2001.
76. Olayanju A, Copple IM, Bryan HK, Edge GT, Sison RL, Wong MW, Lai ZQ, Lin ZX, Dunn K, Sanderson CM, Alghanem AF, Cross MJ, Ellis EC, Ingelman-Sundberg M, Malik HZ, Kitteringham NR, Goldring CE, and Park BK. Brusatol provokes a rapid and transient inhibition of Nrf2 signaling and sensitizes mammalian cells to chemical toxicity-implications for therapeutic targeting of Nrf2. *Free Radic Biol Med* 78: 202–212, 2015.
77. Pagan J, Seto T, Pagano M, and Cittadini A. Role of the ubiquitin proteasome system in the heart. *Circ Res* 112: 1046–1058, 2013.
78. Peake BF, Nicholson CK, Lambert JP, Hood RL, Amin H, Amin S, and Calvert JW. Hydrogen sulfide preconditions the db/db diabetic mouse heart against ischemia-reperfusion injury by activating Nrf2 signaling in an Erk-dependent manner. *Am J Physiol Heart Circ Physiol* 304: H1215–H1224, 2013.
79. Perez V, D Annunzio V, Mazo T, Marchini T, Caceres L, Evelson P, and Gelpi RJ. Ischemic postconditioning confers cardioprotection and prevents reduction of Trx-1 in young mice, but not in middle-aged and old mice. *Mol Cell Biochem* 415: 67–76, 2016.
80. Perez V, D Annunzio V, Valdez LB, Zaobornyj T, Bombicino S, Mazo T, Longo Carbajosa N, Gironacci M, Boveris A, Sadoshima J, and Gelpi RJ. Thioredoxin-1 attenuates ventricular and mitochondrial post-ischemic dysfunction in the stunned myocardium of transgenic mice. *Antioxid Redox Signal* 25: 78–88, 2016.
81. Pickering AM, Linder RA, Zhang H, Forman HJ, and Davies KJ. Nrf2-dependent induction of proteasome and Pa28alphabeta regulator are required for adaptation to oxidative stress. *J Biol Chem* 287: 10021–10031, 2012.
82. Pillay CS, Hofmeyr JH, and Rohwer JM. The logic of kinetic regulation in the thioredoxin system. *BMC Syst Biol* 5: 15, 2011.
83. Polotsky VY, Savransky V, Bevans-Fonti S, Reinke C, Li J, Grigoryev DN, and Shimoda LA. Intermittent and sustained hypoxia induce a similar gene expression profile in human aortic endothelial cells. *Physiol Genomics* 41: 306–314, 2010.

84. Raj P, Louis XL, Thandapilly SJ, Movahed A, Zieroth S, and Netticadan T. Potential of resveratrol in the treatment of heart failure. *Life Sci* 95: 63–71, 2014.
85. Ramadori P, Drescher H, Erschfeld S, Schumacher F, Berger C, Fragoulis A, Schenkel J, Kensler TW, Wruck CJ, Trautwein C, Kroy DC, and Streetz KL. Hepatocyte-specific Keap1 deletion reduces liver steatosis but not inflammation during non-alcoholic steatohepatitis development. *Free Radic Biol Med* 91: 114–126, 2016.
86. Ramprasath T and Selvam GS. Potential impact of genetic variants in Nrf2 regulated antioxidant genes and risk prediction of diabetes and associated cardiac complications. *Curr Med Chem* 20: 4680–4693, 2013.
87. Ren D, Villeneuve NF, Jiang T, Wu T, Lau A, Toppin HA, and Zhang DD. Brusatol enhances the efficacy of chemotherapy by inhibiting the Nrf2-mediated defense mechanism. *Proc Natl Acad Sci U S A* 108: 1433–1438, 2011.
88. Saitoh M, Nishitoh H, Fujii M, Takeda K, Tobiume K, Sawada Y, Kawabata M, Miyazono K, and Ichijo H. Mammalian thioredoxin is a direct inhibitor of apoptosis signal-regulating kinase (ASK) 1. *EMBO J* 17: 2596–2606, 1998.
89. Sakurai A, Nishimoto M, Himeno S, Imura N, Tsujimoto M, Kunimoto M, and Hara S. Transcriptional regulation of thioredoxin reductase 1 expression by cadmium in vascular endothelial cells: role of NF-E2-related factor-2. *J Cell Physiol* 203: 529–537, 2005.
90. Saremi A and Arora R. Vitamin E and cardiovascular disease. *Am J Ther* 17: e56–e65, 2010.
91. Schroeder P, Popp R, Wiegand B, Altschmied J, and Haendeler J. Nuclear redox-signaling is essential for apoptosis inhibition in endothelial cells—Important role for nuclear thioredoxin-1. *Arterioscler Thromb Vasc Biol* 27: 2325–2331, 2007.
92. Shao D, Oka S, Liu T, Zhai P, Ago T, Sciarretta S, Li H, and Sadoshima J. A redox-dependent mechanism for regulation of AMPK activation by Thioredoxin1 during energy starvation. *Cell Metab* 19: 232–245, 2014.
93. Sussan TE, Jun J, Thimmulappa R, Bedja D, Antero M, Gabrielson KL, Polotsky VY, and Biswal S. Disruption of Nrf2, a key inducer of antioxidant defenses, attenuates ApoE-mediated atherosclerosis in mice. *PLoS One* 3: e3791, 2008.
94. Tang Z, Wang A, Yuan F, Yan Z, Liu B, Chu JS, Helms JA, and Li S. Differentiation of multipotent vascular stem cells contributes to vascular diseases. *Nat Commun* 3: 875, 2012.
95. Tao L, Gao E, Bryan NS, Qu Y, Liu HR, Hu A, Christopher TA, Lopez BL, Yodoi J, Koch WJ, Feelisch M, and Ma XL. Cardioprotective effects of thioredoxin in myocardial ischemia and reperfusion: role of S-nitrosation [corrected]. *Proc Natl Acad Sci U S A* 101: 11471–11476, 2004.
96. Tao L, Jiao X, Gao E, Lau WB, Yuan Y, Lopez B, Christopher T, RamachandraRao SP, Williams W, Southan G, Sharma K, Koch W, and Ma XL. Nitrative inactivation of thioredoxin-1 and its role in postischemic myocardial apoptosis. *Circulation* 114: 1395–1402, 2006.
97. Thimmulappa RK, Lee H, Rangasamy T, Reddy SP, Yamamoto M, Kensler TW, and Biswal S. Nrf2 is a critical regulator of the innate immune response and survival during experimental sepsis. *J Clin Invest* 116: 984–995, 2006.
98. Tkachev VO, Menshchikova EB, and Zenkov NK. Mechanism of the Nrf2/Keap1/ARE signaling system. *Biochemistry (Mosc)* 76: 407–422, 2011.
99. Turoczi T, Chang VW, Engelman RM, Maulik N, Ho YS, and Das DK. Thioredoxin redox signaling in the ischemic heart: an insight with transgenic mice overexpressing Trx1. *J Mol Cell Cardiol* 35: 695–704, 2003.
100. Um HC, Jang JH, Kim DH, Lee C, and Surh YJ. Nitric oxide activates Nrf2 through S-nitrosylation of Keap1 in PC12 cells. *Nitric Oxide* 25: 161–168, 2011.
101. Valcarcel-Ares MN, Gautam T, Warrington JP, Bailey-Downs L, Sosnowska D, de Cabo R, Losonczy G, Sonntag WE, Ungvari Z, and Csiszar A. Disruption of Nrf2 signaling impairs angiogenic capacity of endothelial cells: Implications for microvascular aging. *J Gerontol A Biol Sci Med Sci* 67: 821–829, 2012.
102. Vanden Hoek TL, Li C, Shao Z, Schumacker PT, and Becker LB. Significant levels of oxidants are generated by isolated cardiomyocytes during ischemia prior to reperfusion. *J Mol Cell Cardiol* 29: 2571–2583, 1997.
103. Wakabayashi N, Dinkova-Kostova AT, Holtzclaw WD, Kang MI, Kobayashi A, Yamamoto M, Kensler TW, and Talalay P. Protection against electrophile and oxidant stress by induction of the phase 2 response: fate of cysteines of the Keap1 sensor modified by inducers. *Proc Natl Acad Sci U S A* 101: 2040–2045, 2004.
104. Warabi E, Takabe W, Minami T, Inoue K, Itoh K, Yamamoto M, Ishii T, Kodama T, and Noguchi N. Shear stress stabilizes NF-E2-related factor 2 and induces antioxidant genes in endothelial cells: Role of reactive oxygen/nitrogen species. *Free Radic Biol Med* 42: 260–269, 2007.
105. Watson WH, Pohl J, Montfort WR, Stuchlik O, Reed MS, Powis G, and Jones DP. Redox potential of human thioredoxin 1 and identification of a second dithiol/disulfide motif. *J Biol Chem* 278: 33408–33415, 2003.
106. Wei Y, Gong J, Thimmulappa RK, Kosmider B, Biswal S, and Duh EJ. Nrf2 acts cell-autonomously in endothelium to regulate tip cell formation and vascular branching. *Proc Natl Acad Sci U S A* 110: E3910–E3918, 2013.
107. Wei Y, Liu XM, Peyton KJ, Wang H, Johnson FK, Johnson RA, and Durante W. Hypochlorous acid-induced heme oxygenase-1 gene expression promotes human endothelial cell survival. *Am J Physiol Cell Physiol* 297: C907–C915, 2009.
108. Wu ZK, Pehkonen E, Laurikka J, Kaukinen L, Honkonen EL, Kaukinen S, Laippala P, and Tarkka MR. The protective effects of preconditioning decline in aged patients undergoing coronary artery bypass grafting. *J Thorac Cardiovasc Surg* 122: 972–978, 2001.
109. Xu B, Zhang J, Strom J, Lee S, and Chen QM. Myocardial ischemic reperfusion induces de novo Nrf2 protein translation. *Biochim Biophys Acta* 1842: 1638–1647, 2014.
110. Xu S, He Y, Vokurkova M, and Touyz RM. Endothelial cells negatively modulate reactive oxygen species generation in vascular smooth muscle cells: Role of thioredoxin. *Hypertension* 54: 427–433, 2009.
111. Zakkar M, Van der Heiden K, Luong le A, Chaudhury H, Cuhlmann S, Hamdulay SS, Krams R, Edirisinghe I, Rahman I, Carlsen H, Haskard DO, Mason JC, and Evans PC. Activation of Nrf2 in endothelial cells protects arteries from exhibiting a proinflammatory state. *Arterioscler Thromb Vasc Biol* 29: 1851–1857, 2009.

112. Zhang H, Tao L, Jiao X, Gao E, Lopez BL, Christopher TA, Koch W, and Ma XL. Nitrative thioredoxin inactivation as a cause of enhanced myocardial ischemia/reperfusion injury in the aging heart. *Free Radic Biol Med* 43: 39–47, 2007.
113. Zitta K, Meybohm P, Gruenewald M, Cremer J, Zacharowski KD, Scholz J, Steinfath M, and Albrecht M. Profiling of cell stress protein expression in cardiac tissue of cardiosurgical patients undergoing remote ischemic preconditioning: Implications for thioredoxin in cardioprotection. *J Transl Med* 13: 34, 2015.
114. Zschauer TC, Matsushima S, Altschmied J, Shao D, Sadoshima J, and Haendeler J. Interacting with thioredoxin-1—Disease or no disease? *Antioxid Redox Signal* 18: 1053–1062, 2013.
115. Zweier JL and Talukder MA. The role of oxidants and free radicals in reperfusion injury. *Cardiovasc Res* 70: 181–190, 2006.

Address correspondence to:
Prof. Judith Haendeler
IUF-Leibniz Research Institute for Environmental Medicine
Auf'm Hennekamp 50
40225 Duesseldorf
Germany

E-mail: juhae001@uni-duesseldorf.de

Date of first submission to ARS Central, June 25, 2016; date of final revised submission, November 8, 2016; date of acceptance, December 5, 2016.

Abbreviations Used

AMPK = 5′ AMP-activated protein kinase
AP-1 = activator protein 1
APEX-1 = apurinic/apyrimidinic endonuclease redox effector factor-1
ApoE = apolipoprotein E
ARE = antioxidant response element
ASK-1 = apoptosis signal-regulating kinase 1
EC = endothelial cells
eNOS = endothelial nitric oxide synthase
H_2O_2 = hydrogen peroxide
H_2S = hydrogen sulfide
HIF-1α = hypoxia-inducible factor-1 α
HO-1 = heme oxygenase-1
HOCl = hypochlorous acid
ICAM = intercellular adhesion molecule
IL-1β = interleukin 1β
IL-10 = interleukin 10
IPC = ischemic preconditioning
I/R = ischemia/reperfusion
Keap1 = kelch-like ECH-associated protein 1
LDL = low-density lipoprotein
LPS = lipopolysaccharide
MCP-1 =]monocyte chemoattractant protein 1
MI = myocardial infarction
mRNA = messenger RNA
NADPH = nicotinamide adenine dinucleotide phosphate
NF-κB = nuclear factor kappa-light-chain-enhancer of activated B cells
NO = nitric oxide
Nrf2 = nuclear factor erythroid 2-related factor 2
$ONOO^-$ = peroxynitrite
OxLDL = oxidized LDL
OxPL = oxidized phospholipids
PDGF = platelet-derived growth factor
PKC = protein kinase C
PTM = post-translational modification
ROS = reactive oxygen species
siRNA = small interfering RNA
SIRT1 = NAD-dependent deacetylase sirtuin-1
SMC = smooth muscle cells
SOD = superoxide dismutase
TNF-α = tumor necrosis factor α
Trx-1 = thioredoxin-1
TrxR1 = thioredoxin reductase 1
TXNIP = thioredoxin interacting protein
VCAM-1 = vascular cell adhesion molecule-1
VSMCs = vascular smooth muscle cells
WT = wild type

CDKN1B/p27 is localized in mitochondria and improves respiration-dependent processes in the cardiovascular system – new mode of action for caffeine

Ale-Agha N*, Goy C*, **Jakobs P***, Spyridopoulos I, Gonnissen S, Dyballa-Rukes N, Aufenvenne K, Von Ameln F, Zurek M, Spannbrucker T, Eckermann O, Jakob S, Gorressen S, Abrams M, Grandoch M, Fischer JW, Köhrer K, Deenen R, Unfried K, Altschmied J#, Haendeler J#

Plos Biology. 2018: im Druck *Gleichberechtigte Erstautoren; #Gleichberechtigte Letztautoren

Autoren:

Ale-Agha N: Erstautorin, war an der Planung aller Versuche beteiligt, führte alle Tierexperimente und deren Datenanalyse durch. Schrieb Teile des Manuskripts.

Goy C: Erstautorin, plante mit Frau Haendeler alle Endothelzellversuche, führte alle Zellexperimente und alle Oroborosmessungen und deren Datenanalyse durch. Schrieb Teile des Manuskripts.

Jakobs P: Erstautor, war an der Planung aller Versuche in der Revision beteiligt und führte Zellexperimente und Datenanalyse durch. Schrieb mit Frau Haendeler und Herrn Altschmied die Revision und die Antworten für die Gutachter.

Spyridopoulos I: War an der Konzeption der Studie beteiligt, half mit den statistischen Analysen und korrigierte das Manuskript.

Gonnissen S: Führte zusammen mit Frau Aufenvenne, Herrn Spannbrucker und Frau Ale-Agha Immunfluoreszenzfärbungen durch.

Dyballa-Rukes N: Führte zusammen mit Frau Goy Immunoblots und deren Auswertung durch.

Aufenvenne K: Führte zusammen mit Frau Gonnissen, Herrn Spannbrucker und Frau Ale-Agha Immunfluoreszenzfärbungen durch

Von Ameln F: Führte zusammen mit Frau Goy und Herrn Jakobs Immunoblots durch und isolierte RNA für Transkriptomanalysen. Führte zusammen mit Herrn Eckermann die Klonierungen durch. Führte die Messungen des ATP Gehaltes mit Herrn Altschmied durch.

Zurek M: Etablierte die Zellkultur der kardialen Fibroblasten zusammen mit Herrn Jakobs und führte Immunoblots durch.

Spannbrucker T: Führte zusammen mit Frau Aufenvenne, Frau Gonnissen und Frau Ale-Agha Immunfluoreszenzfärbungen durch.

Eckermann O: Führte zusammen mit Herrn von Ameln die Klonierungen durch. Generierte die Lentiviren und transduzierte kardiale Fibroblasten. Führte die Expressionsnachweise.

Jakob S: Führte alle FACS Messungen und deren Datenanalyse durch.

Gorressen S: Führte zusammen mit Frau Ale-Agha, Herrn Abrams und Frau Grandoch die Experimente an Tieren auf diabetogener Ernährung durch.

Abrams M: Führte zusammen mit Frau Ale-Agha, Frau Gorressen und Frau Grandoch die Experimente an Tieren auf diabetogener Ernährung durch

Grandoch M: Entwickelte zusammen mit Herrn Fischer die Zusammensetzung der diabetogenen Ernährung und konzipierte die Durchführung der entsprechenden Tierexperimente.

Fischer JW: Entwickelte zusammen mit Frau Grandoch die Zusammensetzung der diabetogenen Ernährung und konzipierte die Durchführung der entsprechenden Tierexperimente.

Köhrer K: Führte mit Herrn Deenen die Transkriptomanalysen und deren Auswertung durch.

Deenen R: Führte mit Herrn Köhrer die Transkriptomanalysen und deren Auswertung durch.

Unfried K: Führte mit Frau Ale-Agha und Herrn Altschmied die tierexperimentellen Versuche für die Mitochondrienanalysen durch.

Altschmied J: Senior Autor, hatte mit Frau Prof Haendeler die Idee für die Studie, plante und konzipierte die Versuche. Entwickelte alle Klonierungsstrategien für die notwendigen Expressionsvektoren. Schrieb das Manuskript mit Frau Prof Haendeler, erstellte mit Frau Dyballa-Rukes und Herrn Jakobs alle Abbildungen, schrieb die Revision mit Herrn Jakobs und Frau Haendeler.

Haendeler J: Senior Autorin, hatte die Idee zur Studie, plante alle Experimente. Schrieb und finalisierte das Manuskript mit Herrn Altschmied

Fwd: Your PLOS Biology submission

Von: PLOS Biology <plosbiology@plos.org>
Betreff: Your PLOS Biology submission
Datum: 18. Mai 2018 um 12:06:35 MESZ
An: juhae001@uni-duesseldorf.de

A Decision has been Registered on your Manuscript CDKN1B/p27 is localized in mitochondria and improves respiration-dependent processes in the cardiovascular system - new mode of action for caffeine.

Dear Dr. Haendeler,

On behalf of my colleagues and the Academic Editor, Cecilia Lo, I am pleased to inform you that we will be delighted to publish your manuscript in PLOS Biology.

The files will now enter our production system. You will receive a copyedited version of the manuscript, along with your figures for a final review. You will be given two business days to review and approve the copyedit. Then, within a week, you will receive a PDF proof of your typeset article. You will have two days to review the PDF and make any final corrections. If there is a chance that you'll be unavailable during the copy editing/proof review period, please provide us with contact details of one of the other authors whom you nominate to handle these stages on your behalf. This will ensure that any requested corrections reach the production department in time for publication.

Early Version

The version of your manuscript submitted at the copyedit stage will be posted online ahead of the final proof version, unless you have already opted out of the process. The date of the early version will be your article's publication date. The final article will be published to the same URL, and all versions of the paper will be accessible to readers.

PRESS

We frequently collaborate with press offices. If your institution or institutions have a press office, please notify them about your upcoming paper at this point, to enable them to help maximise its impact. If the press office is planning to promote your findings, we would be grateful if they could coordinate with biologypress@plos.org. If you have not yet opted out of the early version process, we ask that you notify us immediately of any press plans so that we may do so on your behalf.

CDKN1B/p27 is localized in mitochondria and improves respiration-dependent processes in the cardiovascular system - new mode of action for caffeine

Niloofar Ale-Agha[1]†, Christine Goy[1]†, Philipp Jakobs[1]†, Ioakim Spyridopoulos[2], Stefanie Gonnissen[3], Nadine Dyballa-Rukes[1], Karin Aufenvenne[1], Florian von Ameln[1,3], Mark Zurek[1], Tim Spannbrucker[6], Olaf Eckermann[1], Sascha Jakob[1], Simone Gorressen[4], Marcel Abrams[4], Maria Grandoch[4], Jens W. Fischer[4], Karl Köhrer[5], René Deenen[5], Klaus Unfried[6], Joachim Altschmied*#[3], and Judith Haendeler*#[1]

Affiliations:
[1]Heisenberg-group - Environmentally-induced Cardiovascular Degeneration, Medical Faculty, HHU Duesseldorf and IUF-Leibniz Research Institute for Environmental Medicine, Duesseldorf, Germany,
[2]Institute of Genetic Medicine, Newcastle University, Newcastle upon Tyne, United Kingdom,
[3]Core Unit of Biosafety Level 2 Laboratory, IUF-Leibniz Research Institute for Environmental Medicine, Duesseldorf, Germany,
[4]Institute for Pharmacology and Clinical Pharmacology, Medical Faculty, HHU Duesseldorf, Duesseldorf, Germany,
[5]Biological and Medical Research Center (BMFZ), Heinrich-Heine-University, Duesseldorf, Germany,
[6]Environmentally-induced Skin and Lung Aging, IUF-Leibniz Research Institute for Environmental Medicine, Duesseldorf, Germany

*To whom correspondence should be addressed:
Judith Haendeler, E-mail: juhae001@uni-duesseldorf.de
and
Joachim Altschmied, E-mail: joalt001@uni-duesseldorf.de

† those authors contributed equally to this work
# those authors contributed equally to this work

Short title: Mitochondrial p27 in concert with caffeine in the cardiovascular system

Abbreviations

CDKN1A - Cyclin Dependent Kinase Inhibitor 1A

CDKN1B - Cyclin Dependent Kinase Inhibitor 1B

CDI - cyclin dependent kinase inhibitor

aa - amino acid

Trx-1 - Thioredoxin-1

TIM23 - Translocase of inner mitochondrial membrane 23

TOM40 - Translocase of outer mitochondrial membrane 40

HSPA9/GRP75 - Mitochondrial heat shock protein 70 kDa

GO - gene ontology

TGFβ1 - transforming growth factor β 1

αSMA - α smooth muscle actin

siRNA – small interfering RNA

PDE - phosphodiesterase

Abstract

We show that CDKN1B/p27, previously known as a cell cycle inhibitor, is also localized within mitochondria. The migratory capacity of endothelial cells, which needs intact mitochondria, is completely dependent on mitochondrial p27. Mitochondrial p27 improves mitochondrial membrane potential, increases ATP content, and is required for the pro-migratory effect of caffeine. Domain mapping of p27 revealed that the N-terminus and C-terminus are required for those improvements. Further analysis of those regions revealed that the translocation of p27 into the mitochondria and its pro-migratory activity depend on serine 10 and threonine 187. In addition, mitochondrial p27 protects cardiomyocytes against apoptosis. Moreover, mitochondrial p27 is necessary and sufficient for cardiac myofibroblast differentiation. In addition, p27-deficiency and aging decrease respiration in heart mitochondria. Strikingly, caffeine does not increase respiration in p27-deficient animals, whereas aged mice display improvement after 10 days of caffeine in drinking water. Moreover, caffeine induces transcriptome changes in a p27-dependent manner affecting mostly genes relevant for mitochondrial processes. Caffeine also reduces infarct size after myocardial infarction in prediabetic mice and increases mitochondrial p27. Our data characterize mitochondrial p27 as a common denominator, which improves mitochondria-dependent processes and define an increase in mitochondrial p27 as a new mode of action of caffeine.

Author Summary

The protein p27 is a nuclear cell cycle inhibitor that can be shuttled to the cytoplasm to inactivate its inhibitory role, and this mechanism is thought to be used by cancer cells to unlock cell cycle arrest. Recent reports, however, have shown that p27 has other roles independent of cell cycle regulation and it was observed that p27 mutant mice had increased mortality to myocardial infarction. Here, we have analysed the potential role of p27 in the major cell types of the heart and show that it is also present in mitochondria, the

cellular powerhouses, where it fulfils important functions. We find that p27 is required for migration of endothelial cells by enhancing mitochondrial functions, and that caffeine concentrations reached after consumption of four cups of coffee induce its translocation into mitochondria. Moreover, we observe that mitochondrial p27 protects heart muscle cells from cell death and is necessary for the conversion of fibroblasts into mechanically strong, contractile myofibroblasts, a process critical after myocardial infarction. Molecularly, we show that p27 is essential for caffeine-induced gene expression changes that mainly affect mitochondria and for mitochondrial respiration. We conclude that mitochondrial p27 improves mitochondria-dependent processes in heart cells and that physiological concentrations of caffeine have a protective effect.

Introduction

The Cyclin Dependent Kinase Inhibitor 1B, also known as p27, was initially discovered as a nuclear-localized cell cycle inhibitor [1]. Previous data demonstrating that p27 can be exported to the cytoplasm [2,3] were considered as a mechanism to inactivate the cell cycle inhibitory effects of p27 in the nucleus and to allow human cancer cells to escape cell cycle arrest. However, McAllister et al. demonstrated that non-nuclear p27 is required for migration of fibroblasts, since p27-deficient mouse embryonic fibroblasts failed to migrate, while reconstitution with p27 rescued the motility defect. Its pro-migratory effect was independent of its cell cycle arrest functions, but rather required serine 10 phosphorylation-dependent nuclear export and a C-terminal scatter domain [4]. Moreover, it was suggested that knockout of a cell cycle inhibitor like p27 could be beneficial in the experimental setup of myocardial infarction. This was based on the reasoning that myocardial infarction leads to loss of cells in the heart and that enhanced proliferation of cells in p27-deficient mice may result in smaller infarct size and reduced mortality; however, exactly the opposite was observed [5,6]. Moreover, over the last years it has become evident that functional

mitochondria, not only in cardiomyocytes, but also in endothelial cells [7,8] and in cardiac fibroblasts [9] are required for proper functionality of those cells and are essential for protective actions in cardiovascular diseases.

Furthermore, in recent years a number of cohort studies have convincingly demonstrated that habitual coffee consumption is associated with a lower risk to develop type II diabetes [10,11]. Coffee consumption was inversely correlated with total as well as cause-specific mortality, such as heart disease, respiratory disease, stroke, and diabetes, whereas no relation or a positive correlation was found with cancer-related deaths [12,13]. In addition, several studies have shown that consumption of caffeinated coffee is associated with lower risk for coronary heart disease mortality specifically in older subjects [14,15]. Finally, the beneficial effect of caffeine appeared to be dose-dependent as coffee consumption of four cups or more per day resulted in a further reduced risk for adverse events when compared to lower coffee consumption. We established previously that four cups of coffee lead to a serum concentration of approximately 30 µM caffeine in humans [8]. Therefore, mechanisms explaining the protective effects of caffeine should be attributed to serum concentrations of less than 100 µM. Over decades, the effects of caffeine have been ascribed to its antagonist activity on adenosine receptors, inhibition of phosphodiesterases and elevated intracellular calcium levels. Since a raise of intracellular calcium in different cell types requires at least 500 µM caffeine, which in humans would result in lethal intoxication [16-18], effects on intracellular calcium can be excluded as a potential mechanism. Similarly, inhibition of phosphodiesterases by caffeine requires concentrations of 250 µM or higher, depending on the isoforms investigated [19,20]. Studies regarding the responses to activation or inhibition of adenosine receptors in the cardiovascular system are controversial. Activation of the adenosine 2A receptor has beneficial effects in the infarcted porcine myocardium [21], whereas blockade of the adenosine 2A receptor reduces cardiac reactive oxygen species production and expression of NADPH oxidase 2 in the heart [22]. Thus, it remains unclear whether unspecific inhibition of adenosine receptors

or phosphodiesterases by caffeine could explain the protective effects of coffee consumption. Importantly, we demonstrated that caffeine in physiologically relevant concentrations improves the functional capacity of endothelial cells *ex vivo* and *in vivo* in a mitochondria-dependent manner [8].

Given the described protective role of caffeine and its association with mitochondria, we hypothesized that a common denominator exists in endothelial cells, cardiomyocytes and cardiac fibroblasts, which improves the mitochondria-dependent functionalities of those cells *ex vivo* and *in vivo*. Since the role of non-nuclear p27 in non-tumor cells was never examined in detail, we investigated whether p27 is present in the mitochondria, and is indeed required to improve mitochondria-dependent functionalities and whether the protective caffeine effects are causally related to mitochondrial p27, which would present a new mode of action for caffeine explaining its protective function in the cardiovascular system.

Results

Mitochondrial p27 is indispensable for functional improvement of endothelial cells

Physiologically relevant concentrations of caffeine, which have beneficial cardiovascular effects, have been attributed to four or more cups of daily coffee consumption. Four cups of coffee lead to a serum caffeine concentration of approximately 30 µM in humans [8]. Since four or more cups of coffee seem to have a beneficial effect, we used 50 µM caffeine in all cellular studies presented here as well as concentrations of caffeine in the drinking water of mice, which result in approximately 30 - 50 µM in the serum of the animals [8]. To assess a potential involvement of adenosine receptors in the caffeine-mediated effects, we first investigated the impact of caffeine on endothelial cell migration, as a measure for functional capacity, in the presence of adenosine receptor 2A and 2B blockers, SCH442416 and GS6201, respectively. Neither inhibition of adenosine receptor

2A nor 2B changed the ability of 50 μM caffeine to induce migration in human primary endothelial cells (S1 Fig). Moreover, caffeine did not change phosphorylation of phosphodiesterases 4A and 5A, respectively (S2 Fig), which is in accordance with the literature that caffeine concentrations higher than 250 μM are needed to modulate activity of those enzymes and, thus, to change intracellular cyclic nucleotide levels [19,20].

Interestingly, McAllister et al. showed that p27 is necessary for migration of HepG2 cells and embryonic fibroblasts. Furthermore, its pro-migratory effect was independent of its cell cycle arrest functions, but rather required serine 10 phosphorylation-dependent nuclear export and a C-terminal scatter domain [4]. Therefore, we down-regulated p27 with two different small interfering RNAs (siRNAs) (Fig 1A and 1B, S3 Fig) and determined first the effect on cell viability (siRNA1: 106.9 ± 11.9 %; siRNA2: 134.6 ± 21.4 % of scrambled control, n=5, means ± SEM, not significant) as well as on cellular and mitochondrial morphology (S4 Fig). Since transfection of p27-specific siRNAs did neither affect cell viability nor morphology, we next investigated the effect on endothelial cell migration. Basal as well as caffeine induced migration was completely blunted upon knockdown of p27 (Fig 1C). These data demonstrate that primary human endothelial cells require p27 for migration.

Fig 1. p27 is required for endothelial cell migration.

(A, B) p27 was knocked down in endothelial cells by transfection with two different siRNAs targeting the p27 mRNA (p27 siRNA-1, p27 siRNA-2) or a scrambled siRNA (scr) as control, and p27 levels were determined by immunoblot. **(A)** Representative immunoblots, Actin served as loading control. **(B)** Knockdown efficiency was determined by semiquantitative analysis of immunoblots. Data are mean ± SEM, n=5, *p<0.05 versus scr (one-way ANOVA). **(C)** Endothelial cells were transfected with the same siRNAs as before, a wound was set 48 hours after transfection and the cells were treated with 50 μM caffeine for another 18 hours or left untreated. Migratory capacity was assessed by counting cells migrated into the wound using Image J. Data are mean ± SEM, n=5, *p<0.05 vs scr -

184 caffeine, #p<0.05 vs scr +caffeine (one-way ANOVA). Underlying data are provided in S1
185 Data.
186
187 Since functional mitochondria are necessary for endothelial cell migration [8] and
188 protein translocation to these organelles is a major determinant of their functional capacity
189 [23], we wanted to establish a causal link between mitochondria and p27. Therefore, we
190 investigated whether p27 is localized in mitochondria. As shown by immunoblots following
191 biochemical separation, a fraction of p27 is localized in mitochondria. The purity of the
192 mitochondrial preparations was confirmed by detection of the non-mitochondrial protein
193 Thioredoxin-1 (Trx-1) and the mitochondrial Translocase of inner mitochondrial membrane
194 23 (TIM23), respectively. As an additional control, we also detected the Cyclin Dependent
195 Kinase Inhibitor 1A (CDKN1A), also known as p21, a member of the same protein family.
196 As demonstrated in figure 2A, p21 is not localized in the mitochondria and caffeine does not
197 affect the protein levels. Moreover, treatment with caffeine significantly increased
198 mitochondrial p27 (Fig 2A and 2B, S5 Fig). To further verify that p27 is truly localized in the
199 mitochondria and not simply attached to these organelles, we performed a proteinase K
200 digest of isolated mitochondria. As demonstrated in Fig 2C, p27 is indeed localized within
201 the mitochondria. Digestion of the outer mitochondrial membrane with proteinase K in
202 hypotonic buffer results in mitoplasts, mitochondria stripped of their outer membrane,
203 leaving only the inner mitochondrial membrane and the matrix. The immunoblot analysis
204 confirmed loss of Translocase of outer mitochondrial membrane 40 (TOM40), but revealed
205 inner mitochondrial membrane proteins like TIM23, and matrix proteins like the
206 mitochondrial heat shock protein 70, also called heat shock protein 70 kDa protein 9
207 (HSPA9) or GRP75, respectively, and also p27 (Fig 2C). To causally link migration to
208 mitochondrial p27, we cloned targeted variants of p27, which are exclusively localized in the
209 nucleus or mitochondria, and expressed them in endothelial cells. Overexpression of
210 nuclear as well as mitochondrially targeted p27 revealed comparable expression levels (Fig

2D). Moreover, mitochondrially targeted p27 is exclusively found in the mitochondria, conversely, nuclear targeted p27 could only be detected in the nucleus (Fig 2E). We then established a rescue experiment, in which endogenous p27 was first knocked down by siRNAs followed by overexpression of nuclear or mitochondrially targeted p27. Strikingly, only mitochondrially targeted p27 rescued the migratory defect induced by knockdown of p27, whereas nuclear targeted p27 did not improve the migratory capacity (Fig 2F). Next, we investigated whether induction of migration by mitochondrial p27 can be further increased by caffeine. Therefore, we overexpressed mitochondrial p27 in endothelial cells, treated the cells with caffeine and measured migratory capacity; nuclear targeted p27 and an empty vector served as controls. Caffeine increased migratory capacity in cells transfected with the empty vector or expressing nuclear p27 (Fig 2G). Without caffeine, only mitochondrially targeted p27 induced migration of endothelial cells, however, the combination of caffeine and mitochondrial p27 did not show any additive effects. Thus, caffeine and mitochondrial p27 either share a common pro-migratory pathway or each individual stimulus already induced maximal migratory capacity in these cells (Fig 2G). To evaluate whether mitochondrial p27, but not nuclear p27, improves mitochondrial parameters, we measured mitochondrial membrane potential in endothelial cells overexpressing mitochondrial p27 or nuclear p27, respectively. Interestingly, only mitochondrially targeted p27 significantly enhanced mitochondrial membrane potential (Fig 2H).

Fig 2. Mitochondrial p27 is sufficient to induce endothelial cell migration.

(A, B) Endothelial cells were treated with 50 μM caffeine for 18 hours and mitochondrial (mito) and non-mitochondrial (non-mito) fractions were separated. p27 and the closely related p21 protein were detected by immunoblot, TIM23 and Trx-1 served as purity controls for the fractions. **(A)** Representative immunoblots. **(B)** Semiquantitative analysis of mitochondrial p27 normalized to TIM23. Data are mean ± SEM, n=6, *p<0.05 (two-tailed unpaired t-test). **(C)** Proteinase K digestion of mitochondria. The different digestion

conditions yield intact mitochondria (1), mitochondria stripped of attached proteins (2) and mitoplasts (3); 4 denotes complete digestion. p27 and marker proteins for the outer (TOM40) or inner (TIM23) mitochondrial membrane and the mitochondrial matrix (GRP75) were detected by immunoblot. **(D, E)** Endothelial cells were transfected with an empty vector (EV) or expression vectors for nuclear (nuc p27) or mitochondrial p27 (mito p27). Expression and localization of the organelle-targeted p27 proteins was analyzed by immunoblot and immunofluorescence. **(D)** Representative immunoblot, tubulin served as loading control. Due to the presence of a trimeric nuclear localization signal at the C-terminus, the nuclear targeted protein has a larger molecular weight. **(E)** Representative immunostainings: nuclei were visualized with DAPI (blue), mitochondria by staining for TIM23 (red), and the targeted p27 variants by staining for the myc epitope (myc (p27), green). Merge shows an overlay of all fluorescence channels. **(F)** Endothelial cells were transfected with the siRNAs used in figure 1. 48 hours later cells were transfected with an empty vector (EV) or the expression vectors for nuclear (nuc p27) or mitochondrial p27 (mito p27). 3 hours later a wound was set. Migratory capacity was assessed 18 hours later by counting cells migrated into the wound using Image J. Data are mean ± SEM, n=5: p27 siRNA-1/EV, p27 siRNA-2/EV, p27 siRNA-1/nuc p27 siRNA-1/mito p27, n=6: all others, *$p<0.05$ vs corresponding scr, $^{\#}p<0.05$ vs scr/mito p27, $^{\S}p<0.05$ vs p27 siRNA-1/mito p27, $^{\$}p<0.05$ vs p27 siRNA-2/mito p27 (one-way ANOVA). **(G)** Endothelial cells were transfected with an empty vector (EV) or expression vectors for nuclear (nuc p27) or mitochondrial p27 (mito p27). 3 hours later a wound was set and cells were treated with 50 µM caffeine for 18 hours or left untreated. Migratory capacity was assessed by counting cells migrated into the wound using Image J. Data are mean ± SEM, n=5-7, *$p<0.05$ vs EV -caffeine, n.s.=not significant (Mann-Whitney pairwise comparison with Bonferroni-corrected p-values). **(H)** Endothelial cells were transfected with an empty vector (EV) or expression vectors for nuclear (nuc p27) or mitochondrial p27 (mito p27). 24 hours after transfection the mitochondrial membrane potential was measured with JC1 using flow cytometry. Data are

mean ± SEM, n=5, *p<0.05 vs EV, #p<0.05 vs nuc p27, n.s.=not significant (one-way ANOVA). Underlying data are provided in S1 Data.

The N- and C-terminus of mitochondrial p27 with serine 10 and threonine 187 are required for migratory capacity of endothelial cells

Given the novelty of our findings, we wanted to understand which domains in p27 could be responsible for its effects on cell migration and mitochondrial functions. Subcellular distribution of p27 was described to be regulated by phosphorylation of at least four phosphorylation sites at serine 10, threonine 157, threonine 187, and threonine 198, all of which have been suggested to be important for non-nuclear localization. The role of phosphorylation at these sites is discussed controversially, as it could differ dependent on cell and tumor type or organ system. Nevertheless, as nuclear p27 cannot compensate for the loss of migratory capacity after knockdown of the endogenous protein, it is suggestive that these sites may play a role in migration, which depends on mitochondria. Therefore, we decided to generate p27 mutants with a mitochondrial targeting sequence, in which either the N-terminus with serine 10 (ΔN, amino acids (aa) 25-198 retained), the C-terminus with the other phosphorylation sites (ΔC, aa 1-151 retained) or both (ΔN/ΔC, aa 25-151 retained) were deleted, leaving the cyclin dependent kinase inhibitor (CDI) domain intact in every construct (Fig 3A). We first confirmed by immunoblotting that all of the mutants are expressed at comparable levels (Fig 3B). Then, we confirmed that the mutants are exclusively localized in the mitochondria (Fig 3C). Next, we examined their impact on functional capacity of human primary endothelial cells by measuring migration and ATP content. Cells overexpressing the ΔN or the ΔC mutant showed only a reduced migratory capacity compared to full-length p27, whereas the ΔN/ΔC mutant completely lost the ability to induce migration (Fig 3D). Full-length p27 increased mitochondrial ATP content (Fig 3E). In contrast, this was not observed in cells overexpressing any of the p27 deletion mutants

(Fig 3E). These data demonstrate that both the N- and C-terminus of p27 are required for the functional capacity of endothelial cells.

Fig 3. The N- and C-terminus of p27 are required for endothelial cell migration and ATP content.

(A) Schematic representation of mitochondrially targeted p27 deletion mutants lacking the N-terminus (ΔN), the C-terminus (ΔC) or both (ΔNΔC). The full-length protein (fl) and all mutants contain a N-terminal mitochondrial targeting sequence (MTS, red) and a C-terminal myc tag (green), CDI denotes the Cyclin dependent kinase inhibitor domain. Numbers indicate the deletion endpoints within p27. **(B-E)** Endothelial cells were transfected with an empty vector (EV) or expression vectors for the mitochondrially targeted p27 mutants depicted in (A). **(B, C)** Expression and localization of the mitochondrially-targeted mutant p27 proteins were analyzed by immunoblot and immunofluorescence. **(B)** Representative immunoblot, tubulin served as loading control. **(C)** Representative immunostainings: nuclei were visualized with DAPI (blue), mitochondria by staining for TIM23 (red), and the targeted p27 mutants by staining for the myc epitope (myc (p27), green). Merge shows an overlay of all fluorescence channels. **(D)** Migratory capacity was measured in a scratch wound assay by counting cells migrated into the wound using Image J. Data are mean ± SEM, n=6, *$p<0.05$ vs EV, $^{\#}p<0.05$ vs fl mito p27, n.s.=not significant (one-way ANOVA). **(E)** ATP content was measured with a luminometric assay. Data are mean ± SEM, n=5, *$p<0.05$ vs EV, $^{\#}p<0.05$ vs fl mito p27, n.s.=not significant (one-way ANOVA). Underlying data are provided in S1 Data.

To further narrow down the amino acids relevant for mitochondrial p27, we focused on serine 10 and threonine 187 as the more likely candidates for phosphorylation, because threonine 157 and 198 have been described as relevant for p27/cyclin D1/Cdk4 complex assembly and as such for cell cycle regulation [24]. Moreover, for the cardiovascular system, it has been shown that p27 phosphorylation at serine 10 is reduced in murine and

human atherosclerotic arteries and that prevention of this phosphorylation aggravates atherosclerosis independent of cell proliferation [25]. Phosphorylation at threonine 187 has been demonstrated to result in proteasomal degradation of p27 in several cancer cells [26], however, in the cardiovascular system loss of this phosphorylation did not affect aortic p27 protein levels [27]. Therefore, we first examined whether caffeine induces phosphorylation of p27 at serine 10 and threonine 187. Indeed, 50 μM caffeine increased phosphorylation at both sites by approximately two fold (Fig 4A and 4B). Since both the N- and C-terminus are required for the functional capacity of p27 in endothelial cells (Fig 3D and 3E), we generated a mitochondrially targeted, non-phosphorylatable p27(S10A/T187A) double mutant and measured the impact on migratory capacity compared to mitochondrially targeted full-length p27. Besides comparable expression levels between p27 wt and the mutant (Fig 4C), immunostainings confirmed the mitochondrial localization (Fig 4D). Strikingly, overexpression of this mutant did not induce migration in endothelial cells (Fig 4E). Thus, serine 10 and threonine 187, at least in the mitochondrial fraction of p27, are required for migratory capacity. To elucidate whether these two residues are also necessary for the import of p27 into the mitochondria, we generated an analogous, but untargeted p27(S10A/T187A) mutant. Following expression of this variant and the corresponding wildtype protein in endothelial cells, their protein levels in mitochondrial fractions were measured. Interestingly, the ability of p27(S10A/T187A) to become imported into the mitochondria was severely restricted (Fig 4F and 4G), suggesting that the amino acids, which are critical for migratory capacity are also involved in the translocation into the mitochondria.

Fig 4. Serine 10 and threonine 187 of p27 are required for endothelial cell migration and mitochondrial import.

(A, B) Endothelial cells were treated with caffeine for 18 hours or left untreated and phosphorylation of serine 10 (p27 P-S10) and threonine 187 (p27 P-T187) as well as total p27 (p27) were detected by immunoblot. **(A)** Representative immunoblots with the

corresponding loading control (Tubulin) below the respective immunoblot. The asterisk denotes p27 phosphorylated on threonine 187. **(B)** Semiquantitative analyses of the ratio of phosphorylated p27 to total p27 for both phosphorylation events. Data are mean ± SEM, n=7: p27 P-S10, n=6: p27 P-T187, *p<0.05 (two-tailed unpaired t-test). **(C, D)** Endothelial cells were transfected with an empty vector (EV) and expression vectors for mitochondrially targeted p27 (mito p27 wt) or a mutant, in which serine 10 and threonine 187 were replaced by alanine (mito p27 S/T-A). Expression and localization of the corresponding proteins were analyzed by immunoblot and immunofluorescence. **(C)** Representative immunoblot, tubulin served as loading control. **(D)** Representative immunostainings: nuclei were visualized with DAPI (blue), mitochondria by staining for TIM23 (red), and the targeted p27 mutants by staining for the myc epitope (myc (p27), green). Merge shows an overlay of all fluorescence channels. **(E)** Endothelial cells were transfected as in (C), a wound was set and migratory capacity was assessed by counting cells migrated into the wound using Image J. Data are mean ± SEM, n=5, *p<0.05 vs mito p27 wt, n.s.=not significant (one-way ANOVA). **(F, G)** Endothelial cells were transfected with expression vectors for p27 wildtype (wt) or the corresponding S/T-A mutant (S/T-A), both without a mitochondrial targeting sequence. Mitochondrial fractions (mito) were prepared and the expressed proteins were detected by immunoblot. **(F)** Representative immunoblots: the p27 proteins were detected with an anti-myc antibody (myc (p27)), TIM23 served as a loading control and Trx-1 as purity control for the mitochondrial fractions. Analysis of total cell lysates (lysate) ensures similar expression levels. **(G)** Semiquantitiative analysis of mitochondrial p27 normalized to TIM23. Data are mean ± SEM, n=5, *p<0.05 vs p27 (wt) (two-tailed unpaired t-test). Underlying data are provided in S1 Data.

Caffeine effects in the heart are linked to mitochondrial p27

It had been assumed that knockout of a cell cycle inhibitor like p27 could be beneficial in the experimental setup of myocardial infarction. This was based on the

372 reasoning that myocardial infarction leads to loss of cells in the heart and that enhanced
373 proliferation of cells in p27-deficient mice may result in smaller infarct size and reduced
374 mortality. However, exactly the opposite was observed. Mice showed bigger infarct size and
375 the mortality was significantly increased [5,6]. Since functional mitochondria in the heart are
376 required not only to provide energy for the pumping function but also to cope with externally
377 or internally induced changes, e.g. during and after myocardial infarction, we hypothesized
378 that a non-cell cycle related function of p27, according to our data most likely in the
379 mitochondria, could also be important for the heart. Therefore, we first analyzed the role of
380 mitochondrial p27 in cell death induction in cardiomyocytes - a hallmark of cardiac
381 pathologies [28]. We lentivirally expressed mitochondrially targeted p27 in cardiomyocytes
382 and measured basal and oxidative stress-induced apoptosis. Mitochondrial p27
383 dramatically reduced basal apoptosis and completely blunted H_2O_2-induced cell death (Fig
384 5A). As functional mitochondria play a pivotal role in protection against heart disease and
385 p27-deficient mice show increased mortality after myocardial infarction [6], we measured
386 oxygen consumption in heart mitochondria isolated from adult p27-deficient mice and their
387 wildtype littermates as a readout for mitochondrial function. Mitochondria isolated from p27-
388 deficient mice displayed significantly reduced complex I respiration, which demonstrates
389 that those animals have impaired mitochondrial functionality (Fig 5B). To further establish a
390 causal link between caffeine and p27, p27-deficient animals were given 0.05% caffeine in
391 drinking water for 10 days, a concentration, for which we had previously shown to result in a
392 serum concentration of approximately 30 - 50 μM and a time sufficient to completely restore
393 the carotid endothelium after wire injury [8] Strikingly, caffeine did not improve respiration in
394 hearts of p27-deficient mice (Fig 5B), whereas respiration in wildtype littermates was
395 increased by caffeine. Next, we wanted to determine whether a connection between
396 caffeine and mitochondrial p27 also exists on the transcriptome level. Therefore, p27-
397 deficient animals and their wildtype littermates were given 0.05% caffeine in drinking water
398 for 10 days. After that, RNA was isolated from whole hearts and microarray analyses were

performed. As shown in the Venn diagram in Fig 5C, all but 3 of the 245 transcripts differentially expressed after caffeine administration in wildtype mice were p27-dependent, since only 3 were also regulated in p27-deficient animals. Interestingly, among the most highly enriched gene ontology (GO) categories for biological processes are GO-terms describing pathways, which take place in the mitochondria (S1 Table). Strikingly, more than one third of the transcripts in all other gene ontology categories are translated into proteins localized in the mitochondria (S1 Table), demonstrating that the caffeine induced, p27-depdendent transcriptome changes affect to a large part the mitochondria.

Fig 5. Caffeine effects in the heart depend on p27.

(A) The mouse cardiomyocyte cell line HL-1 was lentivirally transduced with an empty vector (EV) or an expression vector for mitochondrially targeted p27 (mito p27) and treated with 500 μM H_2O_2 for 48 hours. Apoptosis was measured as annexin V positive/7-propidium iodide (PI) negative cells by flow cytometry. Data are mean ± SEM, n=5, *p<0.05 vs EV -H_2O_2, $^{\#}$p<0.05 vs EV +H_2O_2 (one-way ANOVA). **(B)** Respiration was determined in isolated heart mitochondria of adult wildtype mice (wt) and p27-deficient littermates (p27ko), who had received drinking water without caffeine (■ wt; ■ p27ko) or water supplemented with 0.05% caffeine for 10 days (■ wt; ■ p27ko). Respiration was measured as oxygen (O_2) consumption was measured without the addition of substrates (mito) and after the successive addition of malate/glutamate (M/G), ADP, rotenone (rot) and succinate (succ) (left panel). The right panel shows a magnification of oxygen consumption after the addition of malate/glutamate and ADP, respectively. Data are mean ± SEM, n=5-8 per group, *p<0.05 vs wildtype without caffeine, n.s.=not significant (one-way ANOVA). **(C)** Adult p27-deficient animals and their wildtype littermates received drinking water or water supplemented with 0.05% caffeine for 10 days. RNAs were isolated from the hearts of those mice and microarray analyses were conducted. Data are represented as Venn diagram. The numbers in the circles indicate the number of regulated transcripts (n=3 animals per genotype and treatment, p<0.05). (●) transcripts differentially regulated by

caffeine in wildtype mice, (●) transcripts differentially regulated by caffeine in the p27-deficient littermates. Underlying data are provided in S1 Data.

Mitochondrial p27 is required for proper cardiac myofibroblast differentiation

Over the last years it has become evident that in several healing processes, including wound healing and the early phase after myocardial infarction, fibroblasts have to differentiate into myofibroblasts to fill the gaps caused by cell loss. Recent findings demonstrated that intact mitochondria are needed for differentiation of fibroblasts into myofibroblasts in response to factors like transforming growth factor β1 (TGFβ1) [9]. Thus, we isolated cardiac fibroblasts from p27-deficient mice and wildtype littermates and induced myofibroblast differentiation by TGFβ in the absence or presence of caffeine. Strikingly, TGFβ1 induced myofibroblast differentiation, measured by the upregulation of α smooth muscle actin (αSMA), only in wildtype cardiac fibroblasts, but not in p27-deficient cells (Fig 6). Moreover, caffeine treatment alone slightly, but significantly increased αSMA levels, probably by improving mitochondrial function, again only in cells isolated from wildtype animals (Fig 6).

Fig 6. p27 is required for myofibroblast differentiation of cardiac fibroblasts.

Cardiac fibroblasts were isolated from hearts of wildtype (wt) mice and p27-deficient (p27 -/-) littermates. Myofibroblast differentiation was induced by treatment with 2 ng/ml TGFβ1 for 48 hours in the presence or absence of 50 μM caffeine. Induction of α smooth muscle actin (αSMA) was detected by immunoblot and immunostaining. **(A)** Representative immunoblots, Vimentin served as loading control. **(B)** Semiquantitative analysis of αSMA normalized to Vimentin. Data are mean ± SEM, n=8: wt untreated, wt +TGFβ1, p27-/- untreated, p27-/- +TGFβ1, n=5: all others, *$p<0.05$ vs wt untreated, $^{\#}p<0.05$ vs wt +caffeine, n.s.=not significant (one-way ANOVA). **(C)** Representative immunostainings: αSMA was stained in red and Vimentin in green, nuclei were counterstained with DAPI (blue), shown are the overlays of all fluorescence channels. Underlying data are provided in S1 Data.

To investigate whether mitochondrial p27 is sufficient to rescue the p27-deficient cells from the differentiation defect, we lentivirally expressed mitochondrially targeted p27 in p27-deficient cardiac fibroblasts. As demonstrated in figure 7, re-expression of mitochondrial p27 restored the ability of p27-deficient cardiac fibroblasts to differentiate into myofibroblasts upon TGFβ1 treatment. Thus, we also established a causal link between mitochondrial p27 and the ability of fibroblasts to differentiate into myofibroblasts.

Fig 7. Mitochondrial p27 restores the impaired αSMA upregulation in p27-deficient cardiac fibroblasts.

Fibroblasts isolated from the hearts of p27-deficient mice were lentivirally transduced with an expression vector for mitochondrially targeted p27 (mito p27) or a corresponding empty vector (EV). **(A)** Representative immunostainings: Representative immunostainings: nuclei were visualized with DAPI (blue), mitochondria by staining for TIM23 (red), and the mitochondrially targeted p27 by staining for the myc epitope (myc (p27), green). Merge shows an overlay of all fluorescence channels. **(B, C)** Myofibroblast differentiation was induced by treatment with 2 ng/ml TGFβ1 for 48 hours and smooth muscle actin (αSMA) was detected by immunoblot. **(B)** Representative immunoblots, Vimentin served as loading control. **(C)** Semiquantitative analysis of αSMA normalized to Vimentin. Data are mean ± SEM, n=5, *p<0.05 vs mito p27 +TGFβ1, n.s.=not significant (one-way ANOVA). Underlying data are provided in S1 Data.

Caffeine - in concert with mitochondrial p27 - is protective in mouse models with mitochondrial dysfunction

One hallmark of the murine and human aging process is reduced mitochondrial respiratory capacity. Therefore, we wanted to determine whether a 10 day treatment with caffeine in 22 months old mice could enhance respiration. Indeed, caffeine increased respiration (Fig 8A). Moreover, the mitochondrial ATP content was increased to roughly the

same extent as the mitochondrial oxygen consumption of complex I (Fig 8B). Interestingly, mitochondrial respiration in hearts of adult p27-deficient mice was similar as in 22 months old wildtype animals (S6 Fig), suggesting that loss of mitochondrial p27 impairs the heart as strongly as aging. This is in accordance with increased infarct size and early mortality after myocardial infarction in p27-deficient mice [6]. Furthermore, 10 days of caffeine treatment in old animals was sufficient to raise the mitochondrial respiration to the levels observed in 6 months old mice (S6 Fig). In addition, the analysis of cardiac mitochondria from old mice showed a roughly twofold increase in mitochondrial p27 content after 10 days of caffeine (Fig 8C and 8D, S7 Fig), demonstrating that caffeine-induced improved respiration is paralleled by an increase in mitochondrial p27. The amount of mitochondrial p27 in heart mitochondria of old mice after caffeine consumption was comparable to mitochondrial p27 in heart mitochondria of 6 months old mice (S6 Fig). Thus, treatment of old mice with caffeine for 10 days markedly improved mitochondrial p27 and thus respiration in the heart. In addition, we also treated adult, 6 months old littermates with caffeine for 10 days and analyzed mitochondrial p27 by immunoblot. Similar to old mice, caffeine also increased mitochondrial p27 in adult, 6 months old mice when compared to their wildtype littermates (Fig 8E and 8F).

Fig 8. Caffeine enhances respiration, ATP content and mitochondrial localization of p27 in old mouse hearts.

(A-D) 22 months old wildtype mice received drinking water (■ old) or water supplemented with 0.05% caffeine for 10 days (■ old+caffeine). **(A)** Oxygen (O_2) consumption was measured in isolated heart mitochondria without the addition of substrates (mito) and after the successive addition of malate/glutamate (M/G), ADP, rotenone (rot) and succinate (succ) (left panel). The right panel shows a magnification of oxygen consumption after the addition of malate/glutamate and ADP, respectively. Data are mean ± SEM, n=6 per group, *p<0.05 (one-way ANOVA). **(B)** Mitochondrial ATP content was measured with a luminometric assay. Data are mean, n=5 per group, *p<0.05 (one-way ANOVA). **(C)** Heart

mitochondria were isolated and p27 was detected by immunoblot, GRP75 and TIM23 served as loading controls. To control for purity of the mitochondria, a total heart lysate (lys) was used in parallel and Vimentin was detected. Shown is a representative Immunoblot. **(D)** Semiquantitative analysis of mitochondrial p27; data are mean ± SEM, n=7 per group, *p<0.05 (one-way ANOVA). **(E, F)** 6 months old wildtype mice received drinking water (■) or water supplemented with 0.05% caffeine for 10 days (■). **(E)** Heart mitochondria were isolated and p27 was detected by immunoblot, GRP75 and TIM23 served as loading controls. To control for purity of the mitochondria, a total heart lysate (lys) was used in parallel and Vimentin was detected. Shown is a representative Immunoblot. **(F)** Semiquantitative analysis of mitochondrial p27; data are mean ± SEM, n=5 per group, *p<0.05 (one-way ANOVA). Underlying data are provided in S1 Data.

Not only aging, but also obesity as well as type II diabetes have been demonstrated to be associated with mitochondrial dysfunction [29,30]. Therefore, we used a second animal model, in which we fed 2 months old mice a diabetogenic diet (S2 Table) for a total of 9.5 weeks leading to obesity and a prediabetic state. After that, mice were separated into two groups, one of which received caffeine in the drinking water for 10 days. Then, ischemia reperfusion injury was set and animals were analyzed three weeks later. We first measured the scar size of the left ventricle and the minimum left ventricular wall thickness in both groups. 10 days of caffeine treatment significantly reduced scar size and improved wall thickness (Fig 9A, 9B and 9C). Next, we investigated whether caffeine induces translocation of p27 into the mitochondria in this mouse model analogous to our observations in cells and in adult, healthy as well as in old mice. Therefore, co-immunostainings of heart slices for p27 and the inner mitochondrial membrane protein TIM23 were performed in the border zone of the infarcted area. Indeed, colocalization of p27 and TIM23 was increased in the animals that had received caffeine, whereas p27 was mostly nuclear in the hearts of the mice on diabetogenic diet without caffeine

supplementation (Fig 9D). To further support the results obtained in tissue slices of the heart, we isolated mitochondria from hearts of mice fed a diabetogenic diet for 11 weeks with the last 10 days on drinking water or water supplemented with caffeine. In accordance with our co-immunostainings in figure 9D, p27 was significantly increased in the mitochondria of mice, which had received caffeine in their drinking water (Fig 9E and 9F, S7 Fig).

These data demonstrate that caffeine treatment in obese mice can reduce myocardial infarction injury and in parallel increase the levels of mitochondrial p27.

Fig 9. Caffeine improves outcomes after myocardial infarction in prediabetic mice and induces mitochondrial translocation of p27.

2 months old wildtype mice were fed a diabetogenic diet for 11 weeks (■). For the last 10 days one group of animals received drinking water supplemented with 0.05% caffeine (■). Afterwards, myocardial infarction was induced by ligation of the left anterior descending coronary artery for 60 minutes followed by reperfusion. 21 days after infarction, hearts were excised, sectioned and the sections stained. **(A)** Representative Gomori stainings of sections of three different hearts for each dietary regimen. **(B)** Infarct size per left ventricle and **(C)** minimum left ventricular (LV) wall thickness in the infarcted myocardium. Data are mean ± SEM, n=8: diabetogenic diet, n=10: diabetogenic diet +caffeine, *p<0.05 (one-way ANOVA). **(D)** Representative immunostainings of border zone sections for each dietary regimen. TIM23 is stained in red, p27 in green, nuclei were counterstained with DAPI (blue), merge shows an overlay of all fluorescence channels. The dotted rectangles indicate the sections shown in higher magnifications. **(E)** Heart mitochondria were isolated and p27 was detected by immunoblot, GRP75 and TIM23 served as loading controls. To control for purity of the mitochondria, a total heart lysate (lys) was used in parallel and Vimentin was detected. Shown is a representative Immunoblot. **(F)** Semiquantitative analysis of mitochondrial p27; data are mean ± SEM, n=5, *p<0.05 (one-way ANOVA). Underlying data are provided in S1 Data.

Discussion

Here, we demonstrate that p27 is localized in the mitochondria. Serine 10 and threonine 187 within p27 are required for import into the mitochondria and functional improvements induced by mitochondrial p27. Moreover, mitochondrial p27 is sufficient to improve cellular processes, which depend on functional mitochondria, in different cells of the cardiovascular system. Moreover, it is suggestive to assume that the translocation of p27 into mitochondria might be critically involved in the improved outcomes after myocardial infarction upon caffeine administration. In summary, we present an increase in mitochondrial p27 as a new mode of action how measurable caffeine concentrations in humans improves the functionality of the cardiovascular system or can even be protective in states associated with increased risk for cardiovascular diseases.

p27 was initially discovered as a nuclear-localized cell cycle inhibitory protein [1]. Previous data demonstrating that p27 can be exported to the cytoplasm [2,3] were considered as a mechanism to inactivate the cell cycle inhibitory effects of p27 in the nucleus and to allow human cancer cells to escape cell cycle arrest. However, McAllister demonstrated that non-nuclear p27 is required for migration of fibroblasts, since p27-deficient mouse embryonic fibroblasts failed to migrate, while reconstitution with p27 rescued the motility defect [4]. Here, we show that only mitochondrial p27, but not nuclear p27 rescues the loss of migratory capacity induced by knockdown of endogenous p27, revealing a causal, direct link between mitochondrial localization of p27 and endothelial cell migration. Moreover, serine 10 and threonine 187 are required for import into mitochondria and the pro-migratory action of mitochondrial p27.

Interestingly, p27 is not the only protein initially described as a cell cycle inhibitor, which was subsequently shown to elicit cytoplasmic and mitochondrial functions. In fact, prohibitin and prohibitin-2 were originally characterized as tumor suppressor proteins with anti-proliferative activity, when present in the nucleus [31-33]. However, when localized in

588 the mitochondria, prohibitins act as mitochondrial membrane bound chaperones for the
589 stabilization of mitochondrial proteins [34], and interaction of prohibitin with subunits of
590 complex I of the respiratory chain increases mitochondrial activity [35]. Similarly, we show
591 here that p27 is localized within the mitochondria, where it improves mitochondrial
592 functions. Interestingly, prohibitin has also been shown to be required for cell migration [36].
593 Thus, it is tempting to speculate that mitochondrial p27 exerts chaperone and/or assembly
594 functions by interacting with mitochondrial proteins such as prohibitins, in analogy to
595 nuclear p27, which is required for Cyclin D-CDK complex assembly [37]. It is important to
596 note that mitochondrial import of the non-phosphorylatable p27 S10A/T187A mutant is
597 markedly impaired. Thus, serine 10 and threonine 187 are not only required for p27
598 functions within the mitochondria, but also for its import into these organelles. Similar to the
599 p27 S10A/T187A mutant also the mutant, which lacks larger regions of the N- and C-
600 termini, showed an impaired impact on migratory capacity compared to intact p27, even
601 when exclusively localized in the mitochondria. These results confirm the importance of the
602 N- and C- termini of mitochondrial p27 and therein serine 10 and threonine 187 for
603 improving migration of endothelial cells.

604 Importantly, preserved endothelial cell function accounts for up to 40% of insulin-
605 mediated glucose metabolism in humans [38]. Thus, caffeine-mediated stimulation of the
606 functional capacity of the endothelium may indeed provide a direct mechanistic link for the
607 inverse relationship between habitual coffee consumption and the risk for developing type II
608 diabetes mellitus [11]. Moreover, our results with the diabetogenic diet in mice demonstrate
609 that caffeine reduces infarct size in obese, prediabetic mice. Since obesity and type II
610 diabetes mellitus increase the risk for myocardial infarction [39,40], coffee consumption, in
611 addition to adequate medication, body weight lowering and moderate exercise, could help
612 to reduce this risk. Interestingly, two large cohort studies revealed an association between
613 coffee drinking and reduced mortality. In a prospective NIH study coffee drinking was
614 inversely associated of with subsequent mortality among 229,119 men and 173,141 women

for deaths due to heart disease, respiratory disease, stroke, injuries and accidents, diabetes, and infections [12]. Similar results were obtained in a study with 521,330 participants in ten European countries [13].

With respect to aging and thus, to the elderly population, our data demonstrate that the mitochondrial capacity of the old heart is improved by caffeine to that of the adult heart. Since improving cardiovascular functionality in the elderly population is of major importance for extending healthspan, coffee consumption or caffeine per se could be considered as an additional protective dietary factor for the elderly population. Indeed, epidemiological analyses provided evidence that habitual intake of caffeinated beverages reduces the risk of heart disease mortality among elderly [14,15]. Moreover, since the caffeine effects are linked to increased mitochondrial p27 and thus improved mitochondrial function, enhancing mitochondrial p27 could serve as a potential therapeutic strategy not only in cardiovascular diseases, but also in improving healthspan.

Materials and Methods

Ethics Statement

The study does not involve human participants and/or tissue. All experimental protocols for animal studies were approved by the Animal Ethics Committee of the LANUV, Duesseldorf (Az.: 84-02.05.50.15.023, Az.: 84-02.04.2016.A204, Az.: 84-02.04.2015.A322). The anethetics used are detailed in the sections *Preparation of mouse heart mitochondria* and *Myocardial ischemia and reperfusion*.

Experimental animals

p27-deficient mice (B6.129S4-*Cdkn1btm1Mlf*/J) [41] were originally obtained from V. Andres (Madrid, Spain) and backcrossed onto C57BL/6NTac (Taconic) for more than 10 generations. Only heterozygous p27-deficient animals were used as breeders and the offspring was genotyped with a multiplex PCR using DNA prepared from tail clips with the

DirectPCR Lysis Reagent (Mouse Tail) (Viagen Biotech). The primers used were p27ko for1 (5'-AGTTGTGCCTTGTATGCTGGT-3'), p27ko rev1 (5'-ACAACAAGCTGGAACCCTGT-3') and mPGKpA for1 (5'-ATTAAGGGCCAGCTCATTCC-3'). Amplifications were performed for 10 cycles with an annealing temperature starting at 65°C and a decrease of 1°C per cycle, followed by 30 cycles with a constant annealing temperature of 56°C; the extension time in all cycles was 30 seconds. Amplification products were resolved on 1.5% agarose gels; the wild-type allele yields a product of 553 bp, the null allele a product of 325 bp. For all experiments, where no p27-deficient littermates were required, C57BL/6 animals were purchased from Janvier.

Isolation and cultivation of cardiac fibroblasts and induction of myofibroblast differentiation

Mice were sacrificed by cervical dislocation, the hearts were excised and all fat and large vessels removed with a scalpel. Hearts were placed in a culture dish with room temperature Phosphate Buffered Saline PBS (Thermo Fisher Scientific) supplemented with 1% penicillin/streptomycin (Thermo Fisher Scientific) and 2 mM $CaCl_2$ ($PBS^{(++)}$) and the blood was squeezed out with tweezers. After transfer to a new culture dish with $PBS^{(++)}$, hearts were chopped into small pieces. The pieces were distributed into two 2 ml eppendorf tubes each containing 1 ml of a freshly prepared, ice-cold collagenase solution (1 U/ml Collagenase NB 8 Broad Range (Serva) in $PBS^{(++)}$, filter sterilized) and incubated for 15 minutes at 37°C with gentle mixing every 5 minutes. The cell-containing supernatants were transferred to 2 ml eppendorf tubes containing DMEM GlutaMAX™ (Thermo Fisher Scientific) supplemented with 20% fetal bovine serum (Thermo Fisher Scientific) and 1% penicillin/streptomycin to stop the collagenase reaction. After centrifugation for 5 minutes at 400 xg at 4°C, the pelleted cells were resuspended in 1 ml DMEM GlutaMAX™/20% fetal bovine serum/1% penicillin/streptomycin and placed on ice. In parallel, the remainder of the heart pieces was digested again with collagenase under identical conditions. The collagenase digestions were repeated until no more pieces were visible. Finally, all cells were pooled, plated onto a 10 cm culture dish and placed in humidified tissue culture

incubator at 37°C in an atmosphere containing 5% CO_2. After 2 hours all non-adherent cells were carefully aspirated off. Attached cells were washed twice with DMEM GlutaMAX™/10% fetal bovine serum/1% penicillin/streptomycin and from then on grown in this medium.

Cell culture

All cells were cultivated in humidified tissue culture incubator at 37°C in an atmosphere containing 5% CO_2. Primary human endothelial cells were obtained from Lonza and cultured in endothelial basal medium supplemented with 1 µg/ml hydrocortisone, 12 µg/ml bovine brain extract, 50 µg/ml gentamicin, 50 ng/ml amphotericin B, 10 ng/ml epidermal growth factor (Lonza), and 10% fetal bovine serum until the third passage. After detachment with trypsin, cells were grown for at least 18 hours before transfection or treatment. All experiments were performed in the presence of complete medium including 10% fetal bovine serum.

The murine cardiac muscle cell line HL-1 [42] was a gift from W.C. Claycomb and was cultivated in Claycomb medium (Sigma Aldrich) supplemented with 1% penicillin/streptomycin, 100 µM norepinepherine (Sigma Aldrich), 2 mM L-glutamine (Sigma Aldrich) and 10% fetal bovine serum for as many passages as the cells showed contractile activity in the culture dish.

The human embryonic kidney cell line HEK293FT was obtained from Invitrogen and cultured in DMEM GlutaMAX™ supplemented with 10% heat-inactivated fetal bovine serum, 1% penicillin/streptomycin, 0.5 mg/ml geneticin (Thermo Fisher Scientific) as selective antibiotic, and 1% non-essential amino acids (Thermo Fisher Scientific).

Cardiac fibroblasts were cultivated in DMEM GlutaMAX™ supplemented with 10% fetal bovine serum and 1% penicillin/streptomycin (Thermo Fisher Scientific). For the induction of myofibroblast differentiation, the cells were grown for 24 hours in DMEM GlutaMAX™/1% fetal bovine serum/1% penicillin/streptomycin before recombinant human transforming growth factor β 1 (TGFβ1; 2 ng/ml) (Peprotech) was added for another 48 hours.

Cell lines and primary murine cardiac fibroblasts were routinely tested to be free of mycoplasmas using a PCR-based approach, which detects the most common species of mycoplasmas and includes appropriate internal and positive controls [43].

Transient transfections

Endothelial cells were transfected on 6 cm culture dishes with 3 µg plasmid DNA and 25 µl Superfect (Qiagen) as described previously with a transfection efficiency of 40% [44]. Endogenous p27 was downregulated by transfection with two different siRNAs (p27 siRNA 1 duplex sense strand: 5'-GCGCAAGUGGAAUUUCGAU-3'; p27 siRNA 2 duplex sense strand: 5'-GAGCCAACAGAACAGAAGA-3') using JetSi reagent (Eurogentec) according to the manufacturer`s instructions. Expression of nuclear or mitochondrially targeted p27 after knockdown of the endogenous protein was achieved by transfection with Superfect (Qiagen) 18 hours later using Superfect as described above.

Measurements of cell viability with 3-(4,5-dimethylthiazol-2-yl)-2,5-diphenyltetrazolium (MTT)

Cells were incubated with 0.25 mg/ml MTT in medium for 4 hours. After removing the medium, cells were washed with PBS and formazan crystals were dissolved with dimethyl sulfoxide (DMSO). The resulting supernatant was measured in a TECAN plate reader at an absorbance of 550 nm. Absorbance of DMSO at 550 nm was subtracted as background.

Scratch wound assay of endothelial cells

For detection of cell migration, wounds were created by scraping confluent cell monolayers with a sterile disposable rubber policeman [45]. Therefore, endothelial cells were grown on 6 cm dishes, which were previously labeled with a trace line. After injury, non-attached cells were removed by gently washing with culture medium. In cases where migration of transfected cells was analyzed, the wound was set 5 hours after transfection. For caffeine treatments, caffeine was added after the wound was set. Endothelial cell migration from the edge of the injured monolayer was quantified by staining the cells with 20 ng/ml DAPI (Carl Roth) in PBS after the cells have been fixed wit 4% paraformaldehyde for 15 minutes at

room temperature and microscopic pictures were taken using a Zeiss Axiovert 100. The cells, which had invaded the wound from the trace line, were automatically counted using the particle analysis feature of ImageJ 1.42q [46] after watershed separation of overlapping nuclei.

Cloning of p27 expression vectors

The human p27 coding sequence (NM_004064) without the translation termination codon was amplified from endothelial cell cDNA with primers containing Sal I and Not I restriction sites and inserted into pCMV/myc/nuc and pCMV/myc/mito (Invitrogen) opened with these enzymes to generate expression vectors for nuclear and mitochondrially targeted p27, respectively. An analogous expression vector for non-targeted p27 was created by inserting the p27 coding sequence into pCMV/myc/cyto (Invitrogen). Deletion mutants were created by amplifying subregions of the p27 coding sequence with appropriate primers and insertion into the same vector backbones. Point mutations were introduced by site-directed mutagenesis using the QuikChange Multi Site-Directed Mutagenesis Kit (Agilent Technologies). The starting plasmids were used as empty vectors in the respective transfection experiments.

The lentiviral transfer vector for the expression vector of mitochondrially targeted p27 was created by inserting a DNA fragment containing the CMV promoter and the p27 coding sequence with the N-terminal mitochondrial targeting sequence from the expression vector for mitochondrially targeted p27 into pLKO.1-puro (Sigma Aldrich), which also served as empty vector for the respective transductions.

The identity of all plasmids was verified by restriction digestion and DNA sequencing. Plasmid DNAs for transfections were purified with the HiSpeed Plasmid Maxi kit (Qiagen) according to the manufacturer's specifications. Concentrations were measured spectrophotometrically using a Nanodrop and the identity and purity of each preparation was reconfirmed by restriction digestion.

Lentiviral production and transduction

VSV-G pseudotyped lentiviral transduction particles were generated as previously described [47]. Briefly HEK293FT cells were cotransfected with a transfer vector and expression vectors for the VSV-G envelope protein and lentiviral Gag/Pol using the Calcium Phosphate Transfection Kit (Invitrogen) according to the manufacturer's instructions. Virus containing culture supernatants were collected over several days, filtered through a 0.45 µm PVDF membrane and concentrated by ultrafiltration using Vivacell 100 ultrafiltration units with a PES membrane and a molecular weight cut off of 100.000 (Sartorius). Concentrated virus particles were dispensed in aliquots and stored at -80°C. Viral titers were determined with the QuickTiter™ Lentivirus Titer Kit (Lentivirus-Associated HIV p24) (Cell Biolabs). HL-1 cells or murine cardiac fibroblasts were transduced with a multiplicity of infection of approximately 20. The day after transduction the cells were washed three times, the medium replaced, and the H_2O_2 treatment was started.

Total cell lysis

Cells were scraped off the plates and centrifuged for 10 minutes at 800 xg at 4°C. After washing with PBS, cells were resuspended in buffer (50 mM Tris/HCl pH 8, 1% IGEPAL CA-630, 150 mM NaCl, 0.1% SDS, 0.5% desoxycholate) supplemented with protease inhibitor cocktail and phosphatase inhibitor cocktail (both Bimake) and lysed for 30 min at 4°C. Lysates were centrifuged at 18.000 xg and supernatants were transferred to fresh, precooled eppendorf tubes.

Fractionation of cells

Cells were scraped off the plates and centrifuged for 10 minutes at 800 xg at 4°C. After washing with PBS, cells were resuspended in mitochondrial isolation buffer (20 mM HEPES, pH 7.4, 10 mM KCl, 5 mM $MgCl_2$, 1 mM EDTA, 1 mM EGTA, 250 mM sucrose), incubated for 3 minutes on ice and then disrupted using a dounce homogenizer. Cellular debris was removed by centrifugation for 10 minutes at 3.000 xg at 4°C. The resulting supernatant was transferred to a new tube and centrifuged again for 15 minutes at 10.000 xg at 4°C. The resulting pellet was washed at least three times with mitochondrial isolation

buffer. Finally, the pellet was resuspended in mitochondrial isolation buffer and used for further analyses. The resulting supernatant was collected as non-mitochondrial fraction.

Proteinase K digestion of mitochondria

Proteinase K digestion of mitochondria was performed essentially as previously described by us [53]. Briefly, to determine where in the mitochondria a protein is localized, 300 µg of mitochondria were distributed in four equal aliquots. Mitochondria were pelleted for 5 minutes at 10.000 xg at 4°C and incubated at 4°C on a shaker in 40 µl of 3 different buffers for 20 minutes. Buffer 1 (isotonic buffer): 250 mM sucrose, 1 mM EGTA, 10 mM HEPES, pH 7, Buffer 2 (hypotonic buffer): 1 mM EGTA, 10 mM HEPES, pH 7, 25 µg/ml proteinase K, Buffer 3 (hypotonic buffer with detergent): 1 mM EGTA, 10 mM HEPES, pH7, 1% Triton-X100, 25 µg/ml proteinase K. After 20 minutes, digestion was stopped by adding phenylmethylsulfonyl fluoride to a final concentration of 2 mM and incubation continued for further 5 minutes with shaking. Aliquot 3 was boiled for 5 minutes in Laemmli-buffer. Aliquot 1 and 2 were washed once with Buffer 1 and resuspended in 40 µl RIPA-buffer (50 mM Tris/HCl pH 8, 1% IGEPAL CA-630, 150 mM NaCl, 0.1% SDS, 0.5% desoxycholate) and boiled for 5 minutes in Laemmli-buffer.

SDS-PAGE and immunoblotting

Electrophoretic separation of proteins with sodium dodecyl sulfate polyacrylamide gel electrophoresis (SDS-PAGE) and blotting onto polyvinylidene difluoride membranes was performed according to standard methods. Detection of the different proteins was performed with antibodies directed against p27 (clone D37H1, Cell Signaling Technology, 1:300), phospho-p27 (S10) (clone EP233(2)Y, Abcam, 1:300), phospho-p27 (T187) (polyclonal, ab75908, Abcam, 1:300), TIM23 (clone 32, BD Biosciences, 1:2000), TOM40 (polyclonal sc11414 and monoclonal, sc365467, Santa Cruz Biotechnology, 1:400), Trx-1 (clone 3A1, Abcam, 1:1000), GRP75 (clone D13H4, Cell Signaling Technology, 1:500), γ-Actin (clone 2-2.1.14.17, Sigma Aldrich,1:5000), α-Tubulin (clone DM1A, Sigma Aldrich, 1:50000), myc-tag (rabbit clone 71D10 or mouse clone 9B11, Cell Signaling Technology,

1:500), Vimentin (clone EPR3776, Abcam, 1:12000), αSMA (polyclonal, ab5694, Abcam, 1:6000), PDE5A (polyclonal, #2395, Cell Signaling Technology, 1:1000), phospho-PDE5A (S92 in mouse, S102 in human) (polyclonal, GTX36930, Genetex, 1:250), PDE4A (polyclonal, ab200383, Abcam, 1:500), phospho-PDE4A (serine 686/688) (polyclonal, NB300-635, Novus Biological, 1:1000). After protein transfer, membranes were incubated with primary antibodies overnight at 4°C before they were washed and incubated with secondary antibodies (anti-mouse IgG, HRP-linked whole Ab from sheep, NA931V, GE Healthcare Life Sciences, anti-rabbit IgG, HRP-linked whole Ab from donkey, NA934V, GE Healthcare Life Sciences) according to standard procedures. Detection was performed by enhanced chemiluminescence using the ECL reagent (GE Healthcare) and standard X-ray films. Semi-quantitative analyses were performed on scanned X-ray films using ImageJ 1.42q [46].

ATP measurements

ATP levels in total cell lysates and mitochondria preparations were determined with the luminescence based ATP Kit SL (BioThema). ATP concentrations were calculated according to the manufacturer's recommendations.

Mitochondrial membrane potential

JC-1 dye exhibits potential-dependent accumulation in mitochondria indicative by a fluorescence emission shift from green (~529 nm) to red (~590 nm). Consequently, mitochondrial depolarization is indicated by a decrease in the red/green fluorescence intensity ratio. Therefore, cells were incubated with JC-1 at a final concentration of 0.5 µM for 30 minutes. Cells were washed twice with PBS, and fluorescence intensities were determined using a FACSCalibur (Becton Dickinson). Mean red JC-1 fluorescence was calculated.

Immunostaining of cells

For the detection of nuclear and mitochondrially targeted p27 cells were fixed in 4% paraformaldehyde and permeabilized using 0.3% Triton-X 100/3% bovine serum albumin in

PBS. For coimmunostaining, cells were first incubated with a mouse antibody against myc-tag (clone 9E10, Santa Cruz Biotechnology, 1:50) at 4°C overnight, a Rhodamine Red-X-conjugated Fab fragment anti-mouse was used as secondary antibody (Jackson ImmunoResearch, 1:300, 1 hour, room temperature). Afterwards, cells were incubated with a rabbit anti-TOM40 antibody (polyclonal, sc11414, Santa Cruz Biotechnology, 1:50) at room temperature overnight and an ALEXA 488 anti-rabbit secondary antibody (Invitrogen, 1:200, 1 hour, room temperature). Nuclei were counterstained with 1 mM TO-PRO-3 Iodide (Thermo Fisher Scientific) in PBS and mounted with ProLong Gold antifade mounting medium (Invitrogen). Cells were visualized with confocal microscopy (Zeiss, LSM 510 META).

For the localization studies of mitochondrially targeted p27 deletion mutants, endothelial cells were stained for mitochondria using Mito Tracker Red CMXRos (Thermo Fisher Scientific, 1:50000, 30 minutes, room temperature). Subsequently, cells were washed with PBS and fixed for 15 minutes with 4% paraformaldehyde. For permeabilization 0.3% Triton X-100 and 3% bovine serum albumin in PBS were used for 15 minutes. Afterwards, cells were incubated with a FITC-coupled anti-myc-tag antibody (clone 9E10, Santa Cruz Biotechnology, 1:50) at 4°C overnight. Nuclei were visualized with 20 ng/ml DAPI in PBS. Cells were washed with PBS and mounted with ProLong Gold antifade mounting medium (Invitrogen).

A direct immunostaining of αSMA and Vimentin was performed in mouse cardiac fibroblasts. Cells were fixed and permeabilized as described above. An Alexa-Fluor 594 conjugated antibody against αSMA (clone 1A4, Abcam, 1:100) and an Alexa-Fluor 488 conjugated anti-Vimentin antibody (clone, D21H3, Cell Signalling Technologies, 1:100) were incubated at 4 °C overnight. Afterwards, nuclei were stained with DAPI and cells were mounted as above. All primary antibodies were diluted in PBS containing 1% bovine serum albumin.

Fluorescence images were taken with a Zeiss AXIOVERT 200 M or a Zeiss Axio Imager M2.

Apoptosis measurement

Detection of apoptosis was performed by flow cytometry using annexinV-APC binding and 7-amino-actinomycin (7-AAD) staining as described previously [48]. Only annexin V positive/ 7-AAD negative cells were counted truly apoptotic.

RNA isolation and microarrays

RNA was isolated from mouse hearts using Trizol according to the manufacturer`s instruction (Invitrogen) and subjected to a second purification step using RNeasy columns (Qiagen). RNA integrity was checked on an Agilent 2100 Bioanalyzer and concentrations determined by photometric Nanodrop measurement. All samples in this study showed common high quality RNA Integrity Numbers (RIN 9.7-10).

To study the differences in gene expression between wildtype mice and their p27-deficient littermates in response to caffeine, we used oligonucleotide based microarrays. The *Mus musculus* AROS Oligo Set V4.0 was obtained from Operon. Oligonucleotides (70 mers) were dissolved in amino spotting buffer to a concentration of 20 µM (Genetix) and spotted onto UltraGap slides (Corning). After the printing process the oligonucleotides were UV cross-linked (630 mJ/cm2) to the slide surface (NCBI Gene Expression Omnibus Platform GPL5403).

Labeled cRNA probes were synthesized from 500 ng of total RNA using the Quick Amp Labeling Kit (one-color; Agilent Technologies) according to the manufacturer's protocol. Prior to hybridization the slides were incubated in a prewarmed BSA blocking solution containing 5x SSC, 0.1% SDS, and 0.1 mg/ml BSA at 42°C for 45 to 60 minutes. Subsequently, slides were rinsed twice in 0.1x SSC for 5 minutes and for 30 seconds in double-distilled water, both at room temperature. The slides were then dried in a nitrogen flow. Cy3-labeled cRNA samples (2.5 µg) were dissolved in hybridization buffer (final concentration 50% formamide, 5x SSC, 0.1% SDS). Hybridization was carried out in a

883 humid chamber at 42°C for 16 h. After the hybridization step, unbound cRNA and
884 hybridization buffer were removed by several washing steps (2 times 10 minutes 2x SSC,
885 0.1% SDS, 5 times 1 minute 0.1x SSC, and 10 seconds 0.01x SSC).
886 Fluorescence signals were visualized by a GenePix 4000B laser scanner (Axon). GenePix
887 Pro software (v. 6.0) was used to calculate fluorescence intensities. Data analyses on
888 microarray probe signal intensities were conducted with GeneSpring GX software (v.
889 11.0.2; Agilent Technologies). Probe signal intensities were quantile normalized across all
890 samples to reduce inter-array variability. Input data pre-processing was concluded by
891 baseline transformation to the median of all samples. To further improve signal-to-noise
892 ratio, a given probe had to be expressed above background (i.e. fluorescence signal of the
893 probe was detected within the 20th and 100th percentiles of the raw signal distribution of a
894 given array) in all three replicates in at least one of two, or both conditions to be
895 subsequently analyzed in pairwise comparisons. Differential gene expression was
896 statistically determined by unpaired T-tests. The significance threshold was set to $p<0.05$.
897 Gene ontology analyses were performed using DAVID [49,50]. GO category enrichment
898 was statistically evaluated by modified Fisher Exact testing in DAVID (EASE scoring).
899 Additionally, fold enrichment was determined as the ratio of two proportions: 1) number of
900 genes associated with a defined biological process in the experimental data set / total
901 number of differentially expressed genes in the experimental data set vs. 2) total number of
902 genes associated with a defined biological process in the reference data set / total number
903 of genes in the reference data set. Information about subcellular localization of differentially
904 expressed transcripts was taken from the COMPARTMENTS database [51].
905 *Preparation of mouse heart mitochondria*
906 Animals were sacrificed by exsanguination under deep anesthesia using Ketamine/Xylazine
907 (12/1.6 mg/kg bodyweight). Hearts were prepared after perfusion with ice cold PBS, cut into
908 half. The halves were snap frozen in liquid nitrogen and stored at -80°C. After thawing,
909 intact heart mitochondria were prepared as described earlier for mitochondria from rat

organs [52]. Buffer volumes were reduced by a factor of approximately 2 due to account for the lower organ size in mice. In detail, fat, clotted blood, auricles and fasciae were removed from dry hearts. Hearts were cut into 1-2 mm pieces. Pieces were collected in 10 ml of washing buffer (0.3 M sucrose, 10 mM HEPES pH 7.2, 0.2 mM EDTA), 250 µl Trypsin (bovine pancreas type I, Sigma) of a 2.5 mg/ml stock solution was added and minced tissue was further homogenized with a Ultra Turrax (IKA-TIO Basic) (3 x 5 seconds). After constant stirring for 15 minutes, 5 ml of mitochondria isolation buffer (20 mM HEPES, pH 7.4, 10 mM KCl, 5 mM $MgCl_2$, 1 mM EDTA, 1 mM EGTA, 250 mM sucrose) containing 3.25 mg Trypsin inhibitor (*Glycine max*, Sigma) was added. Samples were centrifuged for 10 minutes at 900 xg at 4°C to remove debris. The resulting supernatant was transferred to a fresh eppendorf tube and centrifuged again for 15 minutes at 10000 xg at 4°C. After centrifugation the supernatant was discarded and the pellet was rinsed twice with fresh mitochondrial isolation buffer removing the fluffy white outer rim layer. The resulting brown pellet containing intact mitochondria was resuspended in mitochondria isolation buffer.

Mitochondrial respiration

The rate of mitochondrial respiration was monitored at 25 °C using an Oxygraph-*2k* system (Oroboros) equipped with two chambers and DatLab software as previously described with slight modifications [53]. In detail, 200-300 µg heart mitochondria were added to 2 ml of a buffer containing 200 mM sucrose, 10 mM potassium phosphate, 0.1 % bovine serum albumin, 10 mM Tris-HCl, 10 mM $MgSO_4$, and 2 mM EDTA, pH 7.0 and respiration was measured. Oxygen consumption was measured after the addition of the NADH-generating substrates malate (0.5 mM) and glutamate (0.5 mM). Then, ADP (0.15 mM) was added. To inhibit complex I activity, rotenone was added to a final concentration of 100 nM. Then, succinate (10 mM) was added, and complex II dependent respiration was determined. Finally, KCN (2 mM) was added to inhibit complex IV activity.

Heart mitochondria from p27-deficient and wildtype littermates were always measured blinded in parallel using the same conditions. The same setup was applied to measure

respiration of heart mitochondria isolated from mice, which had received caffeine with the drinking water or water. For each preparation a second set of measurements were performed in a cross-over design.

Diabetogenic diet

Male mice at the age of 7-8 weeks were fed a diabetogenic diet (S7200-E010, EF Bio-Serv F1850mod.; containing 24% sucrose, 35.85 % lard, Ssniff) for 9.5 weeks, leading to a prediabetic state and increased body weight gain. After that, animals were randomized to a control group (diabetogenic diet) or a group receiving additionally 0.05% caffeine in the drinking water (diabetogenic diet + caffeine) 10 days prior to ischemia induction. Caffeine treatment was continued until the end of the experiment three weeks post ischemia. The composition of the diabetogenic diet is detailed in S5 table.

Myocardial ischemia and reperfusion

A closed-chest model of reperfused myocardial infarction was utilized. Mice were anesthetized by intraperitoneal injection of ketamine (100 mg/kg body weight) and xylazine (10 mg/kg body weight), intubated and ventilated with a tidal volume of 10 µl/g body weight at a rate of 140 strokes/minutes (two thirds air, one third oxygen and isoflurane 2.0 vol.% (Forene, Abbott GmbH)). Mice were placed in a supine position on a 38°C warmed plate to maintain body temperature. After a left lateral thoracotomy between the third and four rib, the pericardium was dissected and a 7-0 surgical suture was passed underneath the left anterior descending coronary artery (LAD). Both ends of the surgical suture were threaded through a 1 mm section of PE-20 tubing, forming a loose snare around the LAD and were exteriorized to the left side of the thorax. The suture was left in the subcutaneous tissue. At 3 days post instrumentation, the animals were re-anesthetized by mask inhalation of isoflurane 2.0 vol.% and a mixture of one third oxygen and two thirds room air. Mice were placed in a supine position on a 38°C warmed plate to maintain body temperature. The skin was reopened and after dissecting the loop, both ends of the applied suture were gently pulled tight until ST-elevation appeared on the ECG. After 60 minutes of ischemia,

reperfusion was accomplished by cutting the suture close to the chest wall. Reperfusion was confirmed by reduction of ST-elevation. Reperfusion was performed for 21 days. We strictly adhered to ischemia induction between 8 am and 11 am to ensure equal ischemia and reperfusion tolerance.

Wall thickness and scar size determination

Three weeks post ischemia and reperfusion animals were sacrificed by CO_2 and hearts were excised and rinsed in PBS After dehydration, hearts preserved in Roti-Histofix 4% (Carl Roth) for 24 hours were paraffin-embedded and cut into 5 µm sections in 10 levels (à 100 mm) beginning from the apex up to the ligation side, discarding 250 µm between each level. To calculate scar size size, fibrous area and wall thickness, sections were stained with Gomori's one-step trichrome staining. The heat-fixed sections were deparaffinized twice in Roti-Clear (Carl Roth) for 15 minutes, then rehydrated with a graded ethanol series to dH_2O. Sections were incubated in Bouin's solution (Sigma Aldrich) at 58°C for 15 minutes. After 5 minutes rinsing under running water, nuclear staining was performed with Weigert's iron hematoxylin A and B for 5 minutes (1:1, Sigma Aldrich). The sections were rinsed again for 5 minutes with running water followed by 25 minutes incubation with Gomori 's staining solution (chromotrope 2R, methylenblue, glacial acetic acid, phosphotungstic acid). Sections were briefly rinsed with water and 0.5% acetic acid 2x 2min. Then sections were treated with an ascending alcohol series and Roti-Clear (2 x 5 minutes) and covered with Roti-Mount mounting medium (Carl Roth). Images were taken with a Zeiss Axio Imager M2. The circumference of the entire endocardium and epicardium, the thickness and length of the infarcted portion, fibrous area as well as the left ventricle (LV) cavity area were determined using Diskus View software (Hilgers). Setting of the myocardial infarctions and scoring of scar size and left ventricular wall thickness were conducted in a blinded fashion and confirmed by an independent blinded observer.

Immunostaining of heart slices

The sections were stained with antibodies against p27 (polyclonal, PA5-27188, Thermo Fisher Scientific, 1:25) and TIM23 (clone 32, BD Biosciences, 1:100). The sections were deparaffinized with xylene and rehydrated by a descending alcohol series. For p27 and TIM23 a basic target retrieval solution boiled for 20 minutes in Tris/EDTA buffer pH 9.0 (Dako) was required. The sections were cooled down, washed with PBS and incubated with 4% formalin for 20 minutes in a wet chamber. Then slices were rinsed with PBS and were treated with blocking solution Tris Buffered Saline (50 mM Tris-HCl, 150 mM NaCl, 2.5 mM KCl, pH 8.0) supplemented with 10% fetal bovine serum/3% goat serum/0.1%Triton-X 100 for 1 hour in a wet chamber. The sections were incubated with the primary antibodies overnight at 4° C in a wet chamber. Next, the slices were washed with PBS; the incubation with the respective secondary antibodies (anti-rabbit IgG (H+L) cross-absorbed antibody, Alexa Fluor 647, A21244, Thermo Fisher Scientific, 1:200, and anti-mouse IgG (H+L) cross-absorbed antibody, Alexa Fluor 568, A11004, Thermo Fisher Scientific, 1:200) was performed for 1 hour in a wet chamber. The sections were covered with ProLong Diamond antifade mounting medium with DAPI (Invitrogen). Fluorescence images were taken with a Zeiss Axio Imager M2.

Statistics

The number of experiments (n) given in the figure legends represents independent biological replicates. Normal distribution for all data sets was confirmed by Shapiro-Wilk test; homogeneity of variances (from means) between groups was verified by Levene's test. Pairwise comparisons were performed with two-sided, unpaired Student’s t-tests on raw data. Multiple comparisons were performed using one-way ANOVA with post-hoc Tukey HSD test. Sample sizes for experiments, which were based on the respective statistical tests for data analyses, were calculated employing G*Power version 3.1.9.2 [54]. Effect strength for this power calculation was taken from our earlier studies [8,44,53]. Significance level (α-error) and sensitivity (β-error) were set to 0.05 and 0.95, respectively.

Acknowledgments

We thank Vicente Andres for providing us with the initial p27-deficient founder mice.

References

1. Toyoshima H, Hunter T. p27, a novel inhibitor of G1 cyclin-Cdk protein kinase activity, is related to p21. Cell. 1994;78:67-74.

2. Shin I, Yakes FM, Rojo F, Shin NY, Bakin AV, Baselga J, et al. PKB/Akt mediates cell-cycle progression by phosphorylation of p27(Kip1) at threonine 157 and modulation of its cellular localization. Nat Med. 2002;8:1145-1152.

3. Viglietto G, Motti ML, Bruni P, Melillo RM, D'Alessio A, Califano D, et al. Cytoplasmic relocalization and inhibition of the cyclin-dependent kinase inhibitor p27(Kip1) by PKB/Akt-mediated phosphorylation in breast cancer. Nat Med. 2002;8:1136-1144.

4. McAllister SS, Becker-Hapak M, Pintucci G, Pagano M, Dowdy SF. Novel p27(kip1) C-terminal scatter domain mediates Rac-dependent cell migration independent of cell cycle arrest functions. Mol Cell Biol. 2003;23:216-228.

5. Hauck L, Harms C, An J, Rohne J, Gertz K, Dietz R, et al. Protein kinase CK2 links extracellular growth factor signaling with the control of p27(Kip1) stability in the heart. Nat Med. 2008;14:315-324.

6. Konecny F, Zou J, Husain M, von Harsdorf R. Post-myocardial infarct p27 fusion protein intravenous delivery averts adverse remodelling and improves heart function and survival in rodents. Cardiovasc Res. 2012;94:492-500.

7. Quintero M, Colombo SL, Godfrey A, Moncada S. Mitochondria as signaling organelles in the vascular endothelium. Proc Natl Acad Sci U S A. 2006;103:5379-5384.

8. Spyridopoulos I, Fichtlscherer S, Popp R, Toennes SW, Fisslthaler B, Trepels T, et al. Caffeine enhances endothelial repair by an AMPK-dependent mechanism. Arterioscler Thromb Vasc Biol. 2008;28:1967-1974.

9. Negmadjanov U, Godic Z, Rizvi F, Emelyanova L, Ross G, Richards J, et al. TGF-beta1-mediated differentiation of fibroblasts is associated with increased mitochondrial content and cellular respiration. PLoS One. 2015;10:e0123046.

10. van Dam RM, Feskens EJ. Coffee consumption and risk of type 2 diabetes mellitus. Lancet. 2002;360:1477-1478.

11. van Dam RM, Hu FB. Coffee consumption and risk of type 2 diabetes: a systematic review. Jama. 2005;294:97-104.

12. Freedman ND, Park Y, Abnet CC, Hollenbeck AR, Sinha R. Association of coffee drinking with total and cause-specific mortality. N Engl J Med. 2012;366:1891-1904.

13. Gunter MJ, Murphy N, Cross AJ, Dossus L, Dartois L, Fagherazzi G, et al. Coffee Drinking and Mortality in 10 European Countries: A Multinational Cohort Study. Ann Intern Med. 2017;167:236-247.

14. Greenberg JA, Dunbar CC, Schnoll R, Kokolis R, Kokolis S, Kassotis J. Caffeinated beverage intake and the risk of heart disease mortality in the elderly: a prospective analysis. Am J Clin Nutr. 2007;85:392-398.

15. Greenberg JA, Chow G, Ziegelstein RC. Caffeinated coffee consumption, cardiovascular disease, and heart valve disease in the elderly (from the Framingham Study). Am J Cardiol. 2008;102:1502-1508.

16. Fisone G, Borgkvist A, Usiello A. Caffeine as a psychomotor stimulant: mechanism of action. Cell Mol Life Sci. 2004;61:857-872.

17. Banerjee P, Ali Z, Levine B, Fowler DR. Fatal caffeine intoxication: a series of eight cases from 1999 to 2009. J Forensic Sci. 2014;59:865-868.

18. Benowitz NL. Clinical pharmacology of caffeine. Annu Rev Med. 1990;41:277-288.

19. Smellie FW, Davis CW, Daly JW, Wells JN. Alkylxanthines: inhibition of adenosine-elicited accumulation of cyclic AMP in brain slices and of brain phosphodiesterase activity. Life Sci. 1979;24:2475-2482.

20. Daly JW. Caffeine analogs: biomedical impact. Cell Mol Life Sci. 2007;64:2153-2169.

21. Lasley RD, Jahania MS, Mentzer RM, Jr. Beneficial effects of adenosine A(2a) agonist CGS-21680 in infarcted and stunned porcine myocardium. Am J Physiol Heart Circ Physiol. 2001;280:H1660-1666.

22. Ribe D, Sawbridge D, Thakur S, Hussey M, Ledent C, Kitchen I, et al. Adenosine A2A receptor signaling regulation of cardiac NADPH oxidase activity. Free Radic Biol Med. 2008;44:1433-1442.

23. Mokranjac D, Neupert W. Protein import into mitochondria. Biochem Soc Trans. 2005;33:1019-1023.

24. Larrea MD, Liang J, Da Silva T, Hong F, Shao SH, Han K, et al. Phosphorylation of p27Kip1 regulates assembly and activation of cyclin D1-Cdk4. Mol Cell Biol. 2008;28:6462-6472.

25. Fuster JJ, Gonzalez-Navarro H, Vinue A, Molina-Sanchez P, Andres-Manzano MJ, Nakayama KI, et al. Deficient p27 phosphorylation at serine 10 increases macrophage foam cell formation and aggravates atherosclerosis through a proliferation-independent mechanism. Arterioscler Thromb Vasc Biol. 2011;31:2455-2463.

26. Grimmler M, Wang Y, Mund T, Cilensek Z, Keidel EM, Waddell MB, et al. Cdk-inhibitory activity and stability of p27Kip1 are directly regulated by oncogenic tyrosine kinases. Cell. 2007;128:269-280.

27. Sanz-Gonzalez SM, Melero-Fernandez de Mera R, Malek NP, Andres V. Atheroma development in apolipoprotein E-null mice is not regulated by phosphorylation of p27(Kip1) on threonine 187. J Cell Biochem. 2006;97:735-743.

28. Chiong M, Wang ZV, Pedrozo Z, Cao DJ, Troncoso R, Ibacache M, et al. Cardiomyocyte death: mechanisms and translational implications. Cell Death Dis. 2011;2:e244.

29. Abel ED. Obesity stresses cardiac mitochondria even when you are young. J Am Coll Cardiol. 2011;57:586-589.

30. Lowell BB, Shulman GI. Mitochondrial dysfunction and type 2 diabetes. Science. 2005;307:384-387.

31. Wang S, Fusaro G, Padmanabhan J, Chellappan SP. Prohibitin co-localizes with Rb in the nucleus and recruits N-CoR and HDAC1 for transcriptional repression. Oncogene. 2002;21:8388-8396.

32. Kurtev V, Margueron R, Kroboth K, Ogris E, Cavailles V, Seiser C. Transcriptional regulation by the repressor of estrogen receptor activity via recruitment of histone deacetylases. J Biol Chem. 2004;279:24834-24843.

33. Sun L, Liu L, Yang XJ, Wu Z. Akt binds prohibitin 2 and relieves its repression of MyoD and muscle differentiation. J Cell Sci. 2004;117:3021-3029.

34. Nijtmans LG, de Jong L, Artal Sanz M, Coates PJ, Berden JA, Back JW, et al. Prohibitins act as a membrane-bound chaperone for the stabilization of mitochondrial proteins. Embo J. 2000;19:2444-2451.

35. Bourges I, Ramus C, Mousson de Camaret B, Beugnot R, Remacle C, Cardol P, et al. Structural organization of mitochondrial human complex I: role of the ND4 and ND5 mitochondria-encoded subunits and interaction with prohibitin. Biochem J. 2004;383:491-499.

36. Rajalingam K, Wunder C, Brinkmann V, Churin Y, Hekman M, Sievers C, et al. Prohibitin is required for Ras-induced Raf-MEK-ERK activation and epithelial cell migration. Nat Cell Biol. 2005;7:837-843.

37. Cheng M, Olivier P, Diehl JA, Fero M, Roussel MF, Roberts JM, et al. The p21(Cip1) and p27(Kip1) CDK 'inhibitors' are essential activators of cyclin D-dependent kinases in murine fibroblasts. EMBO J. 1999;18:1571-1583.

38. Mather K, Laakso M, Edelman S, Hook G, Baron A. Evidence for physiological coupling of insulin-mediated glucose metabolism and limb blood flow. Am J Physiol Endocrinol Metab. 2000;279:E1264-1270.

39. Yusuf S, Hawken S, Ounpuu S, Bautista L, Franzosi MG, Commerford P, et al. Obesity and the risk of myocardial infarction in 27,000 participants from 52 countries: a case-control study. Lancet. 2005;366:1640-1649.

40. Laakso M. Hyperglycemia and cardiovascular disease in type 2 diabetes. Diabetes. 1999;48:937-942.

41. Fero ML, Rivkin M, Tasch M, Porter P, Carow CE, Firpo E, et al. A syndrome of multiorgan hyperplasia with features of gigantism, tumorigenesis, and female sterility in p27(Kip1)-deficient mice. Cell. 1996;85:733-744.

42. Claycomb WC, Lanson NA, Jr., Stallworth BS, Egeland DB, Delcarpio JB, Bahinski A, et al. HL-1 cells: a cardiac muscle cell line that contracts and retains phenotypic characteristics of the adult cardiomyocyte. Proc Natl Acad Sci U S A. 1998;95:2979-2984.

43. Uphoff CC, Drexler HG. Detection of mycoplasma contaminations. Methods Mol Biol. 2013;946:1-13.

44. Haendeler J, Hoffmann J, Tischler V, Berk BC, Zeiher AM, Dimmeler S. Redox regulatory and anti-apoptotic functions of thioredoxin depend on S-nitrosylation at cysteine 69. Nat Cell Biol. 2002;4:743-749.

45. Tamura M, Gu J, Matsumoto K, Aota S, Parson R, Yamada KM. Inhibition of cell migration, spreading and focal adhesions by tumor suppressor PTEN. Science. 1998;280:1614-1617.

46. Abramoff MD, Magelhaes PJ, Ram SJ. Image Processing with ImageJ. Biophotonics International. 2004;11:36-42.

47. Goy C, Czypiorski P, Altschmied J, Jakob S, Rabanter LL, Brewer AC, et al. The imbalanced redox status in senescent endothelial cells is due to dysregulated Thioredoxin-1 and NADPH oxidase 4. Exp Gerontol. 2014;56:45-52.

48. Schroeder P, Popp R, Wiegand B, Altschmied J, Haendeler J. Nuclear redox-signaling is essential for apoptosis inhibition in endothelial cells--important role for nuclear thioredoxin-1. Arterioscler Thromb Vasc Biol. 2007;27:2325-2331.

49. Huang da W, Sherman BT, Lempicki RA. Systematic and integrative analysis of large gene lists using DAVID bioinformatics resources. Nat Protoc. 2009;4:44-57.

50. Huang da W, Sherman BT, Lempicki RA. Bioinformatics enrichment tools: paths toward the comprehensive functional analysis of large gene lists. Nucleic Acids Res. 2009;37:1-13.

51. Binder JX, Pletscher-Frankild S, Tsafou K, Stolte C, O'Donoghue SI, Schneider R, et al. COMPARTMENTS: unification and visualization of protein subcellular localization evidence. Database (Oxford). 2014;2014:bau012.

52. Drose S, Brandt U, Hanley PJ. K+-independent actions of diazoxide question the role of inner membrane KATP channels in mitochondrial cytoprotective signaling. J Biol Chem. 2006;281:23733-23739.

53. Haendeler J, Drose S, Buchner N, Jakob S, Altschmied J, Goy C, et al. Mitochondrial telomerase reverse transcriptase binds to and protects mitochondrial DNA and function from damage. Arterioscler Thromb Vasc Biol. 2009;29:929-935.

54. Faul F, Erdfelder E, Lang AG, Buchner A. G*Power 3: a flexible statistical power analysis program for the social, behavioral, and biomedical sciences. Behav Res Methods. 2007;39:175-191.

Supporting information captions

S1 Fig. Caffeine induces migration despite specific adenosine receptor 2A or 2B inhibition.

(A) A wound was set in a confluent monolayer of primary human endothelial cells and the cells were treated with or without 50 μM caffeine and/or 100 nM SCH442416, a specific adenosine 2A receptor inhibitor, for 18 hours. Migratory capacity was assessed by counting cells migrated into the wound using Image J. Data are mean ± SEM, n=5-6, *$p<0.05$ vs untreated, $^{\#}p<0.05$ vs SCH442416, n.s.=not significant (one-way ANOVA). **(B)** A wound was set and cells were treated with or without 50 μM caffeine and/or 100 nM GS6201, a

specific adenosine 2B receptor inhibitor, for 18 hours. Migratory capacity was assessed by counting cells migrated into the wound using Image J. Data are mean ± SEM, n=6-7, *p<0.05 vs untreated, #p<0.05 vs GS6201, n.s.=not significant (one-way ANOVA). Underlying data are provided in S1 Data.

S2 Fig. Caffeine does not induce phosphorylation of PDE4A and PDE5A.

Endothelial cells were treated with 50 μM caffeine for 18 hours and phosphorylation of serine 686 and 688 in PDE4A (PDE4A P-S686/688) and serine 102 in PDE5A (PDE5A P-S102) as well as total PDE4A (PDE4A) and PDE5A (PDE5A) were detected by immunoblot. **(A)** Shown are three independent biological replicates for PDE4A P-S686/688 and PDE4A with the corresponding loading controls (Tubulin). **(B)** Semiquantitative analyses of the ratios of phospho PDE4A to total PDE4A. Data are mean ± SEM, n=5, n.s.=not significant (two-tailed unpaired t-test). **(C)** Shown are three independent biological replicates for PDE5A P-S102 and PDE5A with the corresponding loading controls (Tubulin). **(D)** Semiquantitative analyses of the ratios of phospho PDE5A to total PDE45A. Data are mean ± SEM, n=5, n.s.=not significant (two-tailed unpaired t-test). Underlying data are provided in S1 Data.

S3 Fig. Original blots used for the quantitation of the siRNA-mediated p27 knockdown. p27 was knocked down in endothelial cells by transfection with two different siRNAs targeting the p27 mRNA (p27 siRNA-1, p27 siRNA-2) or a scrambled siRNA (scr) as control, and p27 levels were determined by immunoblot. Shown are the blots for the five biological replicates used for the quantitation shown in Fig 1B. The levels of p27 were normalized to actin or tubulin, respectively.

S4 Fig. siRNA-mediated knockdown of p27 does not affect cellular and mitochondrial morphology. p27 was knocked down in endothelial cells by transfection with two different siRNAs targeting the p27 mRNA (siRNA p27-1, siRNA p27-2) or a scrambled siRNA (siRNA scr) as control. Intact cell morphology is shown in the brightfield images. To show the mitochondrial network and p27 distribution and levels, nuclei were visualized with DAPI

(blue), mitochondria by staining for TIM23 (red), and p27 with a p27 antibody (green). Merge shows an overlay of all fluorescence channels.

S5 Fig. Original blots used for the quantitation of the caffeine-induced mitochondrial translocation of p27.

Endothelial cells were treated with 50 µM caffeine for 18 hours and mitochondrial (mito) and non-mitochondrial (non-mito) fractions were separated. p27 levels in the mitochondrial fractions were determined by immunoblot and normalized to TIM23. Shown are the blots for the six biological replicates used for the quantitation shown in Fig 2B.

S6 Fig. Caffeine improves respiratory capacity and increases mitochondrial p27 in old mice to the level of adult mice.

(A) For better comparability, the data for malate/glutamate- (M/G) and ADP-stimulated respiration of the mitochondria from the hearts of adult wildtype (■ adult wt) and p27-deficient (■ adult p27ko) mice from figure 5B were combined with the data from the mitochondria from 22 months old wildtype mice receiving water (■ old wt) or water with caffeine (■ old wt+caffeine) shown in figure 8A. **(B)** Heart mitochondria from adult wildtype mice, old mice and old mice, which had received drinking water with 0.05% caffeine for 10 days, were analyzed for mitochondrial p27 by immunoblot. To control for purity of the mitochondria, a total heart lysate (lys) was used in parallel and Vimentin was detected. Underlying data are provided in S1 Data.

S7 Fig. Digestion of mouse mitochondria with proteinase K

40 µg of mouse mitochondria from old (22 months) and adult (6 months) mice as well as mice on a diabetogenic diet presented in figures 8C, 8E and 9E were digested with proteinase K to obtain mitoblasts. 40 µg of undigested mitochondria and the resulting mitoblasts are loaded. Immunoblots for p27, TOM40 and TIM23 are shown. The absence of TOM40 and the presence TIM23 verify the proteinase K digest.

S1 Table. Gene ontology terms for biological processes significantly ($p<0.05$) enriched in hearts of wildtype mice after receiving 10 days 0.05% caffeine in the

drinking water compared to animals on drinking water alone, and subcellular localization of gene products.

S2 Table. Composition of diabetogenic diet.

S1 Data. Excel spreadsheet containing, in separate sheets, the underlying numerical data for figure panels 1B, 1C, 2B, 2F, 2G, 2H, 3D, 3E, 4B, 4E, 4G, 5A, 5B, 6B, 7C, 8A, 8B, 8D, 8F, 9B, 9C, 9F, S1A, S1B, S2B, S2D and S6A.

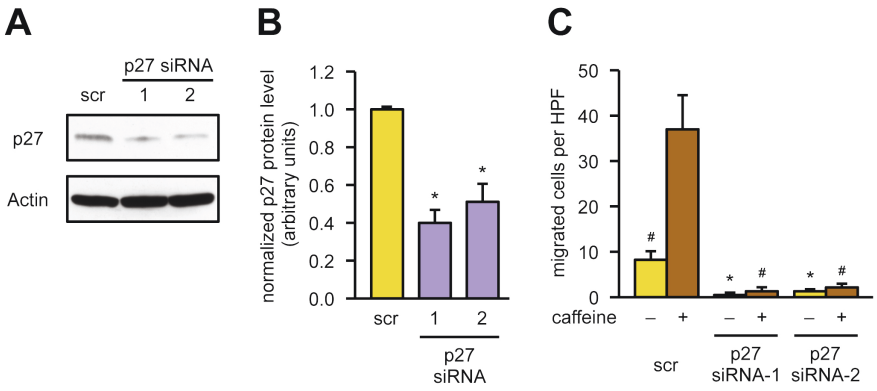
A
p27 siRNA
scr
1
2
p27
Actin
B
normalized p27 protein level
(arbitrary units)
1.2
1.0
0.8
0.6
0.4
0.2
0.0
scr
1
2
p27
siRNA
C
migrated cells per HPF
50
40
30
20
10
0
caffeine
–
+
–
+
–
+
scr
p27
siRNA-1
p27
siRNA-2

figure 1

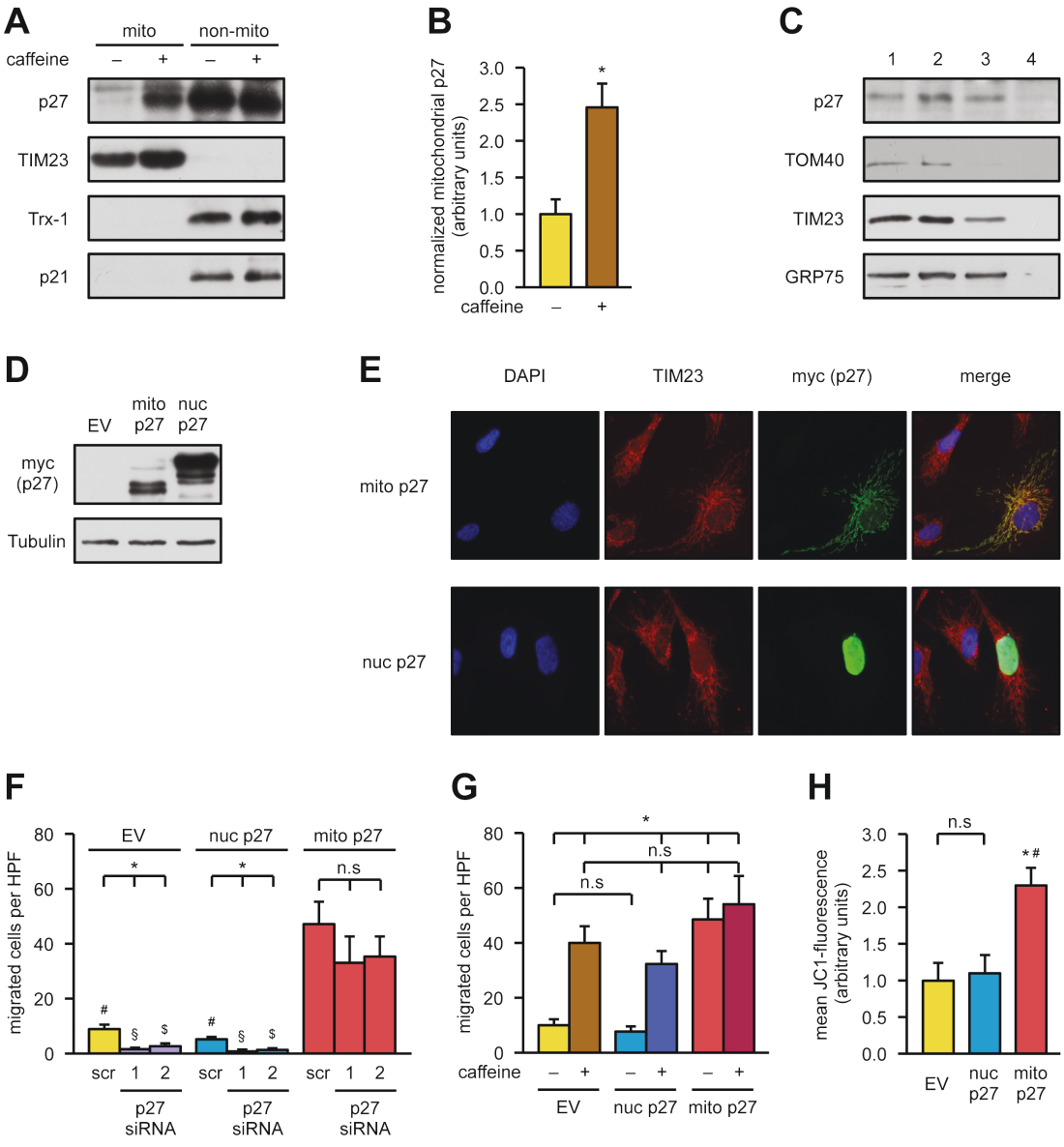
A
mito
non-mito
caffeine
–
+
–
+
p27
TIM23
Trx-1
p21
B
normalized mitochondrial p27 (arbitrary units)
3.0
2.5
2.0
1.5
1.0
0.5
0.0
*
caffeine
–
+
C
1
2
3
4
p27
TOM40
TIM23
GRP75
D
EV
mito p27
nuc p27
myc (p27)
Tubulin
E
DAPI
TIM23
myc (p27)
merge
mito p27
nuc p27
F
migrated cells per HPF
80
60
40
20
0
EV
nuc p27
mito p27
*
*
n.s
#
§
$
#
§
$
scr
1
2
scr
1
2
scr
1
2
p27 siRNA
p27 siRNA
p27 siRNA
G
migrated cells per HPF
80
60
40
20
0
*
n.s
n.s
caffeine
–
+
–
+
–
+
EV
nuc p27
mito p27
H
mean JC1-fluorescence (arbitrary units)
3.0
2.5
2.0
1.5
1.0
0.5
0.0
n.s
*#
EV
nuc p27
mito p27

figure 2

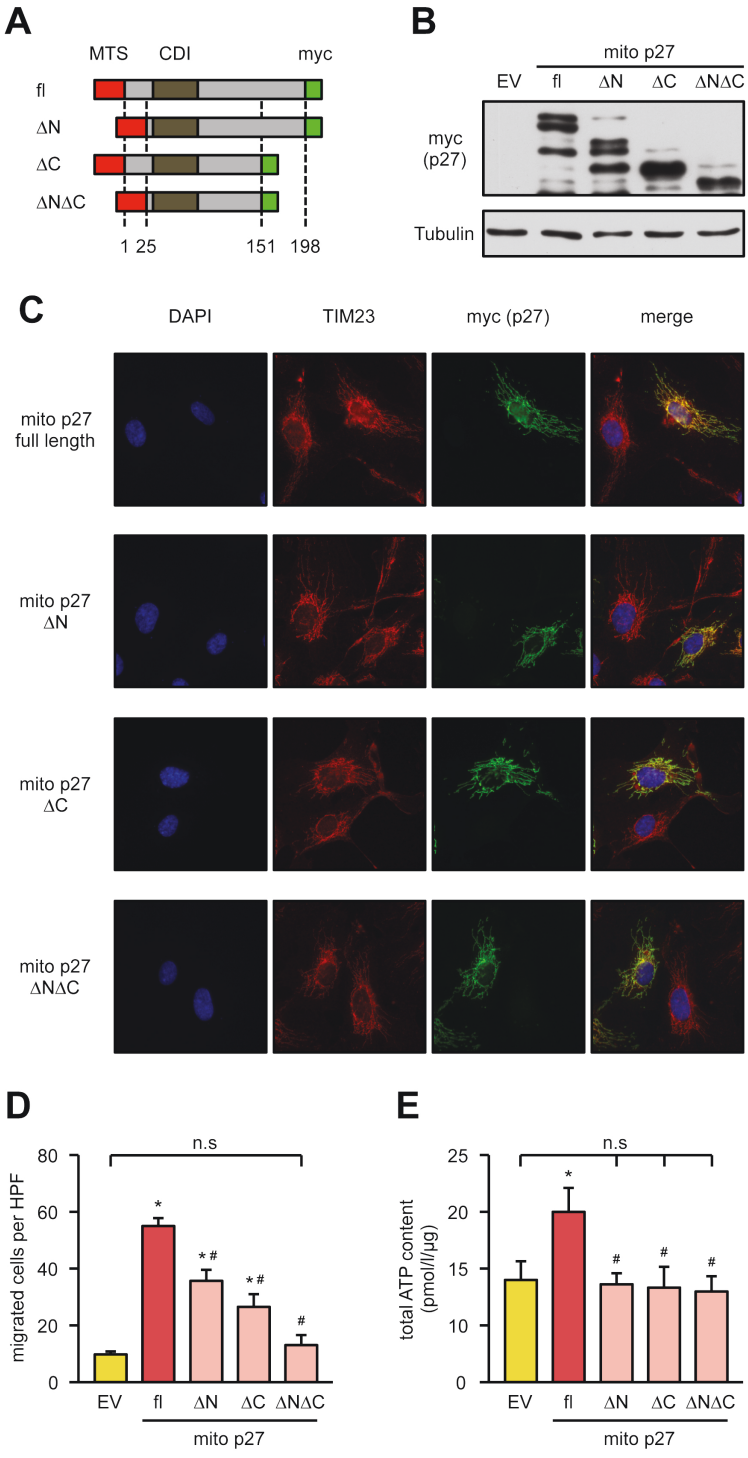
A
MTS
CDI
myc
fl
ΔN
ΔC
ΔNΔC
1 25
151
198
B
mito p27
EV
fl
ΔN
ΔC
ΔNΔC
myc (p27)
Tubulin
C
DAPI
TIM23
myc (p27)
merge
mito p27 full length
mito p27 ΔN
mito p27 ΔC
mito p27 ΔNΔC
D
migrated cells per HPF
n.s
EV
fl
ΔN
ΔC
ΔNΔC
mito p27
E
total ATP content (pmol/l/μg)
n.s
EV
fl
ΔN
ΔC
ΔNΔC
mito p27

figure 3

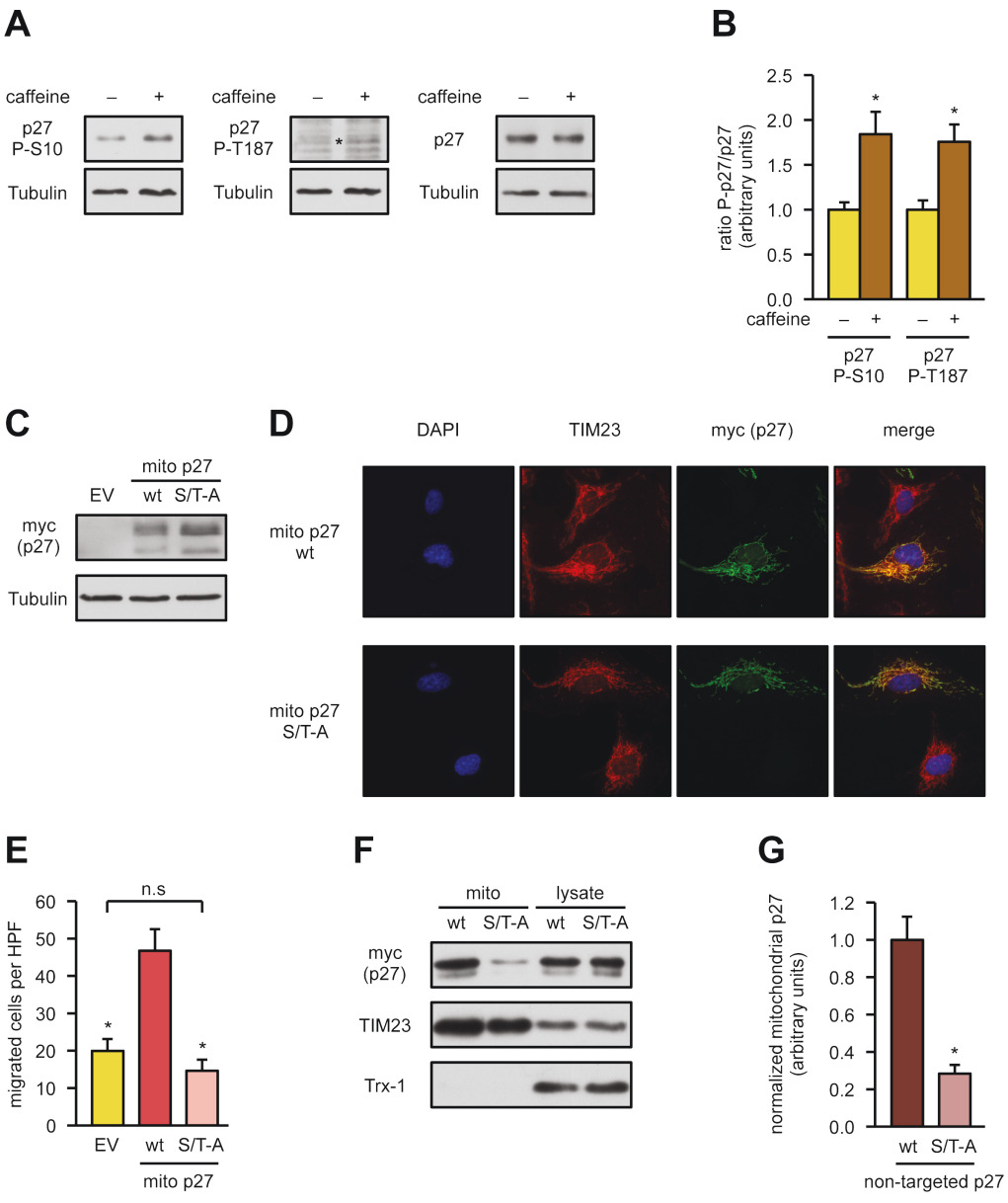
A
caffeine – +
p27 P-S10
Tubulin
caffeine – +
p27 P-T187
Tubulin
caffeine – +
p27
Tubulin
B
ratio P-p27/p27 (arbitrary units)
2.5
2.0
1.5
1.0
0.5
0.0
caffeine – + – +
p27 P-S10
p27 P-T187
C
mito p27
EV wt S/T-A
myc (p27)
Tubulin
D
DAPI
TIM23
myc (p27)
merge
mito p27 wt
mito p27 S/T-A
E
migrated cells per HPF
n.s
60
50
40
30
20
10
0
EV wt S/T-A
mito p27
F
mito lysate
wt S/T-A wt S/T-A
myc (p27)
TIM23
Trx-1
G
normalized mitochondrial p27 (arbitrary units)
1.2
1.0
0.8
0.6
0.4
0.2
0.0
wt S/T-A
non-targeted p27

figure 4

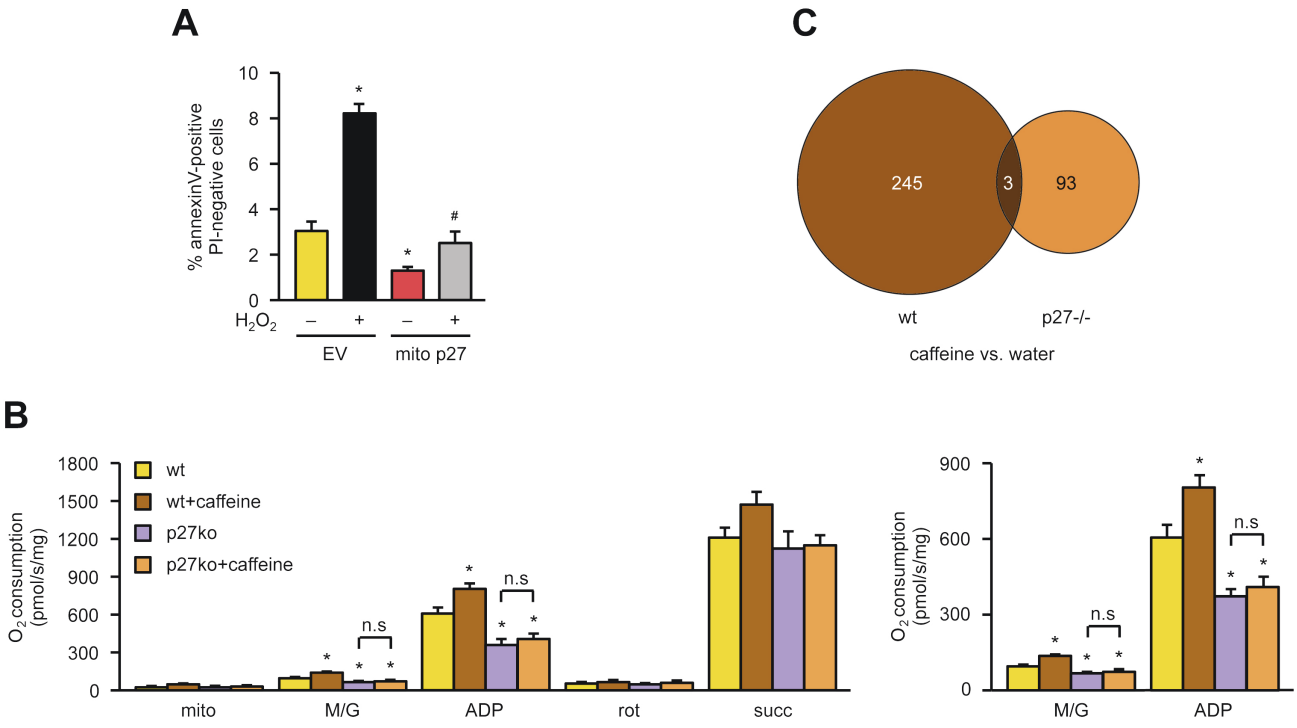
A
10
8
6
4
2
0
% annexinV-positive
PI-negative cells
*
*
#
H2O2
–
+
–
+
EV
mito p27
C
245
3
93
wt
p27-/-
caffeine vs. water
B
1800
1500
1200
900
600
300
0
O2consumption
(pmol/s/mg)
wt
wt+caffeine
p27ko
p27ko+caffeine
n.s
n.s
mito
M/G
ADP
rot
succ
900
600
300
0
n.s
n.s
M/G
ADP

figure 5

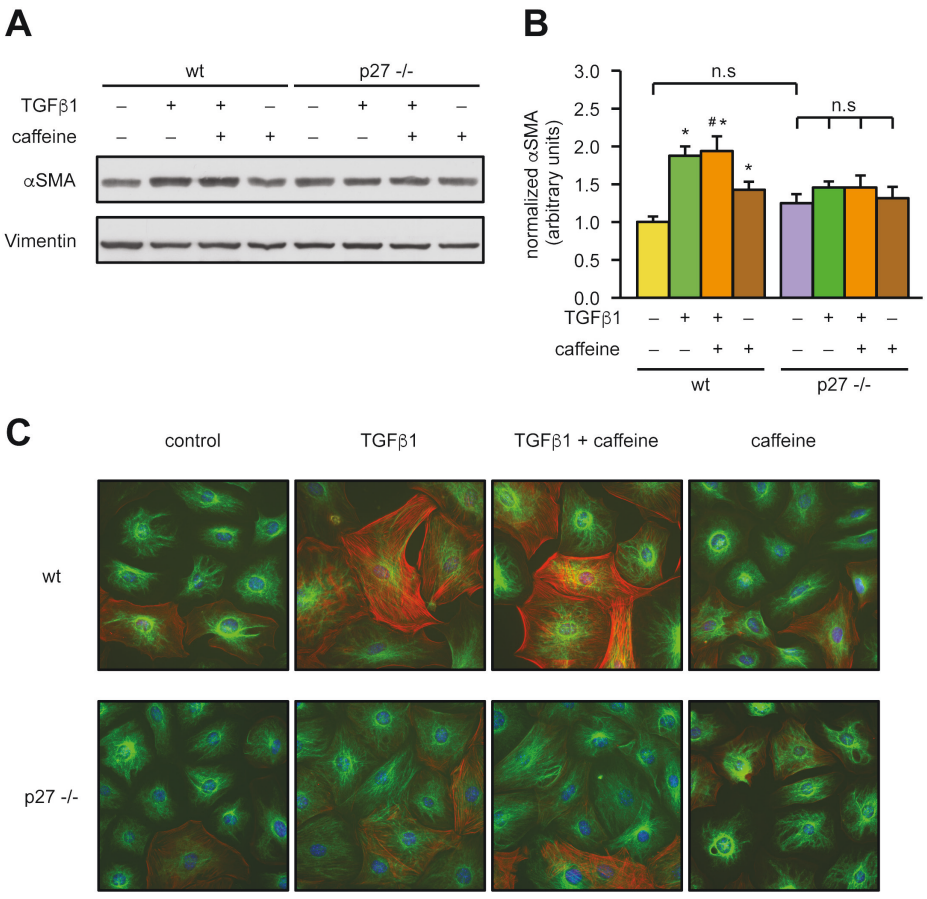
A
wt
p27 -/-
TGFβ1
caffeine
αSMA
Vimentin
B
normalized αSMA (arbitrary units)
3.0
2.5
2.0
1.5
1.0
0.5
0.0
n.s
n.s
*
#*
*
TGFβ1
caffeine
wt
p27 -/-
C
control
TGFβ1
TGFβ1 + caffeine
caffeine
wt
p27 -/-

figure 6

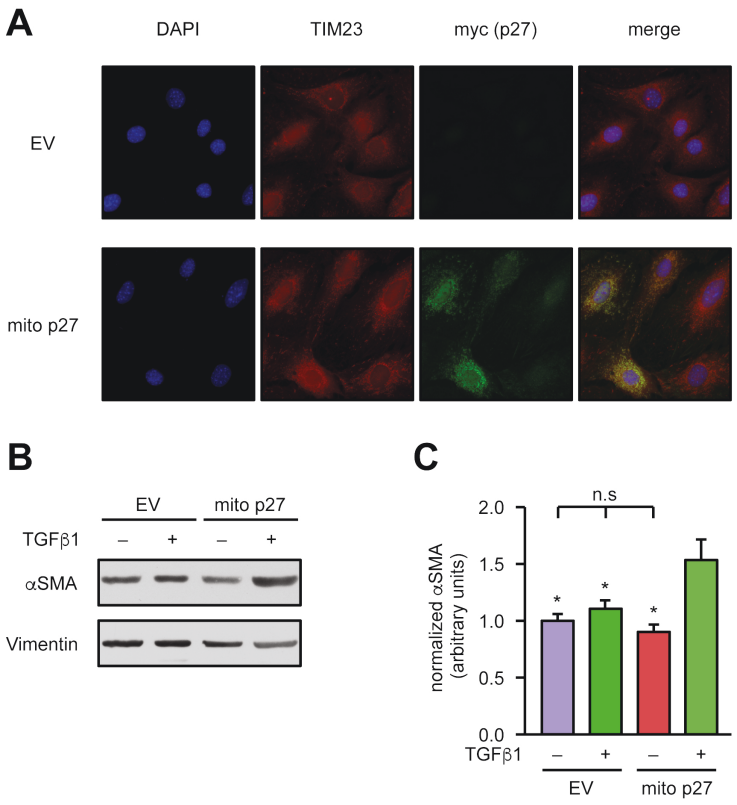
A
DAPI
TIM23
myc (p27)
merge
EV
mito p27
B
EV
mito p27
TGFβ1
–
+
–
+
αSMA
Vimentin
C
n.s
normalized αSMA (arbitrary units)
2.0
1.5
1.0
0.5
0.0
TGFβ1
–
+
–
+
EV
mito p27

figure 7

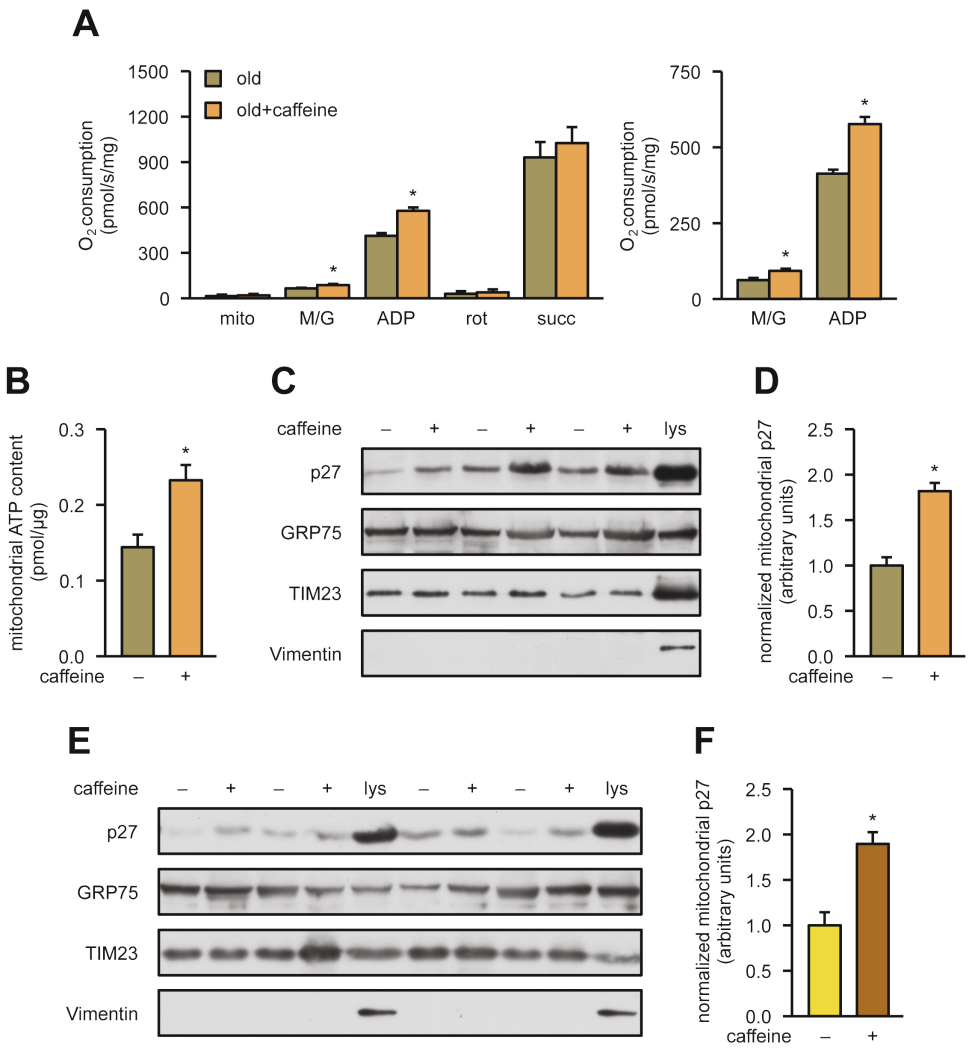
A
1500
1200
900
600
300
0
old
old+caffeine
O2 consumption (pmol/s/mg)
mito
M/G
ADP
rot
succ
750
500
250
0
M/G
ADP
B
0.3
0.2
0.1
0.0
mitochondrial ATP content (pmol/µg)
caffeine – +
C
caffeine – + – + – + lys
p27
GRP75
TIM23
Vimentin
D
2.5
2.0
1.5
1.0
0.5
0.0
normalized mitochondrial p27 (arbitrary units)
caffeine – +
E
caffeine – + – + lys – + – + lys
p27
GRP75
TIM23
Vimentin
F
2.5
2.0
1.5
1.0
0.5
0.0
normalized mitochondrial p27 (arbitrary units)
caffeine – +

figure 8

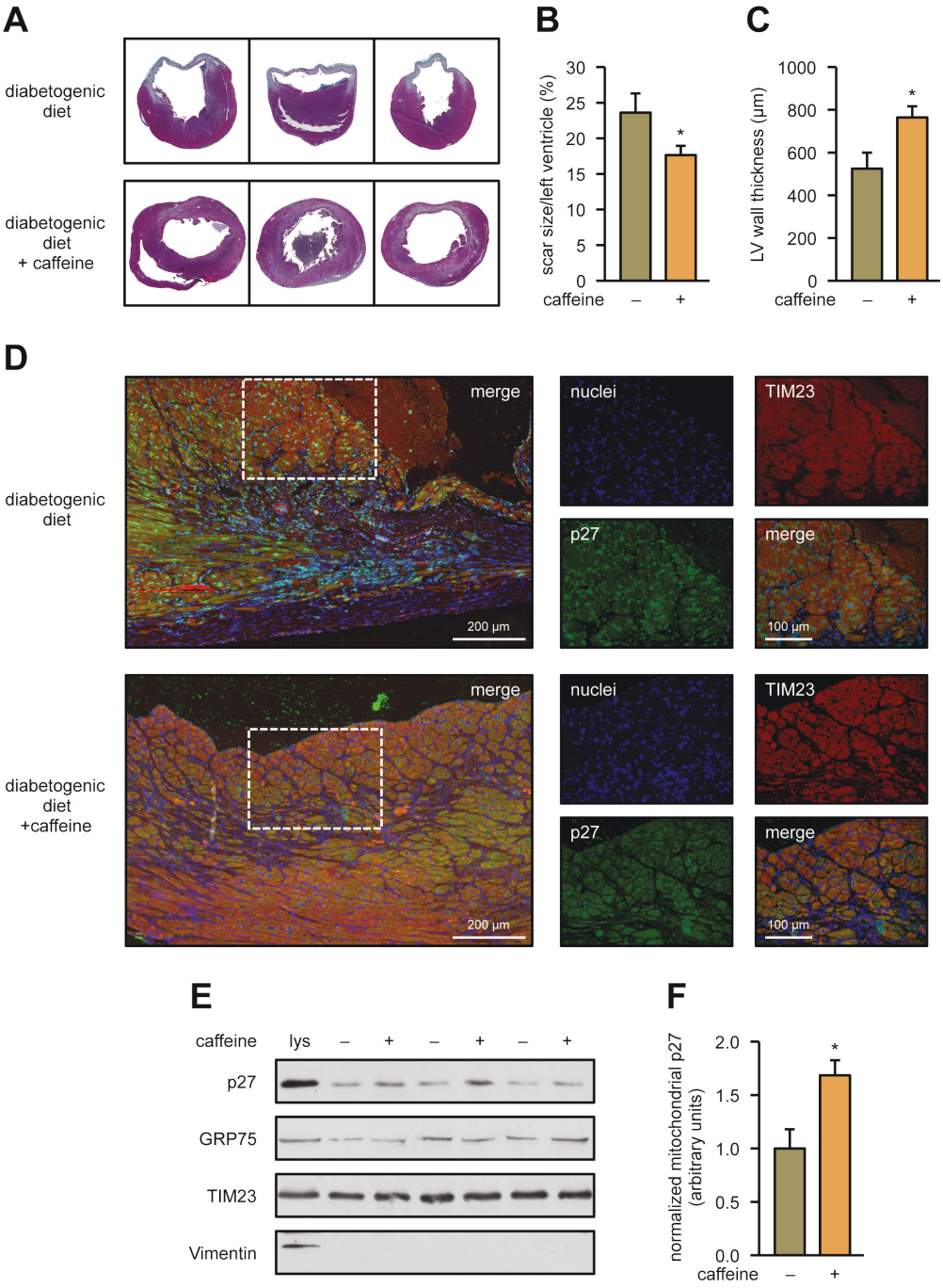
A
diabetogenic diet
diabetogenic diet + caffeine
B
scar size/left ventricle (%)
30
25
20
15
10
5
0
caffeine – +
*
C
LV wall thickness (µm)
1000
800
600
400
200
0
caffeine – +
*
D
diabetogenic diet
merge
nuclei
TIM23
p27
merge
200 µm
100 µm
diabetogenic diet +caffeine
E
caffeine lys – + – + – +
p27
GRP75
TIM23
Vimentin
F
normalized mitochondrial p27 (arbitrary units)
2.0
1.5
1.0
0.5
0.0
caffeine – +
*

figure 9

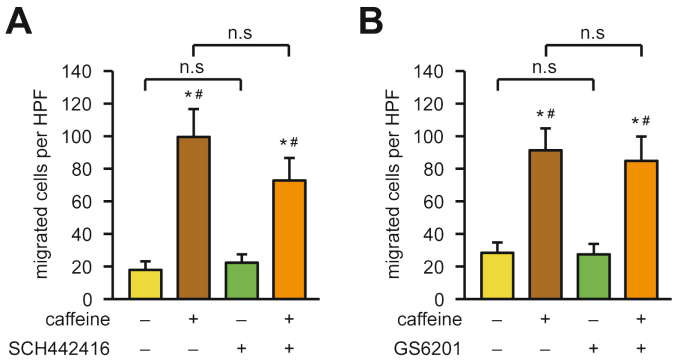

suppl. figure 1

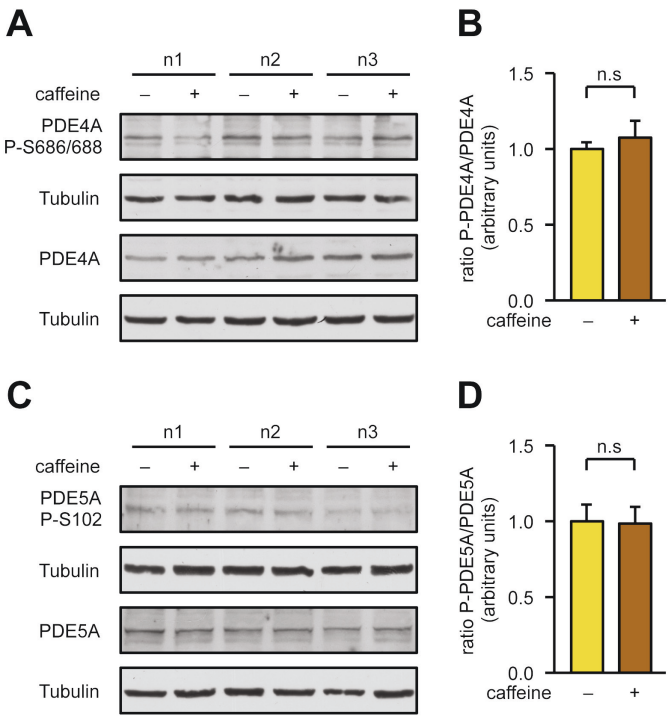

suppl. figure 2

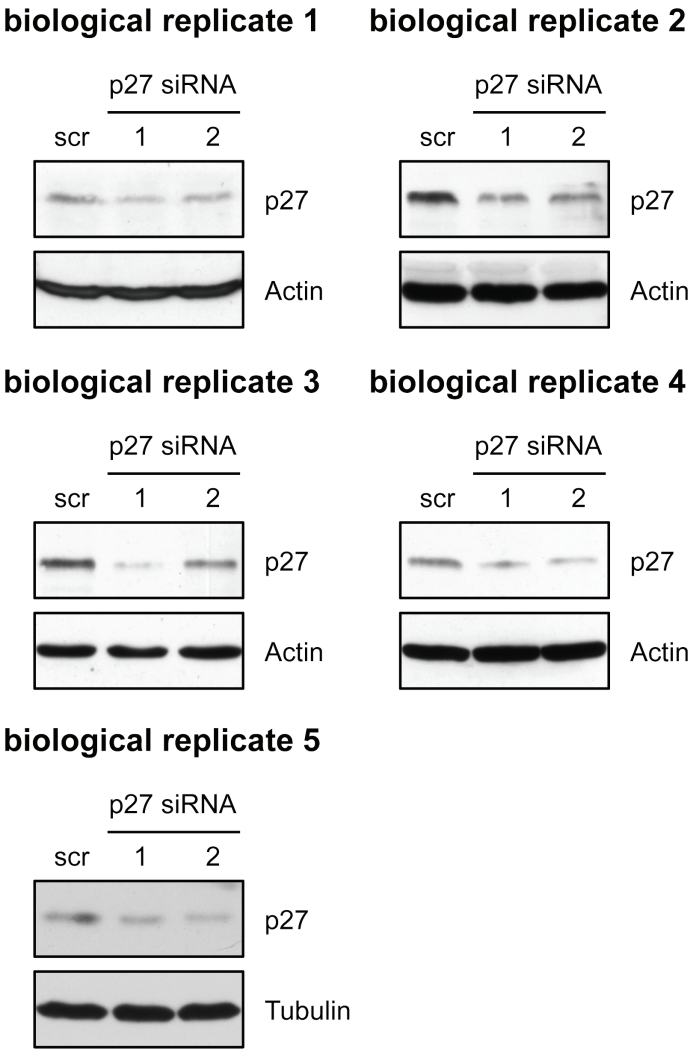

suppl. figure 3

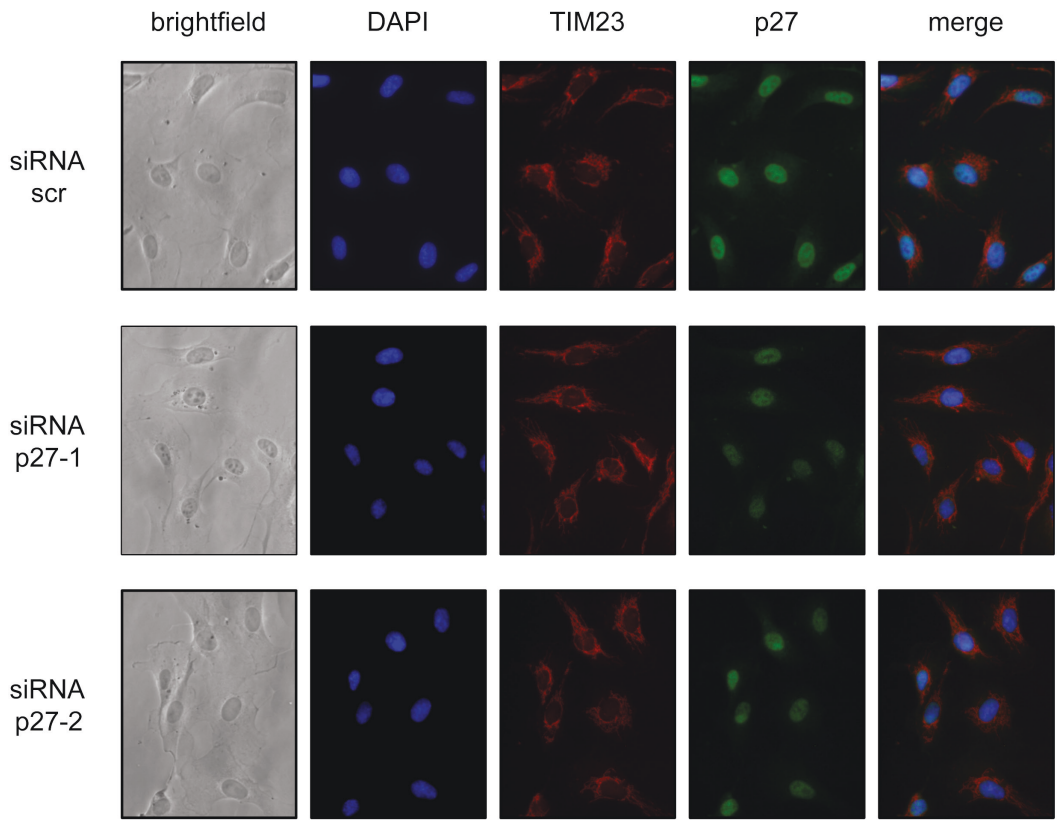

suppl. figure 4

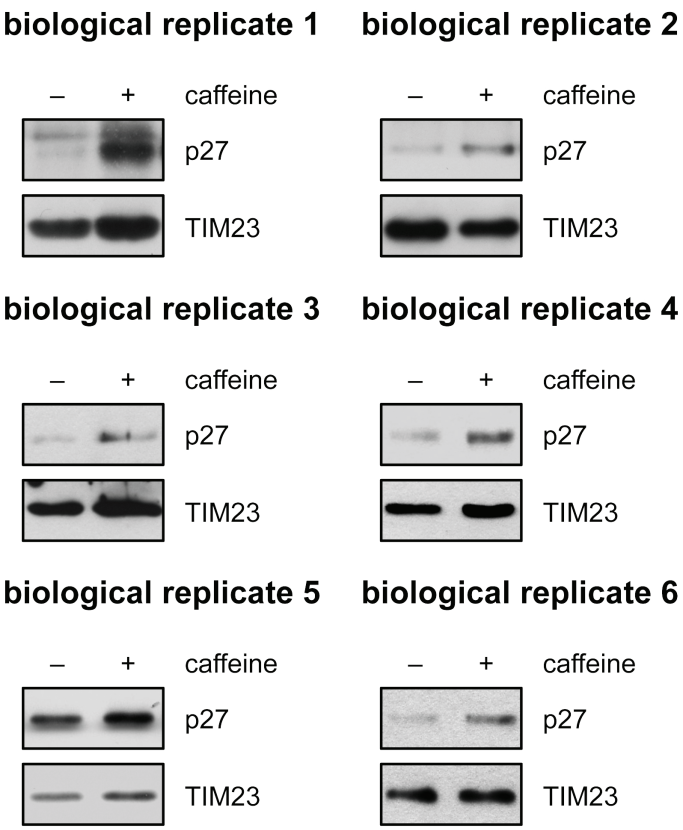

suppl. figure 5

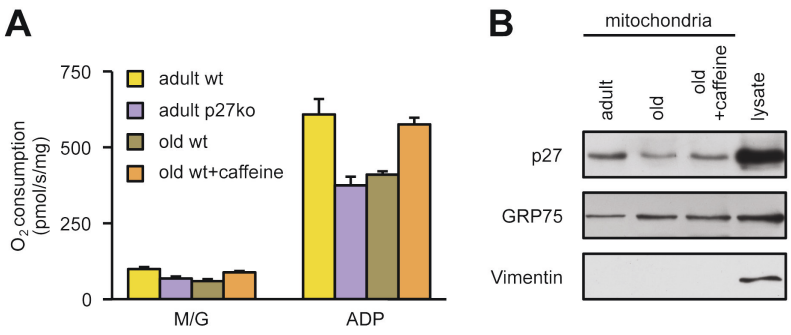

suppl. figure 6

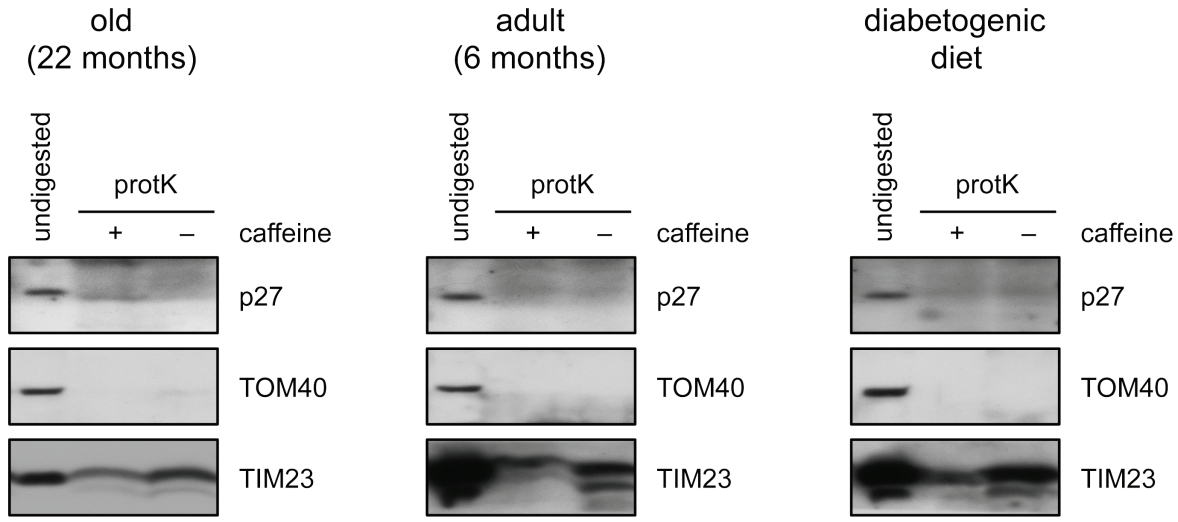

suppl. figure 7

Gene ontology terms for biological processes significantly (p<0.05) enriched in hearts of wildtype mice after receiving 0.05 % caffeine in the drinking water for 10 days compared to animals on drinking water and subcellular localization of gene products. Biological processes taking place in mitochondria are highlighted in yellow, proteins predicted to be localized in mitochondria according to the COMPARTMENTS subcellular localization database are shown in blue.

GO Id	term	genes	fold enrichment	p-value
GO:0003012	muscle system process	SGCE, SGCA	61.09	0.0321
GO:0006086	acetyl-CoA biosynthetic process from pyruvate	**DLD**, **DLAT**	48.87	0.0400
GO:1901029	negative regulation of mitochondrial outer membrane permeabilization involved in apoptotic signaling pathway	**ACAA2**, **SLC25A5**	40.73	0.0478
GO:0022904	respiratory electron transport chain	**IMMP2L**, **NDUFS6**, **ETFDH**	19.29	0.0103
GO:0006099	tricarboxylic acid cycle	**IDH3B**, **DLAT**, **FH1**, **SUCLA2**	16.85	0.0016
GO:0043280	positive regulation of cysteine-type endopeptidase activity involved in apoptotic process	**FIS1**, PPP2CA, **MAPK9**, CYR61	10.18	0.0070
GO:0006936	muscle contraction	**NDUFS6**, MYL1, FKBP1A, HSBP1	9.77	0.0078
GO:0048662	negative regulation of smooth muscle cell proliferation	**MFN2**, CAV1, **COMT**	9.65	0.0381
GO:0008286	insulin receptor signaling pathway	PTPRA, RHOQ, PTPN1, GRB14	9.58	0.0082
GO:0032092	positive regulation of protein binding	CAV1, FKBP1A, AMFR, B2M	7.19	0.0180
GO:0030308	negative regulation of cell growth	CGRRF1, CIRBP, **NDUFS3**, APBB1, DNAJC2	4.89	0.0191
GO:0050821	protein stabilization	LAMP2, ATP1B3, **STXBP1**, TAF9, APBB1	4.77	0.0206
GO:0016192	vesicle-mediated transport	AP3M1, ARF4, BCAP29, **STXBP1**, GOSR2, KDELR1, RTN3	4.02	0.0080
GO:0055114	oxidation-reduction process	**UQCRC2**, UGDH, EGLN3, **UQCRFS1**, **HIBADH**, **NDUFS6**, **PYCR2**, PTGIS, **DLD**, **NDUFS8**, RRM1, **ETFDH**, **OXNAD1**, **NDUFS3**, **ETFB**	2.71	0.0012
GO:0015031	protein transport	CHMP2A, TMED4, SNX6, AP3M1, RAB4A, ARF4, BCAP29, **STXBP1**, VPS35, GOSR2, KDELR1, **DNAJC19**	2.48	0.0091
GO:0006810	transport	**UQCRC2**, CHMP2A, SNX6, ATP1B3, **UQCRFS1**, RTN3, ANK, **NDUFS6**, TMED4, AP3M1, **NDUFS8**, **ETFDH**, BCAP29, VPS35, **NDUFS3**, FYCO1, KDELR1, **ATP5K**, **ETFB**, LAPTM4A, **SLC25A5**, MAGOH, RAB4A, **ABCA8A**, **STXBP1**, **SLC25A12**, ARF4, SYPL, GOSR2	1.94	0.0007

Composition of diabetogenic diet

Crude nutrients	%	Additives	per kg
Crude protein	20.5	Vitamin A [IE/U]	4
Crude fat	36.0	Vitamin D_3 [IE/U]	1
Crude fibre	–	Vitamin E [mg]	75
Crude ash	3.5	Vitamin K_3 [mg]	4
Starch	–	Vitamin C [mg]	–
Sugar	24.0	Copper [mg]	12

Non-canonical activation of the epidermal growth factor receptor by carbon nanoparticles

Stöckmann D*, Spannbrucker T*, Ale-Agha N, **Jakobs P**, Goy C, Dyballa-Rukes N, Hornstein T, Kümper A, Kraegeloh A, Haendeler J, Unfried K

Nanomaterials. 2018; 8, 267 *Gleichberechtigte Erstautoren

Autoren:

Stöckmann D: Erstautor, war an der Planung beteiligt, führte alle Zellexperimente und Datenanalyse durch. Zudem führte er mit Herrn Unfried und Herrn Spannbrucker die Tierexperimente durch.

Spannbrucker T: Erstautor, war an der Planung beteiligt, führte alle Zellexperimente durch. Zudem führte er mit Herrn Unfried und Herrn Stöckmann die Tierexperimente durch.

Ale-Agha N: Führte zusammen mit Herrn Stöckmann Immunfluoreszenzfärbungen durch.

Jakobs P: Führte Immunoblots und deren Datenanalyse durch.

Goy C: Führte Immunoblots und deren Datenanalyse durch.

Dyballa-Rukes N: Führte zusammen mit Herrn Spannbrucker und Herrn Stöckmann Immunoblots durch.

Hornstein T: Führte alle FACS Messungen und deren Analysen durch.

Kümper A: Führte Analysen der Partikelsuspensionen zusammen mit Frau Kraegeloh durch.

Kraegeloh A: Führte Analysen der Partikelsuspensionen zusammen mit Herrn Kümper durch.

Haendeler J: War an der Versuchsplanung beteiligt, plante alle Revisionsversuche, schrieb und bearbeitete das Manuskript.

Unfried K: Senior Autor, hatte die Idee zur Studie, war an der Versuchsplanung beteiligt, schrieb und bearbeitete das Manuskript.

nanomaterials

MDPI

Article

Non-Canonical Activation of the Epidermal Growth Factor Receptor by Carbon Nanoparticles

Daniel Stöckmann [1,†], Tim Spannbrucker [1,†], Niloofar Ale-Agha [1], Philipp Jakobs [1], Christine Goy [1], Nadine Dyballa-Rukes [1], Tamara Hornstein [1], Alexander Kümper [2], Annette Kraegeloh [2], Judith Haendeler [1,3] and Klaus Unfried [1,*]

1 IUF—Leibniz-Institut für Umweltmedizinische Forschung, Auf'm Hennekamp 50, 40225 Düsseldorf, Germany; daniel_stoeckmann@email.de (D.S.); Tim.Spannbrucker@IUF-duesseldorf.de (T.S.); Niloofar.ALE-AGHA@uni-duesseldorf.de (N.A.-A.); Philipp.Jakobs@IUF-duesseldorf.de (P.J.); Christine.Goy@IUF-Duesseldorf.de (C.G.); Nadine.Dyballa@uni-duesseldorf.de (N.D.-R.); Tamara.Hornstein@IUF-duesseldorf.de (T.H.); juhae001@uni-duesseldorf.de (J.H.)

2 INM—Leibniz-Institut für Neue Materialien, Campus D2 2, 66123 Saarbrücken, Germany; akuempi@web.de (A.Kü.); Annette.Kraegeloh@leibniz-inm.de (A.Kr.)

3 Medizinische Fakultät, Heinrich-Heine-Universität Düsseldorf, 40225 Düsseldorf, Germany

* Correspondence: klaus.unfried@uni-duesseldorf.de; Tel.: +49-211-3389-362

† Those authors contributed equally to this work.

Received: 25 February 2018; Accepted: 16 April 2018; Published: 23 April 2018

Abstract: The epidermal growth factor receptor (EGFR) is an abundant membrane protein, which is essential for regulating many cellular processes including cell proliferation. In our earlier studies, we observed an activation of the EGFR and subsequent signaling events after the exposure of epithelial cells to carbon nanoparticles. In the current study, we describe molecular mechanisms that allow for discriminating carbon nanoparticle-specific from ligand-dependent receptor activation. Caveolin-1 is a key player that co-localizes with the EGFR upon receptor activation by carbon nanoparticles. This specific process mediated by nanoparticle-induced reactive oxygen species and the accumulation of ceramides in the plasma membrane is not triggered when cells are exposed to non-nano carbon particles or the physiological ligand EGF. The role of caveolae formation was demonstrated by the induction of higher order structures of caveolin-1 and by the inhibition of caveolae formation. Using an in vivo model with genetically modified mice lacking caveolin-1, it was possible to demonstrate that carbon nanoparticles in vivo trigger EGFR downstream signaling cascades via caveolin-1. The identified molecular mechanisms are, therefore, of toxicological relevance for inhaled nanoparticles. However, nanoparticles that are intentionally applied to humans might cause side effects depending on this phenomenon.

Keywords: tyrosine kinase receptor; caveolin-1; airway epithelium; lung inflammation; protein kinase B

1. Introduction

The epidermal growth factor receptor (EGFR) is an omnipresent receptor tyrosine kinase, which can be activated by the binding of specific ligands. It triggers intracellular signaling pathways involved in a plethora of cellular responses to external stimuli including proliferation, apoptosis, and pro-inflammatory reactions. As a functional protein located in the plasma membrane, the EGFR might be affected when cells are intentionally or unintentionally exposed to nanoparticles. Important evidence for an interference of nanoparticles with EGFR signaling comes from toxicological approaches using different kinds of nanoparticles in various experimental systems. Colloidal nanoparticles consisting of gold, silver, or iron oxide were demonstrated to induce changes in EGFR-dependent signaling

and the expression of gene products regulated by this signaling network in a human epithelial cell line [1]. Earlier investigations of lung epithelial cells exposed to pure hydrophobic carbon nanoparticles demonstrated that a proliferative response on this kind of exposure is mediated by the activation of the EGFR [2,3]. These reactions proved to be specific for nanoparticles since non-nano carbon particles failed to induce these reactions.

The molecular mechanism by which nanoparticles interfere with EGFR-signaling are of particular importance for identifying hazards of nanoparticles and for developing safe nanomaterials [4]. EGFR might be activated by natural ligands released by nanoparticle-triggered cell reactions. Evidence for this kind of mechanism comes from studies with an epithelial cell line exposed to different kinds of environmentally relevant particles and amorphous silica nanoparticles [5,6]. The exposure to these xenobiotics appears to activate TACE (tumour necrosis factor-α-converting enzyme), which is able to shed the ectodomain of TGF-α known as a ligand of EGFR. Signaling events, which are crucial for the pro-inflammatory response in these cells, appears to be activated by this pathway of specific ligand binding. However, the receptor might also be activated by rather unspecific cellular stressors, which are described for oxygen radicals [7]. In our earlier studies, we demonstrated that carbon nanoparticles are able to induce oxidative stress in different kinds of cells [8,9]. The intrinsic oxidative capacity of carbon nanoparticles leads to a rapid generation of reactive oxygen species [10]. In this context, we showed that intracellular reactive oxygen species are crucial for activating proliferative EGFR signaling in lung epithelial cells exposed to carbon nanoparticles [9,10]. Involving membrane-linked src-family kinases (SFK) downstream of EGFR, the activation of protein kinase B (Akt) and proliferative and pro-inflammatory mitogen-activated protein kinase (MAPK) signaling pathways were specifically triggered [11,12]. Molecular analyses of the lipid composition of exposed cells demonstrated that exposure to carbon nanoparticles led to an increase of ceramides in lipid raft membrane fractions, which caused the internalization and activation of the EGFR [9]. Interestingly, ceramide-induced receptor activation could be prevented by stabilizing the EGFR in lipid raft fractions of exposed cells. This effect was achieved by adding ectoine, which is an extremolyte known to stabilize the interaction of membrane proteins with the lipid bilayer [13]. Using this intervention strategy, we were able to demonstrate that the pro-inflammatory effects of nanoparticle-induced EGFR signaling are relevant to in vivo experiments in rats and mice [14].

Based on these previous findings, we now ask whether EGFR activation triggered by carbon nanoparticles involves specific non-canonical mechanisms, which can be distinguished from ligand-dependent activation. As Filosto et al. [15] have shown, non-canonical activation of the EGFR by reactive oxygen species is characterized by src family kinase- (SFK-) dependent processes including the generation of ceramides. After canonical ligand binding, no EGFR homodimers are formed. Moreover, activated monomers are internalized by the formation of caveolae and transported to the perinuclear region where they remain relatively stable compared to ligand-activated homodimers which are, after clathrin-dependent internalization, rapidly subjected to lysosomal degradation [16,17]. In this context caveolin-1, a protein involved in many regulatory processes is of particular importance. The oligomerization of caveolin-1 is the main structural event for the formation of caveolae, which is a specific form of endocytotic membrane invaginations. The lipid composition of the plasma membrane appears to have an impact on EGFR activation mediated by caveolin-1. Ganglioside GM3 has been identified as a negative regulator of EGFR by modulating caveolin-1 levels in raft and non-raft regions of the plasma membrane [18]. In our own studies, we observed a rapid dramatic loss of GM3 accompanied by an accumulation of ceramides after exposure of lung epithelial cells to carbon nanoparticles [9].

The current study aimed to identify signaling events triggered by carbon nanoparticles interacting with epithelial cells. Nanoparticle-specific activation of EGFR was investigated in the model system of the lung epithelium. Using an alveolar type II-derived epithelial cell line (RLE-6TN), we aimed to discriminate non-canonical events from ligand-dependent receptor activation. As a possible mediator of non-canonical EGFR activation, the role of caveolin-1 in lung epithelial cells in vitro

and in vivo was investigated. By comparing molecular events triggered by carbon nanoparticles and the natural ligand of EGFR, the epidermal growth factor (EGF), which is the importance of non-canonical EGFR activation, was elucidated. Employing different kinds of intervention strategies including pharmacological inhibitors also knock out animals for caveolin-1. The relevance of these molecular events was documented.

2. Results

2.1. Particle Characterization

Particles used in this study consist of aciniform, which is an elemental carbon. Carbon nanoparticles (CNP) as well as (non-nano) carbon particles (CP) were characterized for physical properties by using transmission electron microscopy and dynamic light scattering, which was described in the material and methods section and in an earlier publication [19]. Results are shown in Figure S1 and Table S1 in Supplementary Materials.

2.2. Caveolin-1 Is Involved in EGFR Activation after Carbon Nanoparticle Exposure

In the first set of experiments, we aimed to identify signaling events, which allow us to discriminate non-canonical EGFR activation by carbon nanoparticles from ligand-dependent activation. Therefore, the role of caveolin-1 as a potential mediator of these events was investigated in a well characterized rat lung epithelial cell line [20]. Analyses of subcellular localization of EGFR and caveolin-1 were performed by fluorescence microscopy with specific antibodies. Cells either exposed to suspensions of carbon nanoparticles (10 $\mu g/cm^2$) or to EGF as the natural ligand were compared. Earlier, we demonstrated that ceramides are accumulated in the cell membrane after exposure to carbon nanoparticles. Therefore, ceramide (C6) was applied in order to evaluate the role of this nanoparticle-specific event for non-canonical EGFR activation [9]. After five minutes of exposure, all three stimuli led to a translocation of the EGFR from the plasma membrane into the cytoplasm, which is considered a feature of receptor activation (see Figure 1A). Simultaneously, intracellular caveolin-1 accumulation occurred after exposure to carbon nanoparticles and ceramide but not after EGF application. The co-localization of EGFR and caveolin-1 in the cytoplasm of the cells is visualized by the yellow signals in the merge of the images. The co-localization of EGFR and caveolin-1 was only observed after particle and ceramide exposure but not in the presence of the natural ligand EGF. Therefore, the intracellular accumulation of caveolin-1 and its co-translocation with the EGFR can be considered a specific feature that allows to discriminate ligand-dependent from non-canonical receptor activation.

In order to verify the specificity of the observed reactions, a number of molecular events identified earlier to be involved in nanoparticle-specific activation of signaling pathways were investigated by using intervention approaches. Src family kinases (SFK) were inhibited by the pharmacological inhibitor PP2, which specifically and dose dependently diminish downstream signaling [12]. The preventive application of 1 mM ectoine is considered to stabilize EGFR membrane interaction and inhibit the activation and internalization of the receptor. The influence of reactive oxygen species was counteracted by pre-treating the cells with α-tocopherol. Filipin III was used a cholesterol-depleting substance, which is known to prevent the formation of caveolae. All these intervention approaches reduced the internalization and co-localization of EGFR and caveolin-1 after carbon nanoparticle exposure (see Figure 1B). EGF-dependent receptor activation was not influenced by these interventions. From these data points, we can conclude that formation of reactive oxygen species, activation of SFK and structural changes of the membrane including the formation of caveolae are essential components of non-canonical EGFR activation by carbon nanoparticles.

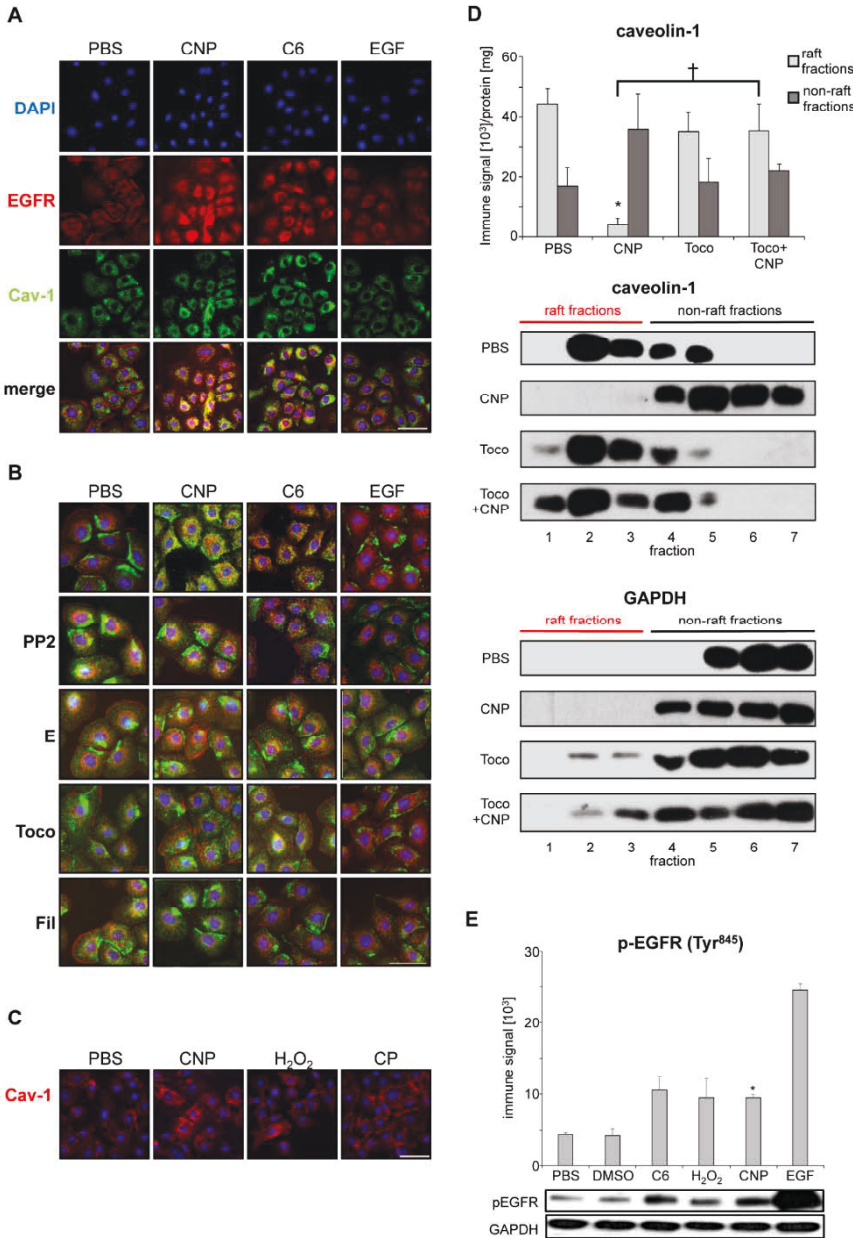

Figure 1. Caveolin-1 and EGFR co-localization as a feature of non-canonical EGFR activation. Epithelial cells (RLE-6TN) were exposed (5 min) to carbon nanoparticles (CNP), non-nano carbon particles (CP), each 10 μg/cm^2, (50 μM) H_2O_2, (5 μM) C6 ceramide, or EGF (100 ng/mL), respectively. (**A**) Subcellular localization of EGFR (red Alexa flour 594) and caveolin-1 (green Alexa flour 488). Co-localization is visualized by the yellow color in merged images; (**B**) Subcellular localization of EGFR and caveolin-1 in cells pre-treated with inhibitors of carbon nanoparticle-specific signaling prior to particle or EGF exposure: SFK inhibitor PP2 (10 μM), 1 mM ectoine (**E**), 75 μM α-tocopherol (Toco), and 1 μg/mL filipin III (Fil). Co-localization is visualized by the yellow color in merged images; (**C**) Subcellular localization of caveolin-1 (red Alexa fluor 594) after exposure to carbon nanoparticles (CNP), carbon particles (CP), or hydrogen peroxide (H_2O_2); (**D**) Quantification and representative Western blots of caveolin-1 in lipid raft fraction of RLE-6TN cells exposed to CNP (10 μg/cm^2). Raft and non-raft fraction were isolated from density gradients after ultracentrifugation. Pre-treatment of cells with α-tocopherol (Toco) was applied as an antioxidant strategy. GAPDH was used as a control protein not associated with lipid rafts. The bars in the graph represent the additive immune signals of raft and non-raft fractions, which was indicated in the representative original Western blots; (**E**) Quantification and representative Western-blot of EGFR phosphorylation at Tyr^{845}. Nuclei were stained with DAPI (blue). Scale bars represent 20 μm; *, which was significantly different to PBS control ($p < 0.05$); †, significantly different from CNP alone ($p < 0.05$).

The specificity of the translocation of caveolin-1 from the plasma membrane to the cytoplasm induced by carbon nanoparticles was tested by applying particulate and non-particulate control substances (see Figure 1C). The relevance of reactive oxygen species for signal induction was demonstrated by the translocation of caveolin-1 in cells exposed to hydrogen peroxide (50 µM). Non-nano carbon particles (CP) with a primary size of >200 nm (see supplementary files for particle characterization) were not able to trigger the specific signaling events. In our earlier studies, we were able to show that these particles at equal mass doses are not able to trigger EGFR translocation and activation as well as subsequent signaling steps and endpoints [3,9,12]. Dose response experiments suggest that this effect is linked to the considerably reduced surface area of the bigger particles compared to the nanoparticles of equal mass.

The activation of the EGFR by carbon nanoparticles is associated with the shift of the receptor molecule from detergent-resistant lipid rafts to non-raft membrane compartments that can be separated by density centrifugation [21]. We investigated whether caveolin-1 behaves similarly to EGFR in these kind of analyses. Western-blot analyses of density gradient fractions reveal that, after exposure to carbon nanoparticles caveolin-1, EGFR is shifted from the raft to the non-raft fractions (see Figure 1D). This effect could be prevented by the pre-treatment of the cells with the antioxidant α-tocopherol.

As proof of principle that co-localization and translocation of both proteins reflect receptor activation, the activating phosphorylation of the EGFR under the chosen experimental conditions has to be demonstrated. In earlier studies, we demonstrated that Tyr^{1173} phosphorylation as a marker of EGFR autophosphorylation is triggered by carbon nanoparticles through reactive oxygen species and ceramide accumulation [9]. We now tested the phosphorylation status of the receptor at Tyr^{845}. This SFK-dependent phosphorylation has been described to be crucial for kinase activity of the EGFR [22–24]. Figure 1E demonstrates that conditions under which intracellular co-localization of caveolin-1 and EGFR occurs, the amount of EGFR that is phosphorylated at Tyr^{845} is significantly increased. A similar reaction was observed when EGF was applied as a positive control.

2.3. Carbon Nanoparticles Induce Higher Order Structures of Caveolin-1

The formation of caveolae is accomplished by structural organization of caveolin molecules [25]. Oligomerization of caveolin-1 as well as its interaction with other structural proteins like cavins is an essential pre-requisite of caveolar invaginations [26]. As the application of filipin III inhibited EGFR translocation after carbon nanoparticle exposure (see Figure 1B), the formation of caveolae might be a critical step in non-canonical EGFR activation. Protein interactions can be observed by crosslinking proteins in intact cells, by applying the membrane permeable substance DSP (dithiobis-succimidylpropionate), and through subsequent protein analysis [27]. In order to test whether caveolae formation is involved in carbon nanoparticle-induced signaling processes, we quantified the formation of high molecular weight protein structures (>350 kDa) containing caveolin-1 under different exposure conditions (see Figure 2). In semi-quantitative Western-Blot analyses, we were able to demonstrate that treatment of the cells with carbon nanoparticles as well as with C6 ceramide led to an increase in high molecular weight caveolin-1 protein complexes while the treatment with EGF failed to induce this reaction (see Figure 2A). Increasing the antioxidant capacity of the cells by applying *N*-acetylcysteine as well as by adding the membrane-coupled antioxidant α-tocopherol, both reduced the amount of caveolin-1 protein complexes significantly (see Figure 2B,C). As expected, filipin III as an inhibitor of caveolae formation prevented the carbon nanoparticle-induced caveolin-1 protein complexes (see Figure 2D). These data strongly suggest that internalization of EGFR after carbon nanoparticle exposure of lung epithelial cells depends on the formation of caveolae.

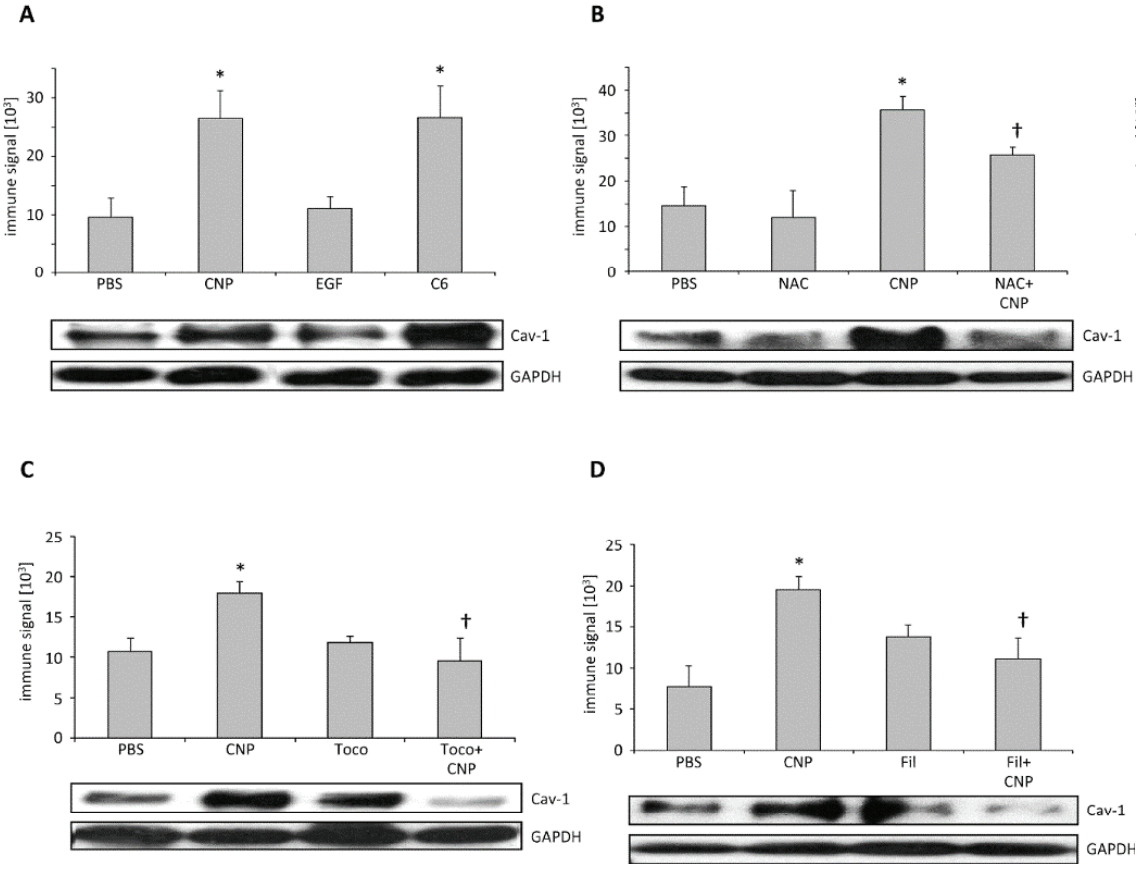

Figure 2. Caveolin-1 protein complexes in dithiobis-succimidylpropionate (DSP)-cross-linked protein extracts. After exposure RLE-6TN cells were treated with DSP (1 mM, 1 h at 4 °C) to stabilize higher order caveolin-1 structures to be detectable by Western blotting. Means and standard errors as well as representative Western-blots are depicted. (**A**) Cells were exposed (5 min) to CNP (10 μg/cm^2), EGF (100 ng/mL), or C6 ceramide (5 μM). Cell were pre-treated with (18 h) *N*-acetylcysteine (NAC, 1 mM); (**B**), or 1 h with α-tocopherol (Toco, 75 μM) (**C**), or filipin III (Fil, 1 μg/mL) (**D**). *, significantly different to PBS control ($p < 0.05$). †, significantly different from CNP alone ($p < 0.05$).

2.4. Non-Canonical EGFR Activation In Vivo

The activation of MAPK signaling pathways via EGFR was identified as a specific mechanism by which carbon nanoparticles induce endpoints like proliferation, apoptosis, and pro-inflammatory responses in lung epithelial cells [3,28]. The in vivo relevance of this cellular reaction was earlier demonstrated in the lungs of animals exposed to carbon nanoparticles [29]. Investigations of signaling events after particle exposure demonstrated that the activation of the MAPK Erk1/2 and protein kinase B (Akt) are mediated by EGFR activation [11]. These EGFR-specific signaling pathways allowed us to test the relevance of caveolin-1-dependent EGFR activation in vivo. The specific appearance of phosphorylated forms of Erk1/2 and Akt was used as an indicator of non-canonical EGFR activation in vivo. The application of carbon nanoparticles in the lungs of animals is a well-established experimental system in which the specific interaction of nanoparticles with the airway epithelium can be investigated. Signaling events triggered by the particles as well as physiological reactions can be studied in tissue samples. The use of animals that lack the caveolin-1 gene due to genetic modification tested the relevance of non-canonical EGFR activation via caveolin-1 in vivo [30]. We, therefore, employed the system of pharyngeal aspiration of carbon nanoparticles (2.5 mg/kg) in the lungs of caveolin-1 knock out mice and their wild type littermates. The induction of signaling events was investigated 6 h after exposure (see Figure 3). At this time point after exposure, signaling events in

lung epithelial cells are activated while inflammatory responses are still not at the peak. As described earlier, lungs of caveolin-1 deficient animals show morphological changes [30]. In hematoxilin eosin (HE) stained lung sections of these animals, we observed a mild phenotype of slightly thickened septa (see Figure 3A). Lung sections immuno-stained for caveolin-1 clearly show that this protein is present in wild type littermates. EGFR as well as the phosphorylated forms of Akt an Erk1/2 were detectable in lung epithelial cells. Exposure of WT-animals appeared to increase the activating phosphorylation of Akt and Erk1/2 while this reaction was not observed in exposed knock out animals. In order to verify this finding, the amount of phosphorylated signaling proteins was determined in protein preparations from lung homogenates. In these semi-quantitative analyses, the levels of phosphorylated Akt (see Figure 3B) and phosphorylated Erk1/2 (see Figure 3C) in relation to the respective amounts of total protein was elevated only in exposed WT animals. In animals lacking caveolin-1, both proteins were not activated after exposure to carbon nanoparticles.

The lack of caveolin-dependent activation of the Akt Erk1/2 signaling cascade is also obvious at the level of the inflammatory response in the lungs triggered by the nanoparticles. Neutrophilic granulocytes and macrophages as the major inflammatory cells were determined in lung lavages of exposed mice (see Figure 3D). In earlier studies, we were able to demonstrate that membrane-dependent signaling in lung epithelial cells is a major driver of neutrophil recruitment in the lung after particle exposure [14]. Accordingly, we now observed that the impairment of non-canonical EGFR activation in caveolin-1 deficient mice led to a marked reduction of this pro-inflammatory response. At the level of macrophages, such effects are not observed at this early time point after exposure. Caveolin-1 knock-out mice appear to have elevated macrophage numbers. This phenomenon appears not to influence the inflammatory response on nanoparticles. The results of the animal experiments demonstrate that carbon nanoparticles are able to address non-canonical EGFR activation via caveolin-1 in epithelial cells in vivo. However, the relevance of these signaling events in lung epithelial cells for nanoparticle-induced lung inflammation as a possible health effect of inhaled nanoparticles in humans is documented.

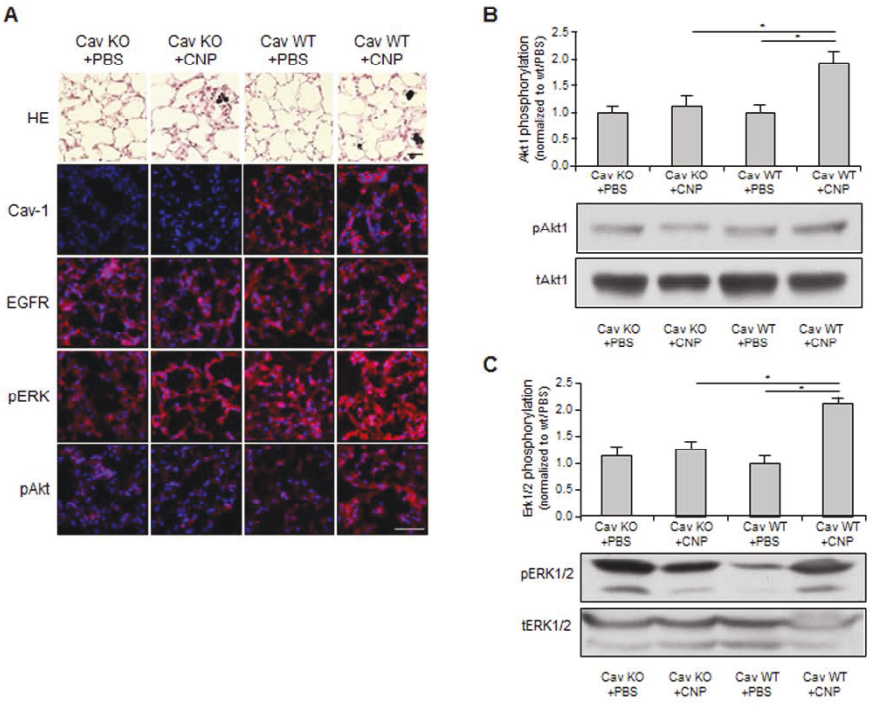

Figure 3. *Cont.*

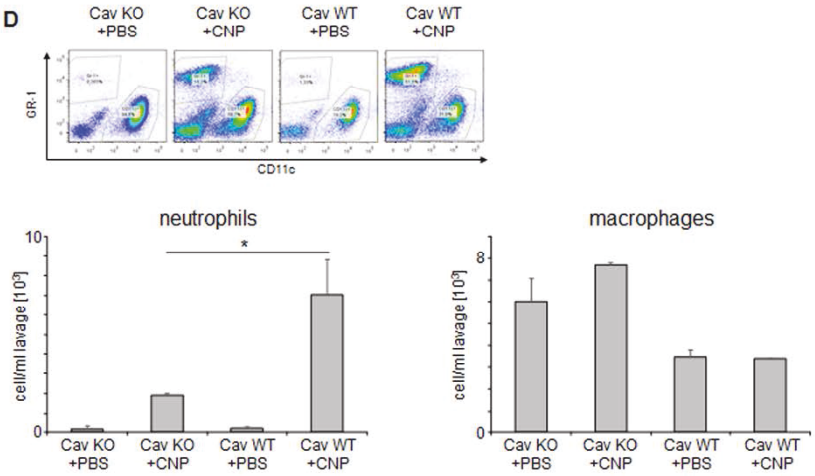

Figure 3. Non-canonical EGFR signaling in vivo. Caveolin-1 knock-out mice and their wild type littermates were exposed to carbon nanoparticles (CNP, 2.5 mg/kg) (or saline as control) by pharyngeal aspiration. Six hours after this single exposure, animals were sacrificed and subjected to bronchoalveolar lavage (BAL) followed by lung tissue preparation. (**A**) Immunohistochemistry from frozen sections of lung tissue. Lungs were either stained with Hematoxilin/Eosin (HE) or immunostained (red) for caveolin-1 (Cav-1), EGFR, phosphorylated Erk1/2 (pERK), or phosphorylated Akt (pAkt) and counterstained with DAPI (blue); (**B**) Relative phosphorylation of Akt in lung homogenates of animals were exposed as indicated. Means and standard errors of immune signals of phosphorylated Akt relative to total Akt and representative Western-blots; (**C**) Relative phosphorylation of Erk1/2 in lung homogenates of animals was exposed as indicated. Means and standard errors of immune signals of phosphorylated Erk1/2 relative to total Erk1/2 and representative Western-blots; (**D**) Flow cytometric analyses of lung lavages with respect to inflammatory cells. GR-1 positive cells (neutrophils) and CD11c positive cells (macrophages) were quantified per mL lung lavage. Scale bars represent 50 µm. *, significantly different from untreated control ($p < 0.05$).

3. Discussion

The presented data demonstrate that EGFR is an important regulator of cellular functions and tissue homeostasis, which can be activated by carbon nanoparticles in epithelial cells via a non-canonical mechanism. This depends on caveolin-1. The induction of higher order structures built by caveolin-1 after carbon nanoparticle exposure and the suppressive effect of the inhibitor filipin III indicate that the formation of caveolae is a critical step involved in these cellular reactions. Our earlier studies identified Akt as a key signaling enzyme downstream of EGFR, which is also responsible for activating MAP-kinases Erk1/2 after nanoparticle exposure [11]. The in vivo experiments demonstrate that this specific signaling cascade, which is responsible for regulating epithelial tissue homeostasis and pro-inflammatory reactions in lungs exposed to nanoparticles depends on the structural protein caveolin-1. Furthermore, the inhibitor experiments demonstrate that signaling events upstream of EGFR activation include the generation of reactive oxygen species and the accumulation of ceramides in lipid raft membrane fractions, which we earlier identified as specific for the interaction of carbon nanoparticles with lung epithelial cells, are causative for the non-canonical activation of the EGFR.

Carbon nanoparticles can be considered model particles for combustion-derived environmental nanoparticles [31]. The inhalation of these particles has been linked to many pathological endpoints including neutrophilic lung inflammation and chronic obstructive pulmonary disease (COPD). Recent investigations have shown that lung epithelial cells are the most relevant cell type for the induction of neutrophilic lung inflammation triggered by carbon nanoparticles [32]. As the current data clearly demonstrate the link between non-canonical EGFR activation in this cell type and neutrophilic lung

inflammation, the induction of this pathway may be considered as a measure for the toxicity of inhaled particles.

Besides toxicologically relevant incidents, carbon nanoparticles as well as other poorly soluble particles might be intentionally applied to the human body. There are a number of strategies that aim to employ carbon-based nanomaterials for diagnostic and therapeutic approaches in humans [33–35]. To our knowledge, a possible interference of these strategies with EGFR signaling is usually not tested. However, nanoparticle-based approaches that aim to suppress EGFR activity, like in tumor therapy, might have the side effect of an activation of this receptor pathway. Our in vivo findings indicate that these nanoparticle-specific effects can occur in vivo and can lead to physiological responses. Yet, there are applications in which the activation of membrane receptor kinases is wanted such as in regenerative therapy [36]. Recent developments of drug delivery systems aim to use nanoparticles for the application of growth factors among therapeutic targets [37]. By choosing appropriate carrier nanoparticles, non-canonical activation of EGFR and possibly other membrane receptor kinases could increase the effectivity of such therapeutic approaches.

4. Materials and Methods

4.1. Reagents

Carbon nanoparticles (CNP Printex 90, Degussa, Essen, Germany) and carbon particles (H. Haeffner, Chepstow, UK) were used for exposure experiments suspended in phosphate buffered saline (PBS). Particle characteristics as well as characteristics of the suspensions were determined as described earlier [19]. Physicochemical characteristics as well as methods of characterization are provided in the supplementary file.

4.2. Cell Culture and Exposure

RLE-6TN cells (ATCC, Manassas, VA, USA) were cultured as described earlier [3]. Cells grown to a confluence of 70–80% were used for exposure experiments. In order to discriminate exposure effects from serum-induced reactions, cells were kept at low serum conditions (0.5% fetal calf serum) for 20 h. Immediate early reactions of particle cell interaction were monitored five minutes after exposure to particle concentrations of 10 $\mu g/cm^2$, which proved to be a relevant exposure dose that does not induce cytotoxicity, according to our earlier studies [3].

Inhibitors were added to the cells at 18 h (NAC (1 mM)), 4 h (ectoine (1 mM)), or 60 min with alpha-tocopherol (75 Mm), PP2 (10 μM), and filipin III (1 μg/mL) [38] prior to treatment with CNP (10 $\mu g/cm^2$), CP (10 $\mu g/cm^2$), C6-ceramide (5 μM), H_2O_2 (50 μM), or EGF (100 ng/mL). EGF (R&D Systems, Abingdon, UK) and ectoine ((*S*)-2-methyl-1,4,5,6-tetrahydropyrimidine-4-carboxylic acid, LPS-free, ultrapure 99%, bitop AG, Witten, Germany) were solubilized in sterile PBS. Filipin III (from *Streptomyces filipinensis*, Sigma-Aldrich Chemie, Schnelldorf, Germany), PP2 (Calbiochem, Schwalbach, Germany), and DSP (dithiobis-succimidylpropionate, Thermo Scientific, Waltham, MA, USA) were solubilized in DMSO (dimethyl sulfoxide) and diluted in PBS to the indicated concentrations. α-tocopherol (D-alpha-tocopherol succinate, semi-synthetic, Sigma-Aldrich Chemie, Schnelldorf, Germany) was solubilized in ethanol and further diluted in PBS before use. In experiments using these compounds, respective vehicle controls were performed. The effect of DMSO on lipid raft composition was investigated as described before [9]. DMSO treated samples showed no difference to PBS treated samples.

4.3. Protein Isolation

The cells were lysed on ice in modified radio immunoprecipitation assay buffer (25 mM Tris-Cl pH 7.4, 150 mM NaCl, 0.1 mM EDTA, 1% Nonidet P-40, 0.1% SDS, 1% deoxycholate, 0.025% NaN_3, 1% protease inhibitor cocktail, 1% phosphatase inhibitor cocktail (both inhibitor cocktails from Sigma)), which was described in Reference [39]. Protein crosslinking by dithiobis-succimidylpropionate (DSP)

was performed as described [27]. Cells were rapidly cooled to 4 °C prior to 1 h incubation with DSP (1 mM) at 4 °C. Crosslinking was stopped by adding 1 M Tris/HCl pH 7.4 (15 mM) prior to protein preparation. Afterwards, proteins were isolated as described above. Detergent resistant membrane raft fractions were isolated and detected as described earlier in Reference [9]. Cells were mechanically disrupted and treated with Triton X-100 (4-(1,1,3,3-tetramethylbutyl)phenyl-polyethylene glycol, 1%). Raft and non-raft fractions were collected from density gradients after ultracentrifugation. Raft fractions were identified by the presence of the raft marker ganglioside GM1 in dot blot assays, as described [9].

4.4. Protein Analyses

Western blotting was performed as described earlier [9]. Equal amounts of total cell protein (5–40 µg) were separated by using SDS-PAGE (7.5% or 10%) and transferred onto PVDF membranes (Hybond-P, Amersham Biosciences, Little Chalfont, UK). DSP-cross-linked caveolin-1 protein complexes were separated on 5% PAGE gels [26]. Unless otherwise stated, all antibodies were from Cell Signaling Technology (Danvers, MA, USA). The antibodies used include caveolin-1 (Upstate Biotechnology, Lake Placid, NY, USA), phospho-EGFR (Tyr^{845}), Akt, phospho-Akt (Ser^{473}), p44/42 MAPK, phospho-p44/42 MAPK (Thr^{202}/Tyr^{204}), and GAPDH (Imgenex Corp., San Diego, CA, USA). Signal strength was detected using the ECL Plus Western Blotting Detection System (Bio-Rad, Hercules, CA, USA). Band intensities from X-ray films (immune signal) were used for statistical calculations. The depicted graphs show either absolute immune signals (high molecular caveolin-1 complexes, EGFR $pTyr^{845}$) or signals relative to the respective total proteins (Erk1/2, Akt).

4.5. Immunostaining

Cells were treated with 4% paraformaldehyde (20 minutes, room temperature). Permeabilisation and blocking was achieved by incubation with 3% bovine serum albumin and 0.3% Triton X-100 in PBS. Slides were incubated with primary antibodies (1:50) overnight at 4 °C, Akt, phospho-Akt (Ser^{473}), Erk1/2, phospho-p44/42 MAPK (Thr^{202}/Tyr^{204}) (Imgenex Corp., San Diego, CA, USA). After 1 h of incubation with secondary antibodies (Alexa Fluor 594 or Alexa Fluor 488, 1:800 or 1:500; Invitrogen, Darmstadt, Germany), nuclei were counterstained by mounting with prolonged gold anti-fade mounting medium with DAPI (1:2000, Invitrogen). Cells were visualized using an Axiovert 200M microscope using (Zeiss, Jena, Germany, 400-fold enlargement, under oil). As control for the specificity of the reactions, mock immunostainings without primary antibodies were performed.

4.6. Animal Experiments

All animal experiments were approved by the local authorities in accordance with the German animal welfare legislation. Caveolin-1 knock-out mice [30] were generated by the group of T. Kurzchalia (Dresden, Germany). Knock-out and wild type mice were obtained by mating of heterozygous animals. Littermates either homozygous knock-out or wild type were used. Adult animals of both sexes were exposed as described earlier [19] by single pharyngeal aspiration of particle solutions (n = 4) or PBS (n = 3). Animals were sacrificed six hours after exposure. Broncho alveolar lavage was prepared from each lung. Lung tissue was sampled for histopathology. Lung sections (4–6 µm) were made from cryo-preserved lung tissue. Immunostainings were performed with the respective antibodies and fluorescent secondary antibodies, which were followed by embedding the sections in mounting medium that contains DAPI. Parallel sections were stained with hematoxylin/eosin. Immunostainings were analyzed microscopically. As a control for the specificity of the reactions, mock immunostainings without primary antibodies were performed. For semi-quantitative analyses of signaling proteins, tissue samples from two independent animal experiments were used (PBS n = 4–5, CNP n = 7–8).

Broncho alveolar lavages were subjected to differential cell counting. Inflammatory cells were discriminated by flow cytometry by employing a FACScanto II Flow Cytometer (BD Bioscience, BD

Bioscience, Franklyn Lake, NJ, USA). Data were analyzed using FlowJo 7.6.5 software. Fluorescently labelled CD11c (N418) and GR-1 (RB6-8C5) (both BioLegend San Diego, CA, USA) were used to monitor changes in the inflammatory status of the lungs, which are reflected by shifts in the percentages of macrophages and neutrophils.

4.7. Statistical Analyses

For statistical analyses, one-way ANOVA followed by Bonferroni post hoc testing was performed using IBM SPSS statistics 22 (IBM Corp., Armonk, NY, USA). Results from Western-blot analyses of phosphorylated proteins were tested for statistical significance with Mann-Whitney U test. The sample size of the animal experiment was determined by power calculation using G*Power 3.1.9.2. Unless not otherwise stated, all experiments were performed as three independent replicates. Differences were considered as significant when $p < 0.05$. Bar graphs show means ± SEM.

Supplementary Materials: The following are available online at http://www.mdpi.com/2079-4991/8/4/267/s1, Figure S1: Transmission elecron micrograph of CP after drying a particle suspension (H_2O) on a holey carbon film, Table S1: Physical characteristics of CNP suspension in PBS.

Acknowledgments: The research was funded by Deutsche Forschungsgemeinschaft: individual grants UN110/4-1 and HA 2868/11-1 as well as from Research Training Group 1427). P.J. is fellowship holder in the International Research Training Group 1902. The authors acknowledge support of their work at INM and IUF in the frame of the Leibniz Research Alliance Nanosafety. The excellent technical assistance of Petra Groß, Tracy Klitz, and Winfried Brock is gratefully acknowledged.

Author Contributions: D.S. and T.S. conducted all cell experiments and analyses. Both contributed to the design of the experiments. N.A.-A. and D.S. performed immunostainings and histology. P.J., C.G., T.S., and N.D.-R. performed Western-blots, A.Kü. and A.Kr. performed analyses of particle suspensions. K.U., D.S., T.S., and T.H. performed animal experiments and subsequent analyses. J.H. and K.U. designed experiments and wrote and edited the manuscript.

Conflicts of Interest: The authors declare no conflict of interest.

References

1. Comfort, K.K.; Maurer, E.I.; Braydich-Stolle, L.K.; Hussain, S.M. Interference of silver, gold, and iron oxide nanoparticles on epidermal growth factor signal transduction in epithelial cells. *ACS Nano* **2011**, *5*, 10000–10008. [CrossRef] [PubMed]
2. Tamaoki, J.; Isono, K.; Takeyama, K.; Tagaya, E.; Nakata, J.; Nagai, A. Ultrafine carbon black particles stimulate proliferation of human airway epithelium via egf receptor-mediated signaling pathway. *Am. J. Physiol. Lung Cell. Mol. Physiol.* **2004**, *287*, L1127–L1133. [CrossRef] [PubMed]
3. Sydlik, U.; Bierhals, K.; Soufi, M.; Abel, J.; Schins, R.P.; Unfried, K. Ultrafine carbon particles induce apoptosis and proliferation in rat lung epithelial cells via specific signaling pathways both using egf-r. *Am. J. Physiol. Lung Cell. Mol. Physiol.* **2006**, *291*, L725–L733. [CrossRef] [PubMed]
4. Unfried, K.; Albrecht, C.; Klotz, L.-O.; Von Mikecz, A.; Grether-Beck, S.; Schins, R.P.F. Cellular responses to nanoparticles: Target structures and mechanisms. *Nanotoxicology* **2007**, *1*, 52–71. [CrossRef]
5. Ovrevik, J.; Refsnes, M.; Totlandsdal, A.I.; Holme, J.A.; Schwarze, P.E.; Lag, M. TACE/TGF-alpha/EGFR regulates CXCL8 in bronchial epithelial cells exposed to particulate matter components. *Eur. Respir. J.* **2011**, *38*, 1189–1199. [CrossRef] [PubMed]
6. Skuland, T.; Ovrevik, J.; Lag, M.; Schwarze, P.; Refsnes, M. Silica nanoparticles induce cytokine responses in lung epithelial cells through activation of a p38/TACE/TGF-alpha/EGFR-pathway and NF-kappabeta signalling. *Toxicol. Appl. Pharmacol.* **2014**, *279*, 76–86. [CrossRef] [PubMed]
7. Goldkorn, T.; Balaban, N.; Matsukuma, K.; Chea, V.; Gould, R.; Last, J.; Chan, C.; Chavez, C. EGF-receptor phosphorylation and signaling are targeted by H_2O_2 redox stress. *Am. J. Respir. Cell Mol. Biol.* **1998**, *19*, 786–798. [CrossRef] [PubMed]
8. Buchner, N.; Ale-Agha, N.; Jakob, S.; Sydlik, U.; Kunze, K.; Unfried, K.; Altschmied, J.; Haendeler, J. Unhealthy diet and ultrafine carbon black particles induce senescence and disease associated phenotypic changes. *Exp. Gerontol.* **2013**, *48*, 8–16. [CrossRef] [PubMed]

9. Peuschel, H.; Sydlik, U.; Grether-Beck, S.; Felsner, I.; Stockmann, D.; Jakob, S.; Kroker, M.; Haendeler, J.; Gotic, M.; Bieschke, C.; et al. Carbon nanoparticles induce ceramide- and lipid raft-dependent signalling in lung epithelial cells: A target for a preventive strategy against environmentally-induced lung inflammation. *Part. Fibre Toxicol.* **2012**, *9*, 48. [CrossRef] [PubMed]
10. Weissenberg, A.; Sydlik, U.; Peuschel, H.; Schroeder, P.; Schneider, M.; Schins, R.P.; Abel, J.; Unfried, K. Reactive oxygen species as mediators of membrane-dependent signaling induced by ultrafine particles. *Free Radic. Biol. Med.* **2010**, *49*, 597–605. [CrossRef] [PubMed]
11. Unfried, K.; Sydlik, U.; Bierhals, K.; Weissenberg, A.; Abel, J. Carbon nanoparticle-induced lung epithelial cell proliferation is mediated by receptor-dependent akt activation. *Am. J. Physiol. Lung Cell. Mol. Physiol.* **2008**, *294*, L358–L367. [CrossRef] [PubMed]
12. Peuschel, H.; Sydlik, U.; Haendeler, J.; Buchner, N.; Stockmann, D.; Kroker, M.; Wirth, R.; Brock, W.; Unfried, K. C-SRC-mediated activation of ERK1/2 is a reaction of epithelial cells to carbon nanoparticle treatment and may be a target for a molecular preventive strategy. *Biol. Chem.* **2010**, *391*, 1327–1332. [CrossRef] [PubMed]
13. Roychoudhury, A.; Haussinger, D.; Oesterhelt, F. Effect of the compatible solute ectoine on the stability of the membrane proteins. *Protein Pept. Lett.* **2012**, *19*, 791–794. [CrossRef] [PubMed]
14. Sydlik, U.; Gallitz, I.; Albrecht, C.; Abel, J.; Krutmann, J.; Unfried, K. The compatible solute ectoine protects against nanoparticle-induced neutrophilic lung inflammation. *Am. J. Respir. Crit. Care Med.* **2009**, *180*, 29–35. [CrossRef] [PubMed]
15. Filosto, S.; Khan, E.M.; Tognon, E.; Becker, C.; Ashfaq, M.; Ravid, T.; Goldkorn, T. Egf receptor exposed to oxidative stress acquires abnormal phosphorylation and aberrant activated conformation that impairs canonical dimerization. *PLoS ONE* **2011**, *6*, e23240. [CrossRef] [PubMed]
16. Goldkorn, T.; Filosto, S.; Chung, S. Lung injury and lung cancer caused by cigarette smoke-induced oxidative stress: Molecular mechanisms and therapeutic opportunities involving the ceramide-generating machinery and epidermal growth factor receptor. *Antioxid. Redox Signal.* **2014**, *21*, 2149–2174. [CrossRef] [PubMed]
17. Balbis, A.; Parmar, A.; Wang, Y.; Baquiran, G.; Posner, B.I. Compartmentalization of signaling-competent epidermal growth factor receptors in endosomes. *Endocrinology* **2007**, *148*, 2944–2954. [CrossRef] [PubMed]
18. Wang, X.Q.; Sun, P.; Paller, A.S. Ganglioside induces caveolin-1 redistribution and interaction with the epidermal growth factor receptor. *J. Biol. Chem.* **2002**, *277*, 47028–47034. [CrossRef] [PubMed]
19. Kroker, M.; Sydlik, U.; Autengruber, A.; Cavelius, C.; Weighardt, H.; Kraegeloh, A.; Unfried, K. Preventing carbon nanoparticle-induced lung inflammation reduces antigen-specific sensitization and subsequent allergic reactions in a mouse model. *Part. Fibre Toxicol.* **2015**, *12*, 20. [CrossRef] [PubMed]
20. Driscoll, K.E.; Carter, J.M.; Iype, P.T.; Kumari, H.L.; Crosby, L.L.; Aardema, M.J.; Isfort, R.J.; Cody, D.; Chestnut, M.H.; Burns, J.L.; et al. Establishment of immortalized alveolar type II epithelial cell lines from adult rats. *Cell. Dev. Biol. Anim.* **1995**, *31*, 516–527. [CrossRef]
21. Mineo, C.; Gill, G.N.; Anderson, R.G. Regulated migration of epidermal growth factor receptor from caveolae. *J. Biol. Chem.* **1999**, *274*, 30636–30643. [CrossRef] [PubMed]
22. Wu, W.; Graves, L.M.; Gill, G.N.; Parsons, S.J.; Samet, J.M. Src-dependent phosphorylation of the epidermal growth factor receptor on tyrosine 845 is required for zinc-induced ras activation. *J. Biol. Chem.* **2002**, *277*, 24252–24257. [CrossRef] [PubMed]
23. Wu, W.; Wages, P.A.; Devlin, R.B.; Diaz-Sanchez, D.; Peden, D.B.; Samet, J.M. SRC-mediated EGF receptor activation regulates ozone-induced interleukin 8 expression in human bronchial epithelial cells. *Environ. Health Perspect.* **2015**, *123*, 231–236. [CrossRef] [PubMed]
24. Mueller, K.L.; Powell, K.; Madden, J.M.; Eblen, S.T.; Boerner, J.L. EGFR tyrosine 845 phosphorylation-dependent proliferation and transformation of breast cancer cells require activation of p38 mapk. *Transl. Oncol.* **2012**, *5*, 327–334. [CrossRef] [PubMed]
25. Sargiacomo, M.; Scherer, P.E.; Tang, Z.; Kubler, E.; Song, K.S.; Sanders, M.C.; Lisanti, M.P. Oligomeric structure of caveolin: Implications for caveolae membrane organization. *Proc. Natl. Acad. Sci. USA* **1995**, *92*, 9407–9411. [CrossRef] [PubMed]
26. Hansen, C.G.; Nichols, B.J. Exploring the caves: Cavins, caveolins and caveolae. *Trends Cell Biol.* **2010**, *20*, 177–186. [CrossRef] [PubMed]

27. Ludwig, A.; Howard, G.; Mendoza-Topaz, C.; Deerinck, T.; Mackey, M.; Sandin, S.; Ellisman, M.H.; Nichols, B.J. Molecular composition and ultrastructure of the caveolar coat complex. *PLoS Biol.* **2013**, *11*, e1001640. [CrossRef] [PubMed]
28. Kim, Y.M.; Reed, W.; Lenz, A.G.; Jaspers, I.; Silbajoris, R.; Nick, H.S.; Samet, J.M. Ultrafine carbon particles induce interleukin-8 gene transcription and p38 mapk activation in normal human bronchial epithelial cells. *Am. J. Physiol. Lung Cell. Mol. Physiol.* **2005**, *288*, L432–L441. [CrossRef] [PubMed]
29. Autengruber, A.; Sydlik, U.; Kroker, M.; Hornstein, T.; Ale-Agha, N.; Stockmann, D.; Bilstein, A.; Albrecht, C.; Paunel-Gorgulu, A.; Suschek, C.V.; et al. Signalling-dependent adverse health effects of carbon nanoparticles are prevented by the compatible solute mannosylglycerate (firoin) in vitro and in vivo. *PLoS ONE* **2014**, *9*, e111485. [CrossRef] [PubMed]
30. Drab, M.; Verkade, P.; Elger, M.; Kasper, M.; Lohn, M.; Lauterbach, B.; Menne, J.; Lindschau, C.; Mende, F.; Luft, F.C.; et al. Loss of caveolae, vascular dysfunction, and pulmonary defects in caveolin-1 gene-disrupted mice. *Science* **2001**, *293*, 2449–2452. [CrossRef] [PubMed]
31. Donaldson, K.; Tran, L.; Jimenez, L.A.; Duffin, R.; Newby, D.E.; Mills, N.; MacNee, W.; Stone, V. Combustion-derived nanoparticles: A review of their toxicology following inhalation exposure. *Part. Fibre Toxicol.* **2005**, *2*, 10. [CrossRef] [PubMed]
32. Chen, S.; Yin, R.; Mutze, K.; Yu, Y.; Takenaka, S.; Konigshoff, M.; Stoeger, T. No involvement of alveolar macrophages in the initiation of carbon nanoparticle induced acute lung inflammation in mice. *Part. Fibre Toxicol.* **2016**, *13*, 33. [CrossRef] [PubMed]
33. Misra, S.K.; Ohoka, A.; Kolmodin, N.J.; Pan, D. Next generation carbon nanoparticles for efficient gene therapy. *Mol. Pharm.* **2015**, *12*, 375–385. [CrossRef] [PubMed]
34. Modugno, G.; Menard-Moyon, C.; Prato, M.; Bianco, A. Carbon nanomaterials combined with metal nanoparticles for theranostic applications. *Br. J. Pharmacol.* **2015**, *172*, 975–991. [CrossRef] [PubMed]
35. Zhang, C.; Lei, S.; Zhang, Z.; He, J.; Xiao, S.; Fan, P.; Xie, J.; Gu, X.; Li, Y.; Zheng, W. Evaluation of the clinical value of carbon nanoparticles as lymph node tracer in differentiated thyroid carcinoma requiring reoperation. *Int. J. Clin. Oncol.* **2016**, *21*, 68–74.
36. Huynh, E.; Li, J. EGF and EGFR: Promising targets for modulating inflammation and mucosal healing therapy in IBD. *Inflamm. Cell Signal.* **2015**, *2*. [CrossRef]
37. Gainza, G.; Villullas, S.; Pedraz, J.L.; Hernandez, R.M.; Igartua, M. Advances in drug delivery systems (DDSS) to release growth factors for wound healing and skin regeneration. *Nanomedicine* **2015**, *11*, 1551–1573. [CrossRef] [PubMed]
38. Henriksen, L.; Grandal, M.V.; Knudsen, S.L.; van Deurs, B.; Grovdal, L.M. Internalization mechanisms of the epidermal growth factor receptor after activation with different ligands. *PLoS ONE* **2013**, *8*, e58148. [CrossRef] [PubMed]
39. Berken, A.; Abel, J.; Unfried, K. Beta1-integrin mediates asbestos-induced phosphorylation of AKT and ERK1/2 in a rat pleural mesothelial cell line. *Oncogene* **2003**, *22*, 8524–8528. [CrossRef] [PubMed]

Induction of cellular senescence and loss of gap junctional intercellular communication by carbon nanoparticle exposure of lung epithelial cells

Spannbrucker T*, Ale-Agha N*, Goy C, Dyballa-Rukes N, **Jakobs P**, Altschmied J, Unfried K, Haendeler J

Exp Gerontol. 2018; in Revision *Gleichberechtigte Erstautoren

Autoren:

Spannbrucker T: Erstautor, war an der Planung und Durchführung der Versuche beteiligt, führte die Datenanalyse durch und war zudem am Entwurf des Manuskriptes beteiligt.

Ale-Agha N: Erstautorin, war an der Planung und Durchführung aller Versuche beteiligt, führte alle Mikroinjektionen und deren Datenanalyse durch und war zudem am Entwurf des Manuskriptes beteiligt.

Goy C: Führte zusammen mit Frau Dyballa-Rukes und Herrn Jakobs die Immunoblots und deren Datenanalyse durch. Korrigierte Teile des Manuskripts.

Dyballa-Rukes N: Führte zusammen mit Frau Goy und Herrn Jakobs die Immunoblots und deren Datenanalyse durch. Korrigierte Teile des Manuskripts.

Jakobs P: Führte zusammen mit Frau Goy und Frau Dyballa-Rukes die Immunoblots und deren Datenanalyse durch. Korrigierte Teile des Manuskripts.

Altschmied J: war an der Idee und Planung der Versuche beteiligt, gab konstruktive Kritik zum Manuskript und erstellte die finale Korrektur.

Unfried K: war an der Idee und Planung der Versuche beteiligt, gab konstruktive Kritik zum Manuskript und erstellte die finale Korrektur.

Haendeler J: Senior Autorin, hatte die Idee zur Studie, war an der Versuchsplanung beteiligt und schrieb sowie finalisierte das Manuskript.

Ref: EXG_2018_136
Title: Induction of cellular senescence and loss of gap junctional intercellular communication by carbon nanoparticle exposure of lung epithelial cells
Journal: Experimental Gerontology

Dear Professor Haendeler,

Thank you for submitting your manuscript to Experimental Gerontology. I have completed the review of your manuscript and a summary is appended below. The reviewers recommend reconsideration of your paper following major revision. I invite you to resubmit your manuscript after addressing all reviewer comments.

When resubmitting your manuscript, please carefully consider all issues mentioned in the reviewers' comments, outline every change made point by point, and provide suitable rebuttals for any comments not addressed.

To submit your revised manuscript:

- Log into EVISE® at: http://www.evise.com/evise/faces/pages/navigation/NavController.jspx?JRNL_ACR=EXG
- Locate your manuscript under the header 'My Submissions that need Revisions' on your 'My Author Tasks' view
- Click on 'Agree to Revise'
- Make the required edits
- Click on 'Complete Submission' to approve

What happens next?

After you approve your submission preview you will receive a notification that the submission is complete. To track the status of your paper throughout the editorial process, log in to Evise® at: http://www.evise.com/evise/faces/pages/navigation/NavController.jspx?JRNL_ACR=EXG.

Enrich your article to present your research with maximum impact. This journal supports the following Content Innovations:

- Explain your research in your own words and attract interest in your work using AudioSlides : 5-minute webcast-style presentations that are displayed next to your published article and can be posted on other websites. You will receive an invitation email to create an AudioSlides presentation within three weeks after your paper has been accepted.

I look forward to receiving your revised manuscript as soon as possible.

Kind regards,

Professor Simm
Editor
Experimental Gerontology

Comments from the editors and reviewers:
-**Reviewer 1**

-

In this paper by Spannbrucker et al., it is suggested that exposure of lung epithelial cells in the absence of inflammatory cells to carbon nanoparticles leads to cellular senescence and loss of gap junctional intercellular communication. It is also suggested that larger particles (non-nanocarbon particles) do not elicit the same effect. Although the study has a nice potential, it seems like the authors have not focused on a particular pathway but test various pathways in general (p21, SIRT1, connexin 43).There are few concerns raised:

1. The authors suggest induction of senescence but they only show increased levels of p21. They do not perform SA-beta-galactosidase assay, BrdU assay etc. They do not show anything on cell proliferation.

For example, this induced senescence is it reversible or irreversible? Would the cells start proliferating again once they divide them and give them the necessary space? Regarding p21, the non-nanocarbon particles exhibit increase as well albeit at lower levels. Nevertheless, just with the p21 levels one cannot rule out the possibility that non-nanocarbon particles also induce epithelial senescence.

2. The same goes for the mRNA levels of connexin 43. Although shown as not significant still the levels upon exposure to CP are downregulated.

3. Figure 4: I am not sure I can see what the authors suggest we see. Maybe a focused photo in a higher magnification would help.

4. Figure 5: It would be nice to show which cells was initially injected. Due to high density of the cells seeded it is a kind of mess to count the communicating cells.

5. The introduction is rather big and vague.

-**Reviewer 2**

-

Spannbrucker and coworkers show that rat lung epithelial cells upregulate p21 and downregulate SIRT1 upon exposure for a week to nanocarbon particles. From this they conclude that this treatment induces senescence as opposed to carbon particles. Finally they show regulation of connexin 43 and claim that the nanocarbonparticles decrease cellular communication via GJIC.

The paper seems pretty preliminary to me and the claim that there is induction of senescence is not backed up by the data at all. I am not convinced by p21 as a sole marker of senescence in rat epithelial cells that are confluent, this could well be a normal stress response reaction. They claim to have shown similar data in a publication before, however, there they used other cell types. Therefore, the model of senescence need to be way better characterized.

The Western blots show no change in connexin 43 at the higher dose of carbon particles, while a change in the IF seems visible that is almost similar to the high nanocarbon particle dose. In addition, the strong decrease in communicating cells at the low dose of nanoparticles would not support that this is dependent on connexin 43 as at this dose no changes in the Westerns are seen. Controls e.g. like knock-down of connexin 43 are missing, further dampening the enthusiasm for this manuscript that stays at a very descriptive and superficial level.

Highlights

Carbon nanoparticles and not carbon particles induce lung epithelial cell senescence

Carbon nanoparticles and not carbon particles induce loss of cell-cell communication

Carbon nanoparticles may induce dysfunctional lung epithelial cells

Induction of cellular senescence and loss of gap junctional intercellular communication by carbon nanoparticle exposure of lung epithelial cells

Tim Spannbrucker[1†], Niloofar Ale-Agha[2†], Christine Goy[2], Nadine Dyballa-Rukes[2], Philipp Jakobs[2], Joachim Altschmied[3], Klaus Unfried[1*], Judith Haendeler[2*]

Affiliations:

[1]Environmentally-induced Skin and Lung Aging, IUF-Leibniz Research Institute for Environmental Medicine, Duesseldorf, Germany

[2]Heisenberg-group - Environmentally-induced Cardiovascular Degeneration, Medical Faculty, HHU Duesseldorf and IUF-Leibniz Research Institute for Environmental Medicine, Duesseldorf, Germany,

[3]Core Unit of Biosafety Level 2 Laboratory, IUF-Leibniz Research Institute for Environmental Medicine, Duesseldorf, Germany,

*To whom correspondence should be addressed:

Judith Haendeler, E-mail: juhae001@uni-duesseldorf.de

and

Klaus Unfried, E-mail: Klaus.unfried@uni-duesseldorf.de

† those authors contributed equally to this work

Abstract

Inhalation of combustion-derived particles is associated with the development of age-related diseases like chronic obstructive pulmonary disease and idiopathic pulmonary fibrosis. In both diseases senescence of lung epithelial cells has been observed. Employing an in vitro system of repetitive exposure to pure carbon nanoparticles we asked whether this kind of particles are able to induce epithelial senescence which might be accompanied by a loss of functionality at the level of gap junctional intercellular communication. Non-cytotoxic doses of carbon nanoparticles but not of bigger carbon particles led to an accumulation of the cell cycle blocking protein p21 as well as a loss of both redox sensitive histone deacetylase SIRT1 and connexin-43. Gap junctional cell cell communication detected by microinjection of fluorescent lucifer yellow was dramatically decreased after exposure. This loss of functionality was caused by a probably senescence-associated reduction of the mRNA expression of connexin-43. As the experimental system was chosen to study the effects of pure carbon nanoparticles in the absence of inflammatory cells, the data indicate that cumulative long term exposure of the lung epithelium to low doses of combustion-derived nanoparticles might contribute to epithelial senescence and age-associated diseases of the airways.

Keywords: senescence; lung epithelial cell; carbon nanoparticles; cell communication

1. Introduction

The inhalation of carbonaceous nanoparticles has been identified as a hazard for cardiovascular and pulmonary human diseases (Donaldson et al., 2005). Environmental (mostly traffic-related) air pollution is considered as the major source for these toxic particles. However, technologically produced carbon nanoparticles (carbon blacks) have also been shown to cause adverse health effects in humans after inhalation (Zhang et al., 2014). In the airways, chronic exposure to particulate air pollution has been shown to contribute to the development of age-related diseases like chronic obstructive pulmonary disease (COPD) and idiopathic pulmonary fibrosis (IPF) (Faner et al., 2012).

Both diseases show features of premature lung aging and cellular senescence. Tissue analyses of samples from IPF as well as from COPD patients show that lung epithelial cells in both diseases exhibit typical markers of senescent cells like the accumulation of cell cycle blocking proteins p21 and p16 (Disayabutr et al., 2016; Houssaini et al., 2018). In COPD the reduced proliferative and regenerative capacity of senescent lung cells may cause the formation of emphysema (Bartling and Hofmann 2018; Chilosi et al., 2013). In IPF, senescence-associated changes in cellular signalling of epithelial cells appear to be involved in processes like epithelial to mesenchymal transition and tissue remodelling (Selman et al., 2016). In both diseases the involvement of senescence associated secretory phenotypes is suggested to contribute to the severe changes in lung tissue structure (Kumar et al., 2014).

The inhalation of particulate xenobiotics may contribute to the pathogenesis of the age-associated diseases by inducing cellular senescence in the lung epithelium. This effect could be triggered by the direct interaction of particles with lung epithelial cells. This particular mechanism appears to be particularly relevant for inhaled nanoparticles, which - because of their small size - are not specifically recognized and cleared from the lung by macrophages (Geiser et al., 2005). However, inhaled particles also induce an inflammatory reaction dominated by neutrophilic granulocytes, which may also contribute to the induction of senescence in the lung epithelium. Indications that inhaled toxicants are able to trigger cellular senescence in the airway epithelium so far mostly come from investigations with tobacco smoke as the main cause of COPD. In the lung epithelium of COPD patients and of smokers a dramatic loss of the redox-sensitive histone deacetylase SIRT1, a regulator of metabolic pathways and senescence, was observed (Rajendrasozhan et al., 2008). The overexpression or pharmacological activation of SIRT1 in experimental systems was able to prevent emphysema formation (Yao et al., 2012). As the molecular mechanism causing the loss of SIRT1 and the induction of cellular senescence, the oxidative stress caused by tobacco smoke was suggested. Oxidants have shown to modify SIRT1 in a way that leads to decreased enzyme activity and increased proteasomal degradation (Caito et al., 2010).

Therefore, oxidative stress either induced by the inhaled xenobiotics or by an inflammatory oxidative burst may contribute to the induction of cellular senescence in the lung epithelium.

However, as tobacco smoke is a highly complex mixture of particulate and volatile xenobiotics, the relevance of such mechanisms for environmental or technologically produced carbon nanoparticles is not clear. Our own earlier studies give indications that the exposure of the lung epithelium to pure carbon nanoparticles also induces cellular senescence (Buchner et al., 2013). For these studies we established a cell culture model using confluent cell layers of an alveolar lung epithelial cell, which was exposed repetitively for 14 days with particle doses not inducing cytotoxicity. In these cells we observed elevated levels of reactive oxygen species in parallel to an accumulation of p21 protein levels.

The molecular mechanisms by which inert poorly soluble pure carbon nanoparticles induce intracellular oxidative stress and cellular senescence are not fully understood (Unfried et al., 2007; Weissenberg et al., 2010). However, the comparison of chemically identical particle types differing in their primary particle size indicates a particular role of physical particle characteristics in this pathogenic mechanism (Peuschel et al., 2012). At constant mass doses, only carbon nanoparticles with a primary diameter of 20 nm induced intracellular oxidative stress and subsequent signalling events, while non-nano carbon particles (primary diameter 350 nm) failed to induce these reactions. Besides the primary size, the particle samples differ in their reactive surface area by a factor of 40. It is, therefore, assumed that the reactive surface area is a particle characteristic, which specifically influences nanoparticle cell interaction.

Cellular senescence is associated with the loss of cellular function. The communication of lung epithelial cells via gap junctions appears to be an important mechanism for the regulation of inflammatory reactions (Freund-Michel et al., 2016; Losa et al., 2011). Moreover, there are also indications that lung epithelial cells are able to communicate with mesenchymal cells via gap junction intracellular communication (GJIC) (Badri et al., 2011). Earlier studies using microinjection of a fluorescent dye demonstrated that GJIC in lung epithelial cells was reduced after exposure to carbon nanoparticles for a few hours (Ale-Agha et al., 2010). The loss of GJIC was accompanied by an acute translocation of connexin-43 from the plasma membrane to the cytoplasm. As connexin-43 appears to be down regulated during aging in other systems (Nagibin et al., 2016), age-associated down regulation of this key protein of GJIC might be an additional feature of nanoparticle induced epithelial senescence.

The current work aimed to investigate the direct influence of carbon particles of different sizes on cellular senescence of lung epithelial cells. We used a well established cell culture model to specifically investigate the induction of cellular senescence by carbon particles without additional influences of inflammatory cells recruited to the airways. The specificity of

such reactions was investigated by applying two different doses of particles, which earlier proved to be not cytotoxic (Buchner et al., 2013). The application of two chemically nearly identical particles, which differ in primary size and therefore also in their reactive surface area (see table 1) allowed to investigate the role of these physical particle characteristics for the induction of epithelial cellular senescence. Furthermore, as a parameter of epithelial function, GJIC was investigated by fluorescent dye injection and expression analyses of connexin-43 after repetitive exposure of lung epithelial cells.

2. Material and methods

2.1 Particles and particle suspensions

Carbon nanoparticles (CNP, Printex 90 were obtained from Degussa (Germany) and carbon particles were from H. Haeffner (CP, Chepstow, UK; as Huber 99). As described earlier, particles and particle suspensions were characterized for their physical characteristics (table 1) (Kroker et al., 2015; Peuschel et al., 2012).

Table 1: Physical characteristics of carbon particles and particle suspensions

sample	primary size [nm]	zeta potential [mV]	surface area [m^2/g]	size in suspension [nm] *peak 1*	size in suspension [nm] *peak 2*	size in suspension [nm] *peak 3*
CNP	20	-22.4	442	887 (±197) 88.8%	118 (±126) 10.5%	1798 (±3114.8) 0.7%
CP	350	-16.0	10.6	359 (±22 100%)		

For each experiment, stock suspensions of particles (1 mg/ml) were freshly prepared in PBS by sonication for 15 min at 50–60 Hz, 120 W (Sydlik et al., 2006). The suspensions were applied to confluent monolayers of RLE-6TN cells to achieve the indicated doses.

2.2 Cell culture

RLE-6TN rat lung epithelial cells (Driscoll et al., 1995) derived from alveolar type II cells were purchased from ATCC and cultivated at 37°C in a humidified atmosphere with 5% (v/v) CO_2 and held in Ham's F-12 (Sigma, Germany) supplemented with (final concentrations) 5% (v/v) fetal calf serum (FCS,Sigma), 1% (v/v) of Glutamax (Invitrogen), and penicillin/streptomycin(Sigma).

2.3 Cell exposure

Confluent monolayers of cells were exposed to particle suspensions each second day for 14 days to achieve doses of either 1µg/cm^2 or 10µg/cm^2 of particles, at each time. Prior to each exposure, the culture medium was changed. Two days after the last exposure, cells were harvested for analyses or used for immunostaining or analyses of gap junctional intercellular communication (GJIC).

2.4 Determination of gap junctional intercellular communication (GJIC)

GJIC was determined as described earlier (Ale-Agha et al., 2010). Cells were grown on 6 cm dishes and exposed to CNP or CP as described above. GJIC was determined by microinjecting the fluorescent dye Lucifer Yellow CH (Sigma; 10% (w/v) in 0.33 M LiCl) into selected cells by means of a micromanipulator and a microinjector system (Eppendorf, Hamburg, Germany). One minute after injection, fluorescent cells surrounding the cells loaded with the dye were counted and taken as a measure of GJIC. Ten individual cells were loaded with dye per dish and means of the numbers of fluorescent neighboring cells were calculated (Ale-Agha et al., 2009).

2.5 Western blotting, immunocytochemistry

For Western blotting, cells were lysed in RIPA (50 mmol/l TRIS-HCl pH 8,0, 1 % IPEGAL CA630, 150 mmol/l NaCl, 0,1 % SDS, 0,5 % Desoxycholat) and protein concentrations determined in Bradford assay (Bio-Rad, Hercules, USA). Samples were applied to SDS–polyacrylamide gels of 10% (w/v) acrylamide, followed by electrophoresis and blotting. Immunodetections were performed using the following antibodies rabbit polyclonal anti-Cx43 (Sigma-Aldrich, St. Louis, U.S.A.; 1:1500), p21 (Abcam, Cambridge, UK; 1:500), SIRT1 (Cell Signaling Technology, Danvers, U.S.A.; 1:500), src (Cell Signaling Technology, Danvers, U.S.A.; 1:500). As secondary antibodies, horseradish peroxidase conjugated goat anti-rabbit antibodies were used (GE Healthcare, Chicago, U.S.A.; 1:5000). All antibody incubations were in 5% (w/v) nonfat dry milk in Tris-buffered saline containing 0.1% (v/v) Tween 20 (TBST). Semi-quantitative analyses were performed on scanned immunoblots using ImageJ. For immunocytochemistry, cells were grown on glass coverslips and treated with carbon nanoparticles or carbon particles as described above. Following the respective experimental treatments, cells were washed with PBS and fixed for 15 min with 4% of formaldehyde, and washed three times with PBS. Non-specific binding sites were blocked for 15 min at room temperature with 3% (v/v) normal goat serum (Sigma) diluted in PBS containing 0.3% (v/v) Triton X-100. For detection of Cx43, cells were incubated with polyclonal rabbit anti-connexin-43 (1:1500) diluted in PBS containing 1% (v/v) goat serum overnight at 4°C. Antibodies were removed and cells washed three times with PBS, followed by incubation with an Alexa 488-coupled goat anti-rabbit IgG (H + L; 1:500) for 1 h at RT. For actin filaments staining RLE were stained with Alexa Fluor 568-coupled phalloidin for 30 min at RT (Invitrogen, Karlsruhe, Germany). Nuclei were stained with 4′,6-diamidino-2-phenylindole (DAPI, Invitrogen, Karlsruhe, Germany). Cells were washed and mounted with ProLong Gold antifade mounting medium (Invitrogen, Karlsruhe, Germany). Fluorescence images were taken with an AXIOVERT 200 M microscope (Zeiss, Jena, Germany, 1:40 oil).

2.6 Real-time PCR measurements of relative mRNA levels

RNA was isolated using Trizol reagent according to the manufacturer's protocol (Invitrogen, Karlsruhe, Germany). Gene-specific mRNA levels were determined by semi-quantitative real-time PCR. Therefore, the RNA concentration was measured photometrically. Aliquots of total RNA were reverse transcribed using the Superscript™ III First-Strand synthesis system (Invitrogen, Karlsruhe, Germany). The PCR reactions were carried out using SYBR® Green PCR Master Mix (Applied Biosystems, Darmstadt, Germany). The following primer pairs were used: hmrCx43 for (5′- ACGAGGTATCAGCACTTTTCT-3′), hmrCx43 rev (5′-ACAGCCACACCTTCCCT-3′), hmRPL32 for (5′-GTGAAGCCCAAGATCGTCAA-3′), hmRPL32 rev (5′-TTGTTGCACATCAGCAGCAC-3′).

2.7 Statistics

For statistical analyses two-sided, unpaired student's t-test was used. Data are presented as means +/- SEM.

3 Results

3.1 Carbon particles increase p21 protein levels in lung epithelial cells

In our earlier studies we observed that repetitive exposure of lung epithelial cells with non-cytotoxic doses of 10µg/m^2 of carbon nanoparticles led to an accumulation of p21 as a feature of cellular senescence (Buchner et al., 2013). In the first experiment we now asked whether this reaction is specific for carbon nanoparticles compared to bigger non-nano carbon particles induced by lower amounts of carbon nanoparticles and by non-nano carbon particles. Cells were exposed every second day with the indicated doses of particles for 14 days. Cells were harvested for the analysis of proteins two days after the last exposure. Western blot analyses revealed that carbon nanoparticles significantly increase p21 protein levels at any given dose (Figure 1). The exposure to similar doses of non-nano carbon particles induced much lower p21 levels, indicating that at the chosen mass doses carbon nanoparticles are more potent to trigger p21 protein induction and thus, probably epithelial cell senescence. To further analyse the induction of senescence by carbon particles, we next investigated SIRT1.

3.2 Carbon nanoparticles induce loss of SIRT1 protein levels in lung epithelial cells

SIRT1 has been described to be downregulated in different aging and senescence models. Therefore, we used the same experimental design as for p21. Compared to control treatment, no significant reductions of SIRT1 levels were observed with both concentrations of carbon particles (Figure 2). However, exposure to 10µg/cm^2 carbon nanoparticles led to a dramatic loss of SIRT1. The slight reduction of SIRT1 levels by exposure to the lower dose of carbon nanoparticles appears to indicate a dose dependency in the reduction of SIRT1 levels. Thus, our data show that only carbon nanoparticles, but not non-nano particles reduce SIRT1 protein levels.

3.3 Carbon nanoparticles induce downregulation of connexin-43 and change its cellular localization in lung epithelial cells

Next, we investigated whether connexin-43 - one of the most important connexins in the lung - is regulated by carbon particles. Thus, we first determined connexin-43 mRNA levels. As demonstrated in figure 3a only carbon nanoparticles significantly reduced connexin-43 mRNA expression. To confirm the mRNA data on protein level, we next performed immunoblot experiments. Only in cells treated with carbon nanoparticles a significant reduction of total connexin-43 protein levels was observed (figure 3b). In order to investigate the subcellular localization of connexin-43 after particle treatment, we performed connexin-43 immunostainings in lung epithelial cells. Immunofluorescence analyses of cells exposed to

carbon nanoparticles demonstrated loss of connexin-43 within the plasma membrane. These findings were not observed in cells treated with carbon particles. Thus, these data would suggest that long term treatment with non-cytotoxic doses of carbon nanoparticles not only leads to signs of cellular senescence but also to loss of GJIC.

3.4 Loss of GJIC in cells exposed to carbon nanoparticles

Therefore, we next measured GJIC by injecting the fluorescent dye lucifer yellow into single cells and counted the number of adjacent stained cells (figure 5). The repetitive treatment with both doses of carbon nanoparticles led to a dramatic loss of GJIC compared to control cells as well as carbon particles treated cells. Thus, our data indicate that only nanoparticles induce loss of cell-cell communication.

4 Discussion

Due to the amount of carbon nanoparticles in ambient air pollution or at occupational settings humans can be exposed to these particulate xenobiotics for long time periods. Chronic exposure to particulate air pollution has been associated with the occurrence of biomarkers for COPD (Schikowski et al., 2014). Particularly the clear correlation of life long exposure to traffic-related air pollution and COPD in a cohort of elderly women suggests the induction of premature lung aging by this environmental stress (Schikowski et al., 2005; Unfried et al., 2016). The current work aimed to find indication that such effects can be triggered in lung epithelial cells by carbon nanoparticles as a major component of air pollution. As human real life cumulative exposure cannot be perfectly reproduced *in vitro* or in animal experiments *in vivo*, exposure models have to be applied. In order to study the induction of cellular senescence by carbon nanoparticle exposure we chose a well characterized mechanistic model, in which we applied cumulative doses of particles over a time period of 14 days. The microscopic analyses of this study (figures 4 and 5) again demonstrated that this treatment has no cytotoxic effect on cells, as observed earlier (Buchner et al., 2013). This model allowed to investigate the effects of carbon nanoparticles on lung epithelial cells without the effects of inflammatory cells, which might contribute to oxidative stress or interfere with the senescence associated secretome (Kumar et al., 2014; Nel et al., 2001). The relevance of data obtained with the chosen cell has earlier been demonstrated for signalling events triggered by carbon nanoparticles when these data were compared to *in vivo* data from exposed animals (Autengruber et al., 2014; Sydlik et al., 2009). The chosen particle types and doses aimed to investigate the specificity of the induction of senescence by carbon nanoparticles in comparison to carbon particles.

The performed studies demonstrate that repetitive treatment with 10µg/cm^2 carbon nanoparticles specifically triggers the accumulation of p21, the loss of SIRT1 and connexin-

43. These features of cellular senescence are accompanied by a loss of epithelial cell function at the level of GJIC. The control particles, which are characterized by a bigger primary particle size appear not to induce these effects. Thus, the reduced surface area of non-nano particles compared to nanoparticles might be responsible for these differences. In earlier studies, we aimed to perform dose response experiments with respect to surface area rather than to mass (Peuschel et al., 2012). These results indicated that signalling processes indeed could be triggered by higher doses of non-nano particles. However in the current study it turned out that under repetitive conditions such high mass concentrations of carbon nanoparticles would interfere with the chosen assays.

The loss of histone deacetylase SIRT1 in the airways so far was observed in macrophages and lung epithelial cells after exposure to tobacco smoke or in the chronic inflammation leading to COPD (Rajendrasozhan et al., 2008; Yao et al., 2012). Our data for the first time demonstrate that similar effects can be triggered in the absence of inflammatory cells by pure carbon nanoparticles carrying virtually no organic compounds (Borm et al., 2005). Although not yet corroborated in an *in vivo* system, these data indicate that long term exposure to combustion-derived nanoparticles below the threshold dose for the induction of lung inflammation may contribute to the cellular senescence of epithelial cells and to the development of age-associated pulmonary diseases.

Cellular senescence in this study is associated with the dramatic loss of epithelial functionality at the level of GJIC. In earlier studies an acute redistribution of connexin-43 from the plasma membrane to the cytoplasm was responsible for the loss of GJIC after exposure to combustion-derived nanoparticles. In the recent study after repetitive long term exposure, however, we can attribute the loss of GJIC to the downregulation of connexin-43 at the mRNA level. Besides the reduction of connexin-43, the intracellular distribution of the protein does not resemble the typical feature of redistribution due to acute stress triggered by particles (Ale-Agha et al., 2010). However, we have to acknowledge that the dramatic loss of GJIC appears not to be completely represented at the level of mRNA and protein. This effect might be due to a combination of senescence-associated down regulation of connexin-43 and a loss of the protein at the plasme membrane. Nevertheless, the study clearly demonstrates that only carbon nanoparticles, but not carbon particles in non-cytotoxic and non-inflammatory doses induce senescent lung epithelial cells.

5 Conclusion

In conclusion the study demonstrates that carbon nanoparticles, but not bigger carbon particles induce cellular senescence accompanied by a loss in GJIC in lung epithelial cells. The data indicate that long term exposure to low doses of combustion-derived nanoparticles

might lead to epithelial senescence even in the absence of inflammation and contribute to the development of age-associated lung diseases.

6 Acknowledgements

We thank Florian von Ameln for excellent technical assistance.

7 Funding

The research was funded by grants from the German Research Foundation (DFG) HA2868/10-1/-2, HA2868/11-1 and UN110/4-1.

8 Figure legends

Figure 1. Exposure to carbon particles increases p21 protein levels in lung epithelial cells. RLE-6TN cells were exposed to carbon particles (CP) or carbon nanoparticles (CNP) each second day with the indicated doses for 14 days, c denotes the untreated control. P21 levels were determined by immunoblot, Src served as loading control. **(A)** Representative immunoblots. **(B)** Semiquantitative analysis of p21 normalized to Src. Data are mean ± SEM, n=4-5, *p<0.05 (two-sided, unpaired t-test).

Figure 2. Exposure to carbon nanoparticles decreases SIRT1 protein levels in lung epithelial cells. RLE-6TN cells were exposed to carbon particles (CP) or carbon nanoparticles (CNP) each second day with the indicated doses for 14 days, c denotes the untreated control. SIRT1 levels were determined by immunoblot, Src served as loading control. **(A)** Representative immunoblots. **(B)** Semiquantitative analysis of SIRT1 normalized to Src. Data are mean ± SEM, n=6, *p<0.05 (two-sided, unpaired t-test).

Figure 3. Exposure to carbon nanoparticles decreases connexin 43 RNA and protein levels in lung epithelial cells. RLE-6TN cells were exposed to carbon particles (CP) or carbon nanoparticles (CNP) each second day with the indicated doses for 14 days, c denotes the untreated control. **(A)** Connexin 43 transcript levels were determined by semi-quantitative real-time PCR, RPL32 served as reference. Data are mean ± SEM, n=3, *p<0.05 (two-sided, unpaired t-test). **(B, C)** Connexin 43 levels were determined by immunoblot, Src served as loading control. **(B)** Representative immunoblots. **(C)** Semiquantitative analysis of Connexin 43 normalized to Src. Data are mean ± SEM, n=6, *p<0.05 (two-sided, unpaired t-test).

Figure 4. Exposure to carbon nanoparticles leads to internalization of Connexin 43. RLE-6TN cells were exposed to carbon particles (CP) or carbon nanoparticles (CNP) each

second day with the indicated doses for 14 days, c indicates the untreated control. The cells were stained for connexin 43 (Cx43) and actin using phalloidin; nuclei were counterstained with DAPI, merge shows an overlay of all fluorescence channels, the scalebar is 50 µm.

Figure 5. Exposure to carbon nanoparticles impairs cell-cell communication. RLE-6TN cells were exposed to carbon particles (CP) or carbon nanoparticles (CNP) each second day with the indicated doses for 14 days, c denotes the untreated control. On day 14 gap junctional intercellular communication was measured by lucifer yellow dye transfer as described under materials and methods. **(A)** Representative microscopic pictures, merge shows an overlay of the fluorescence channel and the brightfield image. **(B)** Quantitative analysis of intercellular communication. Shown are the numbers of communicating cells, data are mean ± SEM, n=4, *p<0.05 (two-sided, unpaired t-test).

9 References

Ale-Agha, N., Albrecht, C., Klotz, L.O. 2010. Loss of gap junctional intercellular communication in rat lung epithelial cells exposed to carbon or silica-based nanoparticles. Biol Chem. 391,1333-1339;

Ale-Agha, N., Galban, S., Sobieroy, C., Abdelmohsen, K., Gorospe, M., Sies, H., Klotz, L.O. 2009. HuR regulates gap junctional intercellular communication by controlling beta-catenin levels and adherens junction integrity. Hepatology. 50,1567-1576;

Autengruber, A., Sydlik, U., Kroker, M., Hornstein, T., Ale-Agha, N., Stockmann, D., Bilstein, A., Albrecht, C., Paunel-Gorgulu, A., Suschek, C.V., Krutmann, J., Unfried, K. 2014. Signalling-dependent adverse health effects of carbon nanoparticles are prevented by the compatible solute mannosylglycerate (firoin) in vitro and in vivo. PLoS One. 9,e111485;

Badri, L., Walker, N.M., Ohtsuka, T., Wang, Z., Delmar, M., Flint, A., Peters-Golden, M., Toews, G.B., Pinsky, D.J., Krebsbach, P.H., Lama, V.N. 2011. Epithelial interactions and local engraftment of lung-resident mesenchymal stem cells. Am J Respir Cell Mol Biol. 45,809-816;

Bartling, B., Hofmann, H.S. 2018. Reduced proliferation capacity of lung cells in chronic obstructive pulmonary disease. Z Gerontol Geriatr;

Borm, P.J., Cakmak, G., Jermann, E., Weishaupt, C., Kempers, P., van Schooten, F.J., Oberdorster, G., Schins, R.P. 2005. Formation of PAH-DNA adducts after in vivo and vitro exposure of rats and lung cells to different commercial carbon blacks. Toxicol Appl Pharmacol. 205,157-167;

Buchner, N., Ale-Agha, N., Jakob, S., Sydlik, U., Kunze, K., Unfried, K., Altschmied, J., Haendeler, J. 2013. Unhealthy diet and ultrafine carbon black particles induce senescence and disease associated phenotypic changes. Exp Gerontol. 48,8-16;

Caito, S., Rajendrasozhan, S., Cook, S., Chung, S., Yao, H., Friedman, A.E., Brookes, P.S., Rahman, I. 2010. SIRT1 is a redox-sensitive deacetylase that is post-translationally modified by oxidants and carbonyl stress. Faseb j. 24,3145-3159;

Chilosi, M., Carloni, A., Rossi, A., Poletti, V. 2013. Premature lung aging and cellular senescence in the pathogenesis of idiopathic pulmonary fibrosis and COPD/emphysema. Transl Res. 162,156-173;

Disayabutr, S., Kim, E.K., Cha, S.I., Green, G., Naikawadi, R.P., Jones, K.D., Golden, J.A., Schroeder, A., Matthay, M.A., Kukreja, J., Erle, D.J., Collard, H.R., Wolters, P.J. 2016. miR-34 miRNAs Regulate Cellular Senescence in Type II Alveolar Epithelial Cells of Patients with Idiopathic Pulmonary Fibrosis. PLoS One. 11,e0158367;

Donaldson, K., Tran, L., Jimenez, L.A., Duffin, R., Newby, D.E., Mills, N., MacNee, W., Stone, V. 2005. Combustion-derived nanoparticles: a review of their toxicology following inhalation exposure. Part Fibre Toxicol. 2,10;

Driscoll, K.E., Carter, J.M., Iype, P.T., Kumari, H.L., Crosby, L.L., Aardema, M.J., Isfort, R.J., Cody, D., Chestnut, M.H., Burns, J.L., et al. 1995. Establishment of immortalized alveolar type II epithelial cell lines from adult rats. In Vitro Cell Dev Biol Anim. 31,516-527;

Faner, R., Rojas, M., Macnee, W., Agusti, A. 2012. Abnormal lung aging in chronic obstructive pulmonary disease and idiopathic pulmonary fibrosis. Am J Respir Crit Care Med. 186,306-313;

Freund-Michel, V., Muller, B., Marthan, R., Savineau, J.P., Guibert, C. 2016. Expression and role of connexin-based gap junctions in pulmonary inflammatory diseases. Pharmacol Ther. 164,105-119;

Geiser, M., Rothen-Rutishauser, B., Kapp, N., Schurch, S., Kreyling, W., Schulz, H., Semmler, M., Im Hof, V., Heyder, J., Gehr, P. 2005. Ultrafine particles cross cellular membranes by nonphagocytic mechanisms in lungs and in cultured cells. Environ Health Perspect. 113,1555-1560;

Houssaini, A., Breau, M., Kebe, K., Abid, S., Marcos, E., Lipskaia, L., Rideau, D., Parpaleix, A., Huang, J., Amsellem, V., Vienney, N., Validire, P., Maitre, B., Attwe, A., Lukas, C., Vindrieux, D., Boczkowski, J., Derumeaux, G., Pende, M., Bernard, D., Meiners, S., Adnot, S. 2018. mTOR pathway activation drives lung cell senescence and emphysema. JCI Insight. 3;

Kroker, M., Sydlik, U., Autengruber, A., Cavelius, C., Weighardt, H., Kraegeloh, A., Unfried, K. 2015. Preventing carbon nanoparticle-induced lung inflammation reduces antigen-specific sensitization and subsequent allergic reactions in a mouse model. Part Fibre Toxicol. 12,20;

Kumar, M., Seeger, W., Voswinckel, R. 2014. Senescence-associated secretory phenotype and its possible role in chronic obstructive pulmonary disease. Am J Respir Cell Mol Biol. 51,323-333;

Losa, D., Chanson, M., Crespin, S. 2011. Connexins as therapeutic targets in lung disease. Expert Opin Ther Targets. 15,989-1002;
Nagibin, V., Egan Benova, T., Viczenczova, C., Szeiffova Bacova, B., Dovinova, I., Barancik, M., Tribulova, N. 2016. Ageing related down-regulation of myocardial connexin-43 and up-regulation of MMP-2 may predict propensity to atrial fibrillation in experimental animals. Physiol Res. 65 Suppl 1,S91-s100;
Nel, A.E., Diaz-Sanchez, D., Li, N. 2001. The role of particulate pollutants in pulmonary inflammation and asthma: evidence for the involvement of organic chemicals and oxidative stress. Curr Opin Pulm Med. 7,20-26;
Peuschel, H., Sydlik, U., Grether-Beck, S., Felsner, I., Stockmann, D., Jakob, S., Kroker, M., Haendeler, J., Gotic, M., Bieschke, C., Krutmann, J., Unfried, K. 2012. Carbon nanoparticles induce ceramide- and lipid raft-dependent signalling in lung epithelial cells: a target for a preventive strategy against environmentally-induced lung inflammation. Part Fibre Toxicol. 9,48;
Rajendrasozhan, S., Yang, S.R., Kinnula, V.L., Rahman, I. 2008. SIRT1, an antiinflammatory and antiaging protein, is decreased in lungs of patients with chronic obstructive pulmonary disease. Am J Respir Crit Care Med. 177,861-870;
Schikowski, T., Adam, M., Marcon, A., Cai, Y., Vierkotter, A., Carsin, A.E., Jacquemin, B., Al Kanani, Z., Beelen, R., Birk, M., Bridevaux, P.O., Brunekeef, B., Burney, P., Cirach, M., Cyrys, J., de Hoogh, K., de Marco, R., de Nazelle, A., Declercq, C., Forsberg, B., Hardy, R., Heinrich, J., Hoek, G., Jarvis, D., Keidel, D., Kuh, D., Kuhlbusch, T., Migliore, E., Mosler, G., Nieuwenhuijsen, M.J., Phuleria, H., Rochat, T., Schindler, C., Villani, S., Tsai, M.Y., Zemp, E., Hansell, A., Kauffmann, F., Sunyer, J., Probst-Hensch, N., Kramer, U., Kunzli, N. 2014. Association of ambient air pollution with the prevalence and incidence of COPD. Eur Respir J. 44,614-626;
Schikowski, T., Sugiri, D., Ranft, U., Gehring, U., Heinrich, J., Wichmann, H.E., Kramer, U. 2005. Long-term air pollution exposure and living close to busy roads are associated with COPD in women. Respir Res. 6,152;
Selman, M., Lopez-Otin, C., Pardo, A. 2016. Age-driven developmental drift in the pathogenesis of idiopathic pulmonary fibrosis. Eur Respir J. 48,538-552;
Sydlik, U., Bierhals, K., Soufi, M., Abel, J., Schins, R.P., Unfried, K. 2006. Ultrafine carbon particles induce apoptosis and proliferation in rat lung epithelial cells via specific signaling pathways both using EGF-R. Am J Physiol Lung Cell Mol Physiol. 291,L725-733;
Sydlik, U., Gallitz, I., Albrecht, C., Abel, J., Krutmann, J., Unfried, K. 2009. The compatible solute ectoine protects against nanoparticle-induced neutrophilic lung inflammation. Am J Respir Crit Care Med. 180,29-35;

Unfried, K., Albrecht, C., Klotz, L.-O., Von Mikecz, A., Grether-Beck, S., Schins, R.P.F. 2007. Cellular responses to nanoparticles: Target structures and mechanisms. Nanotoxicology. 1,52-71;

Unfried, K., Kramer, U., Sydlik, U., Autengruber, A., Bilstein, A., Stolz, S., Marini, A., Schikowski, T., Keymel, S., Krutmann, J. 2016. Reduction of neutrophilic lung inflammation by inhalation of the compatible solute ectoine: a randomized trial with elderly individuals. Int J Chron Obstruct Pulmon Dis. 11,2573-2583;

Weissenberg, A., Sydlik, U., Peuschel, H., Schroeder, P., Schneider, M., Schins, R.P., Abel, J., Unfried, K. 2010. Reactive oxygen species as mediators of membrane-dependent signaling induced by ultrafine particles. Free Radic Biol Med. 49,597-605;

Yao, H., Chung, S., Hwang, J.W., Rajendrasozhan, S., Sundar, I.K., Dean, D.A., McBurney, M.W., Guarente, L., Gu, W., Ronty, M., Kinnula, V.L., Rahman, I. 2012. SIRT1 protects against emphysema via FOXO3-mediated reduction of premature senescence in mice. J Clin Invest. 122,2032-2045;

Zhang, R., Dai, Y., Zhang, X., Niu, Y., Meng, T., Li, Y., Duan, H., Bin, P., Ye, M., Jia, X., Shen, M., Yu, S., Yang, X., Gao, W., Zheng, Y. 2014. Reduced pulmonary function and increased pro-inflammatory cytokines in nanoscale carbon black-exposed workers. Part Fibre Toxicol. 11,73;

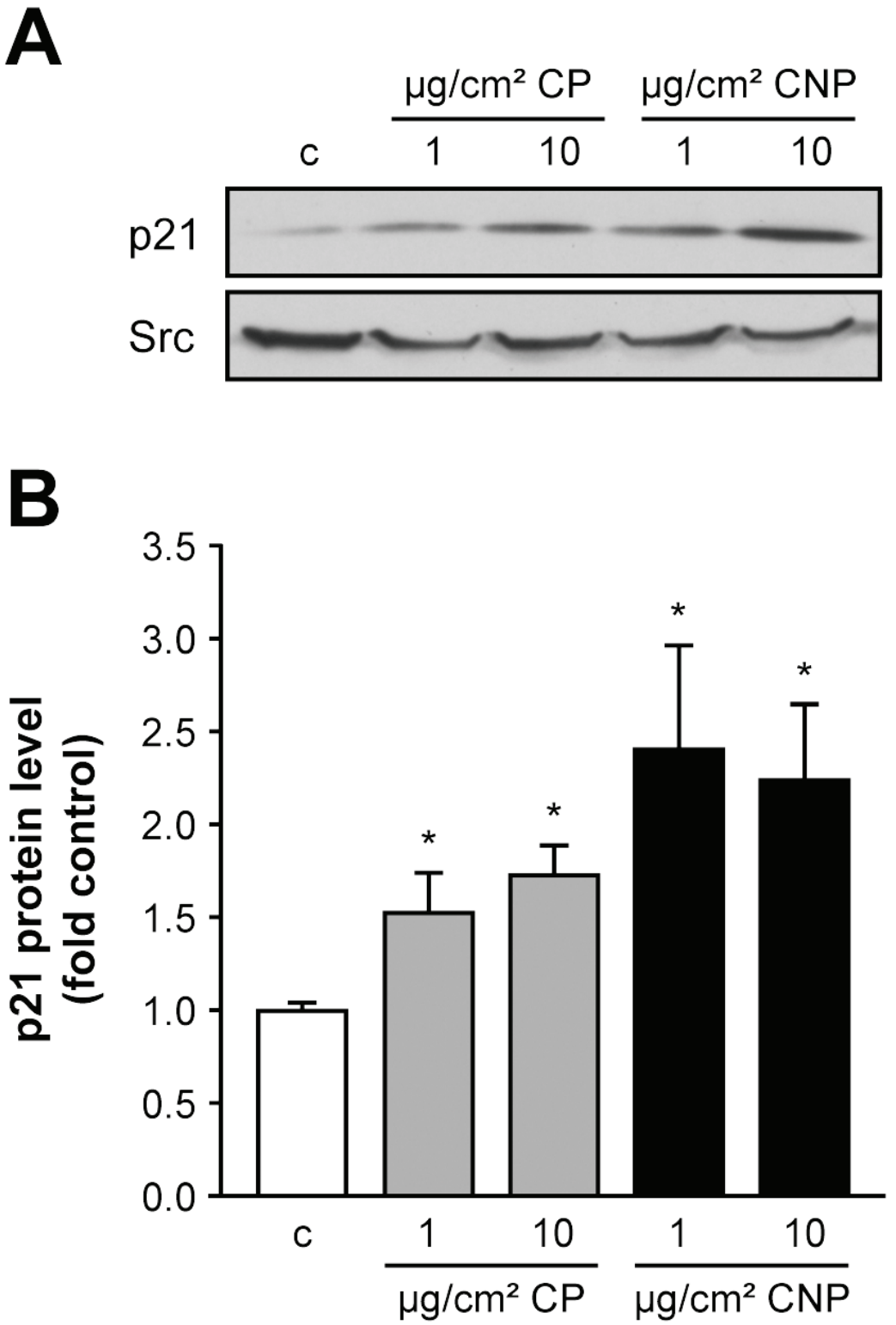

Spannbrucker, Ale-Agha et al.
figure 1
(6.97 cm wide/1 column fitting)

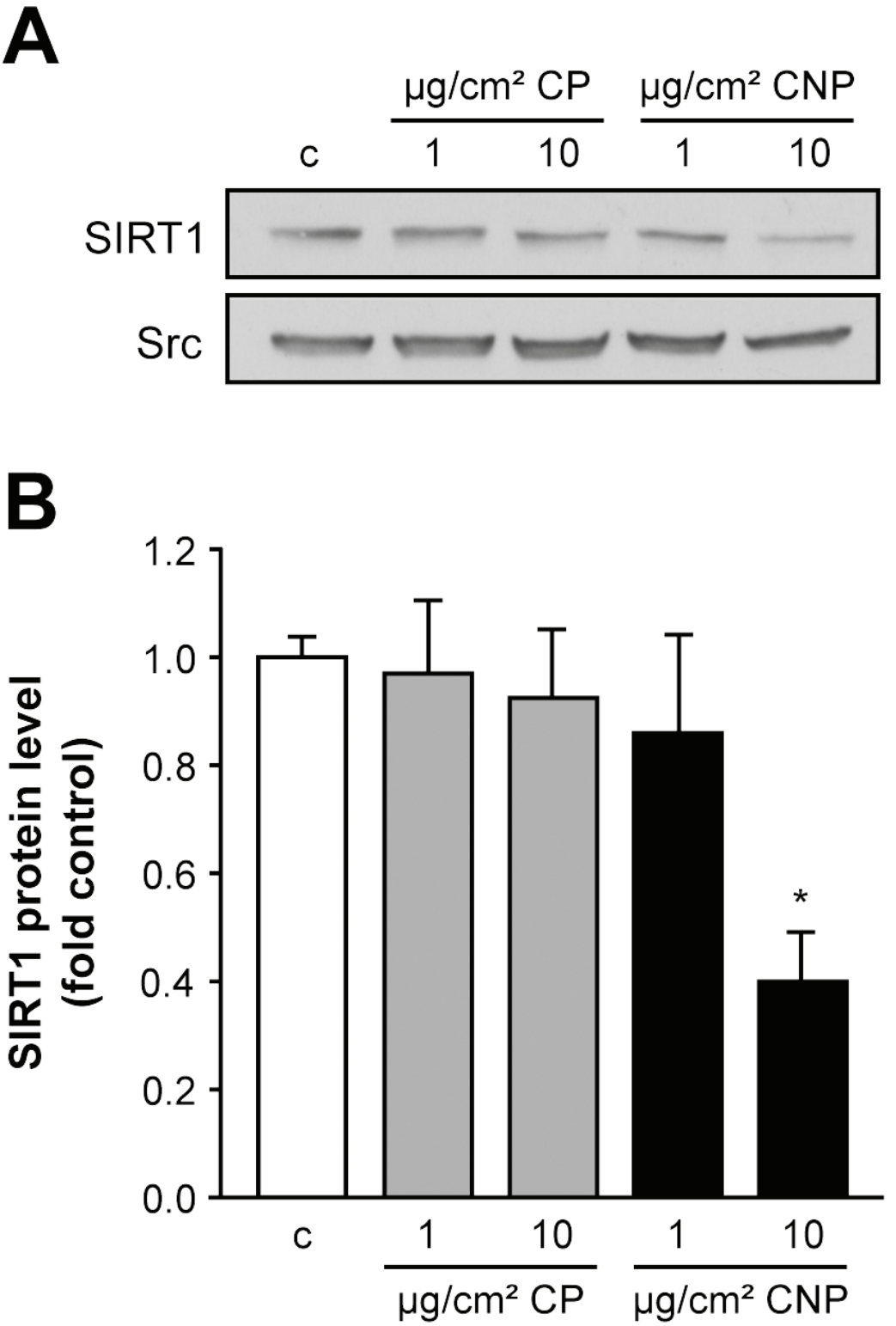

Spannbrucker, Ale-Agha et al.
figure 2
(6.97 cm wide/1 column fitting)

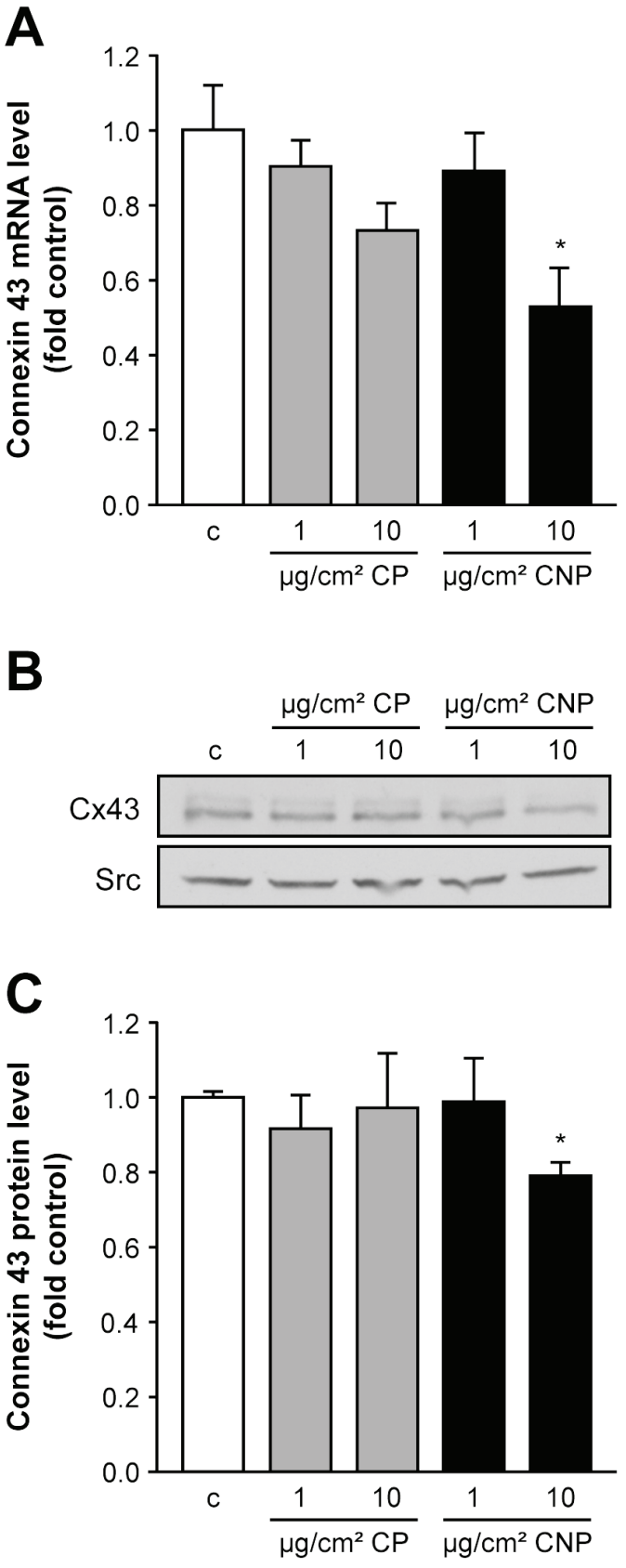

Spannbrucker, Ale-Agha et al.
figure 3
(6.97 cm wide/1 column fitting)

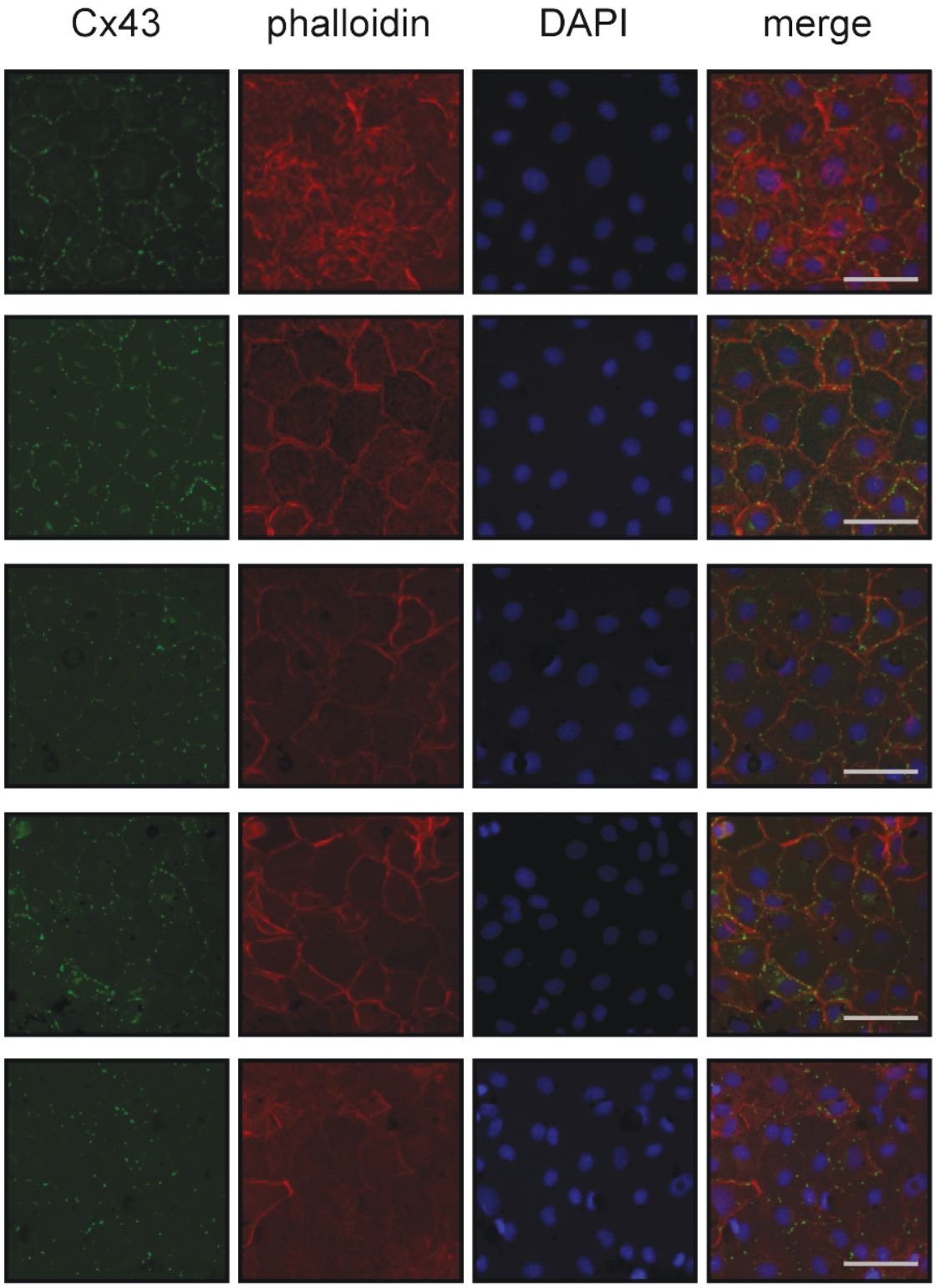

Spannbrucker, Ale-Agha et al.
figure 4
(8.45 cm wide/1 column fitting)

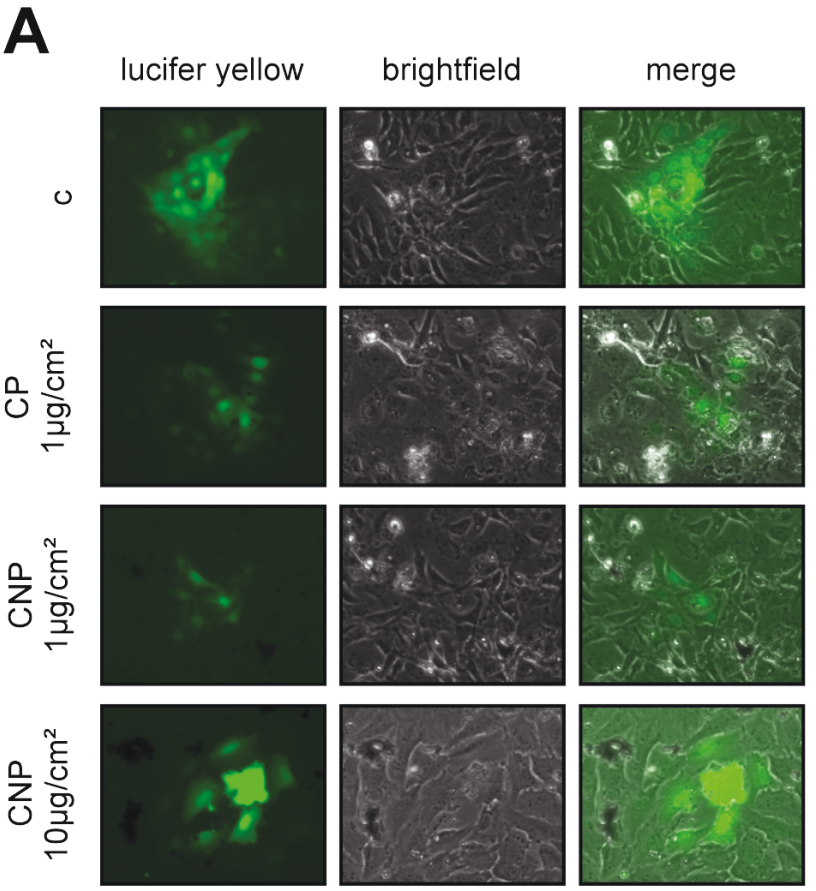

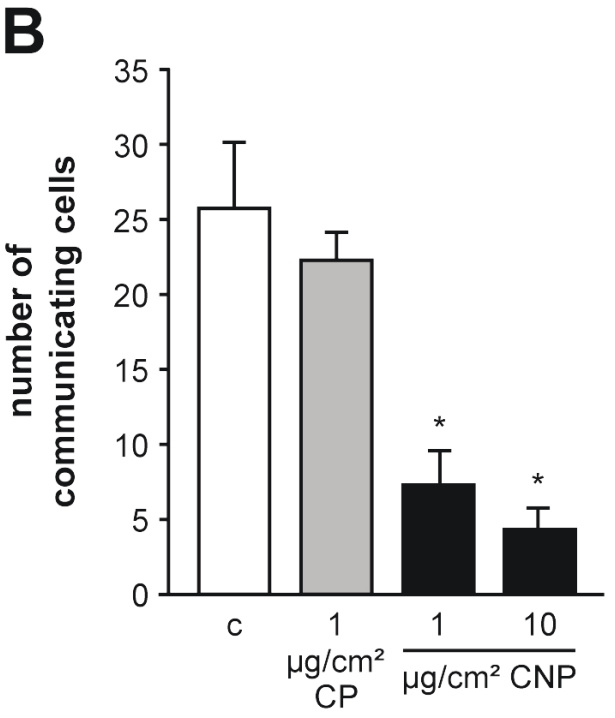

Spannbrucker, Ale-Agha et al.
figure 5
(7.95 cm wide/1 column fitting)

Danksagung

Mein größter Dank gilt an Jojo Haendeler und Yogi Altschmied für die Möglichkeit, an einem solch interessanten Thema zu arbeiten und mir die Chance zu geben, es bei verschiedenen Konferenzen mit anderen Wissenschaftlern zu diskutieren. Außerdem möchte ich mich für den regen Austausch während der Promotion sowie die gehaltvollen Diskussionen bei der Erarbeitung dieser Doktorarbeit bedanken.

Des Weiteren danke ich Prof. Dr. Axel Gödecke für die Übernahme des Zweitgutachtens.

Ein großer Dank gilt auch den Mitgliedern des internationalen Graduiertenkollegs (IRTG1902) für die Unterstützung während der Promotion sowie die vielen gemeinsamen Aktivitäten innerhalb und außerhalb des Promotionslebens. In diesem Zusammenhang möchte ich mich ebenfalls bei dem amerikanischen Partnerlabor an der Universität von Virginia in Charlottesville unter der Leitung von Norbert Leitinger bedanken, bei dem ich in dem sechsmonatigen Austausch eine abwechslungsreiche Zeit sowohl innerhalb als auch außerhalb des Labors hatte. Mein Dank gilt der DFG, die mich über das IRTG1902 während meiner Promotion gefördert und die es ermöglicht hat, den Austausch in Amerika zu finanzieren.

Ich möchte mich bei meiner Arbeitsgruppe bedanken, die mich während der Promotion in besondere Weise unterstützt und all meine Launen während dieser Zeit akzeptiert hat. Insbesondere danke ich Anna für die großartige Betreuung, bei der neben der Forschung auch der Spaß nie zu knapp kam. Auch gilt mein Dank in besonderer Weise Fee, die nicht nur tapfer das Büro und Labor mit mir teilte, sondern auf die ich mich in jeglicher Art und Weise verlassen konnte. Des Weiteren danke ich Florian, Nadine, Olaf, Kirsten, Steffi, Nilo, Karin, Tim, Mark, Sabrina, Sascha, Sabine und Klaus für die besonders intensive Unterstützung bei der experimentellen Durchführung meiner Arbeit und für die vielen lustigen Stunden während und außerhalb der Arbeit.

Ein Dank gilt ebenso Sandra Berger, der Koordinatorin des IRTGs, die mir während der Zeit mit Rat und Tat zu Seite stand und viele gemeinschaftliche Aktivitäten innerhalb des IRTGs organisiert hat.

Ganz herzlich danke ich meinen Eltern Marion und Willi sowie meinen Geschwistern Daniel und Christina. Ohne deren Unterstützung, die ich während meines gesamten Lebens erfahren habe, wäre ich nicht das, was ich jetzt bin. Des Weiteren möchte ich mich bei meiner Freundin Carmen bedanken, die es selbst in den stressigsten Situationen immer geschafft hat, mich abzulenken und wieder aufzubauen.